TECHNISCHE UNIVERSITÄT MÜNCHEN

Fakultät für Medizin

Lehrstuhl für Diabetesforschung/ Beta-Zellbiologie

TUM Medical Graduate Center (MGC)/ HELENA

Functional analysis of *Pitchfork* and *G protein-coupled associated sorting protein 2* in the mouse

Daniela Maria Padula

Vollständiger Abdruck der von der Fakultät für Medizin der Technischen Universität München zur Erlangung des akademischen Grades eines

Doktors der Naturwissenschaften

genehmigten Dissertation.

Vorsitzender:

Univ.- Prof. Dr. Mathias Heikenwälder

Prüfer der Dissertation:

1. Univ.- Prof. Dr. Heiko Lickert
2. Priv.- Doz. Dr. Thomas Floss

Die Dissertation wurde am 17.06.2014 bei der Technischen Universität München eingereicht und durch die Fakultät für Medizin am 22.10.2014 angenommen.

„Wer das Ziel nicht kennt,
wird den Weg nicht finden.“ (Christian Morgenstern)

Acknowledgements

First and foremost I would like to thank my PhD advisor, Professor Heiko Lickert, director of the Institute of Diabetes and Regeneration Research, for giving me the unique opportunity to compile this interesting PhD thesis in an environment most scientists can only dream of. Thank you for your expertise in embryology and beta-cell biology, the continuous guidance, ideas and funding. Your enthusiasm for science was contagious and motivational for me even during tough times of my project.

For the successful teamwork, all the ideas and fruitful discussions within our cilia meetings and all the molecular methods I learned, I'd like to thank Dr. Bomi Jung. Thank your for your helpful corrections and your support through the most difficult time of writing.

Dr. Ingo Burtscher designed and generated the Pifo conditional allele, introduced me to the confocal laser scanning microscopy and provided me with his expertise in cloning techniques. Thank you for your help and support during the last four years.

With progression of my project from embryology to adult mouse metabolism, new questions emerged. Dr. Jantje Gerdes, junior group leader, helped me to navigate through the field of metabolism and insulin resistance. Thank you for your expertise on the field and for answering all my questions.

I`d like to thank Anne Theis for the introduction to mouse work and technical support with my experiments, but also for the personal support and for her friendship. For aggregations I'd like to thank Heide Oller and Angelika Ziegler. Thank you for the good times at the Isar.

I'd like to thank my office mates and friends Moritz Gegg, Martin Preusse, Stefanie Willmann and Silvia Engert for their support and good discussions, but also for all the fun we had during these years. Thank you, Martin, for the statistical evaluation of the neural tube stainings. Thank you, Donna, for proof reading my thesis. I'd like to thank all the members of the AG Lickert for a source of friendship and for good advice and collaborations. Special thanks to all collaboration partners and thank you for the resulting papers.

Lastly, this thesis is what it is today because of all the love and encouragement from my family. I'd like to thank my parents for raising me with a love for science and for supporting me with all my pursuits. I'd like to thank my sister, Claudia, for time outs, I needed to move forward. For the encouragement and for inspiring discussions I'd like to thank Karl-Heinz. And most of all I'd like to thank you, Florian, for loving and believing in me and for the support, encouragement and patience during all these years. Thank you, family.

Abstract

Primary cilia (PC) are important for motility and signal transduction. Vertebrates have adopted the PC as a signaling center to orchestrate and transduce signals, such as Ca^{2+}, Sonic Hedgehog (Shh), platelet-derived growth factor receptor (PDGFR) and others. In a microarray-based screen with the aim to identify novel genes implicated in embryonic pattern formation, we identified *Pitchfork (Pifo)* as an important regulator of left-right asymmetry and cilia disassembly (Kinzel et al. 2010). Pifo is expressed in regions of high Shh signal activity and Pifo haploinsufficient mutant embryos exhibit polydactyly, a phenotype caused by Shh-mediated limb bud (LB) patterning defects. Collectively, these data suggested that Pifo could be a Shh target gene and might act in the Shh pathway. This was the central hypothesis of this PhD thesis which we set out to test functionally in the mouse model system. In order to understand the role of Pifo in more detail, an interactom study (in cooperation with Prof. Marius Ueffing) was performed to identify protein-protein interaction partners. One of the most interesting hits of this screen was the G protein-coupled receptor associated sorting protein 2 (Gprasp2). In primary LB cultured cells (PLCs) as a model for Shh signaling we could show that Pifo and Gprasp2 form a heterotrimeric complex with the main seven transmembrane receptor of the Hedgehog (Hh) pathway, Smoothened (Smo). This heterotrimeric complex is formed in a Shh-dependent manner and necessary for the transport of Smo to the PC for Shh signal transduction. Both, knock-out (KO) of Pifo or Gprasp2 in PLCs lead to defects in Smo PC translocation and Shh pathway activation (Jung et al. 2014, submitted). To translate these findings to the *in vivo* model, we generated conditional (CKO) and constitutive Pifo KO mice. Analysis of neural tube (NT) patterning that is very sensitive to changes in Shh pathway activation revealed minor reduction in motoneuros at E10.5. Similar results we obtained in *Gprasp2* gene trap (GT) mutant embryos. Further molecular characterization of the Pifo KO mice suggests that the KO allele generated is likely a hypomorphic allele where almost half of the mRNA and likely protein is generated. This allowed us to overcome the previously reported lethality and to study the role of *Pifo* as a potential ciliopathy gene in the adult mouse. As both genes, *Pifo* and *Gprasp2*, are expressed in the pancreatic islets, I focused my analysis on systemic metabolic control and a potential involvement of these genes in the pathogenesis of diabetes. I could show that Pifo homozygous mice show impairment in insulin-secretion of pancreatic β-cells. Under challenged high fat diet (HFD) conditions, Pifo homozygous mice become glucose intolerant as a result of β-cell mass decline due to reduced proliferation. We propose to have generated a mouse model system to study T2D susceptibility upon genetic predisposition. On the other hand, Gprasp2 GT mutant adult mice developed obesity and liver steatosis under normal chow conditions. Surprisingly, Gprasp2 GT mutant males overcame obesity upon HFD feeding, suggesting that the phenotype is not fat-diet induced and therefore a novel mous model system in order to study carbohydrate metabolism. Taken together, this PhD thesis provides a novel mechanism of Hh signal transduction by the discovery of the heterotrimeric Pifo-Gprasp-Smo transport complex and links these newly discovered Shh components to clinically observed ciliopathy phenotypes, i.e. obesity and diabetes.

Contents

1 Introduction

1.1 Chapter I Development

1.1.1 Mouse development

1.1.1.1 Early mouse development

The murine development starts with the fertilization of the egg in the oviduct. 24 hours later the zygote starts to divide and another day later, at the eight-cell stage compaction occurs, where the blastomere starts to increase in size and polarize in an apical-basal manner. The morula is formed during this process and results at embryonic day (E)-3.5 in the blastocyst, consisting of the trophectoderm (TE) and the inner cell mass (ICM). The octamer binding transcription factor (TF) 3/4 (*Oct3/4)* and *Nanog* positive inner cell mass is at pluripotent state and will give rise to the embryo proper and the primitive endoderm (PE), whereas the TE will form the extra embryonic placenta (Martin 1981; Takaoka and Hamada 2012; Dietrich and Hiiragi 2007; Niwa et al. 2005). At that time the blastocyst implants into the uterine wall after it has hatched out of the zona pellucida. Morphological changes and cell fate specification take place from blastocyst state (E3.5) until early gastrulation (E6.5).

1.1.1.2 Formation of the body axis

During gastrulation the pluripotent epiblast gives rise to the three principal germ layers, ectoderm, mesoderm, and endoderm. In contrast to the mouse, in human, the gastrulation occurs relatively early after 14 days of fertilization, if one considers the average 266 days of pregnancy. The onset of mouse gastrulation occurs after 7.5 days of the 20 days of pregnancy in total. But before gastrulation starts at E6.0, the mouse embryo consists of a hemispherical epithelial cell layer, the epiblast. The epiblast is characterized by its pluripotent potential, as it is able to differentiate into all cell types of the embryo. It is surrounded with visceral endoderm (VE) and extra embryonic ectoderm which form the placenta and the yolk sac, respectively. At that stage the embryo possesses no information about later head or tail region as the primitive streak, which specifies the three body axes is being formed 12 hours later, at E6.5 with the onset of gastrulation (**Figure 1**). With the onset of *forkhead box protein A2* (*Foxa2)* expression, cells of the epiblast start to migrate towards the VE. *Foxa2* expression starts in the pre-streak stage embryo in the posterior epiblast and the VE. At that stage, *Foxa2* positive cells intermingle slightly with brachyury (T) positive cells (Ang and Rossant 1994; Burtscher and Lickert 2009). At E7.0 mid-streak stage, these two populations separate and Foxa2 positive cells are preferentially found in the proximal part of the posterior epiblast, whereas T positive cells are located to the distal part. The T positive cells will give rise to the mesoderm, whereas Foxa2 positive cells will form the definitive endoderm (DE) and the axial mesoderm, including node and noto chord (NC) cells. The mesoderm lies between the epiblast and the endoderm/ DE (**Figure 1**). Foxa2 is further important for the activation of Dkk1, Cer and Lefty1, which are important Wnt and Nodal antagonists (Glinka et al. 1998; Perea-Gomez et al. 2002; Piccolo et al. 1999). At E7.5, the node an important organizing center forms, which was first identified by Spemann and Mangold in 1924 (Spemann and Mangold 2001). Cells located in the dorsal blastopore lip of the amphibian embryo have the ability to induce a complete secondary axis. This was not only possible in the embryos of the

same species, but also between embryos of different species. Analogous organizers were identified also in the fish, chick, rabbit, mouse and *Xenopus* (Beddington 1994; Kinder et al. 2001; Shih and Fraser 1996; Tam et al. 1997). Foxa2 is necessary for the DE, node and NC as the organizer structures do not form in Foxa2$^{-/-}$ mutant embryos. The mutants die very early due to pattern defects of the primary body axis (Tamplin et al. 2008; Weinstein et al. 1994).

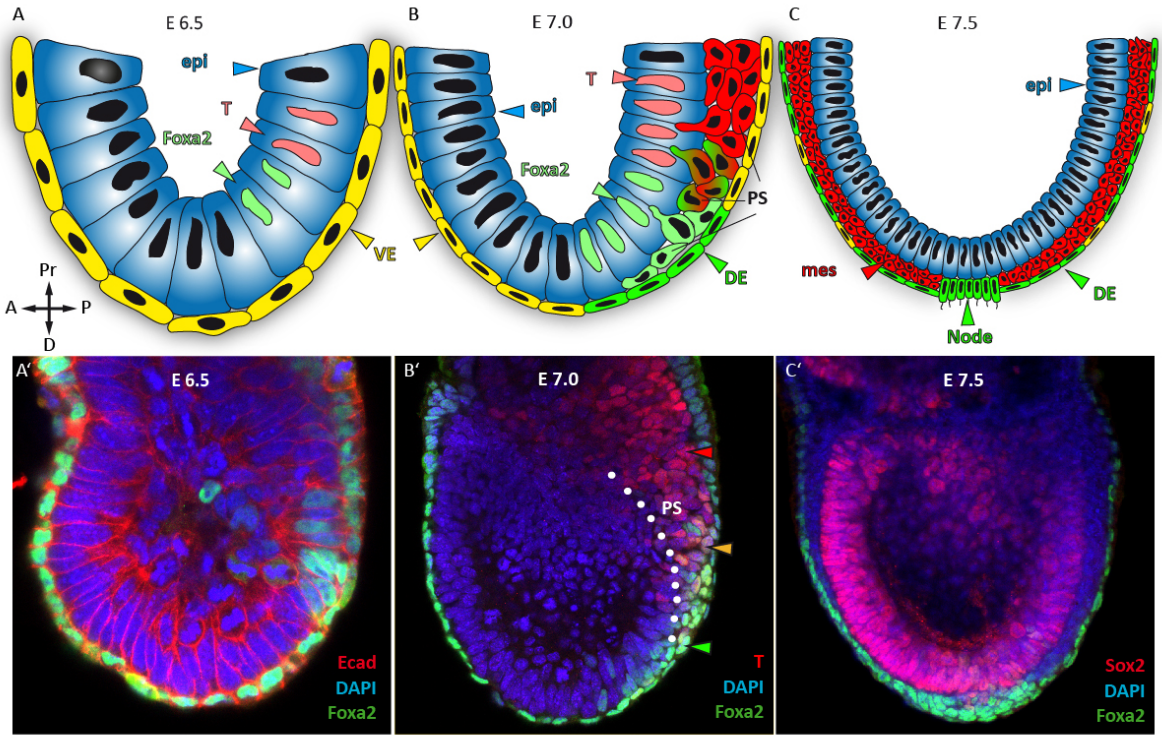

Figure 1 Endoderm formation. (A, A') Embryonic day E6.5, Brachyury (T) and forkhead box protein A2 (Foxa2) are synthesised in a mutually exclusive manner in the epiblast (epi). (B, B') During gastrulation, T^{+} and Foxa2^{+} cells undergo epithelial-to-mesenchymal transition (EMT) and invade into the primitive streak (PS). (C, C') After gastrulation at E7.5, mesoderm (mes), definitive endoderm (DE), and the node are built. Anterior-posterior (A-P), proximal-distal (Pr-D), visceral endoderm (VE). (Burtscher , Engert , Hasenöder , Padula , Lickert . BIOspektrum, Sept. 2011, Volume 17, Issue 5, pp 520-523, modified).

The embryonic node is a transient structure at the anterior end of the primitive streak (PS), which has a pit shaped structure (**Figure 1**). The mono-ciliated node cells (´9+0` axonemal structure), with the exception of being motile, are surrounded by monociliated crown cells in a horseshoe shaped pattern. The primary cilia (PC) (1.1.2.1) of the pit cells are rotating counterclockwise during late head-fold stage (E7.75) in order to generate a leftward flow of the surrounding extracellular fluid to transport a morphogen to the left side (Nonaka et al. 2005). In Kif3A or Kif3B mutant mice, where nodal cilia are absent, and the nodal flow can therefore not be established, the left-right (L-R) axis is disrupted (Supp et al. 1997). After gastrulation the head folds at the anterior side of the embryo, which is often described as head fold stage with an early onset at E7.75. With this the generation of the somites from the presomitic mesoderm begins and the anterior intestinal port forms. A similar fold arises later in the posterior part of the DE from cells moving anteriorly which form the caudal intestinal port. The most anterior and posterior parts of the DE form the ventral gut tube and all organs that

will arise from that, while the midline endoderm gives rise to the dorsal part of the gut tube and the associated organs, respectively (Lewis and Tam 2006). While the gut closes at E8.5 – 9.5, the embryo turns so that the dorsal side faces the outside and the ventral side lines.

1.1.2 Cilia biology and the Sonic Hedgehog pathway

1.1.2.1 The primary cilium: a sensory organelle

PC appear in all eukaryotes ranging from single-celled green algae to human and are found on almost all cells of the organism, with few exceptions such as cells of the myeloid or lymphoid origin (Michaud and Yoder 2006). A PC consists of a microtubule- (MT-) based structure called axoneme (**Figure 2**). With the invention of the electron microscopy *Fawcett et al.* discovered the '9 + 2` structure of motile cilia with an axoneme consisting of nine outer MT and a central MT doublet pair (Fawcett 1954). In addition, they showed that cilia are enclosed by the plasma membrane (PM) and expand from the basal body (BB). The BB originates from the centrosome, which is comprised of the mother and daughter centriole, surrounded by a cluster of proteins called the pericentriolar matrix (Luders and Stearns 2007). Depending on the tissue and its function two types of cilia exist; motile and immotile cilia. Motile cilia on ependymal cells lining brain ventricles circulate cerebrospinal fluid. Cilia on multiciliated epithelial lung cells are important for mucociliary clearance and cilia on cells lining the oviducts transport the oocyte and flagella agitate germ cells. Non-motile cilia on the other hand, are characterized by a '9 + 0` structure, an axoneme consisting of nine outer MT doublets lacking the central MT pair. One exception are the primary node cilia, as they exhibit a '9 + 0` structure together with a twirling movement. This movement is necessary in order to generate the embryonic leftward nodal flow and the establishment of a morphogen gradient important for L-R axis determination (Tanaka, Okada, and Hirokawa 2005). PC, persist in almost all cell types (renal tubules, pancreatic or bile ducts, bone and cartilage, retina, cochlea, developing heart, fibroblasts, kidney and Schwann cells, etc.) and serve as mechano- or chemosensors (Barnes 1961; De Robertis and Franchi 1956; Grillo and Palay 1963; Sorokin 1962; Ware, Aygun, and Hildebrandt 2011).

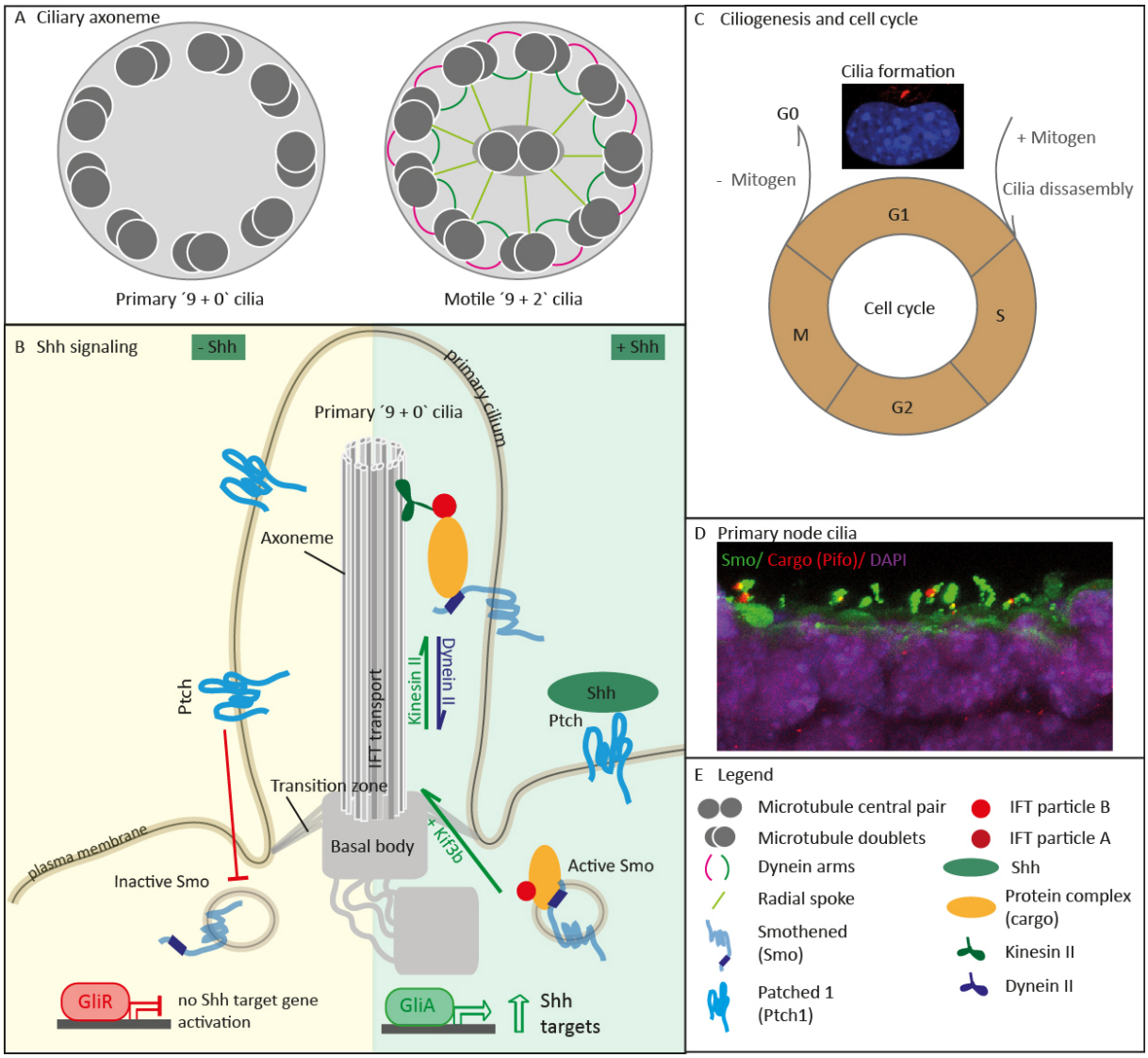

Figure 2 Cilia biology. (A) Schematic few of the ciliary axoneme structures: Primary non-motile (´9 + 0`) and motile (´9 + 2`) ciliary structures. (B) Intraflagellar transport (IFT) and Sonic Hedgehog (Shh) signaling. In the absence of Shh ligand, Patched 1 (Ptch1) inhibits Smoothened (Smo), which stays in its inactive form in the cytoplasm and cannot enter the PC. Mainly Gli repressor (GliR, Gli family zinc finger) is produced, which lacks the transcriptional activator domain and inhibits target gene activation. In the presence of Shh ligand, Ptch1 exits the primary cilium (PC) and Smo as well as other proteins/ transcription factors enter the ciliary compartment. Through unknown mechanisms this leads to an accumulation of the activated form of Gli (GliA) that induces Hh target gene activation in the nucleus. (C) Ciliogenesis and the cell cycle. Cells exit the cell cycle when mitogens are lacking, get ciliated in G0 phase of the cell cycle, and become Shh responsive. The addition of mitogens leads to a re-enty into the cell cycle. (D) Confocal laser scanning microscopy (LSM) of embryonic node showing Smo (green) at the PC and the adaptor protein (Pifo*, red). *Pitchfork (Pifo) is transported along the axoneme. Nuclei are stained by 4', 6-Diamidin-2-phenylindol (DAPI, purple). (E) Legend referring to B.

1.1.2.1.1 Primary cilia and the cell cycle

PC are post-mitotic structures as they are built in G0 or G1 phase when cells exit the cell cycle (**Figure 2**C). To induce ciliogenesis in cell culture, cells are cultured under serum-free conditions (lacking growth mitogens). During cytokinesis each daughter cell carries one centrosome, consisting of two centrioles. Cell cycle re-entry (G1 to S phase transition) induces the disassembly of the PC triggered by addition of serum or mitogens in cell

culture. At the G1 to S phase transition centrosomal duplication takes place (Hinchcliffe et al. 1999). Centrioles lengthen and centrosomes separate in G2 phase of the cell cycle to form the spindle pole bodies during mitosis. The ciliary disassembly program involves two main players, namely Aurora A (AurA) kinase and human enhancer of filamentation 1 (HEF1), plus dynein light chain Tctex type 1 and Pitchfork (Pifo) (Kinzel et al. 2010; Li et al. 2011; Pugacheva et al. 2007). HEF1 and AurA kinase are sequentially activated after serum starvation and subsequent mitogen stimulation, leading to an activation of histone deacetylase 6 (HDAC6) at the axoneme, which facilitates cilia disassembly by deacetylating stabilized and therefore acetylated MTs. It was further shown that HEF1 and AurA kinase inhibition blocks the disassembly of the PC and that a constitutive activation of both accelerates the process. Our laboratory has shown that Pifo is involved in ciliary disassembly where it accumulates at the BB and participates in the ciliary disassembly process working along with AurA (Kinzel et al. 2010). Haploinsufficiency for Pifo causes over-duplicate of the centrioles in S phase and formation of multipolar spindles during mitosis. A mutant form of *Pifo* identified in human ciliopathy (1.2.4) patients, *R80K*, inhibits AurA kinase activation and revealed a similar mitosis defect. In human patients loss of *PIFO* can block ciliary disassembly. Interestingly, accelerated cilia disassembly for example was found in patients with Joubert syndrome, due to a mutation in the inositol polyphosphate-5-phosphatase E (INPP5E), a lipid phosphatase exclusively localized at the basal end of the cilia (Bielas et al. 2009). These data suggest that failure in cilia disassembly can cause ciliopathy phenotypes in human.

1.1.2.1.2 Primary cilia dysfunction and ciliopathies

The important role for PC and BB proteins and their influence in development and later diseases has been elucidated with studying mutant mice (Goetz and Anderson 2010). Chick mutants with disrupted talpid3, which encodes a centrosomal protein important for cilia formation, exhibit developmental defects and polydactyly due to disfunctional Hh signaling (Ede and Kelly 1964). Mutants disrupting BB proteins cause human ciliopathies and also affect Hh signaling. Examples are oral-facial-digital syndrome 1 (OFD1), meckel syndrome type 1 (mKs1), fantom (Ftm, or rPGrIP1l), and Ellis–van Creveld syndrome protein (evC) (Delous et al. 2007; Ferrante et al. 2006). All these mutants exhibit abnormal or even absent cilia leading to developmental defects on the severity of the mutation. Polydactyly, a Shh mutant-like phenotype has also been found in patients with Bardet-Biedl syndrome (BBS) and Meckel syndrome (MKS)(Delous et al. 2007; Zaghloul et al. 2010). The BBS is characterized by the appearance of several symptoms, which not necessarily have to appear all in one patient. Most patients suffer from retinal dystrophy, followed by adipositas, polydactyly, mental retardation and/ or renal disease. Even more severe and lethal is the prognosis of MKS. Besides from severe malformations of the central nervous system (CNS) the fetus develops polycystic kidney diseases, polydactyly and severe defects in multiple inner organs. *Kinzel et al.* identified the PIFO R80K mutation in a fetus with MKS (*situs inversus* and polycystic kidney disease), suggesting that PIFO might be a ciliopathy gene. The Alström syndrome (ALMS) is another disease affecting the function of the PC (Girard and Petrovsky 2011). It is an autosomal-recessive disorder caused by mutations in ALMS1. By contrast, BBS is caused by mutations in several genes involved in PC function. Although, both syndromes cause equivalent levels of obesity, ALMS patients are more likely to develop T2D in young age. It is thought, that ALMS1 has a role in β-cell function and/or peripheral insulin signaling pathway. Furthermore, defects in cilia trafficking genes, like the motor dynein DNAI2 have been found

in patients with PC dyskinesia (PCD) (Loges et al. 2008). In PCD patients the motile cilia, which line the upper and lower respiratory tract, are defective, the disease is therefore also known as immotile cilia syndrome. If a disturbed L-R organization like *situs inversus* and *situs ambiguous* additionally occurs, which is observed in 50 % of PCD patients, the symptoms are summarized under the name Kartagener's syndrome. Recent studies have shown that cilia are also important in sensory tissues. Several retinal disease proteins have been found localized to the PC (Liu et al. 2007). Photoreceptors connect the outer light-responsive segment and the cell body with the help of cilia, and many mutations in genes encoding proteins involved in ciliogenesis or IFT transport lead to photoreceptor degradation. Retinis pigmentosa (RP), characterized by the degradation of the photoreceptor and subsequent cell death, is a clinical phenotype of a number of human ciliopathies. Defects in IFT88 and different MT proteins, and mutations in X-linked retinitis pigmentosa GTPase regulator (RPGR) account for a variety of RP affection (Khanna et al. 2005; Zhao et al. 2003). Cilia are also required in the cochlea, a sensory organ of the inner ear. Here cilia are important to establish the correct polarity of the sensory hair cells, as deficits lead to hearing loss (Moore et al. 2006).

1.1.2.2 Sonic Hedgehog identification

Hedgehog (Hh) was first identified in *Drosophila melanogaster* by Christiane Nuesslein-Volhard and Erich Wieschaus in a screen for embryonic patterning genes for which they later received the Nobel prize (Nusslein-Volhard and Wieschaus 1980). They showed that Hh is essential for the segmentation pattern of the fly embryo. There are three Hh orthologs in mammals, namely Indian Hedgehog (Ihh), Desert Hedgehog (Dhh) and Sonic Hedgehog (Shh), with Shh being the best studied. Shh functions as a long range morphogen, that is secreted from the NC and patterns the floor plate (FP) as well as the ventral region of the neural tube (NT). Cells respond to this morphogen by inducing different target genes at different concentrations (**Figure 3**). To become biologically active Shh undergoes post-translational modifications. The precursor protein is autolytically cleaved and lipidmodified (Dessaud, McMahon, and Briscoe 2008). The C-terminus is cholesterol modified and the N-terminus palmitoylated. Release of Shh requires a multi-pass transmembrane protein, called Dispateched1 (Disp1). Disp1 mutants severely disrupt ventral NT patterning, where Shh is necessary for specification of neuronal cell types (1.1.1). In vertebrates Shh signaling is essential for the embryonic development of many tissues including organizer tissues, such as the node and the NC which determine L-R and D-V asymmetry in the embryo (Zhang, Ramalho-Santos, and McMahon 2001). Furthermore, Shh plays a key role in the central nervous system and the limb bud (LB) where it controls pattern formation (Cruz et al. 2010; Wong and Reiter 2008). Loss of Shh pathway activity leads to a variety of human disease named Hedgehogpathies, which is a subgroup of ciliopathies and includes polydactyly, midline defects like holoprosencephaly, polycystic kidneys, heard defects, retinal degeneration, and many more clinical phenotypes (Cardenas-Rodriguez and Badano 2009; Huangfu et al. 2003; Murdoch and Copp 2010; Tobin and Beales 2008; Goetz and Anderson 2010). Constitutively active Shh signaling leads to over 80 different forms of cancer, e.g. medulablastoma and basal cell carcinoma (Shahi et al. 2010).

1.1.2.2.1 The Sonic Hedgehog pathway

The Zinc finger proteins of the Gli family are TFs, which are involved in the signal transduction of the Shh pathway. In contrast to *Drosophila melanogaster*, vertebrates have adopted the PC as a signaling center. In vertebrates three homologs of the zinc finger protein Cubicus interruptus (Ci) exist: Gli1, Gli2 and Gli3 (Hui and Angers 2011). They were shown to act as bi-functional TFs as through proteolytic processing they are converted from a full length active form (GliA) to a truncated repressor form (GliR), lacking the transcriptional activator domain. The GliR is formed by Gli3 and, to a lesser extent, Gli2. Although, all three Gli proteins contribute to GliA, Gli2 acts as main activator upon Shh pathway stimulation (Hui and Angers 2011). In vertebrates the PC links the activation of Gli TFs with the transcriptional activation of target genes upon Smo translocation. This translocalization was enclosed in *Drosophila* in the absence of Hh signaling. Cis forms a complex with the kinesin-like protein Costal2 (Cos2), the serine/ threonine kinase Fused (Fu), and the suppressor of fused (Sufu) (Goetz and Anderson 2010). Patched 1 (Ptch1) prevents the translocalization of Smo to the cell surface. In the presence of Shh ligand Fu phosphorylates kinesin-like protein Cos2. This modification in combination with the recruitment of Smo may lead to the disassembly of the Cis-Cos2-Fu-Sufu complex and a subsequent inhibition of CiR formation and accumulation of CiA. In vertebrate the PC coordinates the Shh signal transduction in a similar way: In the absence of the Shh ligand, its transmembrane receptor Ptch1 inhibits the accumulation of Smo, a seven-transmembrane protein, in the PC, blocking the downstream signal transduction cascade (Corbit et al. 2005). Smo controls both activation of Gli TFs and their proteolytic processing into the GliR form (Huangfu and Anderson 2006). In the presence of the Shh ligand, Ptch1 releases its repression allowing Smo to translocate to the PC together with cargo (**Figure 2**). Subsequently, protein kinase A (PKA) releases its phosphorylation of the GliR leading to an increase of the GliA form within the cytoplasm. This active form of the Gli TFs can enter the nucleus and transcribe target genes, such as *Gli1* and *Ptch1* but also other target genes like *cyclinD2*, *Pax6*, and *NKX2.2* (Shahi et al. 2010; Winklmayr et al. 2010).

In vertebrates Kif7 (the Cos2 homologue) interacts with all three Gli proteins localizes to the ciliary base in the absence of Shh signaling (Goetz and Anderson 2010). During active Shh signaling Kif7 translocates to the ciliary tip and contributes to the activation of Gli proteins (Goetz, Ocbina, and Anderson 2009). Kif7 at the ciliary base forms a complex with Gli, Sufu and other proteins in order to prevent Gli enrichment within the PC. It also promotes the processing of the GliR (Hui and Angers 2011). In parallel, Sufu at the ciliary tip directly binds Gli proteins, preventing the activation of the pathway in both *Drosophila* and mice (Methot and Basler 2000; Wang et al. 2000; Barnfield et al. 2005). Upon activation of the pathway and subsequent translocation of Smo, the Gli-Sufu-Kif7 complex localizes to the PC immediately, which is negatively regulated by PKA. *Goetz and Anderson* suggested that Kif7 thereby is a positive regulator by prompting Gli2A accumulation in the ciliary tip, by suppressing Sufu. Sufu on the other hand is implicated in suppressing GliA function (Barnfield et al. 2005) and supporting Gli3R formation through the binding of glycogen synthase kinase 3 (GSK-3) (Kise et al. 2009). Moreover, Sufu is thought to be a key regulator of Gli2 and Gli3. Both, Kif7 and Sufu are evolutionary conserved regulators of the Gli protein family. In contrast to *Ptch1* which exhibits a basal expression even in the absence of *Gli2* and *Gli3* (Motoyama et al. 2003), *Gli1* promoter activity is dependent on *Gli2* and *Gli3* expression in early mouse embryos (Bai, Stephen, and Joyner 2004).

Another target gene is the vertebrate *forkhead box A2 (Foxa2)* gene that belongs to a family of TFs consisting of three members, *Foxa1*, *Foxa2*, and *Foxa3*. All three TFs are encoded by individual genes in mammals (Kaestner 2010). All three Shh target genes (*Gli1*, *Ptch1*, and *Foxa2*) are expressed in the embryonic node, the NC, and at later stages in the NT (1.1.1) (Ang and Rossant 1994). *Foxa2* is the first neural-specific Gli target gene identified (Sasaki et al. 1997). In the 3' enhancer region of *Foxa2* a Gli TF binding site (GBS) is located and responsible for Shh-dependent transcription in the ventral NT. *Foxa2* expression is not expressed in the NT in absence of Gli2 and Gli3, even if the pathway is constitutively activated, caused by a *Ptch1* deletion (Motoyama et al. 2003).

1.1.2.2.2 Sonic Hedgehog signaling in the developing neural tube

The NT starts to develop at E7.75 (1.1.1) at the folding neural plate with a graded expression of the receptor Ptch1, which is induced by Shh secreted from the NC (Ribes and Briscoe 2009). The early NT consists of a simple tube which is surrounded by mitotically active neural epithelial cells. It is arranged along a D-V axis with the ventral neurons being pre-assigned to have motor functional control, whereas the dorsal neurons of the NT has the function to command and organize sensory information. With the help of different marker sets, eleven neuronal progenitor subtypes have been identified, which are arranged along the D-V axis of the NT (**Figure 3**). The pattern results from the secretion of different molecules, which provide positional information for the progenitors, namely Wnts, Bmps (secreted from the dorsal side), Shh (secreted from the ventral side of the NT) and fibroblast growth factor (FGF). Shh, released from cells from the NC and FP, forms a gradient along the D-V axis of the NT, with high activity of Shh in the ventral region and lower activity in the more dorsal region. Increased Shh signal and duration is associated with increased Gli2A and decreased Gli3R expression (Dessaud, McMahon, and Briscoe 2008). In the NT, Shh activity controls the specification of neuronal progenitors in a concentration and time dependent manner.

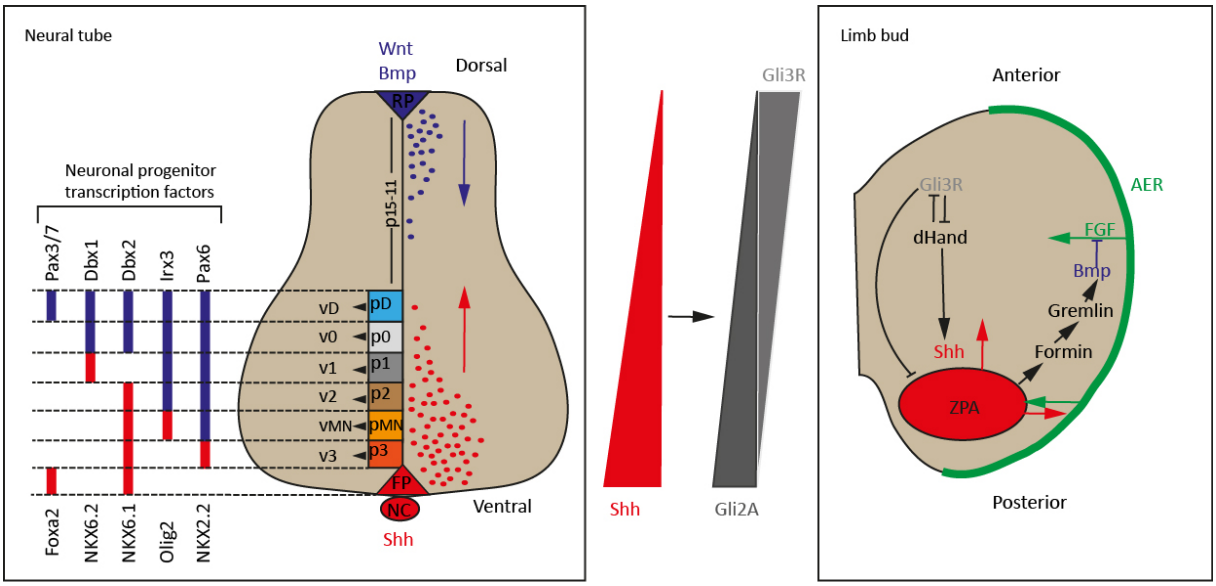

Figure 3 Shh directed neural tube and limb but patterning (Niswander 2003; Ulloa and Marti 2010; Wong and Reiter 2008). The morphogen gradient is formed along the dorsal-ventral (D-V) axis in the neural tube (NT) and similar in the limb bud (LB), along the anterior-posterior (A-P) axis, and released of cells in the zone of polarizing activity (ZPA). Shh is released of cells in the floor plate (FP) and on the contrary bone morphogenic protein (Bmp) and Wnt signaling are released from the roof plate (RP). The ventral region of

the neural tube is patterned through a variety of TFs, which have a distinct regional expression along the Shh gradient (neuronal progenitor TFs). The progenitors (p1-15, pMN and pD, respectively) are localized close to the lumen of the NT and migrate in later differentiated stages (v0-3, vMN and vD, respectively). Gli2A and Gli3R gradients further pattern the neural tube and the LB. For the proper LB growth and identity, next to Shh signaling also fibroblast growth factor (FGF) and Bmp signaling is important.

Similar to the NT, Shh forms a gradient along the anterior-posterior (A-P) axis in the LB of vertebrates (Niswander 2003). It is released from cells in the zone of polarizing activity (ZPA). The proximal-distal (Pr-D) coordination of the limb growth is controlled by *FGF*, which is expressed in the apical ectodermal ridge (AER) of the LB (**Figure 3**). Along with *FGF* and *dHand, GLi3R* regulates the activation of Shh which on the contrary maintains *FGF4* expression in the AER. *Gli3R* is expressed in the anterior region and dHand in the posterior region, mutually restricting their expression (te Welscher, Fernandez-Teran, et al. 2002; te Welscher, Zuniga, et al. 2002). Additionally, it was shown that *Gli3* represses *Gremlin*, which inhibits Bmp signaling. Thereby, the Formin protein maintains the expression of Gremlin. Altogether, these signaling pathway interactions and reciprocal regulations lead to LB patterning and the formation of digit identity in hand and feet.

1.1.2.2.3 Sonic Hedgehog misregulation during development

Shh mutant larvae embryos exhibit a disrupted segmentation pattern, together with short pointy protrusions throughout the body surface, which inspired the scientists to name it “hedgehog” (Nusslein-Volhard and Wieschaus 1980). The $Shh^{-/-}$ mutant mouse embryo exhibits holoprosencephaly, truncated limbs and a disturbed pattern of the NT, as they lack ventral cell types (Eggenschwiler, Espinoza, and Anderson 2001; Chiang et al. 1996). Due to the absent Shh gradient mainly Gli3R is present in the NT and the LB. This results in a specification of only v0 and v1 neurons in the NT and in the limb, were only the anterior-most digit is formed (**Figure 3**) (Wong and Reiter 2008). Mutations in certain ciliary genes such as the motor subunits Kif3a and Kif3b cause an early developmental lethality due to the failure of the L-R axis formation (Hirokawa et al. 2006).

Proteins and protein complexes (cargo) have to be transported along the PC, as there is no protein synthesis occurring within the PC. The transport system is called intraflagellar transport (IFT). Anterograde transport, towards the ciliary tip is achieved by a heterotrimeric kinesin 2 motor, whereas retrograde transport, towards the ciliary base is driven by cytoplasmic dynein 2 motors (Kardon and Vale 2009; Scholey 2008). Together with IFT particles for either anterograde or retrograde transport, these motors build the transport system for multi-subunit protein complexes (cargo, **Figure 2**) (Scholey 2008). Since the millennium evidence has grown that the PC indeed have a function. This was firstly shown by *Pazour GJ et al.* (Pazour et al. 2000) with the IFT88 (intraflagellar transport protein) mutant, which failed to assemble normal cilia in the kidney, leading to polycystic kidney disease (PKD). Ensuing studies could show that the PC is no evolutionary vestige in vertebrates, but serves as sensory organelle in many tissues (Huangfu et al. 2003). IFT mutant embryos affecting proteins for the anterograde transport, such as IFT52, IFT57, IFT88 and IFT172 and kinesin and dynein motor subunits Kif3a, DYNC2H1, respectively all show a disruption of the Shh pathway (Haycraft et al. 2005; Houde et al. 2006; Huangfu and Anderson 2005; Huangfu et al. 2003; Liu, Wang, and Niswander 2005). If the embryo is lacking IFT88 particle for example, it shows as similar NT phenotype as Shh mutants since the ventral

neurons fail to specify, leading to an expansion of dorsal subtypes. Due to the disruption of GliR gradient in the limbs, IFT88 mutants exhibit polydactyly. Gli proteins are important in embryo development as they direct cell determination, specification, proliferation and cell death. *Gli2* and *Gli3* are required for patterning, whereas $Gli1^{-/-}$ mutants in fact were shown to be dispensable for development (Bowers et al. 2012). *Wong and Reiter et al.* reported that $Gli2^{-/-}$ mutant mice show decreased ventral fate and normal digit development, whereas $Gli3^{-/-}$ mutant mice only show a slight expansion of dorsal neuronal fate, as the Shh and Gli2A gradients are present (Wong and Reiter 2008). GliR is crucial for the digit identity and once it is absent in the mutant embryo they exhibit polydactyly due to an up-regulation of Gremlin and dHand normally repressed by Gli3 (Wong and Reiter 2008). Two further conserved key regulators for Gli processing in the Shh pathway were described, namely Kif7 and Sufu. Kif7, being a positive regulator for Shh signaling, and Sufu as negative regulator, promoting the truncation of GliR (Anderson et al. 2012). As described earlier (1.1.2.2) Sufu is located to the ciliary tip, in the absence of Shh ligand where it is involved in the Gli processing into the repressor form. It thereby acts as negative regulator. In keratinocytes *Li et al.* could show in more detail that Sufu forms a complex with Gli2A, which prevents Shh signal activity. Kif7 on the contrary maintains Shh activity by dissociating this complex leading to subsequent Gli2 nuclear translocation (Li, Nieuwenhuis, et al. 2012). Kif7 may also block the function of Sufu at the ciliary tip. Kif7 loss leads to an expansion of dorsal neuronal fate with a loss of ventral neurons and to polydactyly in the LB and embryos die around E10.5 (Cheung et al. 2009; Law et al. 2012; Li, Nieuwenhuis, et al. 2012). In contrast, Sufu embryos exhibit a severely ventralized NT and the embryos die around E9.5 (Tuson, He, and Anderson 2011). The core event in the signal transduction of the Shh pathway is the translocation of Smo to the PC. $Smo^{-/-}$ mutants are stuck in development at E10.5, unable to turn, and with a very poor cranial development (Tran et al. 2008). Due to L-R asymmetry disruption the hearts of Smo mutants fail to fold up and remain as a straight tube (Zhang, Ramalho-Santos, and McMahon 2001). Thus, Smo is important for the transduction of both signals, Shh and Ihh, which have a redundant signaling function in the establishment of L-R axis. In summary the misregulation of Shh ligand, target genes and motor proteins involved in the IFT leads to severe phenotypes in the mouse.

1.1.3 Identification of Pitchfork

In a microarray based screen Foxa2 mutant embryos were compared to wild type (WT) embryos to identify novel organizer genes involved in embryonic pattern formation (Tamplin et al. 2008). Many deregulated endoderm and organizer genes were found and tested for further *in situ* hybridization. Through the screening *Pitchfork (Pifo)* was found which showed a restricted expression to the node. *Pifo* is particularly expressed in ciliated tissues such as node and NT and in tissues receiving Shh signaling (Kinzel et al. 2010). *Pifo* was found to regulate cilia formation and subsequently the L-R asymmetry at the node. In a human cohort study the same heterozygous R80K encoding variant was found in two patients with lethal thoracic-abdominal situs inversus, cystic kidneys, and liver fibrosis, and a patient with isolated double outflow right ventricle. As these data suggested a role for Pifo in ciliopathies, the role of Pifo in cilia formation was investigated in more detail. It was demonstrated that Pifo accumulates specifically at the BB and ciliary necklace during cilia assembly and disassembly, when proteins are delivered to cilia. Pifo was found to colocalize and interact with MT targeting proteins, to be involved in ciliary trafficking, and cilia disassembly by regulating AurA. AurA is important during

cilia disassembly as it deacetylates and destabilizes the axoneme (Pugacheva et al. 2007). Both proteins, Pifo activates AurA and both proteins accumulate at the ciliary base in a cycle-dependent manner. *Kinzel et al.* showed that this process is specifically abolished by the R80K mutation wich leads to the defect in ciliary disassembly, presented in the haploinsufficient embryos with malformed node cilia. As these haploinsufficient embryos further showed L-R asymmetry defects and polydactyly, both described as Shh-like phenotypes, the obvious question was if Pifo is functionally involved in Shh signaling.

1.2 Chapter II Ciliopathies and Diabetes

1.2.1 Diabetes facts

According to the International Diabetes Federation and the Robert Koch Institute in Berlin, around 9 % of the German population developed diabetes in 2013 (Kurth et al. 2009). There is a slight preference of women and people above the age of 50. This is due to the protective effect of estrogen on diabetes, which after the menopause is falling. Together with the fact, that women exhibit a longer life span one can explain the previous mentioned preference for women and older people epidemiologically. However, diabetes has become one of the world-wide most frequent metabolic diseases characterized by elevated blood sugar levels. The clinical diagnosis of diabetes is evident when a patient exhibits persistent hyperglycemia either when the fasting blood glucose exceeds 7.0 mM (126 mg/ dl), the glucose levels two hours after glucose load (oral glucose tolerance test, OGTT) remains above 11.1 mM (200 mg/ dl), or the glycated hemoglobin (HbA1c) is higher than 6.5 %. Human data are not easily transferred into mouse models and the parameter in the mouse models for metabolic measurements differs depending on the genetic background. Moreover, the metabolism of a mouse is different, for example the fasting blood glucose levels range from 4 – 6 mM. In humans there are a variety of forms of diabetes and metabolic syndromes and biologists would like to model these diseases in the pre-clinical mouse model to understand pathomechanisms of the disease and develop strategies for improved therapies. Maturity Onset Diabetes of the Young (MODY) is characteristic as it appears before the age of 25 years with a mainly very mild hyperglycemia and a nonketotic, and noninsulin-dependent form of diabetes. Eleven MODY forms of the autosomal-dominant disease have been identified, so far (Fajans, Bell, and Polonsky 2001). Type 1 and type2 diabetes mellitus (T1D, T2D) are both diagnosed with high blood glucose (hyperglycemia) levels. Type 1 diabetes (T1D) results from both, genetic predisposition and environmental triggers. The insulin producing cells β-cells of the pancreas are attacked by the body`s own immune cells, leading to an absolute insulin deficiency. T1D patients require daily insulin injections. The human leukocyte antigen (HLA) locus -DR4 has been associated with insulin dependent diabetes mellitus (Noble et al. 2008). However, the cause of T1D remains still controversial. The cause of T2D is considered as a combination of environmental factors and genetics (Franks, Pearson, and Florez 2013). Genes like insulin-receptor substrate-1 (IRS-1), glycogen synthase, glucagon receptor, ras-related protein associated with diabetes (RAD), histocompatibility antigens HLA locus-DR4, glycoprotein PC-1, and intestinal fatty acid binding protein (Kahn, Vicent, and Doria 1996), are thought to be involved. There is currently no cure for diabetes, and only a very small percentage of patients with T2D can enhance the condition with the change in life style (performance of exercise and food change). According to the severity of the disease, the patients have to take oral antidiabetic medications or insulin injections. During the last decade scientists have raised two hypotheses: (1) T2D as a cause of β-cell (1.2.2.1) specific insulin resistance, resulting in the failure of the β-cells to produce insulin. (2) T2D as a result of insulin resistance of the peripheral tissue (pancreas, muscle, fat, and liver) and its association with obesity. It occurs before glucose intolerance is detectable (Martin et al. 1992). In more detail, in early stages of the disease, due to partial insulin resistance the still normal β-cells secrete more insulin in order to compensate for the higher metabolic demand. Next, a process called β-cell lipotoxicity occurs, where adipocytes secrete free fatty acids (FFA) and inflammatory cytokines. All this leads to the development of a total defect in insulin secretion, which means for

the β-cells, that they become unable to respond to glucose (Kahn 1994), which subsequently leads to a β-cell failure ensuing in T2D (Petersen and Shulman 2006). In fact, β-cell failure has been described as the first step of whether an insulin-resistant individual will develop diabetes (Cerasi and Luft 1967). Although diabetes is a worldwide hot topic among scientists, the debate whether the β-cells at a certain time point resigns due to insulin resistance, or first undergoes a compensatory mechanism with an insulin overproduction, is still ongoing. It also remains unclear whether obesity is a form of overcompensation and in a long term than leads to T2D.

1.2.2 Pancreas development and function

The pancreas is an endoderm-derived organ that has key regulator function for protein and carbohydrate digestion and glucose homeostasis. The gland lies behind the stomach and surrounds the duodenum. It is divided in two parts: the *head* of the pancreas lies in concavity of the first part of the duodenum and the *tail* is adjacent to the spleen. The pancreas overall consists of an exocrine compartment, the duct and acinar cells and an endocrine compartment the islets of Langerhans. Whereas the exocrine acinar cells secrete zymogens, the duct cells secrete bicarbonate and through its branched structure deliver the zymogens to the duodenum. The islets of Langerhans are the principal source for the production of insulin, required for metabolic homeostasis.

The pancreas originates from a ventral and a dorsal bud that later fuse to form the definitive pancreas in murine development. The earliest progenitors of the pancreas are positive for pancreas and duodenum homeobox protein 1 (Pdx1) and are specified in embryos at seven somite stage around E8.5 (Zaret 2008). At E9.5 a multipotent progenitor domain buds out of the epithelium forming micro lumen which become positive for several markers including Pdx1 (Pan and Wright 2011). At E11.5, random cells start to polarize and constrict, leading to the fusion of the microluminar structures. This process continues with the distinction of tip and trunk when epithelial tubes are formed at E12.5, leading to the secondary transition at E12.5-14.5. At that stage the pancreatic buds are heavily lobulated and differentiated exocrine cells have appeared. At E15.5, the majority of the β-cells is Pdx1 positive and produces high amounts of the hormone insulin (Ahlgren, Jonsson, and Edlund 1996). The islets are initially small clusters and form as mature cell compartment in the last few days of embryonic development and postnatally, which is achieved in humans in the early third of development. In $Pdx1^{-/-}$ deficient embryos, the dorsal pancreatic bud is formed, but the subsequent morphogenesis of the bud is inhibited. This is due to an obstruction of the pancreatic epithelium at E10.5, which leads to the lack of a mature pancreas in mice, as well as in humans (Jonsson et al. 1994). How important the formation of the pancreas is, is seen in $Pdx1^{-/-}$ mutant mice, as they die shortly after birth.

In cell culture experiments with insulinoma cells (INS1), Shh has been shown to activate insulin secretion by activation the Pdx1 promotor (Thomas et al. 2000). The autors also showed an impaired Pdx1 and insulin expression, by inhibiting Shh signal with Cyc in INS1 cells. Contradictory to the evidence from cell culture experiments, are many of the *in vivo* studies, where Shh is only supposed to regulate cell β-cells differentiation. Is Shh signaling important for ß-cell function? How is Shh signaling involved, which mechanism lies behind?

1.2.2.1 Islets of Langerhans

The islets of Langerhans were first identified in 1869 by Paul Langerhans. Nowadays we know that islets consist of different cell types and the cell-type compensation differs between species (Bosco et al. 2010; Kilimnik et al. 2010). When comparing mouse and human islets, it was shown that (1) around 10 % alpha (α-) cells are found in the mouse, whereas 30 % in the human islets (Cabrera et al. 2006). Alpha-cells secrete the hormone glucagon, necessary to increase blood sugar levels when they are too low. (2) β-cells are the main source for insulin and represent around 80 % of the mouse and 70 % of the human islets. (3) Delta (δ-) cells are represented with around 10 % of the islet mass in both, mice and human and produce somatostatin, a peptide hormone regulating repressing insulin and glucagon secretion. A very small portion of cells in both species are formed by the (4) DD (gamma) cells, producing pancreatic polypeptide, which stimulates the gastric juice secretion and (5) epsilon cells, producing ghrelin which induces satiation when present at higher levels.

T2D progresses with the loss or dysfunction of β-cells. They can no longer sustain the elevated insulin amount as a possible result of peripheral insulin resistance. Glucose metabolism requires the transport of glucose into the cell which is achieved by transport of glucose, through the glucose transporter 2 (GLUT2) in mice and GLUT1 in humans. Both are transmembrane carrier proteins (Chakravarthy and Semenkovich 2007). Glucose is metabolized by glycolysis to generate energy in the form of ATP and pyruvate which is necessary to close the ATP sensitive potassium channels (K^+) (Brunham et al. 2007). Potassium channels form a heterotrimeric complex of the subunits sulfonylurea receptor1 (SUR1) with the K^+ ATP channel (Kir6.2). The constant closure of the channels leads to a depolarization of the membrane, leading to the opening of the voltage-dependent calcium (Ca^{2+}) channels, and a subsequent Ca^{2+} influx. Ca^{2+} in turn triggers the release of the insulin into the extracellular space. Obesity is in one-third of the cases the pre-step to diabetes, most likely due to genetic predisposition on the level of β-cells. As earlier discussed, there are a variety inherited forms of MODY concerning mutations in normal β-cell function, such as glucokinase and the TF Pdx1. In obese (non-diabetic) stages, β-cells are able to compensate for a higher insulin demand by increased function and size (Butler et al. 2003; Rhodes 2005). There are certain factors which link obesity and the later onset of diabetes, like the insulin receptor substrate (IRS) TF family. It is considered that insulin triggers an autocrine positive feedback-loop, as it binds its own receptor after secretion. This activates a phosphorylation cascade, which includes tyrosine phosphorylation of the insulin receptor-subunit and the IRS proteins, IRS1 and IRS2 (Borge et al. 2002). IRS1 and IRS2 knockout mice both develop insulin resistance in peripheral tissue, such as muscle, liver and fat (Araki et al. 1994; Withers et al. 1999). $IRS2^{-/-}$ mutant but not $IRS1^{-/-}$ mutant mice develop diabetes, with the whole spectrum of reduction of islets, β-cell mass and insulin. Both are expressed in the pancreas, where they contribute to the peripheral insulin response, but the difference in the phenotypes might lie in their different expression pattern throughout the insulin sensing tissues. Whereas IRS1 is also expressed in adipose tissue and muscle, IRS2 is expresses in adipose tissue, brain, liver and ovary (White 2002). Another good model to study β-cell adaption to metabolic changes is the pregnancy model. The maternal β-cells undergo compensatory proliferation in order to adjust for the increased metabolic load induced by the fetus (Sorenson and Brelje 1997). After delivery, the β-cell mass decreases by a programmed apoptosis of the dispensable β-cells, to return to normal β-cell mass (Bonner-Weir 2000). Beta-cells have a great capacity to adapt to different

metabolic changes, upon obesity or pregnancy for example, but it is considered that they can only adapt for a certain period of time. If the higher demand for insulin is constant, the β-cells exhaust and subsequently the diabetes risk increases.

1.2.2.2 E2F1 β cell cycle

As already mentioned, pancreatic β-cells have to proliferate and constantly adapt to different metabolic needs like pregnancy and obesity and thereby compensate for the different systemic insulin demands. Although β-cells have been shown to have an enormous capacity to self-renewal, it has been reported that upon ageing, the function as well as the proliferation rate of β-cells dramatically lowers in mice and human. In T2D when islets finally fail to compensate for the increased insulin demand, β-cells were found to be reduced, their proliferation impaired and apoptosis increased (Butler et al. 2003; Kloppel et al. 1985; Stamateris et al. 2013). The response to chronically elevated glucose levels in young-adult rat islets for example resulted in an increase of the β-cell mass, whereas in old rats the hyperglycemic state resulted in a β-cell mass decline (Assefa et al. 2014). *Zeng et al*. could show that Pten (phosphatase and tensin homologue deleted on chromosome 10) is involved in cellular aging and senescence, as it blocks the cell cycle re-entry by increasing expression of the cell cycle inhibitor p16ink4a (cyclin-dependent kinase inhibitor 2A, tumor suppressor protein) which is in human encoded by the *CDKN2A* gene (Zeng et al. 2013). When down-regulated, Pten leads to an activation of the E2F TFs and a subsequent methylation of p16ink4a. In the pancreas the CDK4-pRB-E2F1 pathway (cyclin-dependend kinase 4, a cell division protein - retinoblastoma protein, a tumor suppressor protein) mediates pancreatic growth and β-cell proliferation, as well as insulin secretion (Annicotte et al. 2009). Under basal conditions, expression of the potassium channel subunit *Kir6.2* is reduced in β-cells due to complex formation of pRb and E2F1 (which inhibit Kir6.2). In response to increased glucose levels, insulin is secreted, which activates the PI3 kinase, leading to an increase in Cdk4 activity, pRB phosphorylation and subsequent E2F1 transcriptional activity. With a closer look at the target genes, *Fajas et al.* and others could show that Kir6.2 was remarkably reduced in E2F1$^{-/-}$ mutant mice as it in fact was proven to be a direct target of the E2F1 pathway (Annicotte et al. 2009; Fajas et al. 2004). E2F1$^{-/-}$ mutant mice further showed an impaired insulin secretion in response to glucose *in vivo* and *in vitro* with isolated islets, although no difference in insulin content was observed, when compared to wild type (WT) mice (Fajas et al. 2004). Thus, E2F1$^{-/-}$ mutants were insensitive for glibenclamide, an antidiabetic drug, which increases insulin secretion and thereby lowers the blood glucose levels. Glibenclamide constantly closes the SUR1 subunit (sulfonylurea receptor 1) of the potassium channel, leading to a subsequent polarization of the membrane. *Annicotte et al.* could link the E2F1 TF, originally thought to only be involved in the activation of genes involved in the progression of G1 to S phase of the cell cycle, to metabolism (Annicotte et al. 2009). On the one hand, E2F1$^{-/-}$ deficient mice show a reduction in pancreatic size, caused by impaired postnatal pancreatic growth. And on the other hand, E2F1 is highly expressed in non-proliferating pancreatic β-cells. This suggests a role for E2F1 in pancreatic β-cell function and insulin secretion, additional to its effect on β-cell proliferation. Thus, inhibition of Cdk4 resulted in a decreas of Kir6.2 expression, impaired insulin secretion and glucose intolerance in mice. In summary the CDK4-pRB-E2F1 pathway defines a new link between cell proliferation and metabolism.

1.2.3 Role of insulin in peripheral organs

Insulin binds to the alpha-subunits of the insulin receptor (IR), leading to a conformational change, bringing the beta-subunits physically close together. This leads to an auto-phosphorylation and an activation of the tyrosine kinase of the receptor, which in turn allows the binding of several substrates, including IRS1 and IRS2. The IRS proteins thereby function as signaling centers and coordinate and activate different insulin pathway-complexes with different functions (Malaguarnera and Belfiore 2014). IRS proteins interact with the regulatory subunit of the PI3 kinase, leading to an activation of the AKT (protein kinase B) pathway, which propagates the IR metabolic effects like glucose uptake, lipogenesis, glycogen synthesis, fatty acid secretion, and gluconeogenesis by targeting several substrates, including Glut4, and Foxa2. AKT on the other hand activates several downstream cascades, including the mTOR (mechanistic target of rapamycin, serine-threonine kinase) pathway activation which is important for several cellular processes like apoptosis and cancer. Insulin signaling has an overall influence in the whole glucose homeostasis: After food intake, nutrients are absorbed by the gastro-intestinal system into the circulating system via the hepatic portal vein. This is innovated with visceral sensory axons, which exhibit incretin receptors and hormone sensors (glucagon-like peptide 1 (GLP1) receptor, and glucose transporter). The liver senses the ingested nutrients and glucose and according to that releases glucose further in the blood stream. In a second cycle GLP1, a hormone produced in the gut by intestinal L-cells, is released. As it is rapidly degraded by the enzyme dipeptidyl peptidase-4 (DPP4), it has to be constantly reproduced. Together with the elevated blood glucose levels, GLP1 stimulates the production of insulin in pancreatic β-cells and lowers the production of glucagon in pancreatic α-cells. The first phase of insulin release is thought to inhibit hepatic glucose production and the second phase is thought to stimulate the peripheral tissue (muscle, adipose tissue) and the central nervous system (CNS). Glucagon on the other hand causes the liver to convert stored glycogen into glucose (gluconeogenesis), which is released into the bloodstream. Furthermore, insulin and glucagon are part of a feedback-loop in order to keep the blood sugar at an adequate state. A region of the ventral hypothalamus was shown to control the hepatic glucose production. The reduction of insulin receptor (IR) in that region dramatically decreased the insulin sensitivity or led to a total loss of insulin response in the liver (Konner et al. 2007; Obici et al. 2002).

The liver is an endoderm-derived organ and despite it's numerous functions, it is the predominant source for glucose, with a slight contribution of the kidney and the gut (Stumvoll et al. 1995; Troy et al. 2008). Foxa1 and Foxa2 are essential for the specification of foregut endoderm and the liver. When deleted individually, Foxa1 and Foxa2 showed no morphological liver specific defect, but when deleted together, progenitors in the foregut endoderm fail to specify into hepatocytes (Li et al. 2009). The liver not only produces glucose through the process of gluconeogenesis from non-carbohydrate carbon substrates such as pyruvate, lactate, and glycerol, but also stores glucose in form of glycogen (a multibranched polysaccharide of glucose). In fasting periods, the liver utilizes these storages and reduces glycogen through a process called glycogenolysis. This plays an important role in glucose homeostasis (Grayson, Seeley, and Sandoval 2013). If insulin secretion is disturbed, the liver is one of the first organs sensing the changed insulin levels. It is thought that in early stages of T2D the first-phase insulin response is lost, resulting in a rise of hepatic glucose production due to the decrease of the inhibitory effect of insulin on the liver glucose production. The second-phase insulin response is

raised and together with the higher glucose production, it results in a higher peripheral uptake of glucose. As mentioned earlier the debate is still ongoing if due to insulin resistance in the periphery the β-cells compensation is lost, which mediates T2D progression. Or the loss of β-cells function and the subsequent lower amount of insulin are the beginning of the disease. Also the hepatic insulin resistance may contribute to the progression of T2D, through the IRS proteins. Liver specific IRS1 and IRS2 knock-out in mice (highly expressed in WT livers, reduced in diabetic animals and humans) showed that both proteins have complementary roles in the control of hepatic metabolism, with IRS-1 more closely linked to glucose homeostasis and IRS-2 more closely linked to lipid metabolism (Taniguchi, Ueki, and Kahn 2005). Insulin is important for the whole glucose homeostasis and affects the peripheral insulin receiving tissues like the liver, muscle, fat, and brain.

1.2.4 Diabetes and Obesity - link to Ciliopathies

As cilia are located on almost all cells their dysfunction has been linked to multisystem disorders that have been termed ciliopathies. Ciliopathies are described through a large set of mutated or absent ciliary, BB or IFT proteins. Very often several symptoms are clustered and describe a given syndrome. Bardet-Biedl syndrome (BBS) is often called “model ciliopathy” due to its highly pleiotropic appearance with a multisystem involvement. BBS patients suffer from cognitive impairment, genito-urinary tract malformations for example hypogonadism, retinal degeneration, polydactyly, mental retardation, renal malformations, obesity and diabetes. To date, 16 different gene mutations (BBS1-16) have been associated with this disorder (Shen, Yan, and Xiao 2013). The BBS proteins localize to the BB: The BBS chaperonins (BBS6, 10, 12) mediate the assembly of the BBSome (BBS1, 2, 4, 5, 7-9). This complex interacts with BBS3 at the ciliary base, in order to direct the trafficking of cargo to the cilia (Guo and Rahmouni 2011). Like BBS, Alstro¨m’s syndrome (ALS) includes a variety of endocrine phenotypes in humans such as hyperinsulinemia, insulin resistance, T2D and in particular obesity (Marshall et al. 2005). While more than 70 % of BBS patients are overweight, nearly all ALS patients have been reported to be obese. Thus, mice with a mutation in the ALS ortholog show normal birth weight and an age increased hyperhagia and subsequent obesity. These mice also develop insulin resistance and diabetes (Arsov et al. 2006). Symptoms described under ciliopathies very often vary in their severity and unlike many inherited diseases they are not always caused by one single mutation. Thus, several pathways have been reported to be implicated in cilia function and signal transduction such as Wnt and Shh.

1.2.5 Sonic Hedgehog signaling - link to Diabetes

Hh signaling primarly depends on cilia, as shown by many mutations in several Hh related genes (Goetz and Anderson 2010; Ocbina et al. 2011). In MKS1 mutant embryos e.g. the node cilia node cells exhibited mostly amorphous protrusions, which subsequently cause defects in the NT and LB patterning (Cui et al. 2011). Within the NT MKS1 mutant embryos showed an expansion in domains of low-level Shh signaling and a reduction in high-level Shh signaling, due to lower Gli3R expression (Weatherbee, Niswander, and Anderson 2009). MKS1 mutant mice further exhibited polydactyly, polycystic kidneys, situs inversus, heart defects and craniofacial malformations, which all can be linked to defects in Shh signaling. An association with BBS is found in hypomorphic mutants of Meckel syndrome 1 (Meckel-Gruber Syndrome, MKS1) which was classified as BBS13 and in centrosomal protein 290 (CEP290) classified as BBS14, respectively (Waters and Beales 1993). Meckel syndrome is a lethal ciliopathy, which manifests in with occipital encephalocele, polycystic kidneys and post-

axial polydactyly. MKS proteins localize to the transition zones, the basal bodies of sensory cilia, which is an evolutionarily conserved step as in humans this step is equal. Disruption in MKS1, and MKS1 related proteins (MKSR1, MKSR2) as well as MKS6 (CC2D2A), causes ciliogenesis defects in mouse and humans (Bialas et al. 2009; Tallila et al. 2008).

Moreover, Hh signaling is required for proper formation of endocrine and exocrine parts of the developing pancreas and is also active at low levels in the adult β-cells (Lau, Kawahira, and Hebrok 2006; Lau and Hebrok 2010; Cervantes et al. 2010). Thus, ectopic Shh expression has a positive effect on the expression of Pdx1 and subsequent insulin expression (Landsman, Parent, and Hebrok 2011). *Landsman et al.* could further show that β-cell specific increase in Gli2 activity in parallel with the deletion of PC led to glucose intolerance. This increase in Hh signaling accompanies with the dedifferentiation of the β-cells and if this persists, the β-cells lose their insulin secretion ability. Mice with a deletion of Smo in the developing pancreatic epithelium display in adult stages glucose intolerance, increased insulin sensitivity, and reduced total insulin production (Lau and Hebrok 2010). Mutations in the carboxy-terminal domain of Ptch1, as well as Ptch1 heterozygous state were found to decrease both the endocrine and exocrine cell mass in pancreatic islets (Nakayama et al. 2008).

In summary, defects in cilia and Hh genes range from developmental defects to diabetes and obesity (Gerdes, Davis, and Katsanis 2009). Despite from the literature indications of a role for Shh in the pancreas and β-cell function, the precise mechanism of how it acts in the pancreas is still unclear.Therefore, a better understanding of β-cell formation, function and homeostasis could help gain important knowledge for the treatment of diabetes and obesity. There is still a long way in understanding the complexity of the genetic and/ or environmental triggers of the disease. In that sense Hh signaling has gained importance as it controls both development as well as adult organogenesis. Misregulation of Hh signaling was linked to diabetes and obesity. Knowledge of the core mechanism of Shh pathway activation could provide future molecular targets for therapy.

1.3 Aim of this thesis

The aim of this thesis was to characterize potential novel Shh target genes – Pifo and Gprasp2 – in order to understand their function in Shh signaling and a possible link to ciliopathies. Previously, *Kinzel et al.* showed the involvement of Pifo in cilia disassembly (Kinzel et al., 2010). Pifo appears during evolution with vertebrates, which have adopted the PC as the signaling center and is expressed in regions of high Shh activity, suggesting that it might function in the pathway. Thus, haploinsufficient mutants showed polydactyly, likely caused by Shh-mediated LB pattering defects. In order to better understand the role of Pifo and its possible function in the Shh pathway, we generated a conditional Pifo knock-out mouse line. Together with the group of Prof. Marius Ueffing we discovered the interaction of Pifo and Gprasp2, which was found to have the potential to bind 7TMR (Jung et al. 2014, submitted). This suggested that the 7TMR Smo could be regulated by Pifo and Gprasp2. To explore this I investigated whether Pifo and Gprasp2 are targets of the Shh signaling and moreover potentially regulate the Shh pathway. Because of the unknown function of Gprasp2 I generated a GT knock-out mouse line in order to explore its expression and possible function in mouse development and adult organogenesis. Due to their possible involvement in cilia formation and Shh pathway activation I further examined if Pifo and Gprasp2 play a role in adult organogenesis and ciliopathies.

2 Results

The results are subdivided into two chapters. In chapter I I describe the analysis of Pifo and Gprasp2 early mRNA expression and pattern during embryonic development, and their functional involvement in Shh signaling, *in vitro* and *in vivo*. In chapter II I concentrate on the phenotype analysis of Pifo and Gprasp2 targeted mutations, with a main focus on pancreatic islets and a possible impact for diabetes and obesity.

2.1 Chapter I Development

2.1.1 Pifo constructs and expression

2.1.1.1 Analysis of Pifo$^{FD/FD}$ mouse line

2.1.1.1.1 Verification of the Pifo$^{FD/FD}$ targeting construct

Pifo was initially discovered in a microarray-based screen (Tamplin et al. 2008). The aim was to identify novel key players in endoderm development and embryonic pattern formation. *Kinzel et al.* showed that Pifo$^{LacZ/+}$ heterozygous mice die during development, due to L-R patterning formation defects leading to heart failure (Kinzel et al. 2010). In order to investigate the role of *Pifo* not only during development but also in adult tissues and organs, Dr. Ingo Burtscher designed and generated a conditional knock-out (CKO) allele. The targeting vector was used for targeted mutagenesis by homologous recombination in ES cells and the targeting strategy is described in 4.2.2.6.9 (**Figure 4**A). Exons three to six of the open-reading frame (ORF) were flanked by loxP sites (floxed) for Cre-recombinase-mediated excision. Upon germline transmission the neomycin selection cassette was removed by Flp-e-mediated excision in the germ line resulting in Pifo$^{flox/flox}$ mice, which can be used to delete the gene using any Cre-driver line.

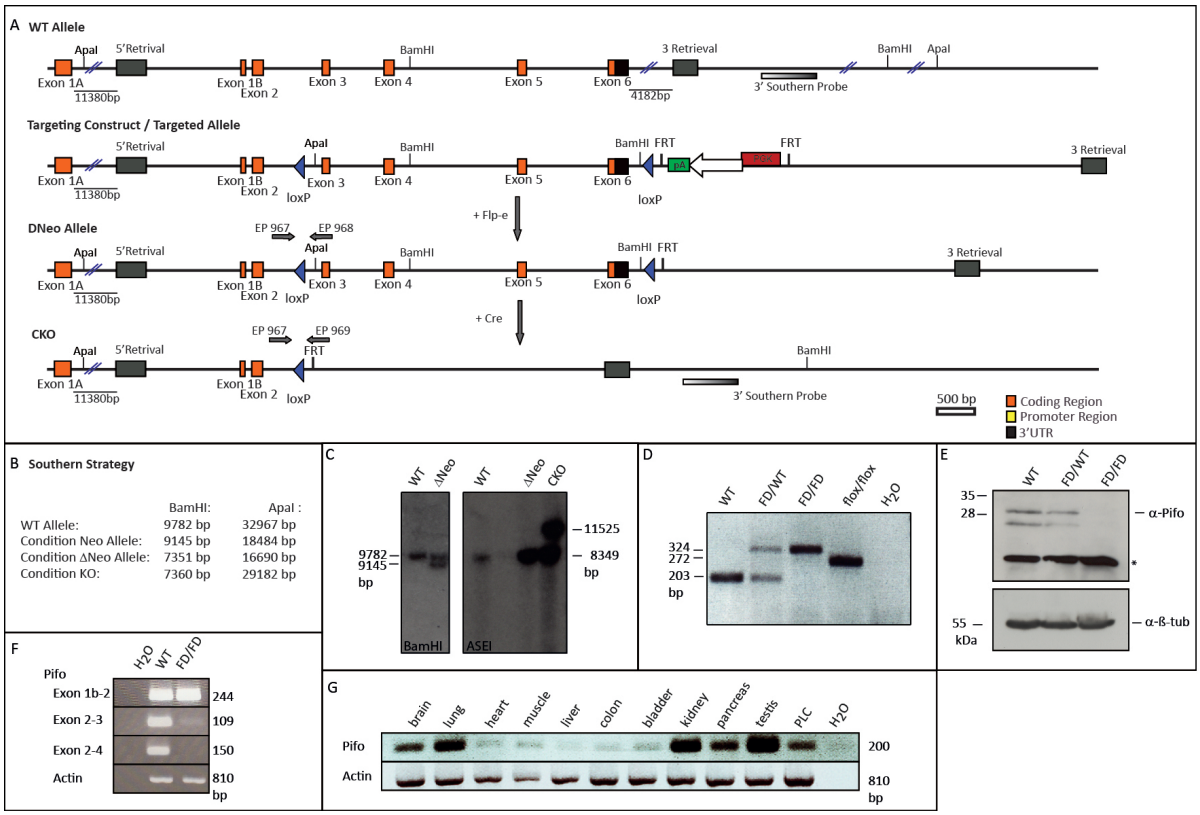

Figure 4 Pitchfork (Pifo) conditional targeting vector and verification of the gene targeting. (A) Scheme of wild-type (WT) and Pifo conditional allele (CKO). Exon three to six are flanked loxP sites and a neo resistance selection cassette which is flanked by FRT sites. When introducing flipase (Flp-e) the deletion of the Neo cassette is triggered (ΔNeo), and introducing Cre recombinase leads to the deletion of the loxP-flanked open reading frame (ORF, coding region), with the recombination of the loxP sites (CKO). Restriction enzyme sites for *ApaI* and *BamHI* are shown. Homology regions for recombination of the targeting construct are indicated as 5'- and 3'-retrieval. The figure is on scale. (B) Southern strategy, showing restriction fragment length polymorphisms form the WT, Pifo targeted (Neo), ΔNeo and CKO alleles. (C) Southern blot of genomic DNA digested with *BamHI* and *AseI* from embryonic stem (ES) cell clones. (D) RT-PCR showing genotyping of WT, flox deleted (FD) Pifo$^{FD/WT}$, Pifo$^{FD/FD}$, and Pifo$^{flox/flox}$ LB cells. (E) Western Blot showing α-Pifo (GordonI) on WT, Pifo$^{FD/WT}$ and Pifo$^{FD/FD}$ testis lysates (80 µg per lane load). For Pifo$^{FD/FD}$ testis lysates the total loss of Pifo protein is shown and beta tubulin (β-tub) as loading control (*unspecific band). (F) RT-PCR using exon spanning primer. (G) RT-PCR using primer EP 970 and EP 971 shows specific band at 200 bp for the *Pifo* mRNA in ciliated tissue. Actin was used as loading control with an expected PCR product at 810 bp.

After the generation of chimeric mice, the loxP-flanked neo selection cassette was removed in the germline by intercrossing with an ubiquitous expressed Cre recombinase deleter mouse strain (ROSA26-Cre) (Soriano 1999). The deletion was confirmed by Southern blot and polymerase chain reaction (PCR) using indicated primers (EP 967, EP 968, and EP 969), resulting in a PCR product of the WT allele of 203 bp, the floxed allele (ΔNeo) of 272 bp, and the flox deleted (FD, CKO) allele of 324 bp (**Figure 4**D, for protocol see 4.2.2.4.1). Western blot (WB) analyses on testis cytoplasmic lysates were performed to confirm the right protein size of 28 kDa and 23 kDa in Pifo WT and heterozygous (Pifo$^{FD/WT}$) lysates (Figure 4E), using a C-terminus directed anti-Pifo antibody (rPifo, Kinzel et al. 2010). The deletion of exons three to six and the subsequent C-terminal epitope of the antibody confirmed the absence of Pifo protein in Pifo$^{FD/FD}$ homozygous lysates. In order to control the deletion on mRNA level, exon-spanning primers were used (**Figure 4**F). The mRNA from exons one to two is clearly transcribed and the gene, thus mRNA deletion starts from exon three onwards. It is therefore likely, that

the residual exon 1A – exon 2 or exon 1B – exon 2 transcript might translate a remaining peptide of 120 Aa. A possible protein residue would need to be further tested by N-terminal directed antibodies, which in case of a protein residue would detect a truncated protein of 12 kDa. This could further mean that we might have created a hypomorphic allele, with only reduced not absent gene function, which might explain the phenotypic discrepancy between the lethal Pifo$^{LacZ/+}$ (Kinzel et al. 2010) and viable Pifo KO alleles. Furthermore, *Pifo* mRNA expression was found in brain, lung, kidney, pancreas and testis; all tissues that are ciliated (Michaud and Yoder 2006, **Figure 4**G), suggesting that Pifo might have a cilia-related function.

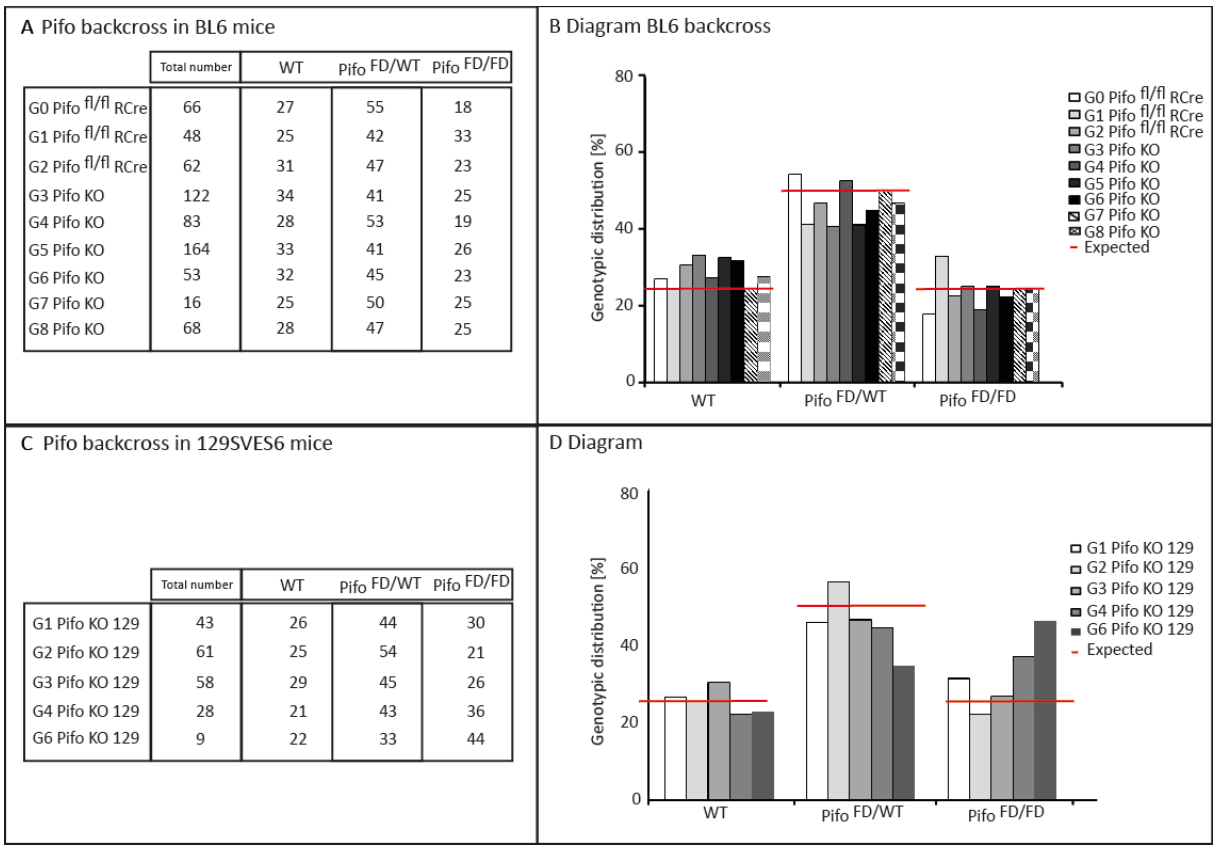

	Total number	WT	Pifo FD/WT	Pifo FD/FD
G0 Pifo fl/fl RCre	66	27	55	18
G1 Pifo fl/fl RCre	48	25	42	33
G2 Pifo fl/fl RCre	62	31	47	23
G3 Pifo KO	122	34	41	25
G4 Pifo KO	83	28	53	19
G5 Pifo KO	164	33	41	26
G6 Pifo KO	53	32	45	23
G7 Pifo KO	16	25	50	25
G8 Pifo KO	68	28	47	25

	Total number	WT	Pifo FD/WT	Pifo FD/FD
G1 Pifo KO 129	43	26	44	30
G2 Pifo KO 129	61	25	54	21
G3 Pifo KO 129	58	29	45	26
G4 Pifo KO 129	28	21	43	36
G6 Pifo KO 129	9	22	33	44

Figure 5 Pitchfork (Pifo) mouse statistics. Backcrossing Pifo KO mouse line in either C57Bl/6J (A, B) or 129SVES6 (C, D) mouse strains and heterozygous intercrosses in various generations. (A, C) The total number and percentage of born wild type (WT), heterozygous (Pifo$^{WT/FD}$), and homozygous (Pifo$^{FD/FD}$) mice are shown after several generation backcrossings (G0-G8). (B, D) The distribution of genotypes shown in A, C is represented in a histogram, respectively. The expected Mendelian ratio for born WT and Pifo$^{FD/FD}$ mice was 25 %, and for born Pifo$^{WT/FD}$ mice 50 %, indicated with a red line.

Pifo$^{FD/WT}$ mice were further backcrossed in either C57Bl/6J or 129SVES6. For all experiments only backcrosses in several generations of C57Bl/6J mice were used. The expected Mendelian ratio was fulfilled as indicated in **Figure 5**D by the percentage of expected offspring (WT and Pifo$^{FD/FD}$ 25 %, Pifo$^{FD/WT}$ 50 %, red lines). Similar results were found when backcrossed in 129SVES6.

2.1.1.2 Pifo embryonic expression using a EUCOMM reporter ES cell line

As cilia are the signaling centers for Shh signaling, and Pifo is found to be expressed in ciliated tissues, I investigated the expression of Pifo in regions of Shh activity, the NT and LB. As antibody stainings and ISH did

not work properly to address this particular question, we decided to use a commercially available reporter ES cell line (Pifo$^{tm1e(KOMP)Wtsi}$, **Figure 6**). In order to analyze the mRNA expression of *Pifo* in embryonic endoderm, we used tetraploid (4n) embryo ↔ ES cell aggregations to generate completely ES cell-derived embryos (Tam and Rossant 2003). Tetraploid (4n) chimeras were generated according to standard protocols (Nagy et al. 1993) from donor YFP-expressing mouse embryos (Hadjantonakis, Macmaster, and Nagy 2002). The extra-embryonic lineages are formed by the tetraploid cells of the embryo and can be identified by YFP expression (Tam and Rossant 2003). Whereas the Pifo$^{tm1e(KOMP)Wtsi}$ ES cells form the embryo proper (YFP^{-}, **Figure 6**B, C). Pifo$^{tm1e(KOMP)Wtsi}$, include a cassette containing a nuclear localization signal (NLS) fused to a lacZ gene encoding for β-gal, which can be used as a transcriptional reporter for the Pifo gene (**Figure 6**A). *Pifo* expression of the tetraploid embryos was subsequently analyzed at E 10.5 (**Figure 6**). In these completely ES cell-derived embryos, *Pifo* expression was found in the ventral region of the NT, the FP, NC and motoneuronal (MN) region, as well as in the mesenchyme and the AER of the LB at E 10.5 (**Figure 6**D-F). These are all regions of Shh activity, which suggests that *Pifo* is a downstream Shh target gene.

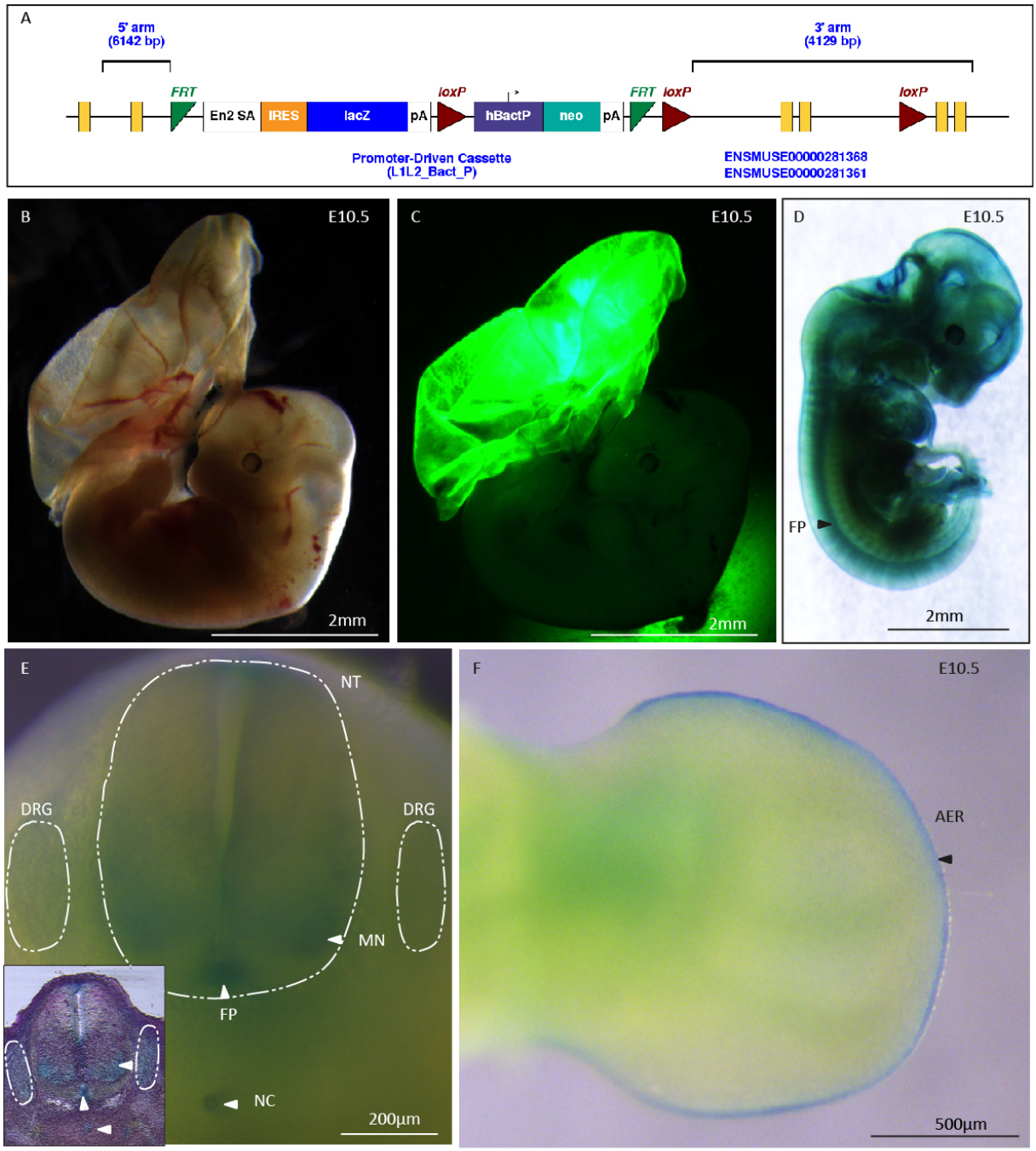

Figure 6 Tissue expression of a *Pitchfork (Pifo)* LacZ knock-in reporter gene. (A) Scheme of Pifo$^{tm1e(KOMP)Wtsi}$ allele. The LacZ reporter and neo resistance cassette are flanked by FRT sites, which can be deleted introducing flipase (Flp-e). In order to delete the neo resistance cassette, and exon three and four, loxP sites are introduced, which can be recombined introducing Cre-recombinase. (B, C) E10.5 tetraploid aggregated embryos in light- and fluorescent images, showing a bright green yolk sac as control and no YVI (WT) contribution to the embryo. (D) LacZ stained and benzyl alcohol : benzyl benzoate (BABB, 1:2) cleared E10.5 embryo with LacZ expression in the floor plate (FP) of the neural tube (NT). (E) NT cross-section showing LacZ expression in the motoneuronal (MN) region, the FP and the notochord (NC). The white dotted line surrounds the NT and the dorsal root ganglia (DRG), respectively. The insert shows a paraffin section with a hematoxilin counterstaining. (F) LacZ expression in the apical ectodermal ridge (AER) of an E10.5 LB.

2.1.1.3 Pifo HPRT reporter mouse line

2.1.1.3.1 Gli binding sites within the Pifo locus

The main transcriptional mediators of Shh signaling are the Glioma TF family (Gli) (Haycraft et al. 2005). In order to answer the question whether *Pifo* is a direct Shh target gene, I performed a bioinformatic promoter analysis using the Genomatix software package. The *Gli* TFs bind with high affinity to the consensus binding sequence GACCACCCA (Winklmayr et al. 2010). The bioinformatic prediction revealed that 11 *Gli* TF binding (GTFB) sites exist between the first two *Pifo* promoter regions, P1 and P2, within intron 1 (Table 1, **Figure 7**). The high frequency of GTFB sites in the cis-regulatory regions of Pifo and its expression in region of Shh signaling, suggests *Pifo* expression might be directly regulated by Gli TFs.

Nr.	Strand	Score	Sequence
1	+	0.891	atgaccaTCCAgaga
2	-	0.906	aaaaCCCCcctatcc
3	+	0.873	cagagctCCCAggga
4	-	0.885	cctcCCCCccctct
5	+	0.812	ccctCCACccacgtg
6	-	0.811	agtcCCACccaaggg
7	+	0.982	accaccaCCCCaacc
8	+	0.886	acgcCCACcccaccc
9	+	0.976	cccaCCCCcccacccc
10	-	0.914	atttCCCCcccacata
11	+	0.922	ctgaCCACtcactct

Table 1 Predicted Gli TF binding (GTFB) sites. Genomatix analysis revealed 11 GTFB sites in the intron one (between exon 1a-1b) of the *Pitchfork (Pifo*) gene. The perfect GTFBS was set with following sequence: GACCACCCA and a deviance of 0.5 %. In red the perfect match is indicated, and small (low-) and big (high-) letters indicate the binding affinity. The score equals the deviation from the consensus GTFB sequence. A perfect match to the GTFB sequence is scored with 1.00

2.1.1.3.2 Generation of a Pifo HPRT reporter mouse line

The presence of 11 GTFB sites within intron 1 of the *Pifo* gene strongly suggests that Pifo is a downstream target of the Shh-Gli pathway. To test this hypothesis and investigate if intron 1 is essential for the spatial and temporal expression of the *Pifo* gene, we used the hypoxanthine phosphoribosyltransferase (HPRT) targeting system (Alten et al. 2012). The advantage of targeting the HPRT locus is twofold. First, one can target single copies of promoter-reporter constructs to a defined locus and therefore can compare reporter gene expression of different constrcuts directly without having position effects multiple integrations of transgenes. Secondly, using the HPRT system the exon 1A-3 of the gene is reconstituted by targeted integration and therefore allows selection and very efficient generation of homologous recombined ES cell clones. Therefore, E14TG2a ES cells

bearing a partial 35 kb null deletion (exon 1A-3) of the HPRT locus were electroporated with targeting constructs containing three predicted promoters around exon 1A and 1B of the *Pifo* gene, including the GTFB site in the large intronic region and a dual lacZ and H2B-Venus reporter cassette flanked by HPRT homologous 5'- and 3'-sequences was cloned (Figure 7). This sequence is capable of restoring a functional HPRT expression. The H47 targeting construct (HPRT WT, 33385 bp) contains the WT *Pifo* sequence including exon 1A, intron 1 with 11 GTFB sites, exon 1B and 2, while GTFB sites three to eight are deleted in the H44 (ΔHPRT, 21896 bp) targeting construct (Figure 7A). Both constructs contain a nuclear localization signal (NLS) fused to a lacZ gene encoding for β-gal (LacZ). The subsequent T2A sequence (4.2.1.1.5) separates the coding sequence for Histone-2B (H2B) fused to a Venus fluorescent reporter gene (Venus), from the NLS-LacZ. After the targeting vectors were introduced by homologous recombination into the genome of E14TG2a ES cells, the selection for the anticipated homologous recombination event used hypoxanthine-aminopterin-thymidine (HAT) media, wherein cell survival is dependent upon HPRT activity. Several HAT resistant colonies were picked and selected in HAT medium, and analyzed by PCR for the correct integration of the targeting vector at the HPRT locus. Correctly targeted ES clones were used to generate chimeras by aggregation to morulae CD1 host embryos. It was previously shown in the lab that the E14TG2a ES cells greatly contribute to chimeric embryos (80-90%), so that we could directly analyze reporter gene expression in the chimeras without germ-line transmission. Chimeras were generated from CD1 morulae.

2.1.1.3.3 Analysis of the Pifo HPRT reporter line

Next, I analyzed whether the chosen promoter sequence is sufficient to drive the LacZ and Venus expression in regions of endogenous Pifo expression. Therefore chimeric embryos were generated using diploid CD1 embryo ↔ ES cell (HPRT WT, ΔHPRT) aggregation technique, allowing us to study mosaic embryos. As the percentage of ES cell contribution is high and the mosaic is always random and different in individual embryos, one can conclude on the temporal and spatial expression by comparing only a few embryos. Thus, using diploid aggregation, without generating germ line chimeras, allowed us a fast analysis of the embryos within 14 days. Using the lacZ reporter, *Pifo* LacZ expression was found in the NT, specifically in the FP and the DRG in E14.5 embryos (Figure 7B, A´, B´, E´, G´). In the kidney *Pifo* LacZ expression was restricted to the collecting ducts and in the brain, to all four choroid plexi (Chlx, Figure 7B, A´, B´, E´, G´). Weaker expression of the LacZ reporter was found in the when the GTFB sites were deleted in the ΔHPRT construct (Figure 7B, C´, D´, F´, H´). These results reveal that deletion of this intronic region including the six GTFB sites, does not changes the spatial and temporal expression pattern of the LacZ reporter, but the expression levels and intensity, indicating that Shh regulates *Pifo* expression levels via GTFB sites. In order to study transgenic reporter gene expression on a cellular level in regions of endogenous *Pifo* expression on a cellular level, I utilized the H2B-Venus fluorescent reporter introduced by the knock-in strategy. Using immunohistochemisty with antibodies against GFP and Pifo antibody I could show that the Venus reporter indeed is expressed in regions where endogenous Pifo protein is localized i.e. the 4th Chlx and the DRG of the NT (**Figure 8**B). Moreover, co-staining with Shh revealed that the WT Pifo promoter H2B-GFP reporter is not only expressed in regions where endogenous protein is localized, but also where the Shh ligand is actively synthesized. These results suggest that Pifo might be under the control of Shh signaling in the DRG and 4th Chlx at E14.5.

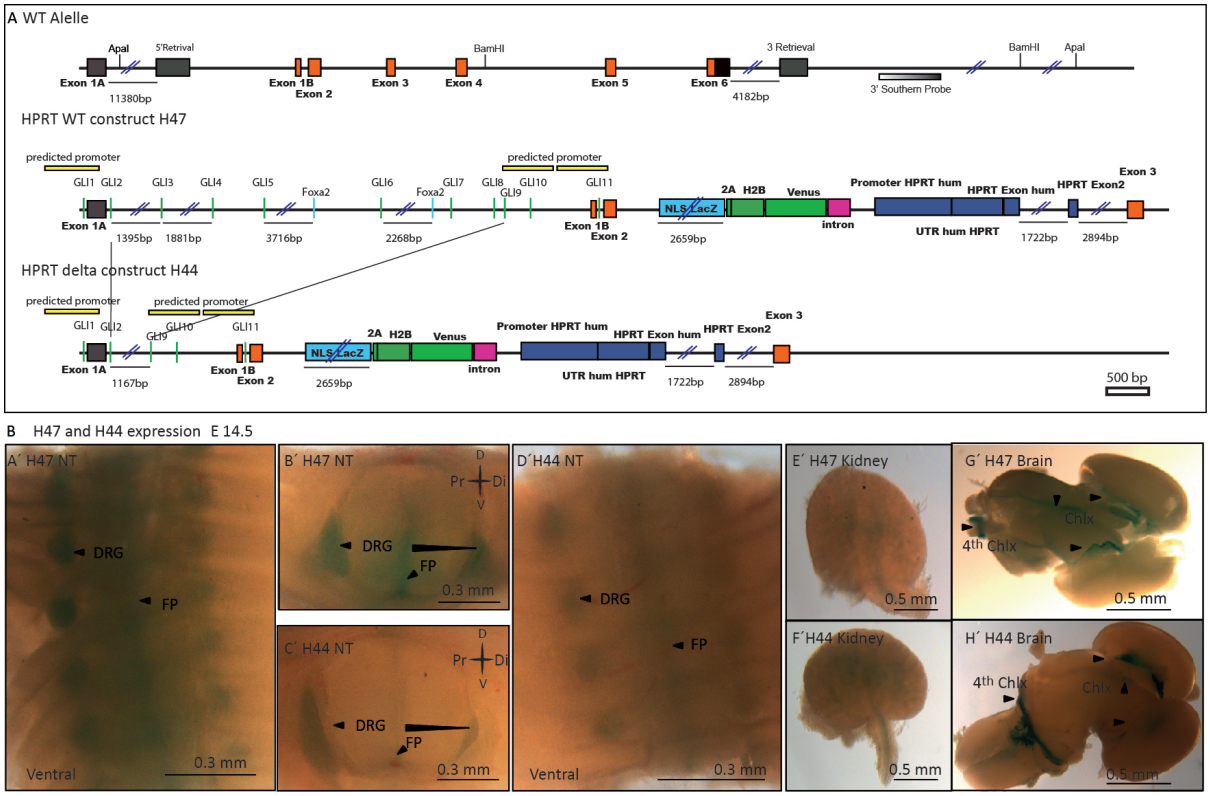

Figure 7 Hypoxantine-phosphoribosyltransferase (HPRT) targeting system. (A) Schematic view of the Pifo wild type (WT) allele compared to the HPRT WT (H47) and ΔHPRT (H44) construct with a deletion of six GTFBS in the H44 construct indicated by two lines. (B) LacZ expression of H47 and H44 constructs in E14.5 embryos. (A´, B´) H47 expression in the neural tube (NT, ventral view) and dorsal root ganglia (DRG), (E´) the kidney, and (G´) choroid plexus (Chlx.). (C´, D´) H44 expression in the NT and DRG, (F´) the kidney, and (H´) the Chlx. Transversal sections B´and C´ of the NT are indicated along the dorsal-ventral (D-V) axis. Bars are shown in each image, respectively.

2.1.1.4 Pifo-(Tg) GBS GFP reporter mouse line

To prove that Pifo is co-expressed in regions of Shh receiving cells, I analyzed a transgenic Shh-Gli reporter Tg(GBS-GFP) mouse line (Balaskas et al. 2012). This mouse line contains eight concatemerized fragments of the FoxA2 enhancer that is a direct target of Shh-Gli and contains consensus GTFB sites (Sasaki et al. 1997). These cis-regulatory elements were cloned upstream of the hsp68 minimal promoter and the enhanced GFP (eGFP) fluorescent reporter gene. Tg(GBS-GFP) mice positive for the Venus reporter were intercrossed and embryos were dissected at E14.5 in order to analyze Pifo expression in Shh-Gli reporter regions (**Figure 8**A). The GFP protein expression was co-localized with Shh and Pifo, in the 1st Chlx, DRG, and MN region of E14.5 embryos as revealed by immunostainings against endogenous Pifo protein using a monoclonal antibody and GFP. These results indicate that Pifo is expressed in regions where Shh is secreted and in cells that receive active Shh signaling. As already mentioned, similar expression was found using HPRT WT (H47) embryos: GFP and Pifo were co-expression with Shh in the 4th Chlx and DRG (**Figure 8**B). In comparison with the HPRT WT (H47) reporter, which has a strong expression in the DRG and the FP, as previously seen by LacZ expression (**Figure 7**B), the Tg(GBS-GFP) reporter exhibit a very weak expression in the MN of the NT, but showed a co-expression

with Pifo antibody in the DRG of E14.5 embryos. In summary, I could show that Pifo is expressed in Shh regions of E14.5 embryos, suggesting a role for Pifo in Shh signaling.

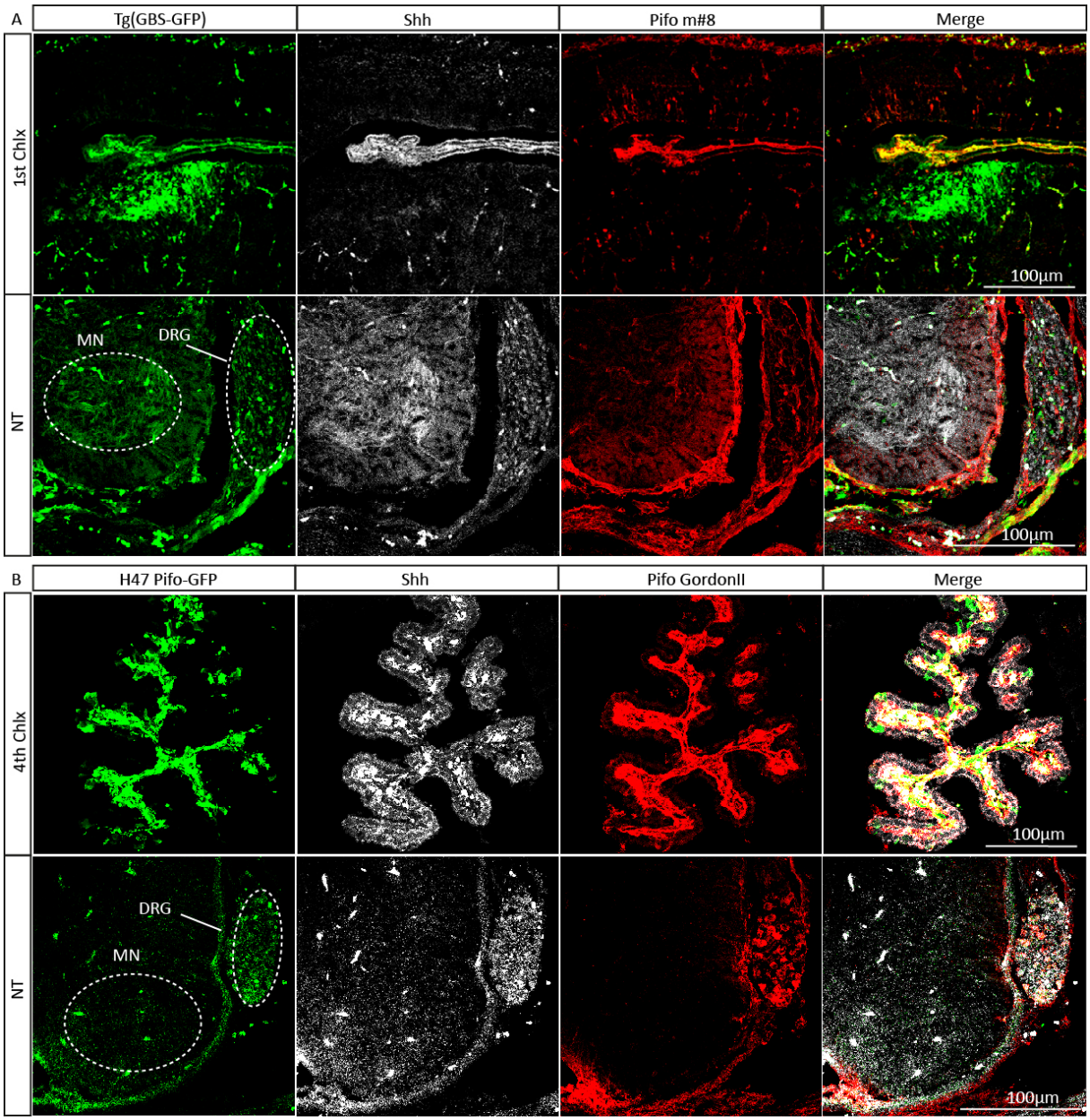

Figure 8 Pitchfork (Pifo) expression in regions of Sonic Hedgehog (Shh) activity. (A) Confocal laser scanning microscopy (CLSM) of cryo-sectioned E14.5 embryos. Transgenic Tg(GBS-GFP) reporter embryo stained for green fluorescent protein (GFP), Shh, and Pifo monoclonal mouse antibody #8, (**Table 2**). GBS-GFP reporter activity revealed that Pifo and Shh are co-expression in the 1st choroid plexus (Chlx) and dorsal root ganglia (DRG) of the neural tube (NT), with a slight expression of GFP-reporter and Shh in the motoneuronal (MN) region. (B) CLSM of cryo-sectioned E14.5 embryos. H47 Pifo-GFP (HPRT) reporter showed a strong co-expression of Pifo and Shh in the 4th Chlx and the DRG, respectively. The MN region of the NT was neg. for the GFP-reporter.

2.1.1.5 Design and generation of a PifoVenus2ALacZ construct

In contrast to our previous analysis which revealed that Pifo is expressed at the node at E7.5 (Kinzel et al. 2010), and in the NT and LB at E10.5 (Figure 7A), the H47 HPRT WT reporter was only weakly expressed and not

detectable before E14.5 in the embryos. This suggests a lack of regulatory regions required to monitor endogenous *Pifo* expression. To circumvent this, and in order to create a tool to monitor early Pifo expression on cellular level, we generated a knock-in reporter construct, a strategy which maintains all cis-regulatory elements. The targeting vector used for recombination in ES cells is described in detail in 4.2.2.6.10. It contains a NLS-LacZ reporter, a coding sequence for H2B fused to a Venus fluorescent reporter gene that is separated by a T2A sequence for biochemical analysis of Pifo protein function. Currently, the construct is finalized and needs to be electroporated in ES cells for gene targeting by homologous recombination (4.2.1.1.4). By generating a Pifo knock-in reporter ES and mouse line, we might have generated a tool, allowing us to analyze Pifo expression in early embryonic stages, adult organs and on cellular levels and molecular levels.

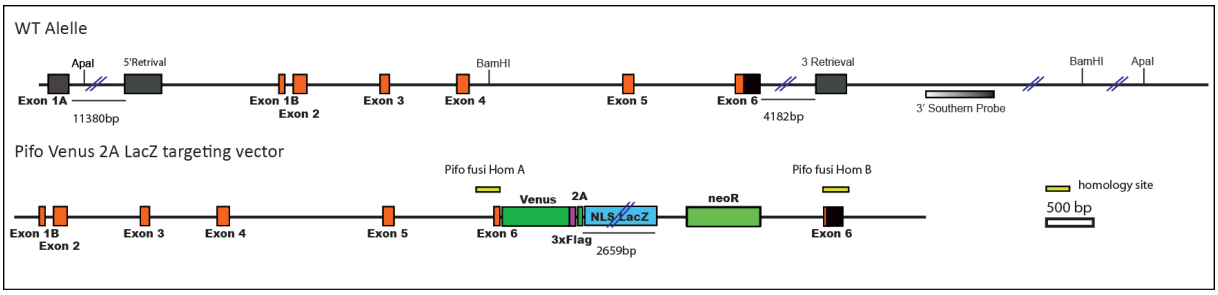

Figure 9 Targeting strategy of the Pifo-Venus-2A-LacZ allele. Pifo WT allele and Pifo-Venus-2A-LacZ targeting vector. The targeting strategy involves fusion of a dual reporter H2B-Venus-T2A-NLS-lacZ in-frame to the coding region of the sixed exon of the gene. The exons are numbered and shown as black and orange boxes. The orange boxes indicate the ORF. The 3' – probe and the, restriction enzyme sites *ApaI* and BamHI are shown on the WT allele, homology sites are indicated on the targeting construct, and the figure is on scale.

2.1.2 Pifo functional analysis

2.1.2.1 Epitopes and Pifo antibody generation

We have created a Pifo KO mouse line which excises exon three to six, which in contrast to our previous published mouse line, Pifo$^{LacZ/+}$, is viable. In order to address the previously raised question of an eventual hypomorphic allele, we wanted to analyze whether the N-terminal part of protein is remaining and/ or functioning in the Pifo KO mouse line. For this purpose, we generated monoclonal antibodies in mouse and rat against different epitopes of mouse Pifo (in collaboration with Dr. Kremmer laboratory, Institute for Molecular Immunology, Figure 10, Table 2, Table 3, 4.2.3.2). Among these, ISO-L/ S (long and short isoform) might give a hint of the possible remaining protein part translated from exon one to three. Thus, as no reporter construct reflected the expression of *Pifo*, these monoclonal antibodies might be valuable to study expression in various tissues and cells, to analyze Pifo subcellular localization, and to analyze protein interactions. Furthermore, *Kinzel et al.* showed that there exist two different *Pifo* mRNA isoforms, a short and a long form, that encode proteins of 207 (23.43 kDa) and 246 (28.16 kDa) amino acids, respectively (Kinzel et al. 2010). To test the specificity of the antibodies, mPifo/ hPifo was overexpressed in HEK293T or IMCD3 cells, respectively, in order to distinguish between the short mouse and the long human isoform. IMCD3 cells were preferentially used in order to determine Pifo ciliary experession, as they showed longer cilia compared to other cell lines, which

simplified subcellular imaging. Subsequently, WB analysis and immunocytochemistry was performed, which were analyzed under a confocal laser scanning microscope (CLSM, IF mP, IF hP). Using cytoplasmic fractionation of adult testis lysates, comparing WT vs. Pifo$^{FD/FD}$, we detected both, the long and short protein isoforms. In **Figure 10**A, B the alignment of different species are shown (adapted from Kinzel et al. 2010), among them the two different mouse isoforms and the human sequence. Thus, the different antibody directed epitops and epitope sequences are presented. N-terminal, ISO-L (antibody #8, see **Table 2**) and C-terminal, ISO-S (antibody #70, see **Table 2**) directed antibodies were used (**Figure 10**C) in order to detect the two isoforms. Both protein isoforms are in line with their expected sizes. **Figure 10**D shows the detection of the long isoform using mPifo and hPifo overexpressed HEK293T and IMCD3 cells, respectively. Mouse monoclonal antibody #56, one of the antibodies generated against epitope ISO-LS was able to detect overexpressed mPifo and hPifo at expected size. We used testis lysates, which is a highly ciliated tissue and Pifo is highly expressed, and the rabbit antibody described in *Kinzel et al.* as control, as it recognizes both isoforms (Kinzel et al. 2010). Thus, testis lysates from WT and Pifo$^{FD/FD}$ mutants were used for further verification of the monoclonal antibodies and revealed that we were able to detect both isoforms (**Figure 10**E). Representative images of imunocytochemistry is shown in **Figure 10**F using mouse monoclonal antibodies as indicated and the Pifo (anti-rabbit, rPifo, Kinzel et al. 2010) and a secondary antibody served as control. Taken together, due to the antibody specificity issues or technical problems such as detection of unspecific bands (**Figure 10**C, α-mPifo #56), weak signals (**Figure 10**C, α-mPifo #47), and overloaded blots (**Figure 10**C, α-mPifo #70) and low protein amounts, further antibody verification is required and ongoing. Subsequently, the hypothesis of an eventual hypomorphic allele needs still to be confirmed. For that reason we selected four mouse and rat monoclonal antibodies for further affinity purification which is still in progress (Dr. Kremmer, Institute for Molecular Immunology).

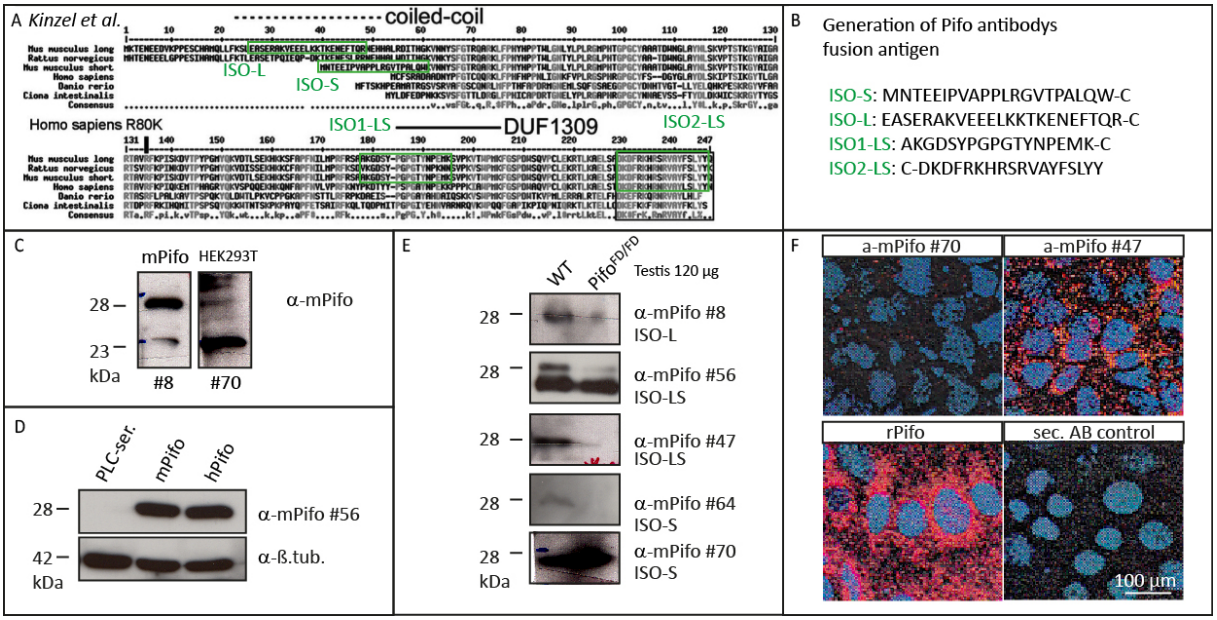

Figure 10 Protein alignment and epitopes for the generation of Pitchfork (Pifo) monoclonal mouse and rat antibodies. (A) Alignment between different species: Mouse isoform (mus musculus, long and short), rat (rattus norvegicus), human (Homo sapiens) and zebrafish (danio rerio), and tunicate (ciona itestinalis), adapted from *Kinzel et al. 2010*. Highly conserved residues between species are indicated in light grey with letters, respectively. The different epitopes are marked with a green square (ISO-L, -S, -LS), referring to the antibody direction. (B) Amino acid sequence of the different antibody-directed epitopes, indicated in A. (C)

Westen blot (WB) analysis of Pifo mouse monoclonal antibodies #8, #70 (**Table 2**), using HEK293T cells over-expressed with mouse Pifo (mPifo). (D) WB using HEK293T cells over-expressed with mPifo and IMCD3 cells over-expressed with human Pifo (hPifo). (E) WB using different epitope directed mouse monoclonal antibodies (#8, #56, #47, #64, #70). (F) Confocal laser scanning microscopy (CLSM) of Pifo mouse monoclonal antibodies (#70, #47, anti-rabbit, rPifo) and secondary antibody control (sec. AB control).

Monoclonal Pifo mouse antibodies											
NR	**Description**	**WB**	**IF mP**	**IF hP**	**WB**	**NR**	**Description**	**WB**	**IF mP**	**IF hP**	**WB**
5	2E6, MG1	+	++	+++	++	31	ISO1-LS, 2F11, M2a	+	+++	+	n.d.
6	ISO-L, 1E11, M2a	+	++	+++	n.d.	37	ISO1-LS, 3B10, MG1	+++	n.d.	n.d.	n.d.
7	ISO-L, 3A9, M2b	n.d	+	+	n.d.	39	ISO1-LS, 1G9, MG1	+++	+++	+	n.d.
8	ISO-L, 1F12, M2b	+++	++	++	+++	41	ISO1-LS, 3B5, M2b	+++	+	+++	n.d.
10	ISO-L, 1EI, M2a	+++	+++	+++	++	43	ISO1-LS, 2C6, M2b	+++	++	++	++
12	ISO-L, 6D11, M2a	n.d.	+++	+++	n.d.	47	ISO1-LS, GC12, M2a,b,	+++	++	++	+++
14	ISO-L, 2H8, M2a	n.d.	+	+++	n.d.	50	ISO1-LS, 7C12, M2a	+	+++	+++	+++
15	ISO-L,2H5, M2a	+++	+	+++	+++	51	ISO1-LS, 7G2, MG3, M2a	+	n.d.	++	++
19	ISO-L, 5B7, M2a	+	+++	+++	n.d.	54	ISO1-LS, 7H1, M2a	+++	++	++	++
20	ISO-L, IF4, M2b	+	+++	+	++	56	ISO1-LS, 8C12, M2a	+++	n.d.	n.d.	++
21	ISO-L, 3GI, M2a	n.d.	+++	+++	n.d.	61	ISO-S, 3D3, M2a	+++	++	++	++
24	ISO-L, 4F6, M2b	+++	+++	+++	+++	62	ISO-S, 1D10, M2a	+++	+++	+++	n.d.
25	ISO-L, 6E7, M2a	++	n.d.	n.d.	++	70	ISO-S, 2D2, M2a	+++	n.d.	n.d.	++

Table 2 Monoclonal Pitchfork (Pifo) mouse antibodies. The table shows the number (NR), a description about the epitopes, and a summary of the Western blot (WB) and immunoflourescence (IF) evaluation of the different mouse monoclonal Pifo antibodies. For IF evaluation confocal laser scanning microscopy (CLSM) was used, and HEK293T cells were over-expressed with mouse Pifo (mPifo, AB30), and IMCD3 cells were over-expressed with human Pifo (hPifo, AB55), respectively. If either of the WB or IF experiments were positive, than the antibody was further tested on wild type (WT) vs. $Pifo^{FD/FD}$ testis lysates, represented in the last WB row of the table. Not detected (n.d.), positive "+" means there is a weak signal, "++" means a good signal and "+++" means a very good signal. Antibodies which were negative for both signals were not selected for this table, in total 74 mouse monoclonal antibodies were tested. Among them four (#8, #47, #56, #70) were selected for further affinity purification.

Monoclonal Pifo rat antibodies								
NR	**Description**	**WB**	**IF mP**	**WB**	**NR**	**Description**	**WB**	**IF mP**	**WB**
2	18H2	++	+	x	48	ISO-LS, 19B5, R2b	++	n.d.	x
4	13A3, 2C	++	n.d.	+++	49	ISO-LS, 17G5, R2b	++	n.d.	+++
5	ISO-L, 24C4, RG1	++	+	x	51	ISO-LS, 10E8 R2a/2c	++	n.d.	x
7	ISO-L, 24A10, RG2	++	+	x	58	ISO-LS, 13C1, R2a	++	+++	x
14	ISO-L, 23D8, R2a	++	+	x	62	ISO-LS, 3A6, R2c	++	n.d.	x
17	ISO-L, 15A9, R2a	++	+++	x	64	ISO-S, 9C12, R2a	++	+	+++
18	ISO-L,19D12, R2a	++	++	x	67	ISO-S, 13E11, R2a	++	n.d.	+++
22	ISO-L, 20E5, RG1	++	n.d.	x	68	ISO-S, 20C2, R2a	++	+++	+++
24	ISO-L, 15I2, R2a	++	n.d.	x	70	ISO-S, 17D2, R2a	++	n.d.	+
27	ISO-L, 14A8, RG1/2a	++	++	x	72	ISO-S, 9A10, RG1/2c	++	n.d.	+

Table 3 Monoclonal Pitchfork (Pifo) rat antibodies. The table shows the number (NR), a description about the epitopes, and a summary of the Western blot (WB) and immunoflourescence (IF) evaluation of the different mouse monoclonal Pifo antibodies. For immunofluorescence evaluation confocal laser scanning microscopy (CLSM) was used, and HEK293T cells were over-expressed with mouse Pifo (mP). If either of the WB or IF experiments were positive, than the antibody was further tested on wild type (WT) vs. $Pifo^{FD/FD}$ testis lysates, represented in the last WB row of the table. Not detected (n.d.), positive "+" means there is a weak signal, "++" means a good signal and "+++" means a very good signal, "x" stands for not tested. Antibodies which were negative for both signals were not selected for this table, in total 78 rat monoclonal antibodies were tested. Among them four (#4, #5, #64, #68) were selected for further affinity purification.

2.1.2.2 Shh target gene expression in Pifo$^{FD/FD}$ embryos

Pifo was reported to be expressed in the node at E7.5, in the MN region and FP of the NT at E12.5, and in the AER of the LB at E12.5 (Kinzel et al. 2010). Moreover, I could confirmed *Pifo* expression in the the MN region and FP of the NT, and the AER of the LB, using the Pifo$^{tm1e(KOMP)Wtsi}$ allele (EUCOMM), and LacZ stainings at E10.5. Thus, the GFP reporter lines additionaly showed expression in Shh high regions in E14.5 embryos. Taken together, these results suggest a role for Pifo in Shh signaling. I therefore analyzed Shh target genes regulation in Pifo$^{FD/FD}$ embryos *in vivo*, in tissues of Pifo expression. Using whole-mount *in situ* hybridization technique I analyzed the mRNA expression of known Shh targets, namely *Ptch1*, *Gli1* and *Foxa2*. In the NT, *Ptch1* mRNA is expressed in the NC at E7.75 and the FP, and at stays express throughout gastrulation. At E9.5, *Ptch1* it is found in the FP of the NT and shows no differences in expression in Pifo$^{FD/FD}$ mutant embryos compared to WT. Similar to *Ptch1*, *Foxa2* is also expressed in the node, NC and FP of the NT. *Su et al.* (Su et al. 2012) reported that *Ptch1* forms a gradient along the ventral NT and *Ocbina et al.* (Ocbina et al. 2011) showed that *Foxa2* is expressed exclusively in the FP at E10.5. *Gli1* showed a weak expression at E7.5 at the node and at E9.5 in the FP of the NT, also in a gradient at the ventral site already reported (Balaskas et al. 2012). At E10.5 *Gli1* is expressed at the NT and LB, with no obvious differences between the genotypes. In summary, I could not detect an obvious difference in mRNA expression of several Shh target genes in different regions of *Pifo* expression and at various stages of early embryo development (E7.5 – E9.5, **Figure 11**), suggesting that *Pifo* has no major impact on Shh signal transduction.

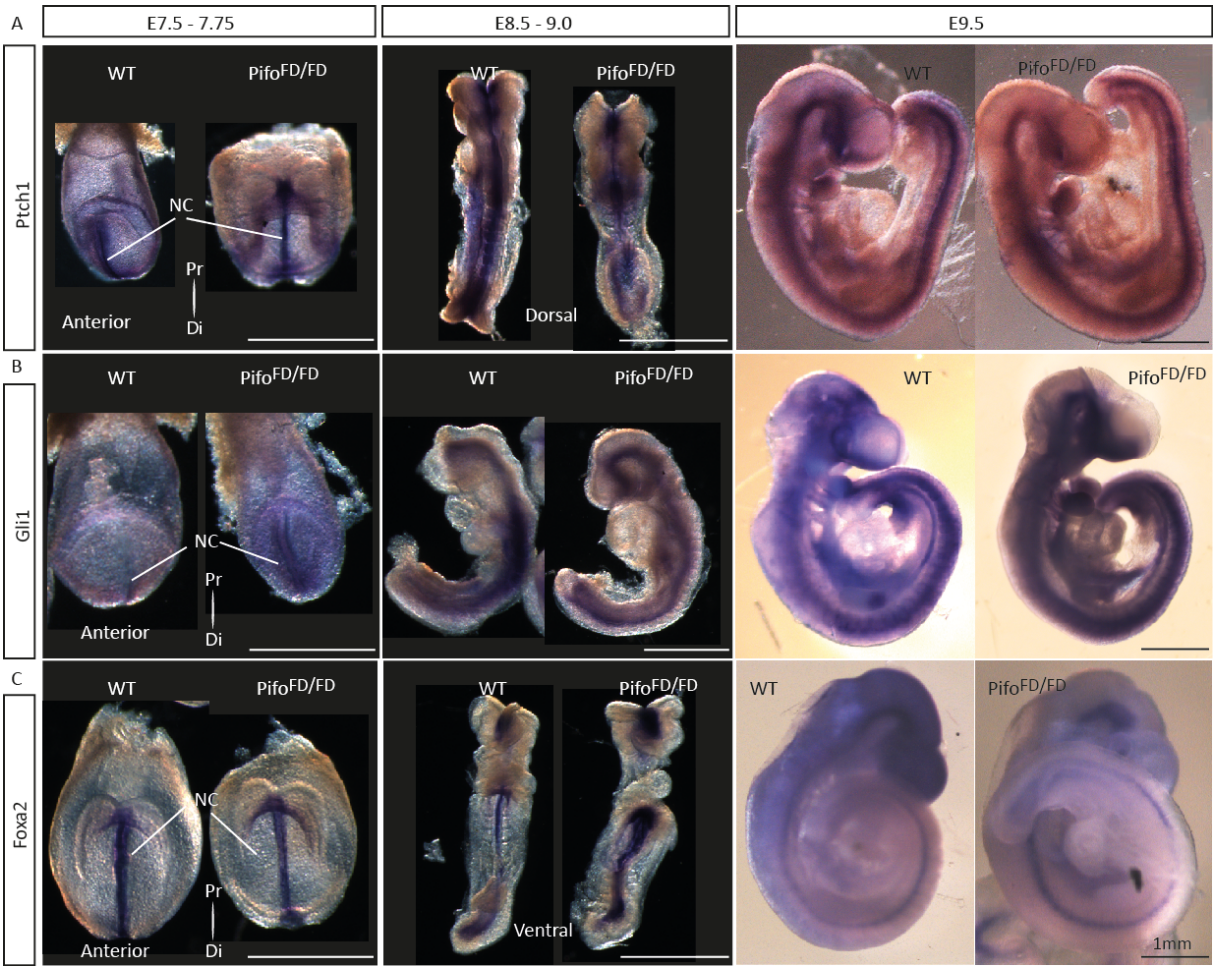

Figure 11 Whole mount *in situ* hybridization of Sonic Hedgehog (Shh) target genes. (A) *Patched 1 (Ptch1)* expression pattern at different embryonic stages (E7.5 – 9.5), respectively. (B) *Gli family zinc finger 1 (Gli1)* expression, and (C) *forkhead box protein A2 (Foxa2)* expression, showing no obvious differences between wild type (WT) vs. Pifo$^{FD/FD}$ embryos. E7.5 – 8.5 embryos are shown in an anterior or posterior view, respectively. Proximal-distal (Pr-Di).

In the LB, *Ptch1* is slightly reduced in the ventral AER of both, fore and hind limb. The AER is exactly the site of *Pifo* expression (**Figure 12**A, B indicated with an asterix), suggesting that a loss of Pifo expression results in Shh target gene reduction. These results might also explain the recent observed polydactyly phenotype (Kinzel et al. 2010). Thus, paraffin sections of whole-mount LacZ-stained embryos further confirmed these results. I showed a weaker expression of *Shh* in the FP of Pifo$^{FD/FD}$ mutant NT, when compared to WT, suggesting a function of Pifo in Shh signal transduction.

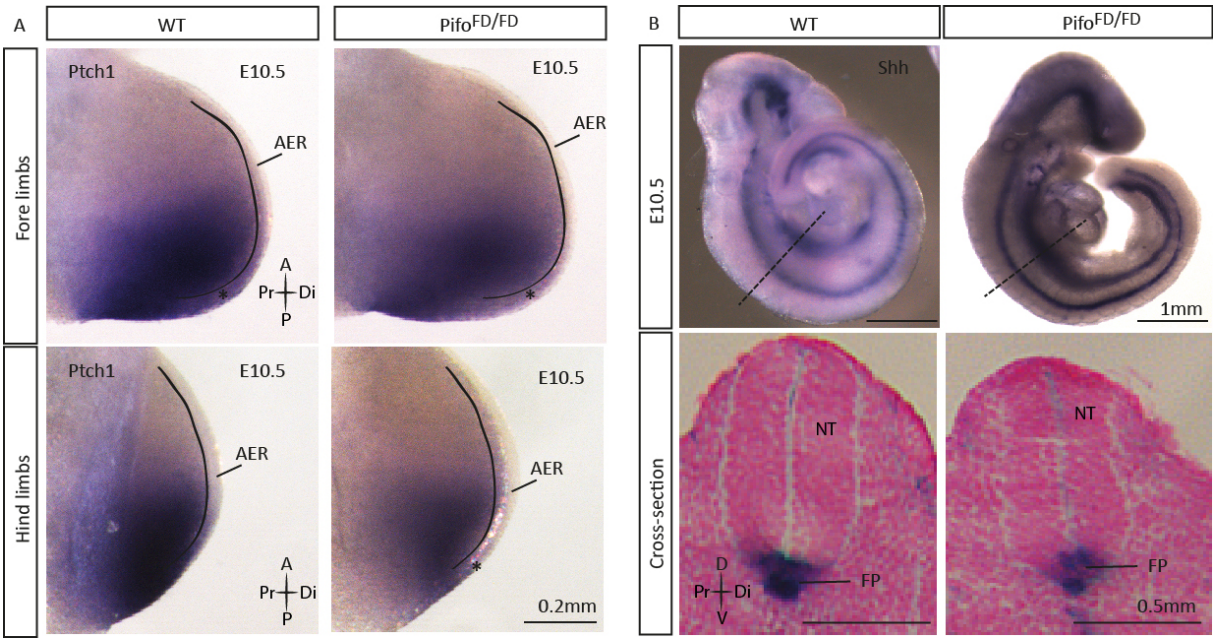

Figure 12 Expression analysis of Shh signaling components *Patched 1 (Ptch1)* and *Sonic Hedgehog (Shh)* in Pifo$^{FD/FD}$ mutant embryos. (A) *Ptch1* LB *in situ* hybridization (E10.5), showing a slight reduction in the apical ectodermal ridge (AER, indicated with an asterix, "*"), in both, fore and hind limb of Pifo$^{FD/FD}$ mutant embryos. Limbs are shown in an anterior-posterior (A-P) orientation. (B) Whole mount *in situ* hybridization of E10 .5 embryos showing no obvious difference in *Shh* expression of wild type (WT) vs. Pifo$^{FD/FD}$ mutant embryos. Neural tube (NT) paraffin cross-sections were counter stained with nuclear fast red and taken as indicated at the heart region (dotted line). They show a slight reduction of *Shh* expression in the floor plate (FP) of the NT in Pifo$^{FD/FD}$ mutant embryos. The sections are shown in a dorsal-ventral (D-V) orientation. Proximal-distal (Pr-Di).

As polydactyly is further described as a Shh-like phenotype (Eggenschwiler, Espinoza, and Anderson 2001; Litingtung et al. 2002; Kinzel et al. 2010), I quantitatively analyzed Shh target genes in WT and Pifo$^{FD/FD}$ mutant embryos. As previous results showed that *Pifo* is expressed in the MN region of the NT (**Figure 6**, **Figure 8**), I dissected the NT of E10.5 embryos as shown in **Figure 13**A and performed real-time quantitative (q-PCR) analysis. This tissue peace was lysed and the total RNA was extracted for cDNA synthesis and qPCR analysis (4.2.2.4.4). This analysis clearly revealed that the known Shh target genes *Ptch1*, *Gli1,2 and 3* are downregulated in the Pifo$^{FD/FD}$ mutant NT. *Gli3* on the other hand was unchanged, when compared to WT controls (**Figure 13**C). In order to prove the deletion of *Pifo* I used exon-spanning primer and could show that around one third of the *Pifo* mRNA is remaining. When analyzing the mRNA expression of the *G-protein coupled associated sorting protein 2 (Gprasp2)* in Pifo$^{FD/FD}$ mutant NT, I saw no difference in mutant vs. control NTs at E10.5. Sufu and Kif7 play regulatory roles in Hh signaling and directly interact with the Gli proteins (Motoyama et al. 2003) and both mRNAs are downregulated in Pifo mutant NTs at E10.5. Furthermore, I confirmed the downregulation of Shh, which is consistent with the whole-mount in situ hybridization data (**Figure 12**B). These data clearly indicate that Pifo is involved in Shh target gene regulation.

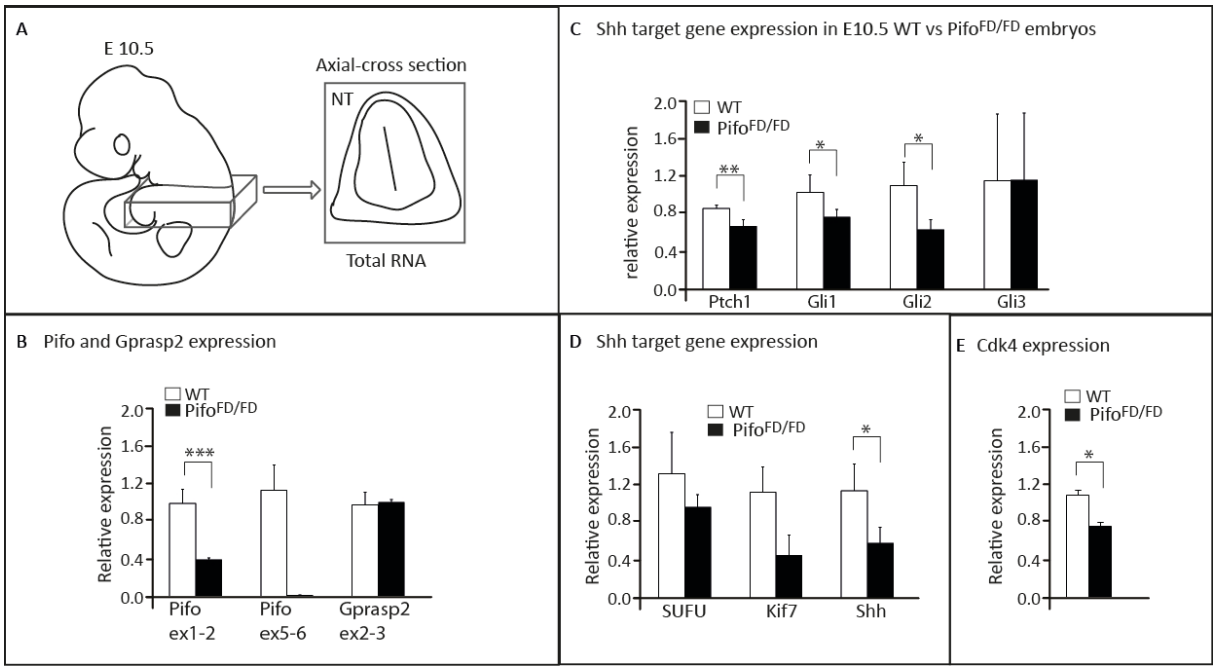

Figure 13 Quantitative *Sonic Hedgehog (Shh*) target gene expression in the embryonic neural tube (NT). (A) Schematic few of the NT dissection of an E10.5 embryo. (B) Real-time quantitative PCR (q-PCR), showing expression of *Pitchfork (Pifo)* with the remaining exon two, and *G-protein coupled associated sorting protein 2 (Gprasp2)* in wild type (WT) vs. Pifo$^{FD/FD}$ mutant dissected NT. (C) P*atched 1 (Ptch1), Gli family zinc finger 1-3 (Gli1-3)* expression. (D) *Suppressor of fused (Sufu), kinesin-like protein 7 (Kif7),* and *Shh* expression, respectively. (E) q-PCR analysis showing *cyclin-dependent kinase 4 (Cdk4*) for G1 phase progression reduction. ($p < 0.05$, "*" is considered to be statistically relevant, $p < 0.01$, "**", is considered to be highly statistically relevant, and $p < 0.001$, "***", is considered to be extremely statistically relevant).

2.1.2.3 Neural tube specification in Pifo$^{FD/FD}$ mutant embryos

A well studied model of Shh-mediated tissue patterning and neuronal cell type specification is the developing NT (**Figure 3**). Here, Shh forms a gradient along the D-V axis with highest levels of pathway activation on the ventral side. As we observed a downregulation of *Shh* and its target genes in Pifo$^{FD/FD}$ mutant NTs, I analyzed the influence of *Pifo* in Shh-driven NT specification. Therefore we made use of the previously described sensitive Shh-Gli reporter Tg(GBS-GFP) mouse line (Balaskas et al. 2012), which was crossed into Pifo$^{FD/FD}$ mice, in order to generate Tg(GBS-GFP/+) and Pifo$^{FD/FD}$;Tg(GBS-GFP/+) mutants. At E9.5 the GBS-GFP activity was analyzed by immunostaining using antibodies directed against GFP and signal activity was quantified by CLSM (**Figure 14**). No significant differences of GBS reporter activity was detected in GBS-GFP/+ vs Pifo$^{FD/FD}$;Tg(GBS-GFP/+) NTs at E9.5. However, we could detect a small, but significant reduction of GBS-GFP reporter activity in the ventral NT of Pifo$^{FD/FD}$;Tg(GBS-GFP/+) mutant embryos at E10.5 (**Figure 15**). Thus, the peak of the GBS-GFP reporter activity was shifted more ventrally in Pifo$^{FD/FD}$;Tg(GBS-GFP/+) mutant embryos (Pifo$^{FD/FD}$, **Figure 15**, red and black lines). Subsequently, marker analysis revealed no differences in Isl1, NKX6.2, and Foxa2 expression between the genotypes. Though, Olig2^{+} was significantly reduced in the ventral NT, suggesting that Pifo plays a role in specifying the MNs of the NT, a region of high Shh activity (**Figure 16**, **Figure 3**).

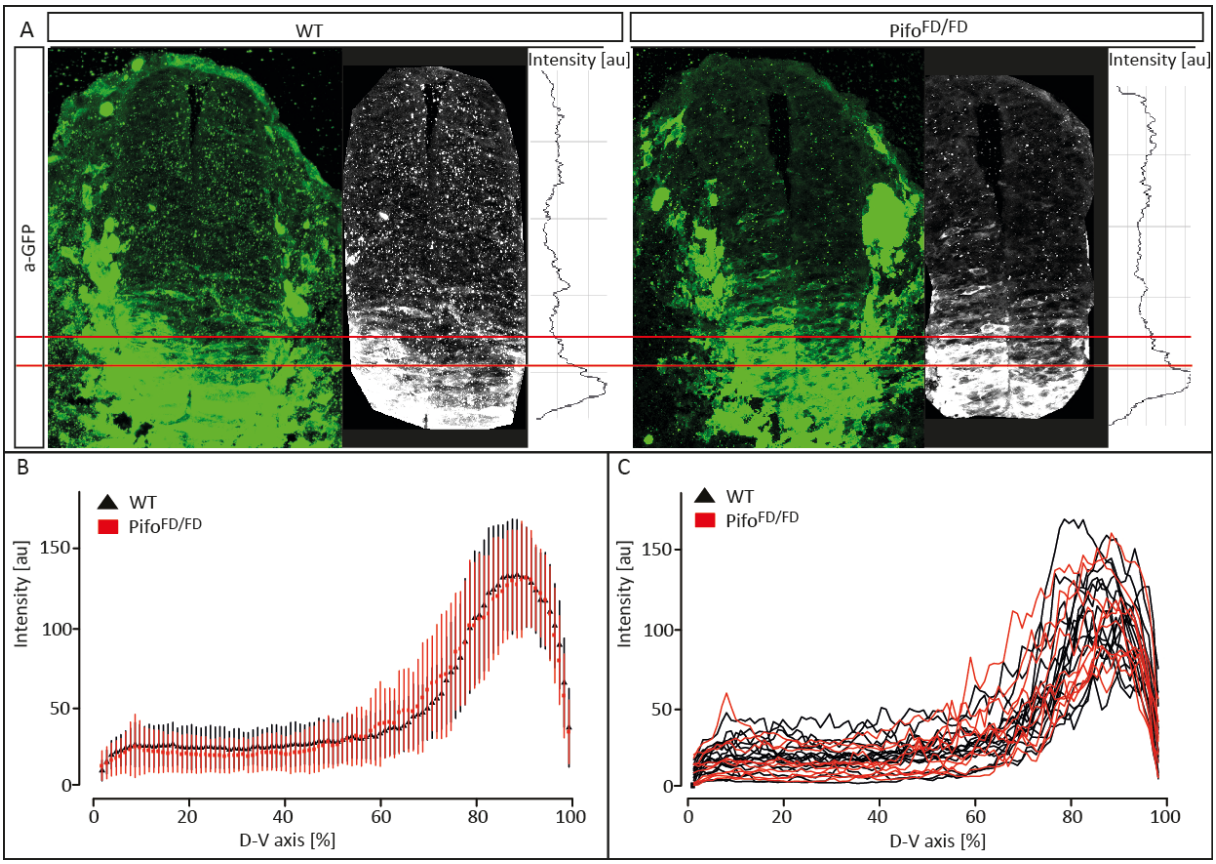

Figure 14 Sonic Hedgehog (Shh) Tg(GBS GFP) expression in the neural tube (NT) of E9.5 embryos. (A) Confocal laser scanning microscopy (CLSM) of a cryo-sectioned E9.5 embryo comparing wild type (WT) and Pifo$^{FD/FD}$ mutant Shh Tg(GBS-GFP) expression, showing the green fluorescence protein (GFP) staining in the NT, the processed image cropped in ImageJ and the GFP intensity along the dorsal-ventral (D-V) axis. (B) WT and Pifo$^{FD/FD}$ mutant GBS-GFP intensities are plotted along the D-V axis showing mean and standard deviations. (C) Single intensity profiles are merged.

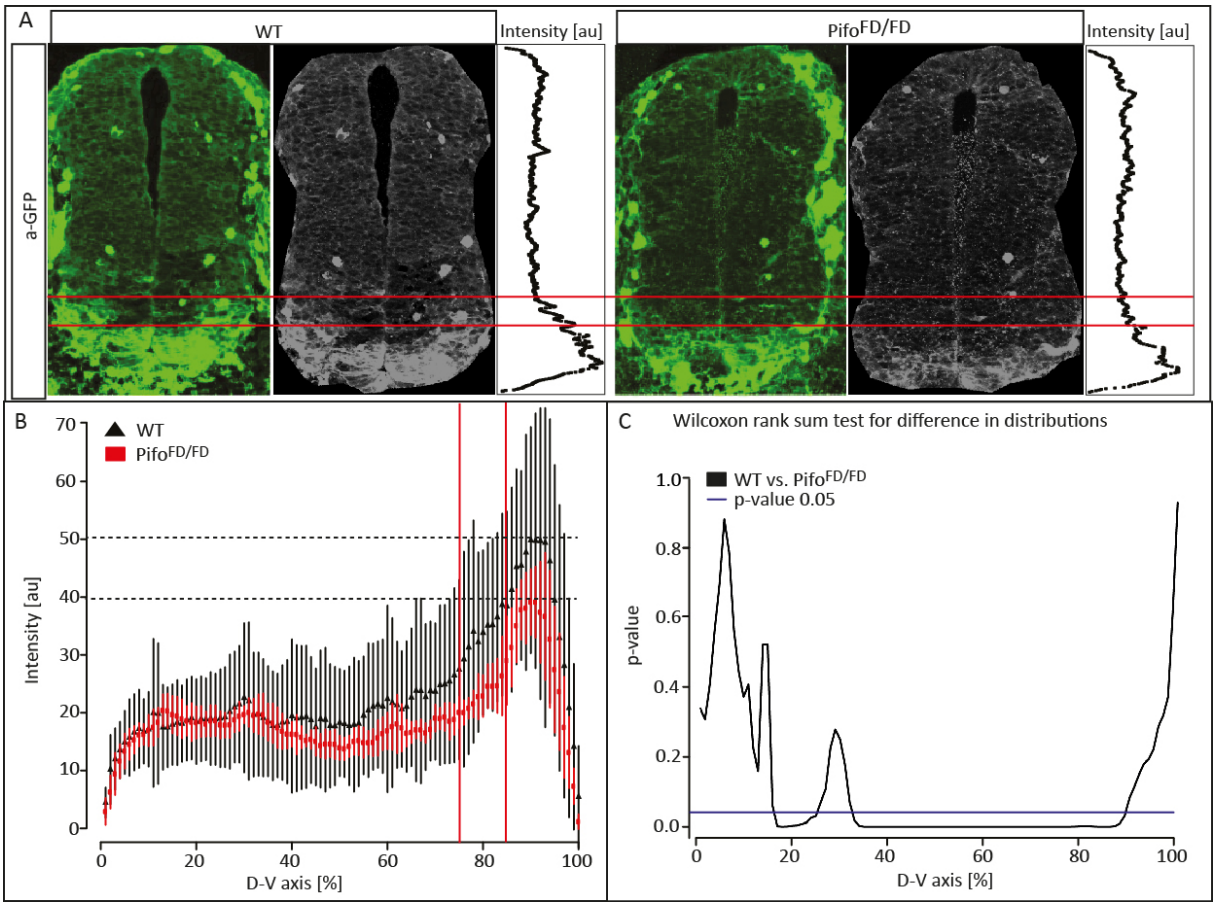

Figure 15 Sonic Hedgehog (Shh) Tg(GBS GFP) expression in the neural tube (NT) of E10.5 embryos. (A) Confocal laser scanning microscopy (CLSM) of a cryo-sectioned E10.5 embryo comparing wild type (WT) and Pifo$^{FD/FD}$ mutant Shh Tg(GBS-GFP) expression, showing the green fluorescence protein (GFP) staining in the NT, the processed image cropped in ImageJ (white) and the GFP intensity plot along the dorsal-ventral (D-V) axis. The red lines show a slight ventralization of Pifo$^{FD/FD}$ mutant embryos. (B) Summary of WT vs. Pifo$^{FD/FD}$ GBS-GFP intensities, plotted along the D-V axis. The red lines indicate the ventralization shown in A, the dottet lines the intensity means. (C) Wilcoxon rank sum test for differences in the distributions.

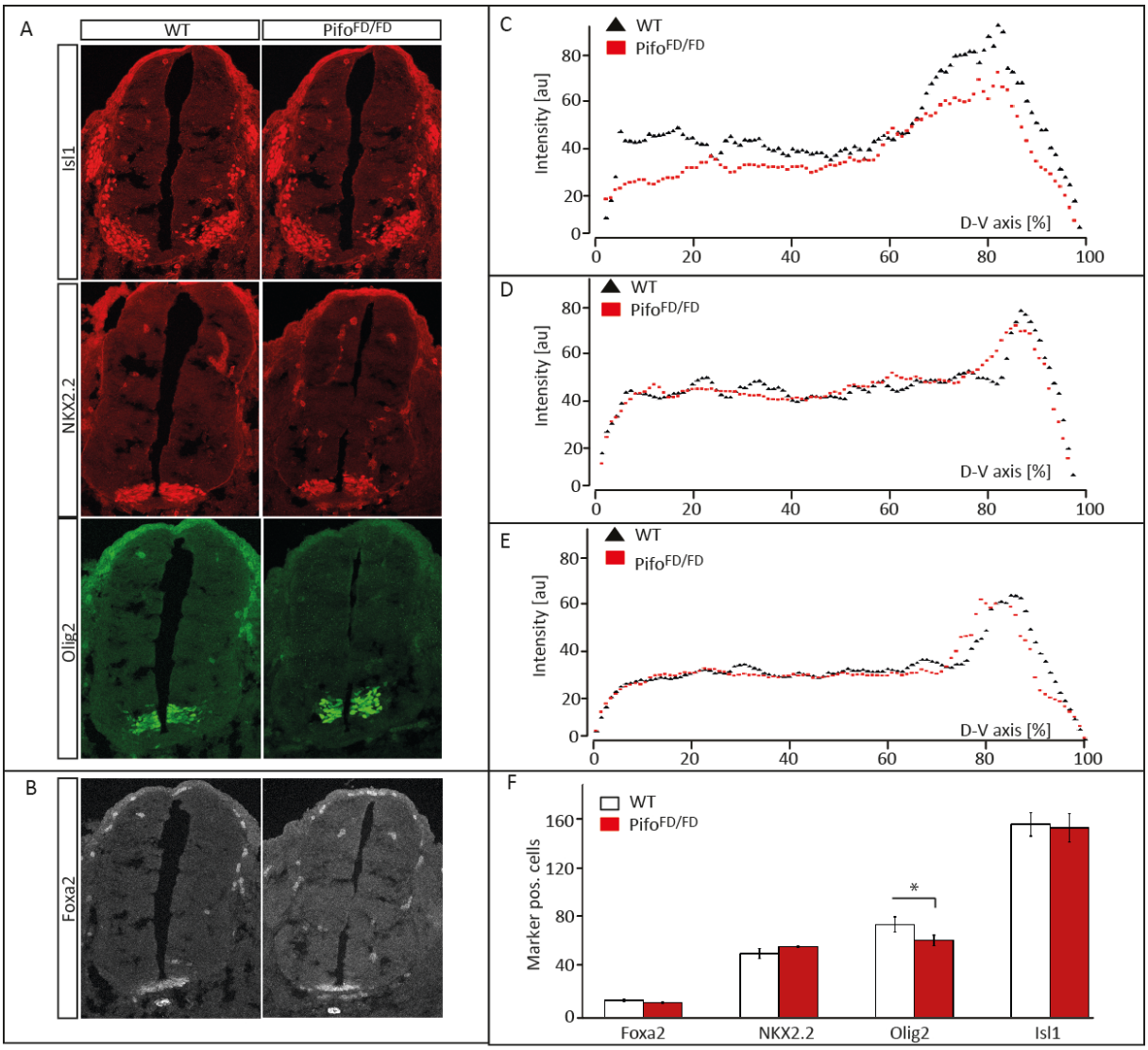

Figure 16 Marker analyses in the neural tube (NT) of E10.5 embryos. (A, B) Confocal laser scanning microscopy (CLSM) of E10.5 embryonic neural tube (NT) sections (14 µm) comparing wild-type (WT) and Pifo$^{FD/FD}$ mutants. (A) Insulin gene enhancer protein 1 (Isl1), NK2 homeobox 2 protein (NKX2.2), and oligodendrocyte lineage TF 2 (Olig2) marker analysis. (B) Forkhead box protein A2 (Foxa2) expression in the floor plate (FP). (C-E) Intensitiy profiles blotted along the dorsal-ventral (D-V) axis of the NT, shown for each neuronal marker (A, B), respectively. (F) Quantitative evaluation of neuronal marker shown in A, B. Olig2 domain was found to be significantly reduced ($p < 0.05$, "*" is considered to be statistically relevant).

2.1.2.4 Pifo Sufu and Pifo Kif7

Sufu and Kif7 are Shh pathway members which were shown to interact with Gli proteins (Goetz, Ocbina, and Anderson 2009). As already metioned the motorprotein Kif7 is supposed to regulate the Shh pathway in a positve, GliA supporting manner, whereas Sufu supresses the GliA (1.1.1). Thus, quanititative analysis showed a downregulation of Sufu and Kif7 in dissected Pifo$^{FD/FD}$ mutant NTs (**Figure 13**D). In order to analyze a possible interaction of Pifo with these two Shh pathway proteins, I analyzed the genetic interaction of Pifo mutants with Sufu and Kif7 mutant mice. Therefore, the Pifo$^{FD/FD}$ mouse line was crossed into the Sufu and Kif7 mutant mouse lines, to generate Sufu$^{-/-}$, Kif7$^{-/-}$ single mutants and Pifo$^{FD/FD}$;Sufu$^{-/-}$, Pifo$^{FD/FD}$;Kif7$^{-/-}$ double knock-out (DKO) mutants. Embryos were isolated at E9.5, genotyped as described (4.2.2.4.1) and subsequently

cryopreserved and sectioned (4.2.6.3). At E9.5 Pifo$^{FD/FD}$;Sufu$^{-/-}$ DKO mutants exhibit the same morphological phenotype as reported for Sufu$^{-/-}$ mutant embryos (**Figure 17**A). Sufu$^{-/-}$ mutants die in utero at approximately E9.5 and the NT and cephalic vesicle fail to completely close (Svard et al. 2006). Sufu$^{-/-}$ mice in principle exhibit and expanded ventral fate along the D-V axis of the NT, missing the dorsal neuronal progenitors (Goetz and Anderson 2010). As Pifo$^{FD/FD}$;Sufu$^{-/-}$ DKO embryos show no difference to Sufu$^{-/-}$ mutants, we conclude that *Pifo* and *Sufu* do not genetically interact. The comparison of Pifo$^{FD/FD}$;Kif7$^{-/-}$ DKOs to Kif7$^{-/-}$ mutants at E9.5 revealed no obvious morphological difference between the two genotypes, either (**Figure 17**B). Both, the Pifo$^{FD/FD}$;Kif7$^{-/-}$ DKOs and the Kif7$^{-/-}$ mutants showed an open NT at the stage of E9.5. Kif7$^{-/-}$ mutant mice exhibit exencephaly and polydactyly and die latest at birth (Cheung et al. 2009). The MN region of Kif7$^{-/-}$ mutant embryos is reported to be expanded more dorsally (Cheung et al. 2009; Goetz and Anderson 2010). As Pifo was has an impact on the ventral fate of the MN region and in order to analyze a possible genetic interaction in more detail, marker analysis of cryo-sectioned embryonic NTs were performed on cellular level using CLSM. Analysis were carried out using Foxa2 as FP marker, NKX2.2 as p3 marker, and Olig2 as MN marker. Although, q-PCR analysis revealed reduced expression of *Sufu*, and *Kif7* in Pifo$^{FD/FD}$ mutant NTs (**Figure 13**C, D), no obvious difference was found when comparing Pifo$^{FD/FD}$;Kif7$^{-/-}$ DKO and Kif7$^{-/-}$ mutant NTs. These results suggest, no direct genetic interaction between *Pifo* and *Sufu* and *Kif7*. It is likely that a transcriptional regulation occurs via the GTFBs.

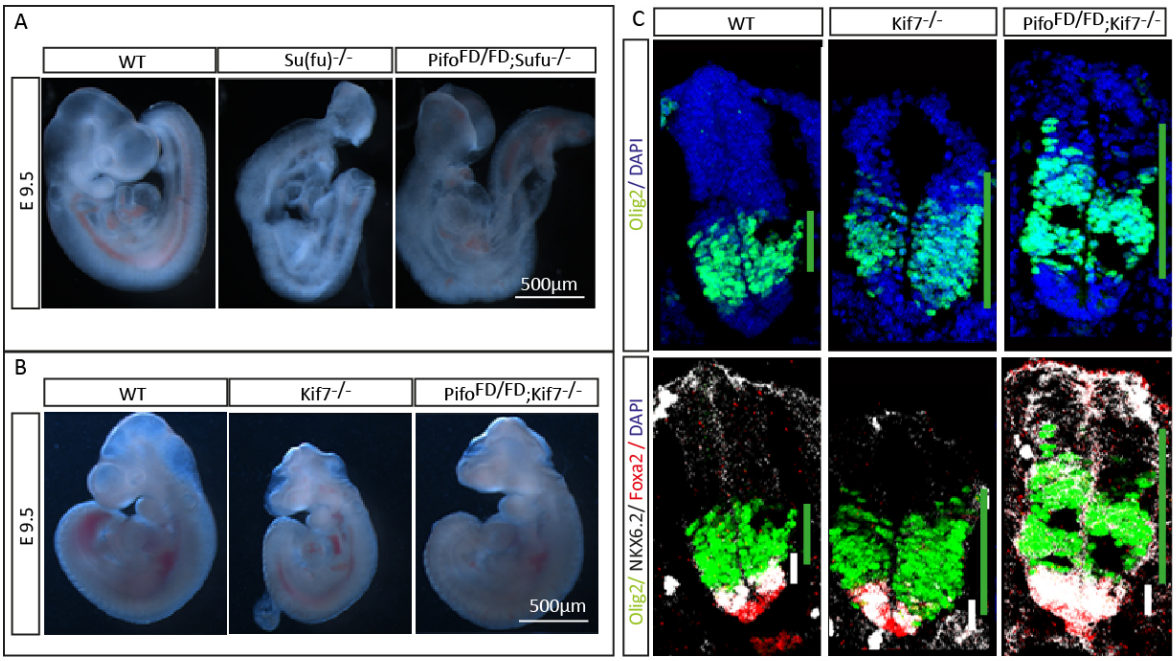

Figure 17 Pitchfork (Pifo) function in Shh pathway. (A) Pifo and suppressor of fused (Sufu) intercrosses, showing wild type (WT), Sufu$^{-/-}$ mutant, and Pifo$^{FD/FD}$;Sufu$^{-/-}$ double knock-out (DKO) embryos at E9.5. (B) Pifo and kinesin family member 7 (Kif7) intercrosses, showing WT, Kif7$^{-/-}$ mutant, and Pifo$^{FD/FD}$;Kif7$^{-/-}$ DKO embryos at E9.5. (C) Confocal laser scanning microscopy (CLSM) of neural tube (NT) cryo-sections (14 µm). Marker analysis of E9.5 WT, Kif7$^{-/-}$, and Pifo$^{FD/FD}$;Kif7$^{-/-}$ DKO embryos revealed no differences between the genotypes. Following marker were used: motoneuronal (MN) marker (oligodendrocyte lineage TF 2, Olig2, green), floor plate marker (forkhead box protein A2, Foxa2, red), and neuronal progenitors marker for v3 region of the NT (NK2 homeobox 2 protein, NKX2.2). Green bars showing the expansion of the Olig2 domain and white bars showing the expansion of the NKX2.2 domain, respectively.

2.1.3 Pifo regulation on cellular level

In order to understand the Pifo regulation in more detail, a cell-based assay was designed using primary limb cells (PLC). As previous shown in section 2.1.1.2, *Pifo* is expressed in the AER of the LB (**Figure 6**F), and haploinsuficiency of *Pifo* in the LB results in polydactyly, which is likely caused by defective Shh signaling. The LB is a Shh receiving and responding tissue and PLCs are a suitable system for answering the question if *Pifo* is a Shh target gene and whether Pifo functions in the Shh pathway. Known Hh target genes, such as *Gli1* and *Ptch1*, respond to Hh stimulation in PLCs. For this reason, I first tested how Pifo and Shh target gene expression reacts in response to Shh, SAG a small molecule acting as Shh agonist, or cyclopamine (Cyc) acting as Shh antagonist. Both, SAG and Cyc act downstream of Shh by modulating Smo activity (**Figure 18**A, B). In contrast to published data (Wang et al. 2009), Cyc incubated cells showed less cilia formation compared to Shh and SAG treated cells (**Figure 18**C). As less cilia formation could influence the results on Shh signal transduction, I excluded Cyc from further analysis. Examination of mRNA expression revealed that similar induction kinetics of *Pifo* was found compared to known Hh target genes, such as *Ptch1*, *Gli1*, and *Gli2* (**Figure 18**D). All target genes, including *Pifo*, were upregulated upon Shh or SAG stimulation and inhibited upon Cyc stimulation, while *Gli3* and *Smo* expression was unchanged upon Shh, SAG, or Cyc stimulation. Protein analysis was carried out using WT compared to H47 HPRT WT reporter PLCs, showing an upregulation of Pifo after two hours of Shh stimulation (**Figure 18**E). Both Pifo protein and then transcriptional Pifo promoter-driven Venus reporter protein quickly accumulate after Shh induction, suggesting that *Pifo* is an immediate early target gene of Shh signaling. We next tested if *Pifo* is required for Shh target gene induction. Comparison of target gene activation in WT and Pifo$^{FD/FD}$ mutant PLCs after 24 hrs of Shh induction, revealed that *Ptch1* and *Gli1* were significantly downregulated in Pifo$^{FD/FD}$ mutant PLCs, suggesting that *Pifo* is required for Hh target gene activation (**Figure 18**F). Quantitative mRNA expression analysis of WT PLCs showed an upregulation of *Gli1* after one hour (**Figure 18**G), *Gli2* was upregulated already after half an hour and consistent with the WB data, *Pifo* was upregulated after two hours of Shh induction (**Figure 18**H). Taken together, the PLC system is a suitable system to study the function of Pifo in Shh signaling, as the cells are ciliated, responsive to Shh, and Pifo is expressed *in vitro*. Thus, *Pifo* is an immediate early Shh target gene as revealed by temporal qPCR and Western blot analysis, suggesting that Pifo is necessary for the activation of Shh target genes and likely a novel Shh pathway component.

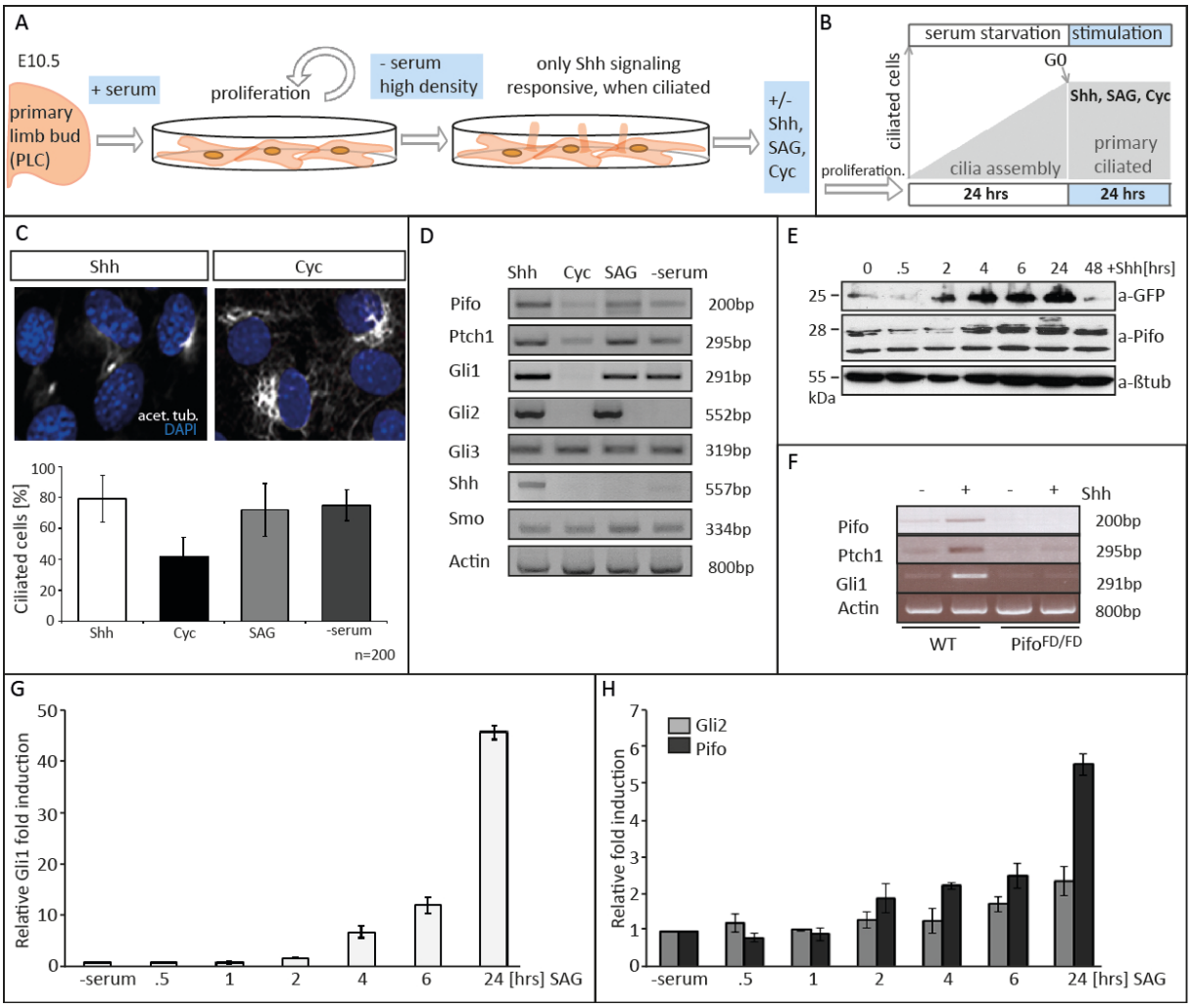

Figure 18 Primary limb bud (LB) cell culture (PLC) system. (A-B) Experimental design: generation of PLCs, and assay-design. (C) Confocal laser scanning microscopy (CLSM) of PLC, using antibodies against acetylated tubulin (acet.tub., white) and 4', 6-diamidino-2-phenylindole (DAPI, blue) to stain nuclei upon Sonic Hedgehog (Shh) or cyclopamine (Smo antagonist, Cyc) treatment for 24 hrs. Evaluation of percentage of ciliated PLCs uopn Shh, Cyc, Shh agonist (SAG) stimulation for 24 hrs and serum control (>200 cilia were counted). (D) RT-PCR data showing target gene activation upon Shh, Cyc or SAG stimmulation over 24 hrs. (E) Western blot (WB) of wild type and H47 WT Pifo-Venus reporter PLCs upon Shh stimmulation over 24 hrs showing Pitchfork (Pifo) and Venus reporter protein production, as revealed by antibodies against GFP and Pifo, respectively. (F) RT-PCR target gene activation upon Shh stimulation comparing WT and Pifo$^{FD/FD}$ mutant PLCs. (G) Real-time quantitative PCR (q-PCR) *relative Gli family zinc finger 1 (Gli1)* target gene up-regulation in WT PLCs upon SAG treatment for 24 hrs. (H) Q-PCR showing relative *Gli2* and *Pifo* target gene upregulation in WT PLCs, upon SAG treatment over 24 hrs.

To analyze the dynamic kinetics of the Pifo requirement for Gli1 activation, immortalized WT and Pifo$^{FD/FD}$ PLCs were generated from the Pifo$^{FD/FD}$ intercrosses and verified by genomic PCR analysis (**Figure 19**A). In order to investigate the requirement of Pifo for Shh the target gene regulation in more detail, time resolved and quantitative WB analysis against Gli1 was performed (**Figure 19**). Already upon loss of one Pifo allele (Pifo$^{FD/WT}$), Gli1 protein was significantly downregulated and almost completely abolished in Pifo$^{FD/FD}$ mutant PLCs after 24 hrs of SAG induction (**Figure 19**B, C). The natural Shh ligand and the Smo receptor anatagonist SAG induced to the same levels *Gli1* target gene in WT PLCs, which was completely blocked upon Pifo deletion (**Figure 19**D). In time-resolved WB analysis Pifo WT PLCs showed a slight increase in Gli1 protein production already 0.5 hrs

after Shh induction with a peak of protein synthesis after 24 hrs. In Pifo$^{FD/FD}$ mutant PLCs early Gli1 synthesis was completely abolished and only low levels were detectable after 24 hrs and 48 hrs of Shh induction. To investigate at which level of the Shh pathway Pifo is required, we furhter analyzed whether the initial step of Shh activation by Smo translocation to the PC was affected in Pifo mutants. Whereas 70-80% WT PLCs show efficient Smo translocation to the PC already within 3 hrs of ligand exposure, Pifo$^{FD/FD}$ mutant PLCs with normally formed PC showed a significant delay in Smo translocation to the PC upon Shh pathway activation (**Figure 19**G). Moreover, CLSM analysis revealed dramatic loss of Smo intensity at the PC of Pifo$^{FD/FD}$ mutant PLCs (**Figure 19**F). Thus, Smo translocation was delayed and decreased in Pifo$^{FD/FD}$ mutant PLCs. Together, these results clearly indicate that Pifo is necessary for Smo translocation to the PC, in a Gli1-mediated manner.

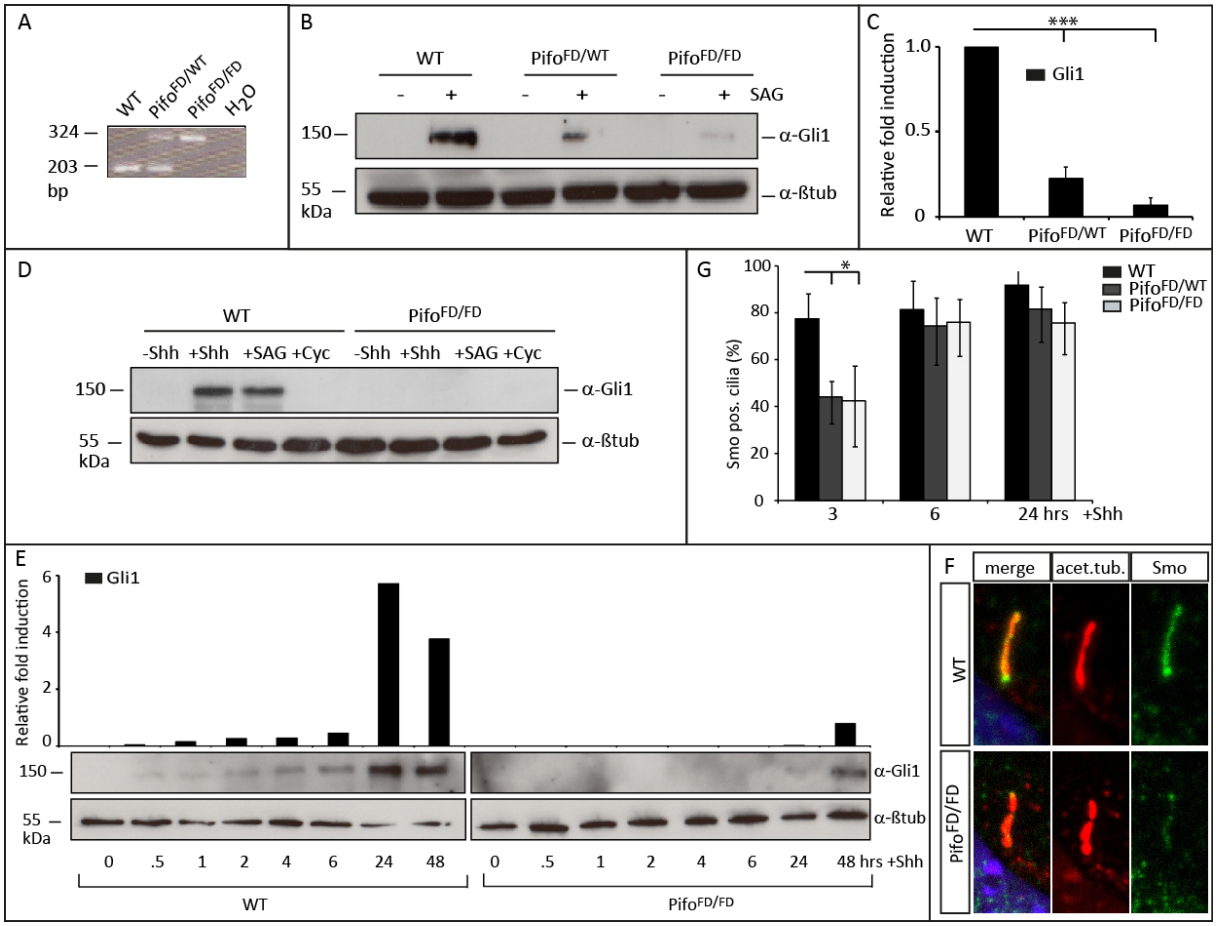

Figure 19 Gli family zinc finger 1 (Gli1) target gene activation and Smothened (Smo) translocation to the primary cilium (PC) in wild-type (WT) and Pitchfork (Pifo) mutant primary LB cells (PLCs). (A) RT-PCR genotyping of PLCs showing WT (203 bp), Pifo$^{FD/WT}$, and Pifo$^{FD/FD}$ (324 bp) bands. (B) Western Blot (WB) for Gli1 using PLCs, showing a reduction in Pifo$^{FD/WT}$ and Pifo$^{FD/FD}$ compared to WT PLCs. (C) Quantification of WB results shown in B. (D) WB for Gli1 using PLCs stimulated 24 hrs with Sonic Hedgehog (Shh), Smoothened agonist (SAG), and Cyclopamine (Cyc). (E) Time-resolved WB for Gli1 over 48 hrs, respectively. (F) Confocal laser scanning microscopy (CLSM) of PLC cilia using antibodies against acetylated tubulin (acet.tub, red), Smo (green), and 4', 6-diamidino-2-phenylindole (DAPI, blue). (G) Quantification of Smo translocation to the primary cilium (PC) after 3, 6, and 24 hrs of Shh stimulation. ($p < 0.05$, "*" is considered to be statistically relevant, and $p < 0.001$, "***", is considered to be extremely statistically relevant)

2.1.4 Pifo and Gprasp2 protein-protein interaction

In order to investigate the function of the Pifo protein in greater detail, we established the Pifo protein-protein interactome in cooperation with Prof. Marius Ueffing (Boldt et al. 2009). The experiment was carried out in primary ciliated HEK393T cells using quantitative stable isotope labeling by aminoacids in cell culture (SILAC). As Pifo was previously indentified to be important for cilia disassembly (Kinzel et al. 2010), the cell assays were performed during ciliary assembly and disassembly by withdrawal or addition of mitogen, respectively. Affinity purification and subsequent mass spectrometry of native protein complexes identified novel Pifo interaction partners, among which Gprasp2 was found. Gprasp2 interacts with huntingtin (Horn et al. 2006), which associates with MT motor proteins and is likely to be involved in intracellular vesicular trafficking. The translocation of Smo to the PC upon Hh induction depends on a conserved hydrophobic and basic residue ciliary targeting motif, that is conserved in several 7TMRs, including rhodopsin (Corbit et al. 2005). Strikingly, Gprasp1 and Gprasp2 bind to the exact same ciliary targeting motive in several 7TM-Gprasp receptors (Simonin et al. 2004). In this regard, one could speculate that Pifo and Gprasp2 might have a potential for trafficking the 7TMR Smo into the PC in Hh signaling.

2.1.5 Analysis of Gprasp2 gene trap mouse line

2.1.5.1 Generation and verification of the Gprasp2 gene trap mouse line

We identified Gprasp2 as novel Pifo interaction partner. To understand the Gprasp2 function in Shh signaling, a gene trapped (GT) Gprasp2 mouse line was generated ($Gprasp2^{Gt(IST12714A6)}$, Tigm Texas A&M Institute for Genomic Medicine, TIGM). We used commercial available Lex3.13 ES cells (C57BL/6N), containing a GT cassette inserted within intron four of mouse *Gprasp2* gene. The GT cassete contains a splice acceptor (LTR1), followed by a NLS fused to a lacZ gene encoding for β-gal (LacZ) under the control of the *Gprasp2* endogenous promoter (**Figure 20**A). The GT vector contains a polyadenylation recognition motif just after the LacZ reporter gene indicating that a putative fusion transcript lacks the whole ORF. It can therefore be assumed that such truncated transcripts do not encode for any functional Gprasp2 polypeptides. Germline chimeras were generated using diploid embryo ↔ ES cell ($Gprasp2^{Gt(IST12714A6}$) aggregation technique and chimeras were further crossed to C57BL/6N mice. As *Gprasp2* is located on the X chromosome, males were either WT or hemizygous (GT/y), when carrying the GT. Females were either WT, heterozygous (GT/x), or homozygous (GT/GT) for the *Gprasp2* GT. PCR genotyping was performed using tail tip genomic DNA or embryonic tissue using a forward primer in combination with a reverse primer within exon five (EP1194, EP1196) of the WT sequence, and a reverse primer located in the lacZ sequence (EP 1195) revealing products of 287 bp and 338 bp for the WT and GT alleles, respectively (**Figure 20**B). In order to confirm the absent Gprasp2 protein in GT mice, I performed WB analysis comparing adult testis lysates from WT and $Gprasp2^{GT/y}$ hemizygous males. This analysis revealed a high specificity of Gprasp2 antibody, as the Gprasp2 protein with a molecular weight of 130 kDa was detected in WT, showing only one band and absent in the $Gprasp2^{GT/y}$ hemizygous males (**Figure 20**C). Intercrosses of WT males with GT/x heterozygous females revealed a genotype distribution of the expected Mendelian ratios for the progeny, with a five percent aberration as shown in **Figure 20**D. Intercrosses of GT/y hemizygous males with WT females revealed 100 % WT males and 100 % GT/x heterozygus females, which were born in accordance with the expected Mendalian ratios. Intercrosses of GT/y hemizygous males and GT/x heterozygous females revealed a 17 % higher preference of for GT/y male offsprings, compared to WT. Though, the Mendelian ratio for female offspring was fulfilled. At the time point of weaning all genotypes were comparable to their WT counterparts, and so far their livespans and fertility are normal. Hemizygous males exhibited increased body weights after approximately four month, which is shown in more detail under 2.2.6.2.

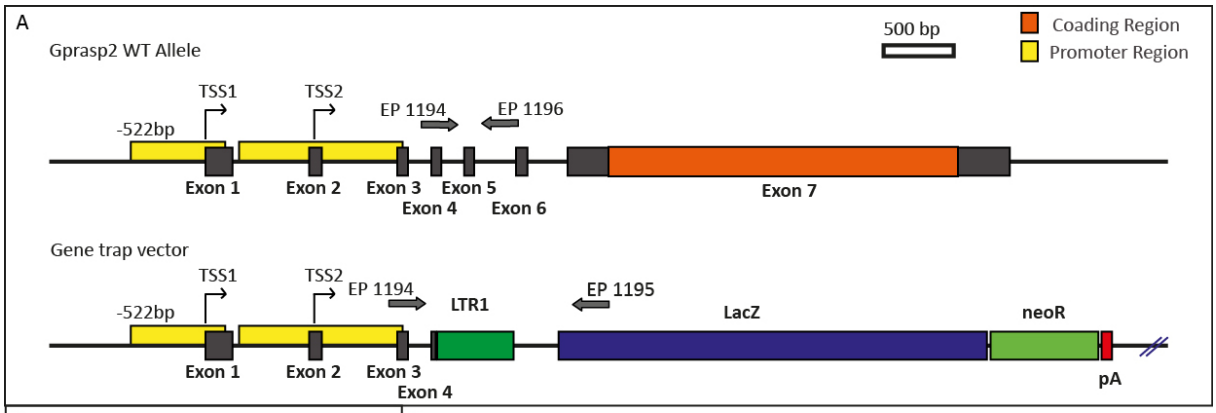

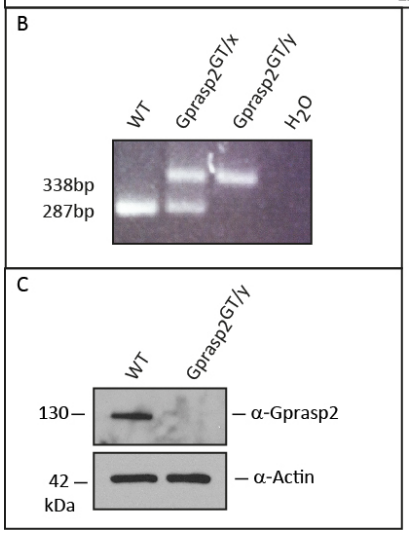

D

WT♂ x GT/x♀	♂ WT	♂ GT/y	♀ WT	♀ GT/x
Total	15	18	16	13
Percent	*45*	*55*	*55*	*45*
Expected	*50*	*50*	*50*	*50*
GT/y♂ x WT♀	**WT**	**GT/y**	**WT**	**GT/x**
Total	20	0	0	32
Percent	*100*	*0*	*0*	*100*
Expected	*100*	*0*	*0*	*100*
GT/y♂ x GT/x♀	**WT**	**GT/y**	**GT/x**	**GT/GT**
Total	14	29	23	23
Percent	*33*	*67*	*50*	*50*
Expected	*50*	*50*	*50*	*50*

Figure 20 G-protein coupled associated sorting protein 2 (Gprasp2) construct and mouse statistics. (A) Gprasp2 wild type (WT) and Gprasp2 gene trap vector sequence. (B) Genotyping of WT, heterozygous female (Gprasp2$^{GT/x}$) and hemizygous male (Gprasp2$^{GT/y}$) mouse tails. (C) Western blot (WB), showing the loss of Gprasp2 protein (130 kDa) in testis lysates (80 µg). Actin was used as loading control. (D) Mouse statistics showing the progenity of intercrosses of WT (male) and GT/x (heterozygous, female), GT/y (hemizygous, male) and WT (female), and GT/y and GT/x. In each panel the total mouse number, the percentage of the born mice, and the expected Mendelian ratios are shown for each genotype.

2.1.5.2 Analysis of embryonic Gprasp2 lacZ expression

Up to date, *Gprasp2* expression was only shown in the nervous system (Gene paint, http://www.genepaint.org/). Since we discovered Gprasp2 as a Pifo interacting protein, and we identified *Pifo* as Shh target, I examined the *Grasp2* LacZ reporter expression at various embryonic stages. Indeed, LacZ expression was detected in neural crest cells, the NT and NC of E8.5 and E9.0 Gprasp2$^{GT/y}$ embryos (**Figure 21**A, B, D-G). At E10.5, the overall LacZ expression was increased in the ventral NT, NC and DRG. Thus, *Gprasp2* LacZ reporter expression was particularly found in the NT and the LBs, tissues receiving Shh signals (**Figure 21**H-K), showing expression similarity to *Pifo*. These results for the first time show *Gprasp2* LacZ reporter expression in early embryonic stages. The expression in the NT and limb in regions of Pifo and Shh activity, suggests a role of Gprasp2 in the Shh pathway.

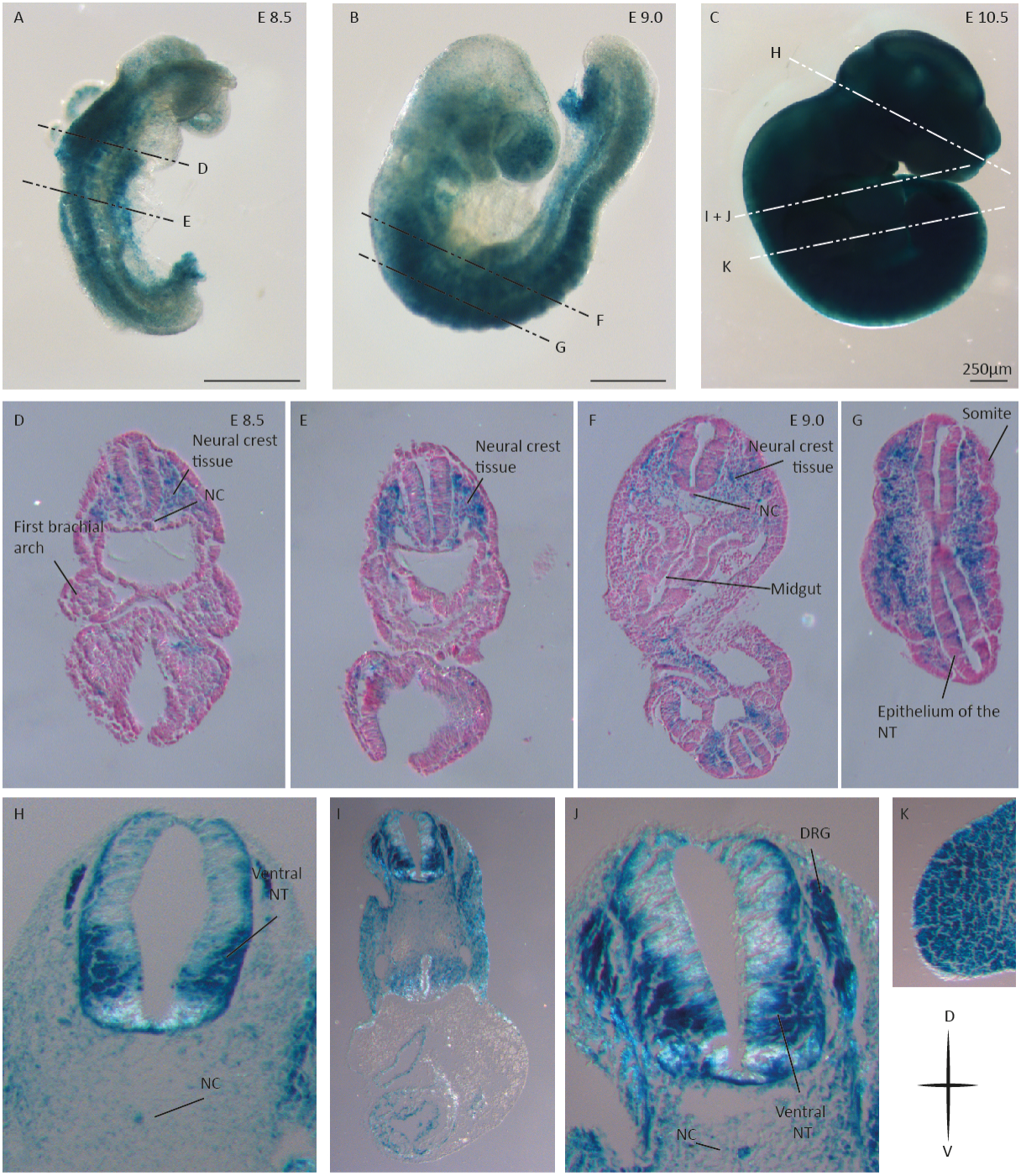

Figure 21 *G-protein coupled associated sorting protein 2 (Gprasp2)* embryonic LacZ expressions. (A-C) E8.5, E9.0, and E10.5 whole mount LacZ stained embryos, respectively. (D-G) Paraffin embedded LacZ stained and cross-sectioned embryos, counterstained with nuclear fast red. (D, E) E8.5 cross-sectioned LacZ stained embryo, section plane indicated in A. Neural crest tissue, notochord (NC), and first brachial arch are indicated. (F, G) Cross-section of E9.0 embryo shown in B. Neural crest tissue, NC, midgut, somites, and neural tube (NT) epithelium are indicated. (H-K) Cross-section of the E10.9 embryo shown in C. Ventral NT, NC, and dorsal root ganglia (DRG) are indicated, K shows the LacZ positive LB section indicated in C.

X-chromosomal inactivation is a vital mechanism for dosage compensation evolved to balance the expression of X-linked and autosomal genes in the two sexes. Due to *Gprasp2* gene location on the X chromosome, I studied *Gprasp2* LacZ reporter expression in the different genders and genotypes. Whole-mount LacZ stainings of Gprasp$^{GT/x}$, Gprasp$^{GT/GT}$, and Gprasp$^{GT/y}$ embryos at E9.5 and E10.5 revealed an ubiquitous LacZ reporter

activiy with distinct expression in the neuronal tissue and LB (**Figure 22**A). Thus, due to X-linked inactivation Gprasp2$^{GT/x}$ embryos showed lower LacZ reporter expression, compared to Gprasp2$^{GT/GT}$ and Gprasp2$^{GT/y}$ embryos. The LacZ reporter activity was analyzed in more detail by cross-sectioning the embryos (**Figure 22**B). Gprasp$^{GT/GT}$ and Gprasp$^{GT/y}$ embryos thereby revealed a distinct expression pattern at E9.5, by showing a V-D LacZ activity gradient in the NT, whereas in Gprasp$^{GT/x}$ embryos only a slight LacZ expression was detected. E10.5 cross-sectioned embryos, showed a more ventral-restricted pattern of the NT, with a LacZ positive NC, FP, and MN region. Taken together, the ubiquitous LacZ reporter activity was increased in the ventral NT and overall weaker in Gprasp2$^{GT/x}$ embryos, suggesting that the expression differences between the genotypes are due to random X-linked inactivation. Thus, the distinct localization to Shh-high activity regions within the ventral NT strongly indicates a role for Gprasp2 in Shh signaling.

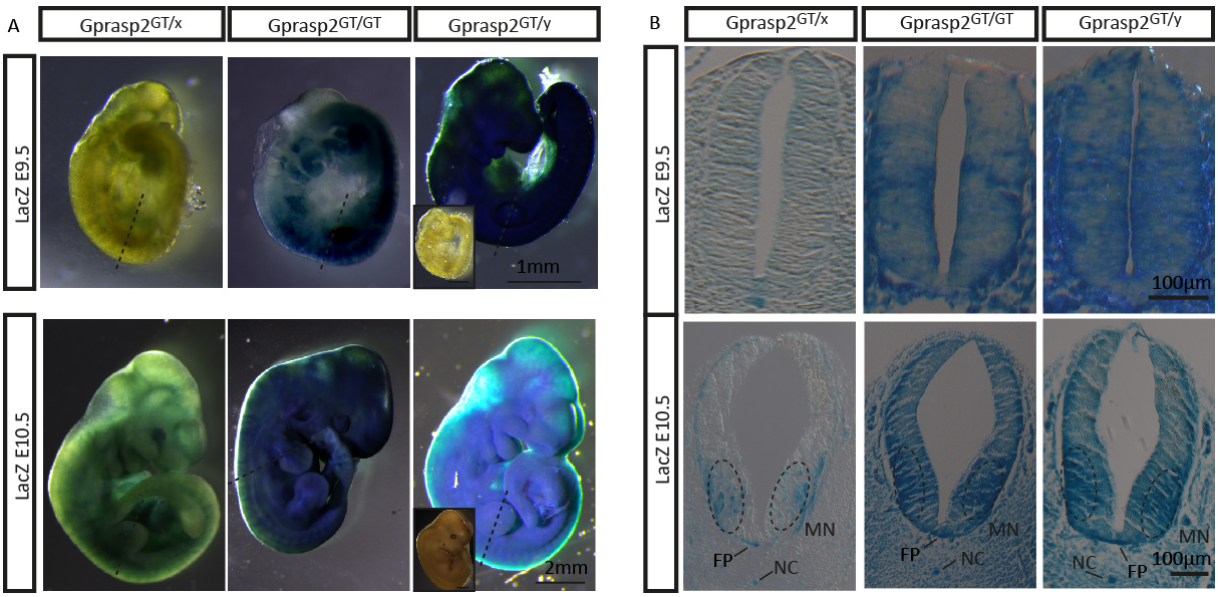

Figure 22 *G-protein coupled associated sorting protein 2 (Gprasp2)* dose dependent LacZ expressions. (A) Whole-mount LacZ expression of E9.5 and E10.5 heterozygous (Gprasp$^{GT/x}$), homozygous (Gprasp$^{GT/GT}$), and hemizygous (Gprasp$^{GT/y}$) embryos. The inserts represent the wild-type (WT) control. (B) Associated paraffin-embedded and cross-sectioned NT are shown, at E9.5 and E10.5. The sections were analyzed at the limb bud (LB) region of the neural tube (NT) as indicated in A. In E10.5 cross-sections, the motoneuronal (MN), floor plate (FP) and the notochord (NC) are indicated.

2.1.5.3 Floor plate and neural tube specification in Gprasp2 mutant embryos

Gprasp2 protein interaction with Pifo and *Gprasp2* expression in regions of high Shh activity led us to test Gprasp2 function in Shh signaling. To address this, chimeric embryos were generated by diploid embryo ↔ ES cell (Gprasp2$^{Gt(IST12714A6)}$) aggregation, which allowed us to study mosaic embryos. During embryo development, the node is a highly ciliated and Shh responsive. Moreover, the localization of Smo to cilia in nodal cells was already characterized (May et al. 2005). In this reason I first analyzed the ciliary translocation of Smo *in vivo*. I used chimeric embryos to analyzing Smo translocation in neighboring nodal WT (YVI^{+}) and Gprasp2 GT (YVI^{-}, **Figure 23**A, B) cells. However, after quantitative image analysis, I did not find any major differences between ciliary Smo of WT and Gprasp2 mutant cells, suggesting no disruption of Smo transport at the node. A temporal

and spatial gradient of Shh is essential for the appropriate ventral NT specification. As *Gprasp2* LacZ expression is detected at more ventral region of the NT, I further examined the possible function in the NT specification, using MN precursor marker Olig2 and definitive MN marker Isl1 (**Figure 23**D). Interestingly, slightly decreased number of Olig2 and Isl1 positive cells were observed in the ventral NT of Gprasp2 mutant (YVI^-) embryos, compared to the WT (YVI^+, **Figure 23**C-F), suggesting a role for Gprasp2 in Shh-dependent specification of the ventral NT.

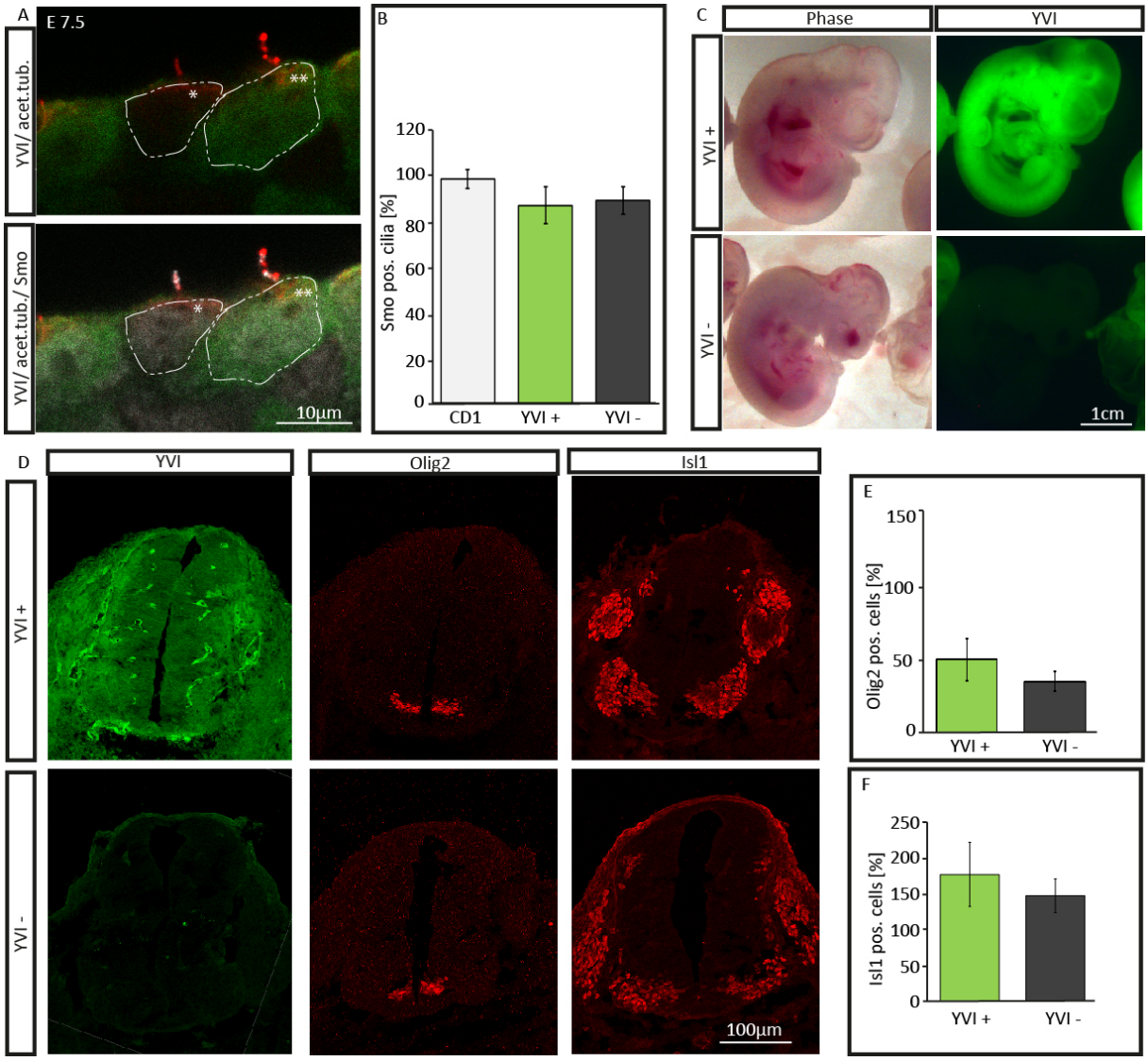

Figure 23 G-protein coupled associated sorting protein 2 (Gprasp2) function in embryonic development. (A) Confocal laser scanning microscopy (CLSM) of the node's Smothended (Smo, white) translocalization to the PC (red) of chimeric embryos at E7.5, showing wild-type (WT, YVI) and Gprasp2 mutant neighboring cells. (B) Quantification of Smo positive cilia (70 cilia) from YVI positive (YVI +) and negative (YVI -) node cells. (C) YVI expression of diploid aggregated E10.5 WT and Gprasp2 mutant embryos, showing phase and fluorescence images. (D) CLSM of cryo-sectioned neural tubes (NT) of YVI + and YVI - E10.5 embryos, shown in A. Marker analysis of green fluorescent protein (GFP, in order to detect YVI), oligodentrocyte TF 2 (Olig2), and insulin gene enhancer protein 1 (Isl1). (E, F) Quantification of Olig2 and Isl1 positive cells, shown in D.

2.1.5.4 Gprasp2 regulation on cellular level

To test whether Gprasp2 has a possible function in Shh signaling we used the *in vitro* PLC culture assay, comparing Gprasp2$^{GT/y}$ PLCs to WT PLCs. I concentrated on Shh target gene *Gli1*, as the Gli family of zinc finger proteins are well-known TFs and targets of Shh signaling. Thus, Gprasp2 interacton partner Pifo, already showed Gli1-mediated regulation. In WB analysis of WT PLCs, Gprasp2 and Gli1 were upregulated upon Shh or SAG and downregulated upon Cyc stimulation after 24 hrs (**Figure 24**A, B). In contrast, Gprasp2$^{GT/y}$ mutant PLCs showed absent Gprasp2 protein and almost completely abolished Gli1 protein, strongly suggesting a role for Gprasp2 in Shh target gene regulation. Time-resolved kinetics in Gprasp2$^{GT/y}$ mutant PLCs revealed a dramatic delay in Gli1 activation, upon SAG stimulation over 24 hrs (**Figure 24**C), similar to Pifo$^{FD/FD}$ mutant PLCs (**Figure 19**E). Next we analyzed whether depletion of Gprasp2 results in a lack of Smo translocation to the PC (**Figure 24**D, E). Whereas 20% of WT PLCs show efficient Smo translocation to the PC within one hour of ligand exposure, Gprasp2$^{GT/y}$ mutant PLCs with normally formed PC barely responded to SAG induced pathway activation. After six hours the peak of 70 % Smo positive cilia is reached in WT PLCs, whereas only 20 % of the Gprasp2$^{GT/y}$ mutant PLCs exhibit efficient Smo translocation. Thus, similar to Pifo$^{FD/FD}$ mutant PLCs, Gprasp2$^{GT/y}$ mutant PLCs show a decrease in Smo intensity along the PC. Together, these results clearly indicate that Gprasp2 is required for Smo translocation to the PC and Gli1-mediated Shh pathway activation.

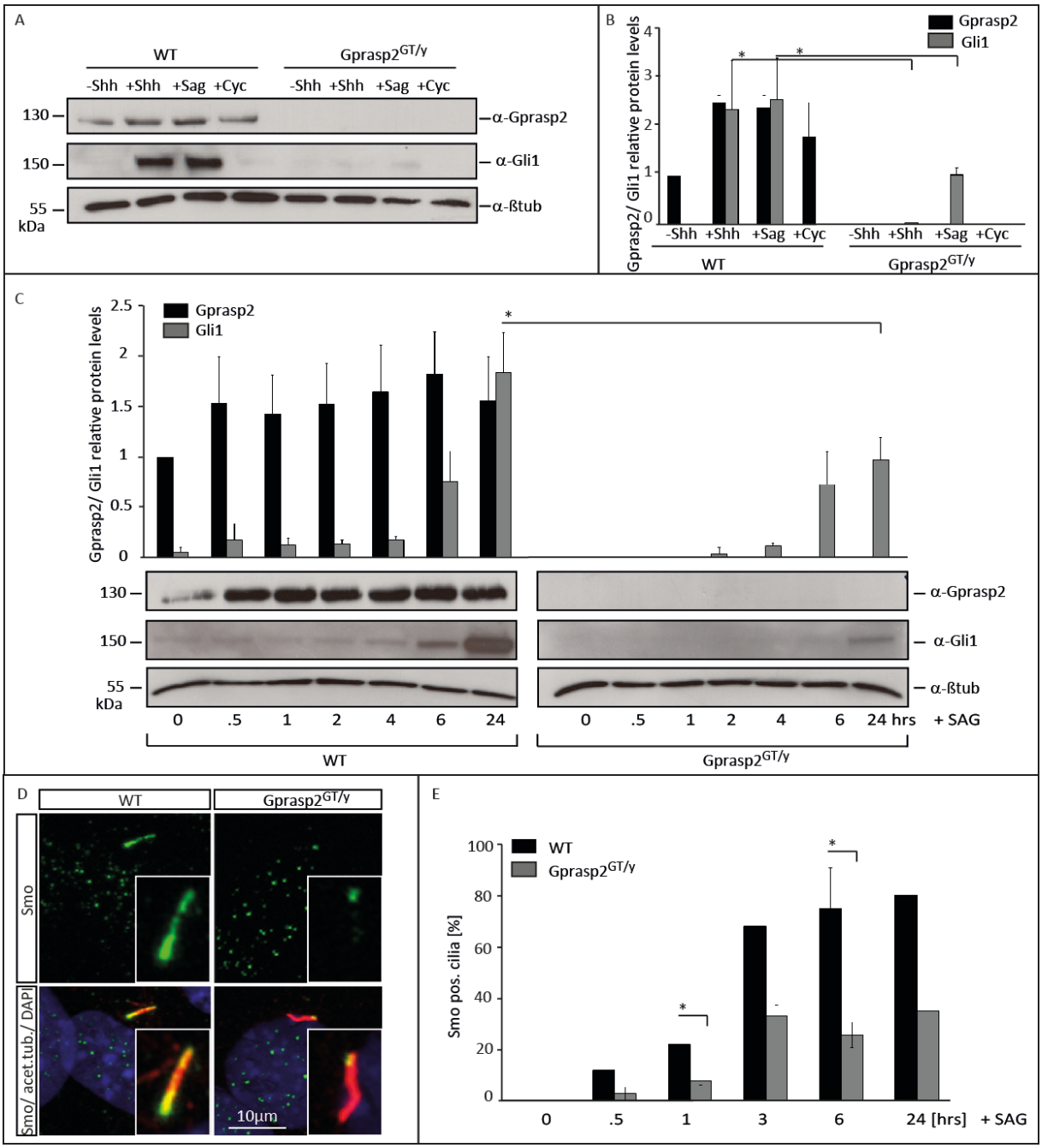

Figure 24 Gli family zinc finger 1 (Gli1) target gene activation and Smothened (Smo) translocalization in G-protein coupled associated sorting protein 2 (Gprasp2) mutant primary limb bud cells (PLCs). (A) Western blot (WB) analysis of Gprasp2$^{GT/y}$ hemizygous vs. wild-type (WT) PLCs. Gprasp2 and Gli1 target gene regulation in Gprasp2$^{GT/y}$ PLCs upon Sonic Hedgehog (Shh), Smothened agonist (SAG), and Cyclopamine (Cyc) stimulation. (B) Quantification of relative protein levels shown in A. (C) WB analysis of Gprasp2 and Gli1 target gene downregulation in Gprasp2$^{GT/y}$ PLCs upon SAG stimulation over 24 hrs. (D) Confocal laser scanning microscopy (CLSM) of Smothened (Smo, green) translocalization to the primary cilium (PC) (acetylated tubulin, acet.tub., red), and 4', 6-diamidino-2-phenylindole (DAPI, blue), in WT and Gprasp2$^{GT/y}$ PLCs after 24 hrs SAG stimulation. The windows on the right bottom show a magnification of the cilia, respectively. (E) Quantification of Smo positive cilia over 24 hrs SAG induction.

2.1.6 Pifo and Gprasp2 double knock-out study

2.1.6.1 Pifo and Gprasp2 co-expression in Shh high regions

We previously found Pifo and Gprasp2 to interact on protein level. Thus, both proteins are expressed in Shh receiving tissues (NT and LB) and are required for Smo translocation to the PC and Gli1-mediated Shh pathway activation. Next, we further studied whether both proteins are co-expressed in the same tissues. In order to address this question I used the previous described reporter lines, Tg(GBS-GFP) and HPRT WT (H47) and immunostainings in order to detect Pifo-Gprasp2-Shh co-expression.

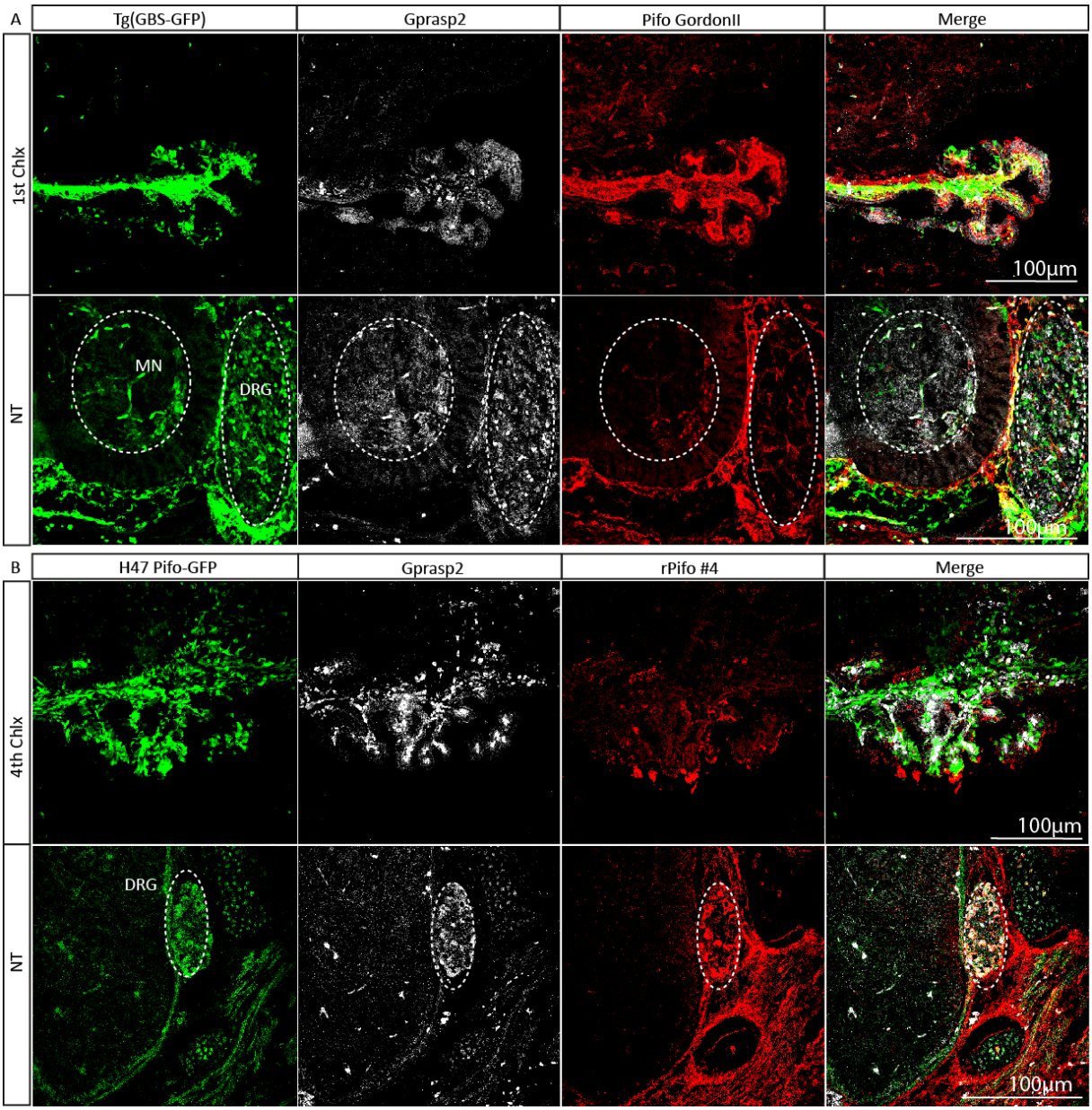

Figure 25 G-protein coupled associated sorting protein 2 (Gprasp2) and Pitchfork (Pifo) co-expression in Sonic Hedgehog (Shh) regions. (A) Confocal laser scanning microscopy (CLSM) of Tg(GBS-GFP), stained for GFP, Gprasp2, and Pifo ant-rabbit, in the choroid plexus (Chlx) and dorsal root ganglia (DRG) of the neural tube (NT). (B) CLSM of HPRT WT (H47) reporter, stained for GFP, Gprasp2, and Pifo (rat, #4, Table 3), respectively.

Using the Tg(GBS-GFP) reporter and co-staining of GFP, Gprasp2 and Pifo revealed a Shh-Gprasp2-Pifo co-localization in the 1st Chlx, MN region and DRG of the NT of E14.5 cryo-sectioned embryos (**Figure 25**). Using the HPRT WT (H47) reporter and co-staining with GFP, Gprasp2 and Pifo revealed a Pifo-Gprasp2 co-localization in the 4th Chlx and DRG of the NT of E14.5 cryo-sectioned embryos. Taken together, Pifo and Gprasp2 are co-localized in Shh receiving tissues, suggesting a joint interaction in Shh signaling.

2.1.6.2 Pifo and Gprasp2 direct interaction

To understand the mechanism underlining the function of Pifo and Gprasp2 in more detail, we analyzed the physical interaction of both proteins within the Shh pathway, using semi-endogenous immunoprecipitation (IP) experiments. 7TMR Smo causes increased Grk2-dependent phosphorylation and association with β-arr2 (Chen et al. 2004) that, in turn, mediates Kif3a motor protein-driven anterograde transport of Smo into the PC for Hh pathway activation (Kovacs et al. 2008). We therefore analyzed the association of Pifo and Gprasp2 with the kinesin motor subunits. Immobilized mPifo (Strep-FLAG-tagged) was subjected to lysates from ciliated PLCs and the protein-protein interaction was analyzed in a time resolved manner upon Shh stimulation. The affinity of Smo and Gprasp2 to Pifo and Kif3b was remarkably increased within first 30 min upon Shh stimulation (**Figure 26**A, B). Next, we performed a co-IP where immobilized mSmo (Strep-His-tagged) was subjected to PLC lysates which were transiently transfected with a HA-tagged hGprasp2 (**Figure 26**E). With the use of antibodies against HA- and His-taggs we could show that Smo directly interacts with Gprasp2. Together with Dr. Bomi Jung we identified the heterotrimeric complex of Pifo-Gprasp2-Smo with Kif3b as the motor transport unit, as Pifo directly interacts with Kif3b and Gprasp2 (**Figure 26**, Jung et al. 2014, submitted). We further summarize, that Gprasp2 acts as an adaptor for the binding of Pifo to Smo, as Gprasp2 but not Pifo directly interacts with Smo. In addition co-expression of Pifo and Gprasp2 was shown in early stages and onset of Shh signaling, by immunostainings of E7.75 embryonic node cilia (**Figure 26**C, D), were Smo, Gprasp2, Pifo, and Kif3b are all expressed. Thus, the percentage of Gprasp2, Pifo, and Kif3b positive cilia are similar, suggesting a co-localization at the PC of the embryonic node. These results show that the heterotrimeric complex proteins are present under physiological conditions as they are co-expressed in vivo. Taken together we have identified a heterotrimeric Pifo-Gprasp2-Smo complex, which requires Shh signaling. Shh induction together with a lack of either Pifo or Gprasp2 leads to failure of Smo translocation to the PC and deficient Shh target gene induction.

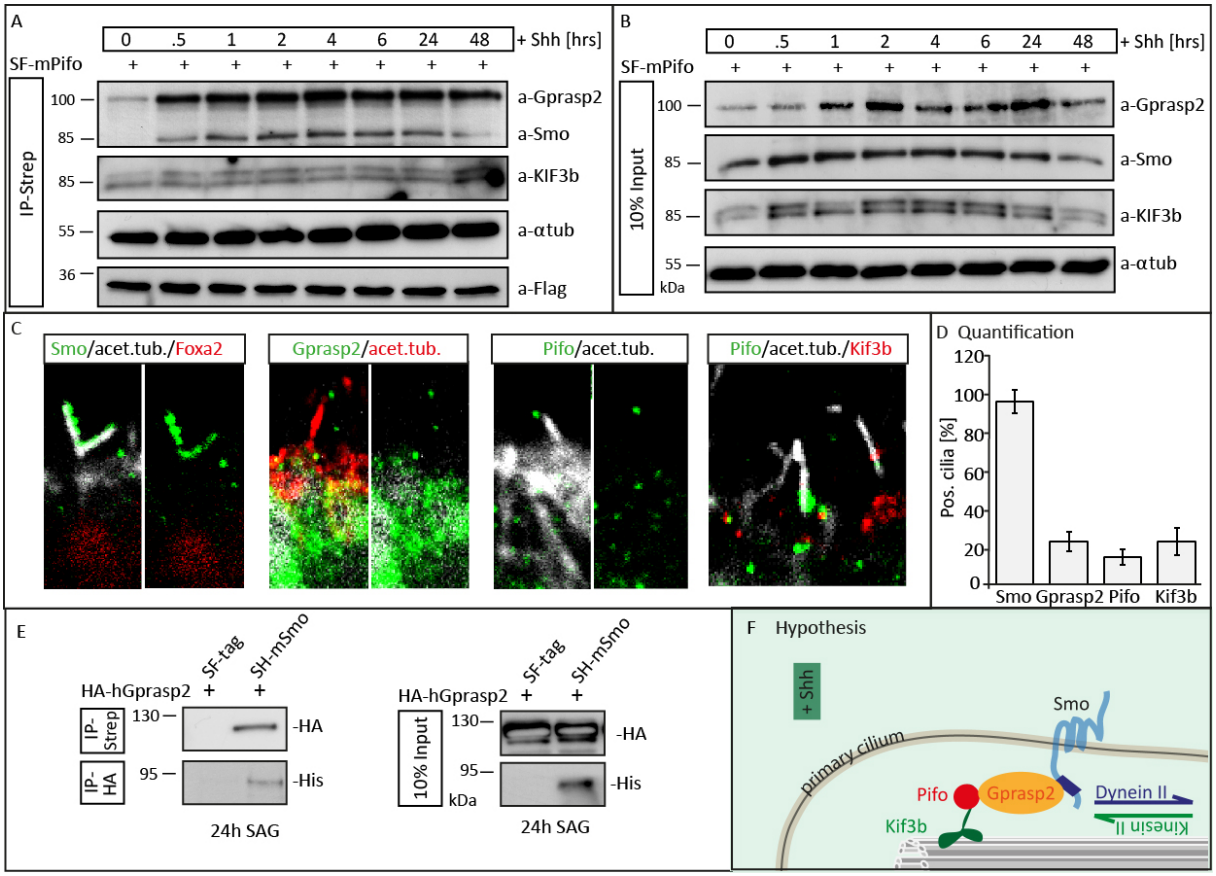

Figure 26 Kinetics of Pifo-Gprasp2-Smo (Pitchfork, G-protein coupled associated sorting protein 2, Smothened) multimeric complex formation upon Sonic Hedgehog (Shh) treatment. (A) Semi-endogenous immunoprecipitation (IP) Strep-Tactin sepharose FLAG-TAP (SF-TAP) coupled mouse Pifo (mPifo, AB30) was subjected to ciliated primary LB cells (PLCs) in a time-manner upon Shh stimulation. Strep-Tactin immunoprecipitation (IP-Strep) was performed over 48 hrs using Gprasp2, Smo, kinesin like protein 3b (Kif3b), alpha tubulin (αtub), and Flag antibodies. (B) Western blot (WB) of 10 % protein input of Gprasp2, Smo, Kif3b, and alpha tubulin as control. (C) Confocal laser scanning microscopy (CLSM) of embryonic node at E7.75, showing Smo, Gprasp2, Pifo and Kif3b at the node cilia, using acetylated tubulin (acet.tub., red) as ciliary marker. (D) Quantification of positive node cilia (three embryos, 100 cilia) shown in C. (E) Co-IP using Strep-His-TAP (SH-TAP) coupled mouse Smo (mSmo) which was subjected to HA tagged human Gprasp2 (hGprasp2). IP-Strep was performed after 24 hrs of Shh agonist (SAG) incubation using anti-HA and anti-His antibodies. 10 % input is shown in the right WB. (F) Hypothesis of a heterotrimeric complex translocalization upon Shh signaling, with Gprasp2 acting as mediator between Pifo and Smo, with Kif3b as motor subunit.

2.1.6.3 Pifo/ Gprasp2 double knock-out mice

In the previous chapter (2.1.6.2) I showed, that we identified a heterotrimeric complex of Pifo-Gprasp2-Smo, which upon Shh stimulation is formed. I could also show that Pifo KO and Gprasp2 GT mouse lines are viable and do not show specific Shh-like phenotypes. As both proteins form a complex, are co-expressed in the same tissues, and regulate Shh target genes, we questioned whether eliminating both genes will lead to a disruption of Shh signaling and elucidate a possible Shh-like phenotype. Therefore I intercrossed both mouse lines, Pifo KO and Gprasp2 GT, as depicted in **Figure 27**A, B. Briefly, statistically a genotypic distribution of 25 % Pifo$^{FD/FD}$ mutants is expected with an equal distribution of the genders (7.75 % Pifo$^{FD/FD}$;Gprasp$^{GT/y}$ and 7.75 % Pifo$^{FD/FD}$;Gprasp$^{GT/GT}$). So far, 43 born bubs revealed four Pifo-Gprasp2 DKOs. The DKOs are viable and reveal no obvious phenotypes. Among the DKO offspring, three males (Pifo$^{FD/FD}$;Gprasp$^{GT/y}$) and one female

(Pifo$^{FD/FD}$;Gprasp$^{GT/GT}$) were born. The expected Mendelian ratio for the DKO is 12.5 %, whereas the actual ratio is 10.75 %. But in order to draw conclusions about the distribution of the Mendelian ratios, we need to genotype further mice, in order to gain a statistically relevant number. Thus, it is likely that the eventual hypomorphic Pifo allele and the remaining protein residual is still functioning, and therefore we observe no complete KO for Pifo. In this regard also the DKO phenotype might be influenced. As both, Pifo$^{FD/FD}$ and Gprasp2 single mutants showed a reduction in MN region of the NT, I preliminarily compared WT and Pifo$^{FD/FD}$;Gprasp$^{GT/GT}$ DKO mutant NT by marker analysis of the MN region at E10.5 (**Figure 27**C). Olig2 and Isl1 marker analysis revealed no obvious difference in ventral NT regions, as both cell types were present. Eventual differences, as shown in Pifo and Gprasp single mutants, have to be elaborated by quantification of Olig2 and Isl1 positive cell numbers. In summary, the intercrossing of Pifo KO and Gprasp2 GT mutant mice revealed that they are viable, yet quantitative phenotype analysis are still in progress.

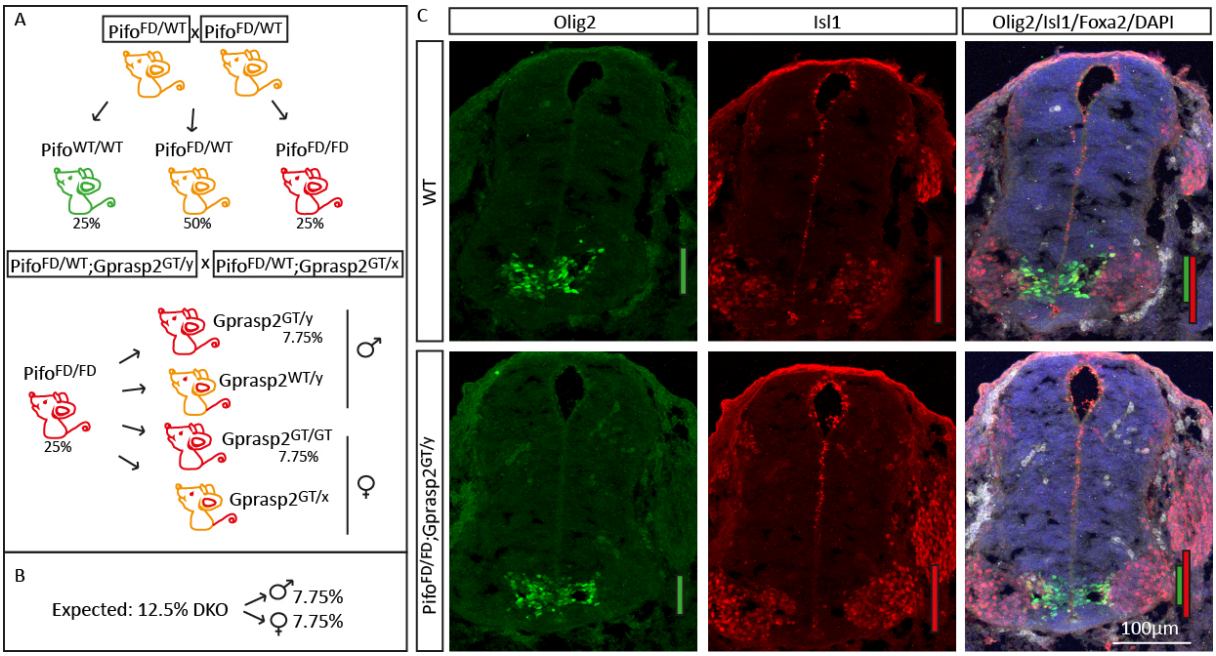

Figure 27 Pitchfork (Pifo) and G-protein coupled associated sorting protein 2 (Gprasp2) double knock-outs (DKO). (A) Crossing scheme depicting Pifo heterozygous intercorsses (Pifo$^{WT/FD}$) with an expected outcome of 25 % Pifo$^{FD/FD}$ mutants. When intercrossing Pifo$^{FD/WT}$; Gprasp2$^{GT/x}$ double heterozygous females with Pifo$^{FD/WT}$; Gprasp2$^{GT/y}$ hemizygous males, 7.75 % of DKO males and 7.75 % of DKO females are expected, due to the Mendelian ratio. (B) Expected DKO statistics, 12.5 %, with half of them expected to be males (7.75 %) and half of them females (7.75 %). (C) Confocal laser scanning microscopy (CLSM) of WT and Pifo$^{FD/FD}$;Gprasp2$^{GT/y}$ DKO mutant embryo showing oligodentrocyte TF 2 (Olig2, green), and insulin gene enhancer protein 1 (Isl1, red). A merge including forkhead box protein A2 (Foxa2, white) and 4', 6-diamidino-2-phenylindole (DAPI, blue) is shown in the last panel. Green bars showing the expansion of the Olig2 domain and white bars showing the expansion of the NKX2.2 domain, respectively.

2.2 II Ciliopathies – Diabetes

2.2.1 Analysis of Pifo in the pancreatic islets

In contrast to previously published data (Kinzel et al. 2010) the Pifo CKO allele enabled us to overcame lethality. Together with the fact that *Pifo* was found to be express in certain ciliated tissues like brain, lung, testis and pancreas (**Figure 4**), we are now able to study the adult phenotype of $Pifo^{FD/FD}$ mutant mice in more detail. Hh signaling in the pancreas is still controversially discussed among scientists. Although, there is evidence that Hh signaling plays a role in pancreas development and function, as concomitant elimination of cilia results in overt Hh activation in pancreatic epithelium and impaired pancreas formation in Gli2 deficient mice (Cervantes et al. 2010).

2.2.1.1 Pifo expression in pancreatic islets

We previously identified Pifo as Shh target gene and discovered its role in Shh signaling. Moreover, we could show that is in deed expressed in the adult pancreas (**Figure 4**). We therefore questioned whether Pifo might have a tissue specific role in the pancreas. In order to analyze the specific site of expression, I isolated pancreatic islets (4.2.1.3.1) from different aged WT mice and co-stained them with Pifo and glucagon, which is a marker for α-cells (**Figure 28**A). CLSM analysis revealed no Pifo-positive α-cell, suggesting that the majority of Pifo-positive cells are most likely β-cells, knowing that around 80 % of the cell types within an islet are β-cells. No obvious difference in Pifo protein expression was found over various ages in WT mice. In order to conclude that Pifo is exclusively expressed in β-cells, a co-staining with NKX6.1 should be performed, using monoclonal antibodies (**Figure 10**). Real-time quantitative PCR revealed a slight decrease in *Pifo* expression in pancreatic WT islets upon aging (3 – 18 months), whereas Gprasp2 expression was rather increased upon aging (**Figure 28**B). Next, *Pifo* mRNA expression in pancreatic islets of three months old WT animals was compared to equal amounts of PLC lysates. RT-PCR showed that *Pifo* is equally expressed in both cell types, PLCs and WT islets (**Figure 28**C). Thus, co-staining of Pifo with a ciliary marker (acet.tub) revealed ciliary localization of Pifo (**Figure 28**D, zoom in). In summary, these results show Pifo expression e.g. in islets β-cells, suggesting a role for Pifo in β-cell function.

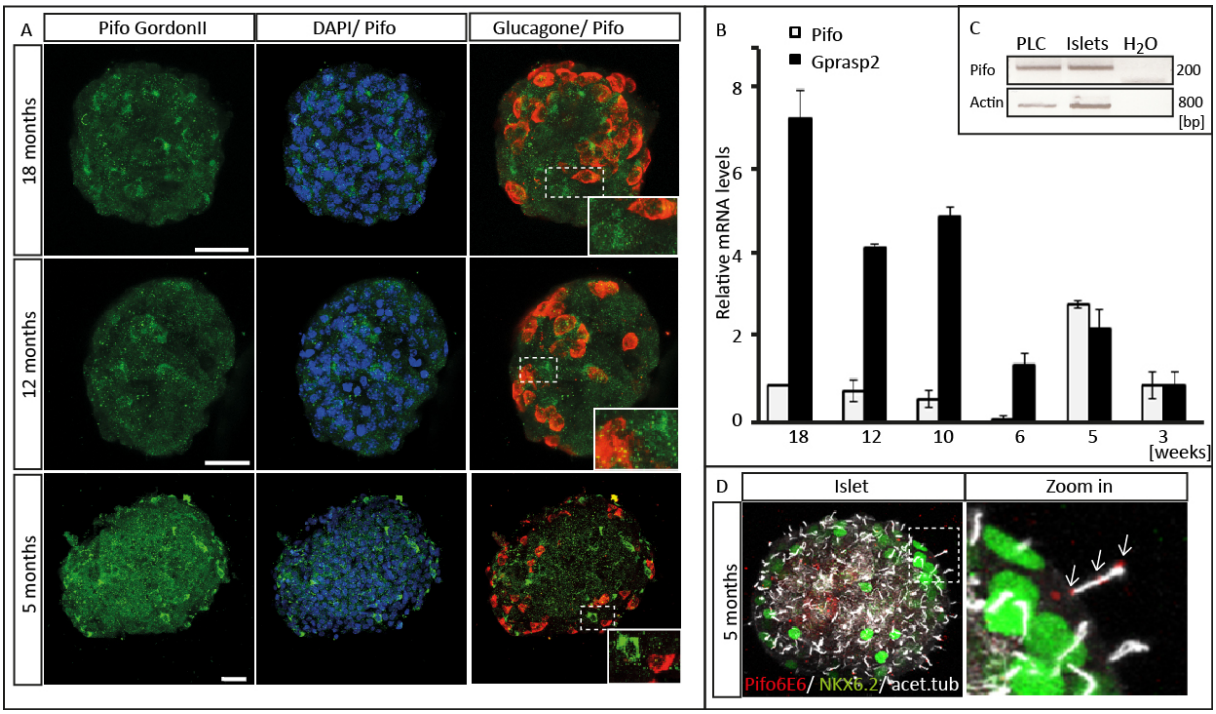

Figure 28 Pitchfork (Pifo) expression in isolated pancreatic islets. (A) Confocal laser scanning microscopy (CLSM) of isolated pancreatic islets, showing Pifo (rabbit, green) expression in β-cells of 5 – 18 months old wild type (WT) islets using glucagone co-staining (α-cell marker, red) and 4', 6-diamidino-2-phenylindole (DAPI, blue). (B) Real-time quantitative PCR (qPCR), showing *Pifo* and *G-protein coupled associated sorting protein 2 (Gprasp2)* expression in 3 – 18 months old isolated WT islets. (C) *Pifo* expression comparing primary LB cells (PLC) and isolated WT islets (3 month) using RT-PCR. (D) Pifo expression (rat, red) in the primary cilium (PC) of an WT islet islets (arrows in the zoom in, dotted line), using co-staining with NK6 homeobox 1 (NKX6.1, green, β-cell marker), and acetylated tubulin (acet.tub, white, cilia marker).

2.2.1.2 Shh *in vitro* assay in pancreatic islets

In order to test, whether pancreatic islets express Hh target genes and are responsive to Shh signaling, I performed an *in vitro* assay and stimulated isolated WT and Pifo$^{FD/FD}$ mutant islets with Shh, or Cyc for 24 hrs. First, Smo and Gli1 were found at the ciliary tip of the PC of isolated WT islets after Shh stimulation (**Figure 29**A, D). Next, I analyzed Shh-dependent translocation to the PC. Upon Shh stimulation, Smo as well as Gli1 translocation to the PC was significantly increased and decreased upon Cyc stimulation (**Figure 29**B). Thus, Smo translocation upon Shh induction, revealed not response in Pifo$^{FD/FD}$ mutant islets at all, when compared to WT islets (**Figure 29**D). Though, there was a basal Smo translocation upon serum free treatment of 60 % in WT and Pifo$^{FD/FD}$ mutant islets. Last, mRNA data show an stimulatory effect of Shh ligand on both mouse forms of *insulin 1* and *2*, as well as on the potassium channel subunit *Kir6.2* (**Figure 29**C), suggesting a role for Shh in insulin secretion. Together, these *in vitro* experiments suggest that Shh has a role in islets function, as it mediates the translocation of Shh pathway proteins to the PC, and stimulates the insulin pathway.

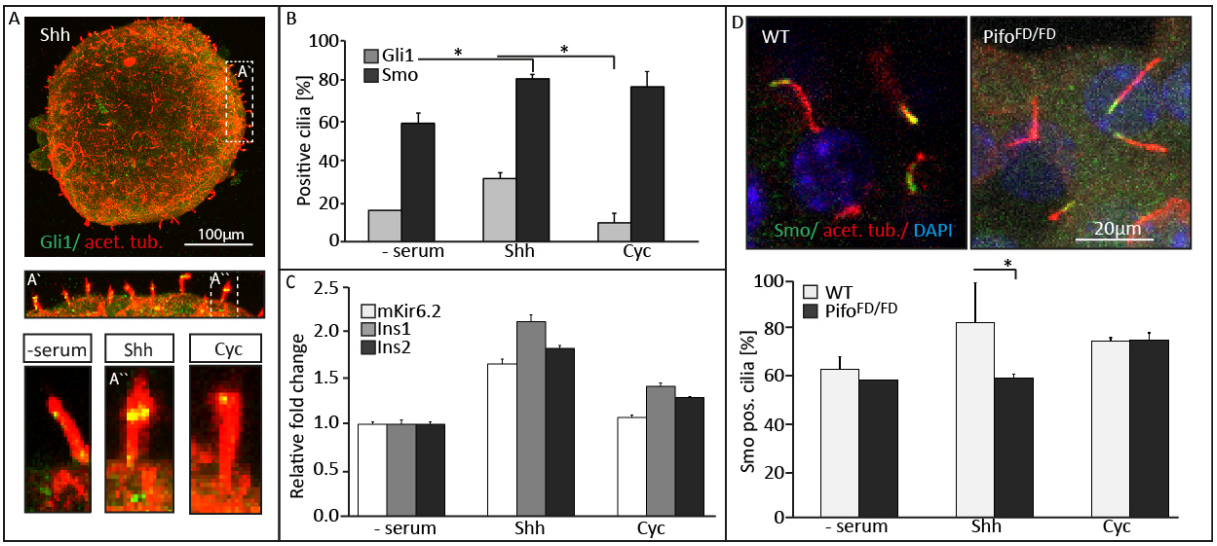

Figure 29 Sonic Hedgehog (Shh) *in vitro* assy on islolated pancreatic islet. (A) Confocal laser scanning microscopy (CLSM) of an isolated wild type (WT) islet stained with Gli family zinc finger 1 (Gli1, green) and acetylated tubulin (acet. tub., red, ciliary marker) after 24 hrs of Shh incubation. (A`) Magnification of the indicated pannel (dottet line). The three lower pannels depict a further magnification, showing single cilia and Gli1 positive staining after 24 hrs of serum free (-serum), (A``) Shh (dottel line in A`), and cyclopamine (Cyc) treatment, respectively. (B) Evaluatin of positive cilia for Gli1 and Smothened (Smo) staining. (C) Real-time quantitative PCR (qPCR), showing relative fold induction of the potassium channel subunit (mKir6.2), insulin 1, 2 (Ins1, 2) of WT islets induced with Shh or Cyc, error bars showing three technical replicates. (D) CLSM of WT and Pifo$^{FD/FD}$ mutant islets comparing Smo positive cilia after 24 hrs of Shh induction. Quantification of Smo positive cilia after serum starvation, Shh or Cyc induction, respectively. ($p < 0.05$, "*" is considered to be statistically relevant).

2.2.1.3 Islet architecture insulin secretion in Pifo$^{FD/FD}$ mutant islets

The islet cell structure is highly ordered and composed primarily of β-cells (80 %) and surrounded by α-cells (20 %), and lower numbers of δ-cells, DD and epsilon cells (Bosco et al. 2010; Kilimnik et al. 2010). Islets are a sensitive read-out system for changed metabolic demand, such as pregnancy, or in insulin-resistant states, as islet and β-cell masses increase to meet metabolic requirements. As Pifo is expressed in pancreatic islets, most likely in β-cells, I examined the influence of Pifo deletion on islets cell composition at various ages (1.5 – 18 months) and compared Pifo$^{FD/FD}$ mutant cryo-sections to WT. In order to distinguish the different cell types within the pancreatic islets CLSM marker analysis was applied, using anti-insulin antibody as β-cell marker and anti-glucagon as α-cell marker (**Figure 30**A). The insulin and glucagon staining of WT and Pifo$^{FD/FD}$ mutant islets revealed no obvious differences. Quantification of positive glucagon cells, in order to analyze the α-cell amount in 2 – 18 months old islets showed also no difference between WT and Pifo$^{FD/FD}$ mutant islets (**Figure 30**C). Though, the cell area of 18 months old Pifo$^{FD/FD}$ mutant islets was significantly decreased (**Figure 30**B), suggesting either higher apoptosis or a cell proliferation defect, though islet cell proliferation is decreased in 17 month old islets to under 1 % proliferation rate (Stolovich-Rain et al. 2012). When investigating the proliferation of 1.5 months old islets by Ki-67 marker analysis, no difference was found in Pifo$^{FD/FD}$ mutant islets, compared to WT (**Figure 30**D). As Shh had an influence on insulin mRNA expression, I in a next step analyzed the glucose stimulated insulin secretion (GSIS) in Pifo$^{FD/FD}$ mutant islets. Therefore, I isolated islets of 1.5 – 9 months old and Pifo$^{FD/FD}$ mutant mice and incubated them for 1 hr in glucose (16.8 mM). Insulin

secretion was analyzed using an Insulin ELISA Kit (Crystal Chem INC.) as described in 4.2.1.3.5. Interestingly, 1.5 months old Pifo$^{FD/FD}$ mutants islets did not respond at all to the glucose exposure, compared to WT (**Figure 30**E). At three and nine months of age the insulin secretion was impaired in Pifo$^{FD/FD}$ mutant islets compared to WT, with an extremely significant decrease in insulin secretion at three months. These results suggest a role for Shh signaling and Pifo in insulin secretion, and moreover an eventual role of Pifo in T2D, as it is characterized by diminished or inappropriate secretion of insulin.

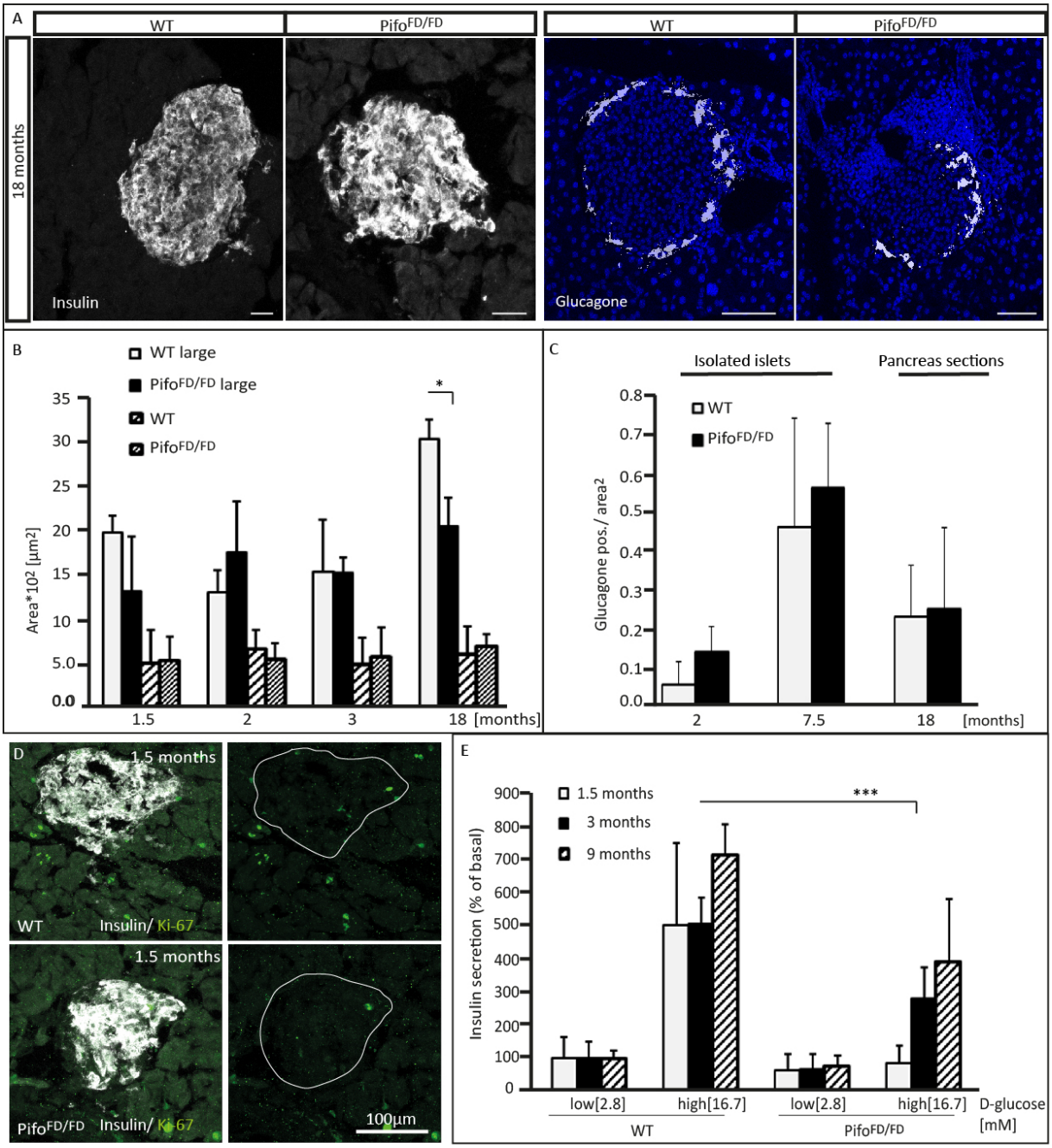

Figure 30 Islet architecture and insulin secretion. (A) Confocal laser scanning microscopy (CLSM) of insulin and glucagone staining of cry-sections of 18 months wild type (WT) and Pifo$^{FD/FD}$ mutant pancreas, respectively. 4', 6-diamidino-2-phenylindole (DAPI, blue) counter staining. (B) Evaluation of islet area after 1.5 – 18 months, respectively, with a significant reduced islet size in large islets of Pifo$^{FD/FD}$ mutant mice after 18 months. (C) Quantification of glucagone positive cells per islet area after 2, 7.5, and 18 months. (D) CLSM of pancreatic sections of 1.5 months old WT and Pifo$^{FD/FD}$ mutant mice, showing insulin (white) and antigen Ki-67 (green, proliferation marker) double staining. (E) Glucose stimulated insulin secretion (GSIS)

after 1.5, 3, and 9 months. Throughout the different months Pifo$^{FD/FD}$ mutant islets show a reduced insulin secretion. ($p < 0.05$, "*" is considered to be statistically relevant, and $p < 0.001$, "***", is considered to be extremely statistically relevant).

2.2.2 Function of Pifo in metabolic control

Glucose is transported through GLUT2 in mice, metabolized by glycolysis in order to generate ATP and pyruvate, necessary to close the ATP sensitive potassium-channels (Brunham et al. 2007). The constant closure of the channels leads to a depolarization of the membrane, an opening of the voltage-dependent Ca^{2+} channels, and a subsequent Ca^{2+} influx and insulin efflux into the extracellular space.

2.2.2.1 Impaired insulin secretion and glucose intolerance

T2D is thought to involve both, a first decline of insulin sensitivity and a decrease in β-cell function, although the order of events is not entirely clear, yet. This can be either due to diminished or inappropriate secretion of insulin or reduced β-cell mass (Prentki and Nolan 2006). It is known that under a normal diet, many gene mutations in mice show no overt phenotypes. For example, mice genetically ablated for macroH2A1, a variant of histone H2A, a key chromatin regulator during cell proliferation and differentiation, show no difference in body weight and sensitivity to glucose or insulin under a chow diet, but under HFD the phenotype evolves (Sheedfar et al. 2014). Thus, a recent study provided a molecular explanation for the decrease in GSIS caused by HFD feeding (Ohtsubo et al. 2011). The mechanism underlying involves the nuclear exclusion of Foxa2 and Hnf1a in β-cells and a subsequent reduction of a glycosyltransferase required to form the N-linked oligosaccharide side chain of GLUT2. This side chain is required for the receptor's cell-surface expression and reduction of GLUT2 side chain leads to receptor internalization, reduced cell-surface expression, and reduced GSIS. As *Pifo* was initially found as Foxa2 target gene, and Pifo$^{FD/FD}$ mutant islets show an impaired insulin secretion, it is likely that Pifo is also involved in the HFD-dependent insulin secretion process. I therefore challenged Pifo$^{FD/FD}$ mutant compared to WT cohorts of eight animals on a 12 week HFD and compared them to WT cohorts. The monitored body weight revealed no significant difference between Pifo$^{FD/FD}$ mutant and WT cohorts (**Figure 31**A). Measuring food consumption revealed, that the overall consumption increased over time, and that Pifo$^{FD/FD}$ mutant animals had a significant higher food-uptake rate compared to WT cohorts (**Figure 31**B). But the body fat detected by NMR measurements revealed no difference between Pifo$^{FD/FD}$ mutant and WT cohorts, suggesting that WAT is not affected (**Figure 31**C). Lack of the anabolic hormone insulin due to an insulin-secretion defect might explain why a higher calorie uptake upon HFD feeding in Pifo$^{FD/FD}$ mutant mice does not lead to increase body weight compared to WT cohorts. But why can Pifo$^{FD/FD}$ mutant mice gain weight at all upon HFD if they have lower insulin amount? Is the insulin amount for GTT and weight gain upon HFD feeding still enough, but too little to store the additional calories from higher food intake? These are questions which we still have to address.

As insulin resistance can be a cause for higher energy storage and in order to investigate where the extra calories were stored after HFD, metabolically active organs were weight (**Figure 31**G). Analyzing the organ weight of liver, epididymal fat pad, and pancreas, no obvious difference was found. But analyzing the liver fat

storage, Pifo$^{FD/FD}$ mutant showed hepatosteatosis (in more detail see **Figure 32**A). Hepatosteatosis is characterized by lipid deposition within the liver and associated with insulin resistance and the metabolic syndrome, by means of hyperglycemia (Cuthbertson et al. 2014). But hepatosteatosis is also found in NAFLD, characterized by decreased insulin signaling leading to hepatic insulin resistance and T2D (Birkenfeld and Shulman 2014). It is therefore likely the extensive lipid storage in Pifo$^{FD/FD}$ mutant mice, is caused by an overall insulin resistance and subsequent β-cell compensation failure. Thus, in accordance with published data the higher calorie uptake of Pifo$^{FD/FD}$ mutant mice could be a result of an overall insulin secretion defect. Blood glucose levels, measured before start of HFD by intraperitoneal glucose tolerance test (ipGTT) showed no difference between four months old WT and Pifo$^{FD/FD}$ mutant cohorts. However, after 12 weeks on HFD Pifo$^{FD/FD}$ mutant cohorts were found to be glucose intolerant (**Figure 31**E, F). Compared to WT, Pifo$^{FD/FD}$ mutants were not able to clear the blood glucose after 60 minutes of glucose injection. Before the start of HFD feeding, basal insulin levels after fasting showed a significant lower amount of insulin in the blood plasma in Pifo$^{FD/FD}$ mice (**Figure 31**D). The plasma insulin response was significantly delayed in Pifo$^{FD/FD}$ mutant cohorts after HFD feeding, as the peak of insulin secretion was found at 30 minutes after glucose injection in WT cohorts, and at 120 minutes in Pifo$^{FD/FD}$ mutant cohorts. The insulin secretion was measured after HFD feeding by GSIS and again found to be lower in Pifo$^{FD/FD}$ mutant islets, compared to WT control islets (**Figure 31**H). Additionally, the total insulin amount was also decreased in Pifo$^{FD/FD}$ mutant cohorts, compared to WT cohorts after 12 weeks of HFD feeding (**Figure 31**I). These results confirm the previous found insulin secretion defect in Pifo$^{FD/FD}$ mutant islets and suggest that compensatory mechanisms are already in place before the HFD challenge, as we detect lesser basal insulin secretion already under chow diet. With the application of an insulin tolerance test (ITT) which is commonly used to evaluate insulin sensitivity, we will be able to assess the sensitivity of insulin-responsive tissues in the Pifo$^{FD/FD}$ mutant mice. Taken together, under normal metabolic conditions Pifo$^{FD/FD}$ mutant mice display lesser total insulin and an insulin secretion defect, without displaying major metabolic defects. However, under HFD challenged conditions the insulin secretion defect is accompanied with glucose intolerance, suggesting a β-cell compensation failure upon HFD. Thus, an ITT will clarify whether this phenotype is due to an insulin resistance of the insulin-responsive tissues.

2.2.2.2 Decrease in beta-cell mass and proliferation after HFD

In the previous chapter I showed that insulin secretion is impaired in Pifo$^{FD/FD}$ mutant mice. It is likely that the insulin secretion defect is due to a lacking compensatory potential of β-cells for the higher insulin demand upon HFD feeding, which results in insulin secretion defect. In order to test a possible β-cell compensation failure, I analyzed the islet architecture in Pifo$^{FD/FD}$ mutant mice. The islet size of six months old HFD Pifo$^{FD/FD}$ mutant mice was similar to WT controls (**Figure 32**B, F). Next, analyzing the cell-composition of Pifo$^{FD/FD}$ mutant islets after 12 weeks of HFD revealed a decline in β-cell mass, compared to WT cohorts (**Figure 32**D). T2D is defined by insulin reduction and subsequent β-cell mass decline. As β-cell mass is controlled by several mechanisms including β-cell proliferation, neogenesis, hypertrophy, and survival, I analyzed β-cell proliferation in Pifo$^{FD/FD}$ mutant mice. Co-stainings of NKX6.1 with the proliferation marker Ki67, revealed a decrease in Pifo$^{FD/FD}$ mutant β-cells proliferation compared to WT (**Figure 32**C, E). Taken together, we have identified HFD-induced T2D in Pifo$^{FD/FD}$ mutant mice, as the β-cells mass declines upon HFD. Whether systemic insulin

resistance or a decreased hepatic insulin signaling is the cause of the Pifo$^{FD/FD}$ mutant phenotype is not clear, yet. Although we identified an insulin secretion defect under normal feeding conditions, under challenged HFD feeding conditions the susceptibility of Pifo$^{FD/FD}$ mutant mice to develop metabolic defects and insulin secretion defects is increased. We therefore discovered a novel mouse model system in order to study challenge induced predisposition to T2D.

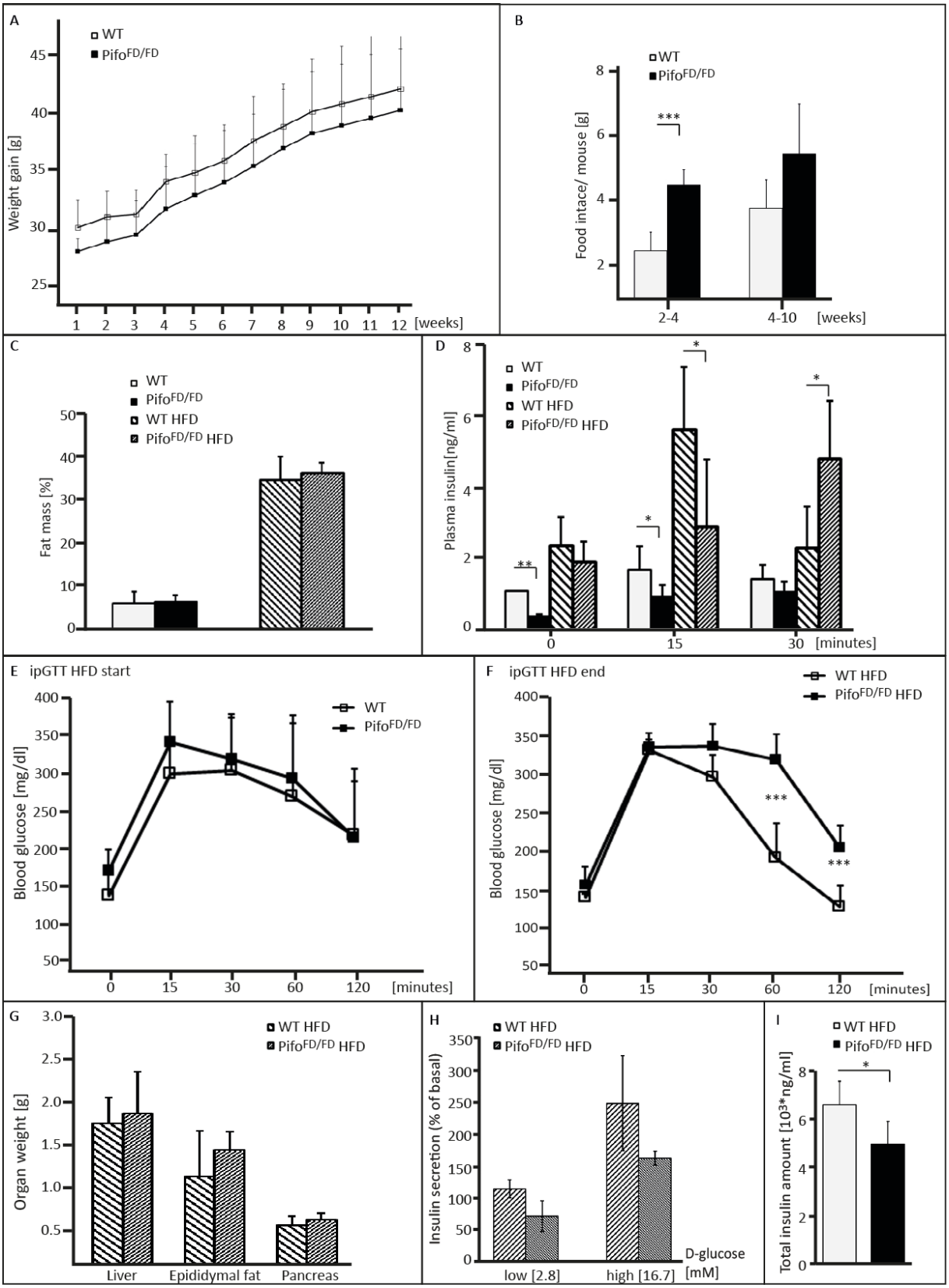

Figure 31 Glucose intolerance and insulin secretion defect after High fat diet (HFD). (A) Weight monitoring over three month of HFD, comparing wild type (WT) and Pifo$^{FD/FD}$ mutant mice (amount/ group = 8). (B) Calculated food intake monitored over the first 2 – 4 and 4 – 10 weeks. (C) Nuclear magnetic resonance (NMR) spectroscopy, before (WT, Pifo$^{FD/FD}$) and after (WT HFD, Pifo$^{FD/FD}$ HFD) HFD. (D) Plasma insulin levels before and after the HFD measured upon intraperitoneal glucose tolerance test (ipGTT). (E) IpGTT before and (F) after 12 weeks of HFD. (G) Organ weight of liver, epididymal fat pads and pancreas after 12 weeks of HFD. (H) In vitro glucose stimulated insulin secretion (GSIS) of islets from HFD mice. Decrease in insulin

secretion, and (I) total amount of pancreatic insulin of three animals after HFD. ($p < 0.05$, "*" is considered to be statistically relevant, and $p < 0.001$, "***", is considered to be extremely statistically relevant).

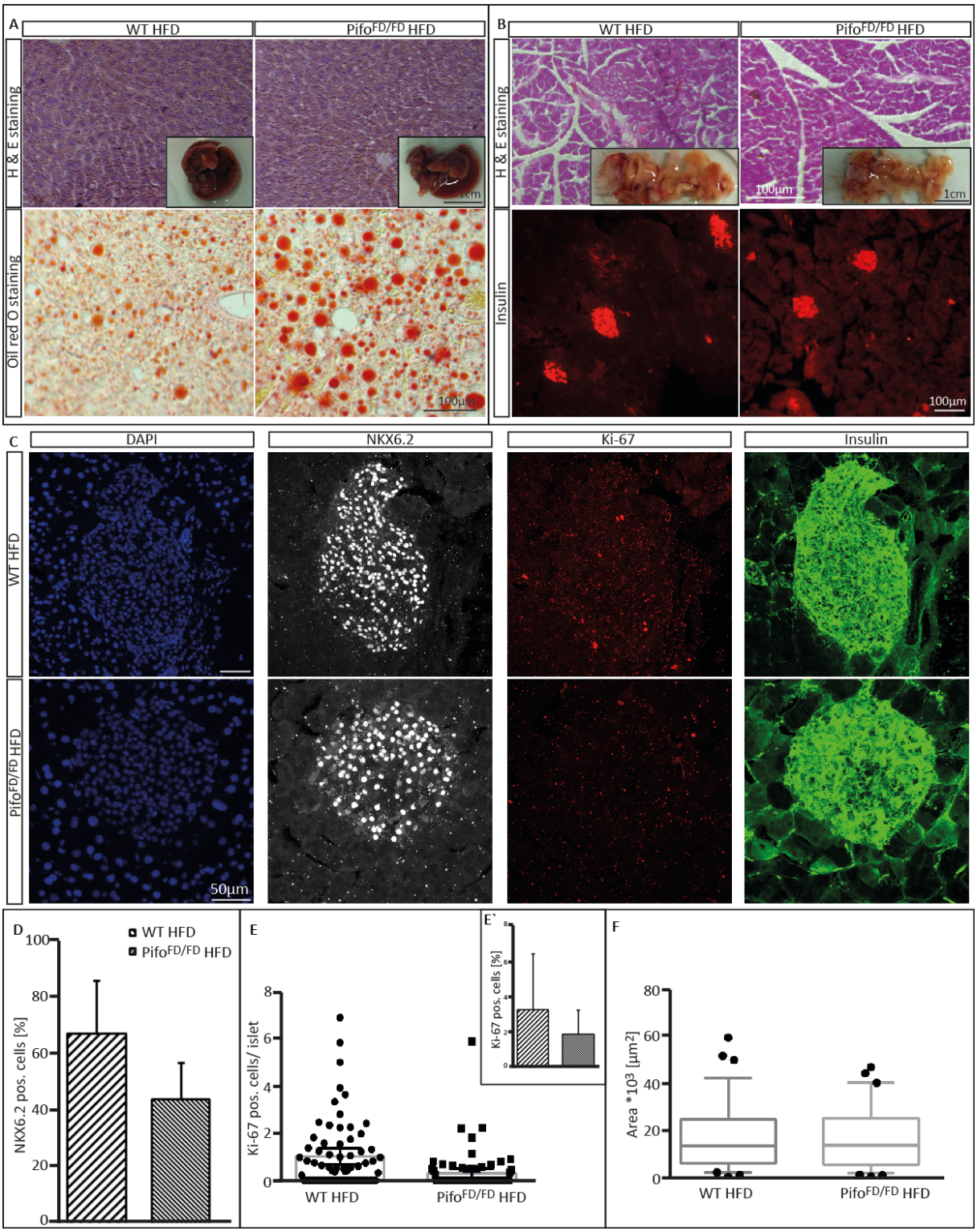

Figure 32 Insulin secretion defect effecting liver and pancreas after high fat diet (HFD). (A) Hematoxylin and eosin (H & E) staining of liver paraffin sections and whole mount liver image (insert), comparing WT and Pifo$^{FD/FD}$ mutant mice. Oil red O staining showing slightly increased amount of fat lipids in Pifo$^{FD/FD}$ mutant liver cryo-sections. (B) H & E staining of pancreas paraffin sections, whole mount pancreas image (insert), and insulin immunofluorescence staining after 12 weeks of HFD. (C) Confocal laser scanning microscopy (CLSM) of 4', 6-diamidino-2-phenylindole (DAPI, blue) counter staining, NK6 homeobox 2 (NKX6.2, white, beta cell marker), Ki-67 (red, proliferation marker), and insulin (green) staining, comparing WT and Pifo$^{FD/FD}$

mutant islets. (D) Evaluation of NKX6.2 positive cells, (E, E`) Ki-67 positive β-cells, and (D) calculation of islet area.

2.2.3 Influence on proliferation during pregnancy

Pregnancy is one of the most robust physiological stimuli of β-cell cell mass expansion in the adult pancreas, shown to be increased by enhanced proliferation of β-cells (Sorenson and Brelje 1997). In order to confirm the proliferation defect of β-cells in $Pifo^{FD/FD}$ mutant mice, the β-cell response was analyzed during pregnancy. For the pregnancy experiment, $Pifo^{FD/FD}$ mutant and WT female mice were mated with WT male mice. Mating was confirmed by the presence of a vaginal plug on the next morning, designated as day 0.5 of gestation. Pancreata of three months old $Pifo^{FD/FD}$ mutant and WT females were analyzed at day 14.5 of pregnancy, as in pregnant rodents, β-cells proliferation increases dramatically, with a peak occurring after mid gastrulation. In accordance with previous results, I could detect an insulin decrease in $Pifo^{FD/FD}$ mutant pancreas sections of pregnant females, when compared to WT (**Figure 33**A, B). Although, the α- (glucagon positive), β- (insulin positive), and δ-cell (somatostatin positive) masses were unaltered, I detected a decrease in proliferation (Ki-67 positive) in $Pifo^{FD/FD}$ mutant females after 14.5 days of pregnancy. Together, with previous observed proliferation decrease upon HFD feeding, these results again suggest a β-cells proliferation defect in $Pifo^{FD/FD}$ mutants.

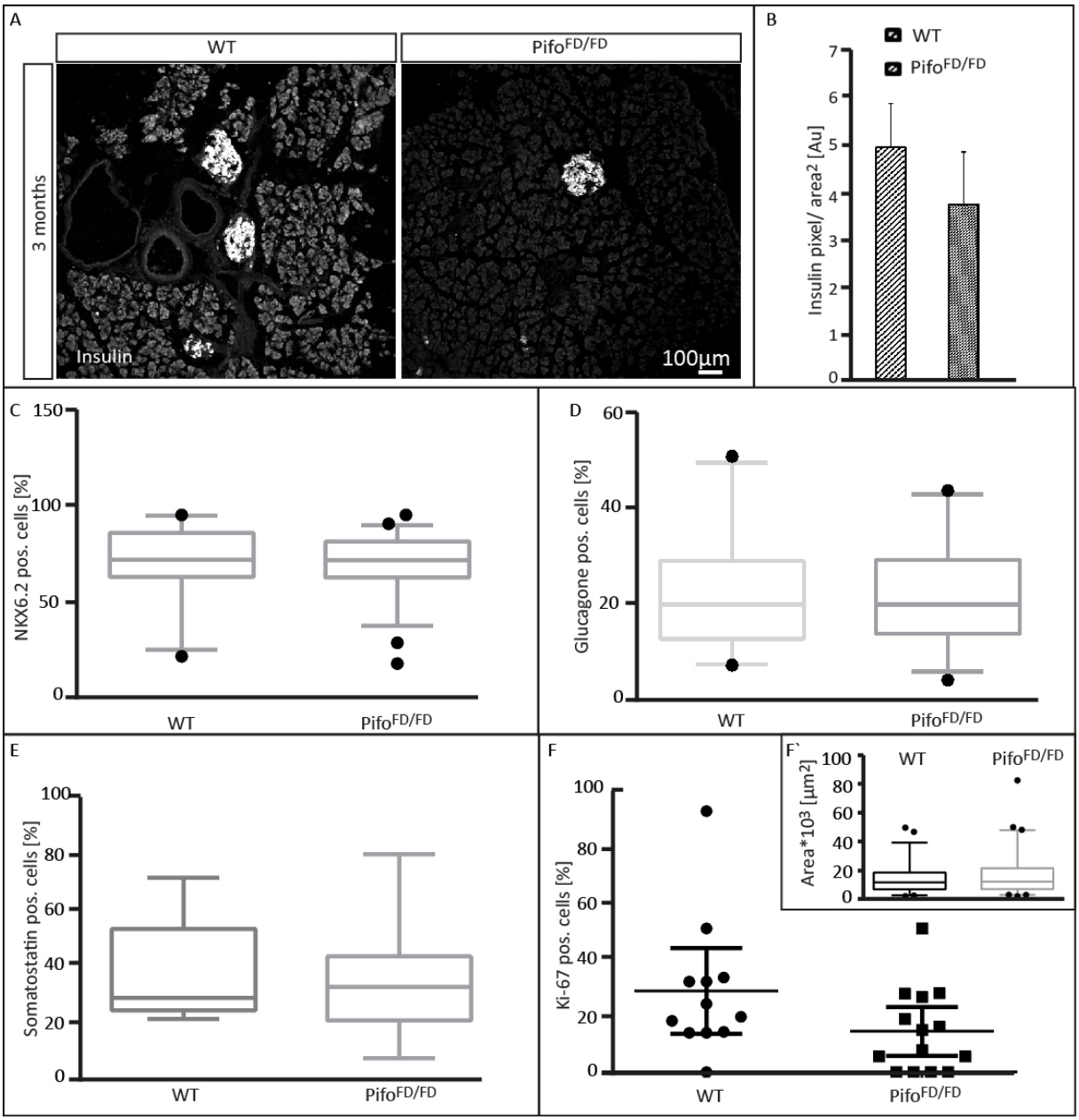

Figure 33 Islet architecture and insulin secretion during pregnancy. (A) Insulin immunofluorescence staining of three months old pancreatic cryo-sections of 14 day pregnant wild-type (WT) and Pifo$^{FD/FD}$ mutant female mice. (B) Evaluation of insulin intensity/ islet area as a measure of insulin secretion. (C) Evaluation of confocal laser scanning microscopy (CLSM) images stained with NK6 homeobox 2 (NKX6.2, beta-cell marker), (D) glucagone (alpha-cell marker), (E) somatostatin (delta-cell marker), and (F) Ki-67 (proliferation marker), comparing WT and Pifo$^{FD/FD}$ mutant cryo-sections. (F`) Evaluation of islet area of WT and Pifo$^{FD/FD}$ mutant pancreatic cryo-sections.

2.2.4 Cell-cycle mechanism

Pifo$^{FD/FD}$ mutant mice develop both, an insulin secretion defect as well as the decline in β-cell mass, accompanied with a proliferation decrease. Thus, *Pifo* is expressed in pancreatic β-cells. To further address which mechanism or pathway is underlying the β-cells proliferation defect phenotype, I concentrated on the previously published CDK4-pRB-E2F1 pathway for β-cell proliferation (Annicotte et al. 2009). It was shown that CDK4-pRB-E2F1 pathway mediates, pancreatic growth and β-cell proliferation (G1 phase), as well as insulin

secretion. Therefore, I first analyzed the expression level of the pathway involved target genes in an age-dependent manner. The pathway target gene p16ink4a e.g., which is a cell-cycle inhibitor, it known to be expressed in aged mice (Zeng et al. 2013). I could confirm the increased expression levels of p16ink4a, encoded by the gene Cdkn2a in humans, which expression is doubled after six months, and further increased upon age in WT islets (**Figure 34**A). Ki-67 expression maximum was also found after six month, with a 5 – 6 fold increase. Although not highly expressed, Cdk4 followed the same expression pattern, with an expression maximum after six months. The two forms of mouse insulin subjected some fluctuations over the age, with an overall higher expression after six months. Next, I compared the target gene expression of 5 – 6 months old WT and $Pifo^{FD/FD}$ mutant islets (**Figure 34**B). Quantitative PCR revealed a dramatic downregulation of *E2F1* TF, a direct target gene of the CDK4-pRB-E2F1 pathway, as well as *insulin 1* in $Pifo^{FD/FD}$ mutant islets compared to WT controls (**Figure 34**B). *P16ink4a* was slightly increased and surprisingly, the *Kir6.2* subunit of the potassium channel, which was reported to act downstream of the *E2F1* TF, was three-fold increased mRNA expression. These results suggest a role for Pifo in the CDK4-pRB-E2F1 β-cell proliferation pathway. In WB analysis, the Cdk4 kinase, important for G1-phase transition, was found to be significantly decreased in the NT of E10.5 $Pifo^{FD/FD}$ mutant islets (**Figure 12**E), suggesting a role for Pifo in cell-cycle regulation. Thus, pRB and E2F1 proteins were downregulated and Kir6.2 protein was upregulated in $Pifo^{FD/FD}$ mutant islets. As the CDK4-pRB-E2F1 pathway previously was linked to insulin secretion and $Pifo^{FD/FD}$ mutant mice developed an insulin secretion defect, I further confirmed these results by GSIS and measurement of total insulin amount in young and old $Pifo^{FD/FD}$ mutant mice (**Figure 34**C, D). I could again show that the insulin secretion is already impaired at two months of age *in vitro*. The total insulin amount is similar in $Pifo^{FD/FD}$, $Pifo^{FD/WT}$, and WT pancreata at two month of age and decreased in $Pifo^{FD/FD}$ mutant islets upon aging, as shown in 11 months old pancreata. Taken together, Pifo is a regulator in the CDK4-pRB-E2F1 pathway, as it directly regulates the target genes and loss of Pifo leads to an impaired insulin secretion. As the Kir6.2 channel is upregulated, the secretion lower, and the total amount of insulin unaltered in $Pifo^{FD/FD}$ mutant pancreata, it is likely that $Pifo^{FD/FD}$ mutant mice compensate the insulin secretion defect with upregulation of the upstream machinery. Thus, as *Pifo* was initially identified as Shh target gene, I preliminarily investigated Shh target gene regulation in $Pifo^{FD/FD}$ mutant islets. Therefore, I compared *Gli1* expression in WT and $Pifo^{FD/FD}$ mutant islets, as previous *in vitro* assays revealed a Gli1-mediated Shh defect in $Pifo^{FD/FD}$ mutant PLCs. *Ptch1* was also analyzed as it is a known Shh target gene. Preliminary q-PCR analysis revealed an induction of *Gli1* and *Ptch1* expression in WT islets after 24 hrs of Shh induction (**Figure 34**F). In fact, *Gli1* as well as *Ptch1* were reduced in $Pifo^{FD/FD}$ mutant islets after 24 hrs of Shh induction. Thus, Gli1 protein was downregulated in $Pifo^{FD/FD}$ mutant islets (**Figure 34**E). This suggests a role for both signaling pathways, Shh and CDK4-pRB-E2F1, in β-cell dysfunction of $Pifo^{FD/FD}$ mutant islets. The connection of both pathways and the precise mechanism how Pifo influences β-cell proliferation and insulin secretion needs to be further elucidated. An approach could be to study the regulation of cyclinD1, which is a G1 to S phase cell-cycle regulator and a Shh target gene (Kenney and Rowitch 2000). Moreover cyclinD1 interacts with Cdk4, which we identified as Pifo interacting protein.

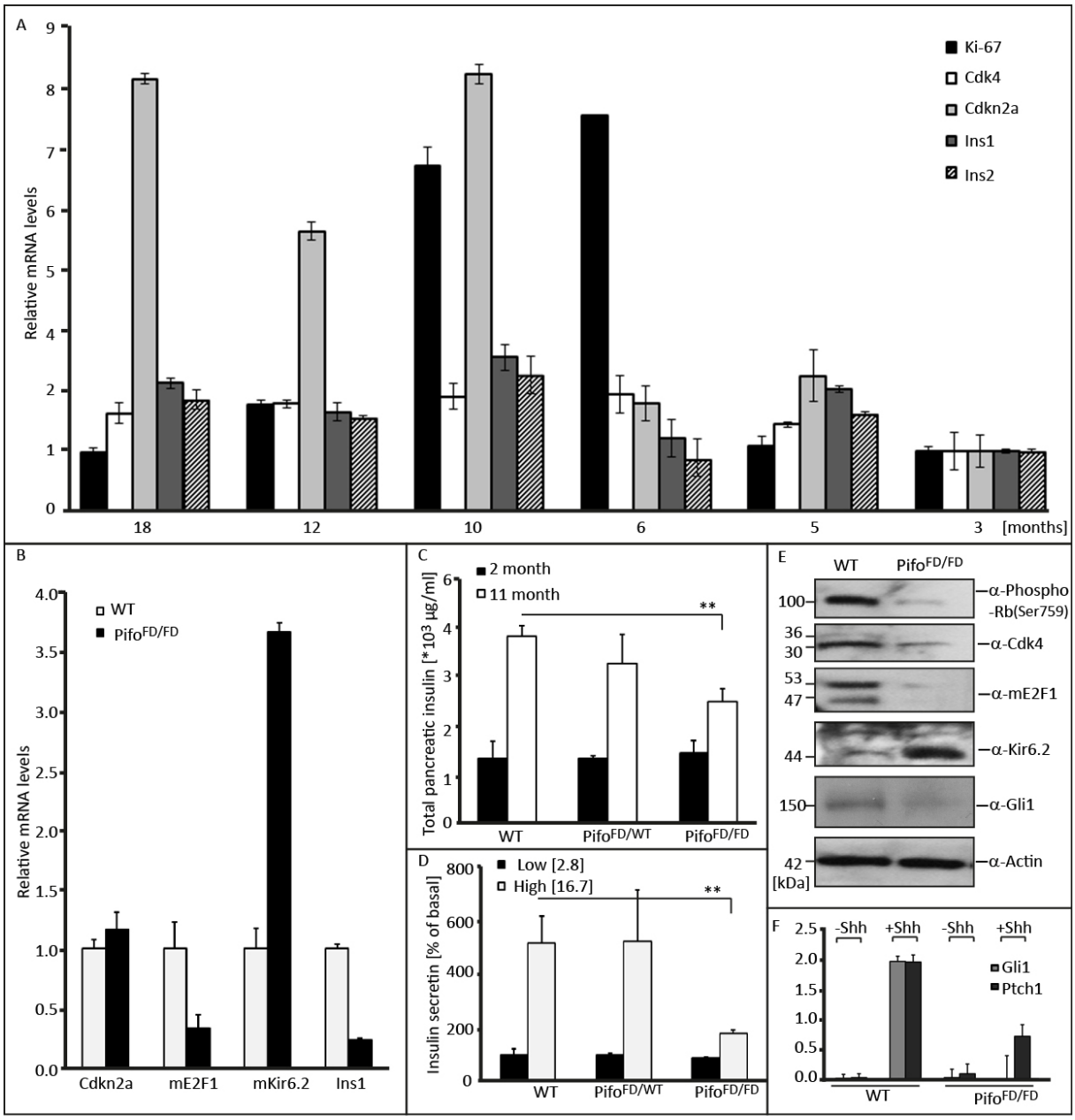

Figure 34 Islet G1-S phase progression and CDK4-pRB-E2F1 (cyclin-dependent kinase 4, retinoblastoma protein, E2F1 transcription factor) pathway activation. (A) Real-time quantitative PCR (q-PCR) showing relative mRNA expression of different proliferation target genes (proliferation marker Ki-67), CDK4 for G1-S phase progression, cyclin-dependent kinase inhibitor 2A (p16ink4a) encoded by Cdkn2a in humans, and insulin type1 and 2 (Ins1, 2) in wild type (WT) islets at different ages (3 – 18 months). (B) Q-PCR of WT vs. Pifo$^{FD/FD}$ mutant6 months old isolated islets. TF mE2F1 and Ins1 are downregulated and the potassium channel subunit mKir6.2 is highly upregulated in Pifo$^{FD/FD}$ mutant islets. (C) Total pancreatic insulin at 2 and 11 months of age, comparing WT, Pifo$^{WT/FD}$, and Pifo$^{FD/FD}$ mutant islets. (D) Glucose-stimulated insulin secretion (GSIS) of two month old WT, Pifo$^{WT/FD}$, and Pifo$^{FD/FD}$ mutant islets, showing a dramatic decrease in insulin secretion in Pifo$^{FD/FD}$ mutants. (E) Western blot (WB) analysis showing downregulation of, p-Rb, Cdk4, mE2F1, and Gli family zinc finger 1 (Gli1, Sonic Hedgehog (Shh) target gene), and up-regulation of Kir6.2 in Pifo$^{FD/FD}$ mutant islets. (F) Q-PCR analysis of Shh induced WT and Pifo$^{FD/FD}$ mutant islets over 24 hrs. Patched 1 (Ptch1), and Gli1 down-regulation in Pifo$^{FD/FD}$ mutant isolated islets. ($p < 0.01$, "**", is considered to be highly statistically relevant).

A main regulation in Pifo$^{FD/FD}$ mutant islets seems to occur at the Kir6.2 subunit, as its expression is dramatically increased, with significant decrease of E2F1 TF, which was previously reported as downstream target of the

CDK4-pRB-E2F1 pathway. In order to test this hypothesis further, I performed an *in vivo* experiment, using glibenclamide which is an antidiabetic drug and used for T2D patients, in order to stimulate the insulin secretion (Ding et al. 2013). The β-cell potassium-channel is composed of Kir6.2 and SUR1 (Inagaki et al. 1995). Glibenclamide acts at the level of the potassium-channel with a constant polarization of the PM, leading to an opening of Ca^{2+} channels and subsequent insulin secretion, and blood glucose decrease. In order to analyze a possible defect of the potassium-channel in $Pifo^{FD/FD}$ mutant mice, I applied glibenclamide to 5 – 6 months old $Pifo^{FD/FD}$ mutant cohorts and compared them to WT controls. Before the application of glibenclamide, at the time point 0, the fasted plasma insulin levels were significantly reduced in $Pifo^{FD/FD}$ mutant cohorts (**Figure 35**A). This is accompanied with the previous observed plasma insulin levels (Figure 31D). Upon glibenclamide applicatin no difference in plasma insulin levels were found in $Pifo^{FD/FD}$ mutant mice compared to WT mice (**Figure 35**B). The ipGTT measurement showed no significant difference between $Pifo^{FD/FD}$ mutant and WT cohorts. These results show that by induced activation of the potassium-channel by glibenclamide, no defect in insulin secretion is measurable, suggesting a defect on the level of Kir6.2 subunit in $Pifo^{FD/FD}$ mutant mice. Thus, mutations in the potassium channel genes KCNJ11 and ABCC8 increases the susceptibility to T2D (Qiu et al. 2014; Takagi et al. 2013). With the influence of Pifo deletion on the potassium channel and the previous found HFD feeding induced β-cells mass decline we might have discovered a novel mouse model system in order to study challenge-induced predisposition to T2D. Through which pathway Pifo is regulated during β-cells progression is not clear, yet. Eventually a connection exists between the CDK4-pRB-E2F1 and Shh pathway.

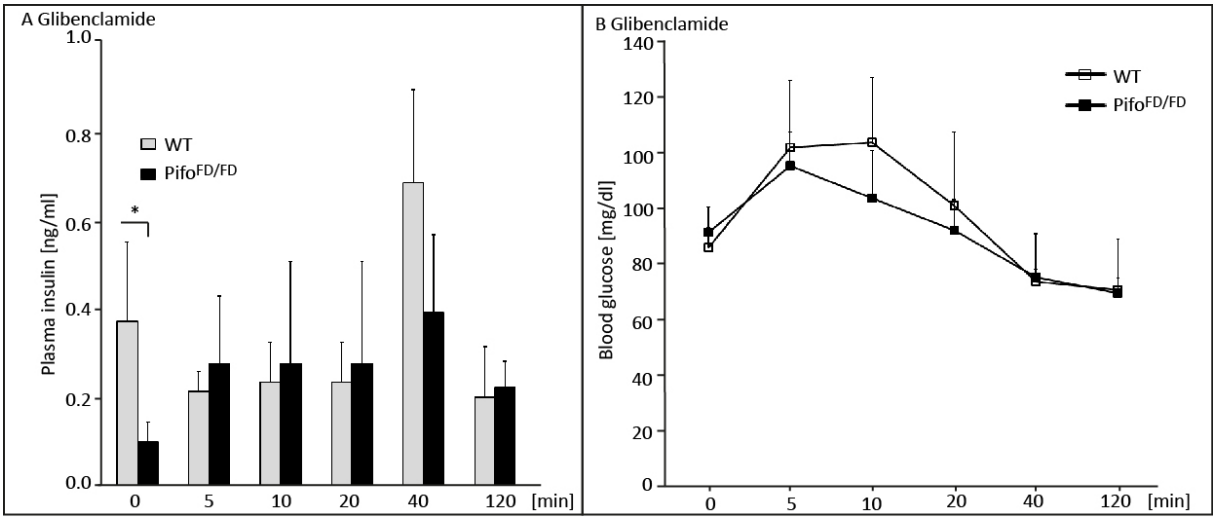

Figure 35 Constant activation of the potassium-channel subunit Kir6.2. (A) Plasma insulin before (0 minutes) and after (5 – 120 minutes) glibenclamide intraperitoneal injection (ip), comparing wild-type (WT) and $Pifo^{FD/FD}$ mutant mice cohorts (amount/ group = 6). (B) Blood glucose was simultaneously measured. ($p < 0.05$, "*" is considered to be statistically relevant).

2.2.5 Pifo SNP in human cohorts

Translating the mouse phenotype into human, our collaboration partner Prof. Harald Steiger and his group in Tübingen found glucose intolerant subjects in pre-diabetic patients with a single nucleotide (SNP) polymorphism in the 3`UTR of the *Pifo* gene (data not shown). When observing the insulinogenic index [(insulin

after 30 min – insulin after 0 min) / (glucose after 30 min – glucose after 0 min)] of these two patients it was lower compared to healthy patients. In one of these patients an additional insulin secretion defect was found. The insulin secretion thereby was calculated as AUC C-peptide 0 – 120 min) / (AUC glucose 0 – 120 min and was found to be reduced. The blood sugar value after two hours of glucose intake was also higher in that patient. These data are comparable to the phenotype found in $Pifo^{FD/FD}$ mutant mice, as they show an insulin secretion defect and glucose intolerance upon HFD, and further suggesting a role for *Pifo* in human diabetic patients.

2.2.6 Analysis of Gprasp2 in adult organs

2.2.6.1 Gprasp2 LacZ expression in lung and pancreas

Gprasp2 was previously identified as Pifo interacting partner. It was shown to form a heterotrimeric Pifo-Gprasp2-Smo complex, which is Gli-mediated and Shh dependent. It is expressed in the NT and LB (**Figure 21**, **Figure 22**). Gprasp2 is located on the X chromosome, and homozygous (Gprasp2$^{GT/GT}$) females and hemizygous (Gprasp2$^{GT/y}$) males are viable and fertile (**Figure 20**).

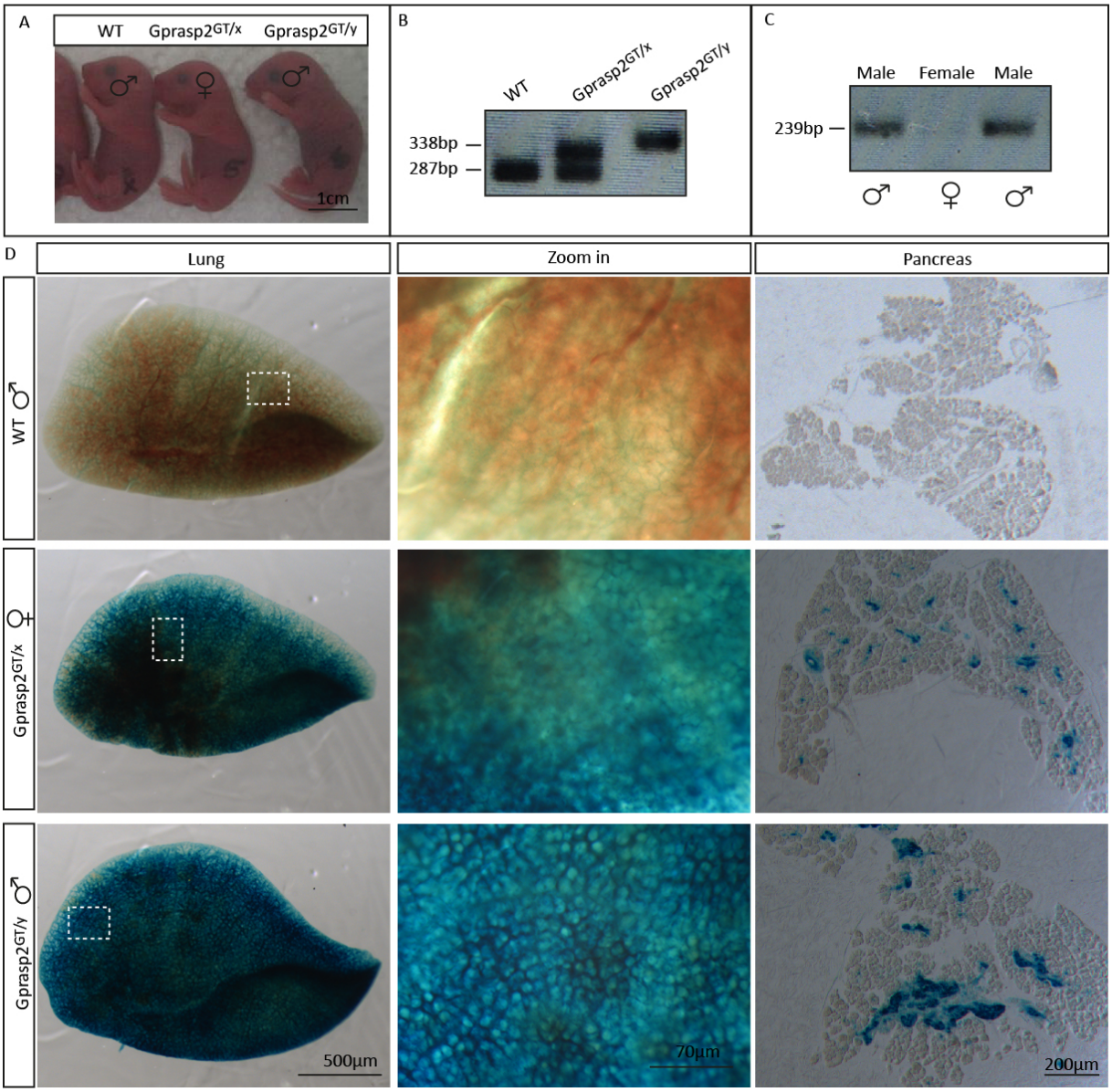

Figure 36 LacZ expression of *G-protin coupled associated sorting protein 2 (Gprasp2)* at postnatal day 1 (P1). (A) Normal appearance of P1 pubs before dissection. (B) RT-PCR showing Gprasp2 genotyping of wild-type (WT), heterozygous (Gprasp2$^{GT/x}$), and hemizygous (Gprasp2$^{GT/y}$) pubs, bands at 338 bp and 287 bp. (C) RT-PCR of SRY genotyping showing a band at 239 bp in case of male confirmation. (D) LacZ staining of whole mount lung, a zoom in (dotted line), and pancreas paraffin sections, for the genotypes shown in A-C, respectively.

In order to further study a possible adult phenotype, the *Gprasp2* LacZ expression in adult tissues was analyzed at postnatal day 1 (P1). WT, Gprasp2$^{GT/x}$ heterozygous and Gprasp2$^{GT/y}$ mutants were compared and LacZ expression was found in the lung and pancreas (**Figure 36**). Compared to the WT control, already Gprasp2$^{GT/x}$ lung showed a strong overall expression. In the pancreas the expression was restricted to the islets of Langerhans, and knowing that the majority of cells within the islets are β-cells, this result might already suggest a role for Gprasp2 in β-cell function.

2.2.6.2 Gprasp2 adult phenotype in liver and pancreas

To analyze the Gprasp2 GT mouse line in more detail, I examined adult mice at 3-6 months. I observed that approximately at the age of five months the Gprasp2$^{GT/y}$ mutant males become obese, compared to WT litter controls, although the onset of diabetes was variable (**Figure 37**A). Therefore, I weighted the mice at the onset of obesity at five months, and compared those to old mice at 18 months (**Figure 37**B). Strikingly, the old Gprasp2$^{GT/y}$ mutant males were indeed, obese. Thus, already at five months the fat-mass percentage of the Gprasp2$^{GT/y}$ mutant males was increased by two folds (**Figure 37**C). In order to analyze the obese phenotype in more detail, I weighted various organs to observe whether Gprasp2$^{GT/y}$ mutants store their energy in form of fat. In fact, Gprasp2$^{GT/y}$ mutants showed higher lipid storage in the liver, and epididymal fat pad, compared to WT cohorts, already at the age of five months (**Figure 37**D). At the age of 18 months the phenotype is more distinct as the liver weight is increased by almost three fold, and the epididymal fad pad weight is increased four fold (**Figure 37**E), suggesting that the obese phenotype becomes more distinct during aging. In order to confirm the steatosis of Gprasp2$^{GT/y}$ mutant livers, I performed an Oil-Red-O staining in order to visualize the higher amount of lipid storage in Gprasp2$^{GT/y}$ mutant liver cryo-sections (**Figure 37**G). As already mentioned, Gprasp2$^{GT/y}$ mutant livers were heavier, subsequently bigger in size, and due to the lipid storage also lighter by visual control. Extensive amounts of fat infiltrating the liver is found in NAFLD, and often observed as one consequence of the current obesity epidemic (Fraulob et al. 2010). As mentioned earlier, there are two theories of how NAFLD evolves: Either by β-cell defect, leading to less insulin production and subsequent fat infiltration, or by insulin resistance of the periphery and the liver, and a subsequent β-cell compensation failure due to an higher insulin demand, leading to T2D (Cuthbertson et al. 2014).

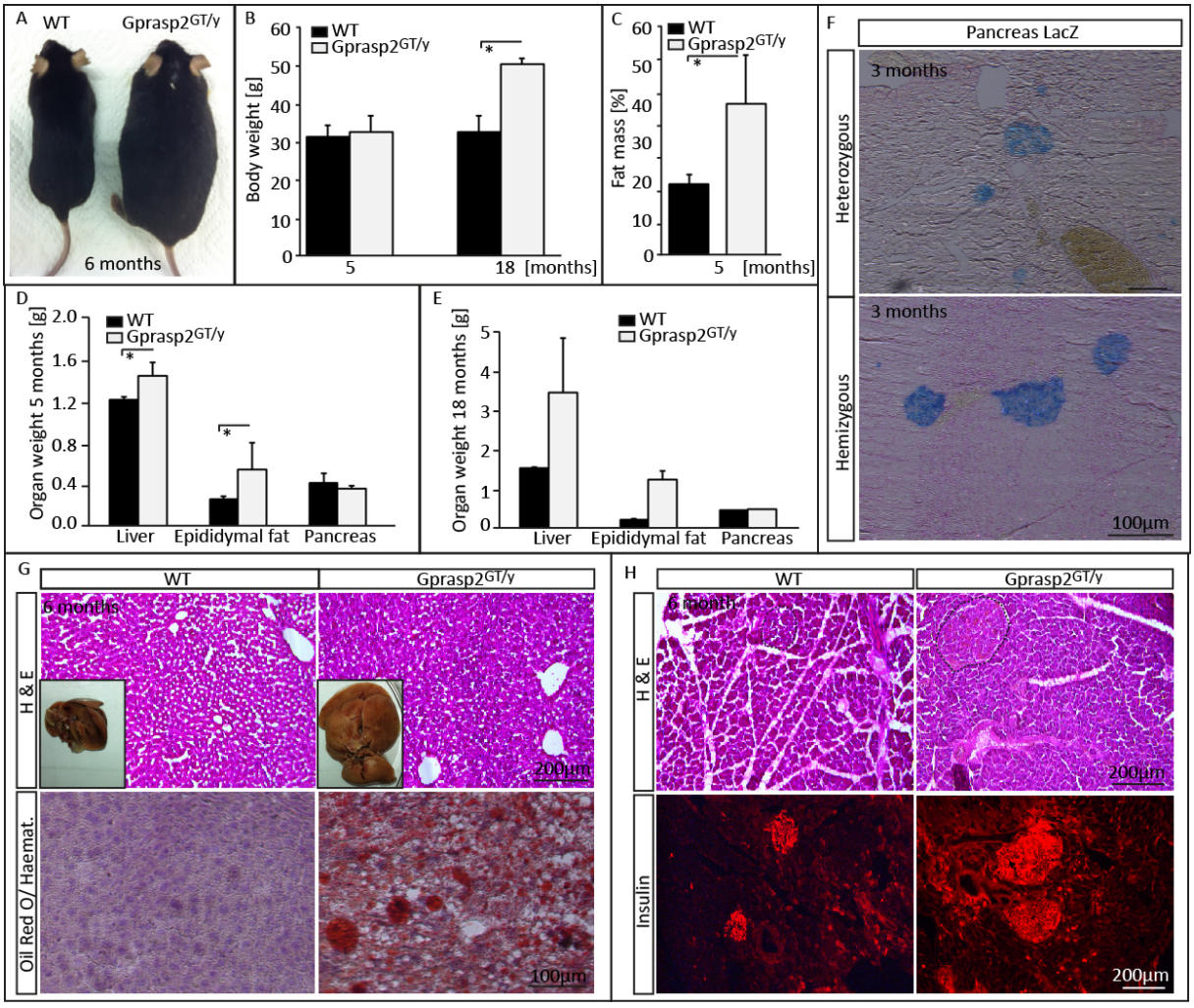

Figure 37 G-protin coupled associated sorting protein 2 (Gprasp2) adult phenotype. (A) Six months, old male mice, showing obesity of the Gprasp2$^{GT/y}$ mutant male (right) compared to the wild-type (WT, left) control. (B) Body weight comparing WT and Gprasp2$^{GT/y}$ mutant males at five months and 18 months, showing a significant increase of Gprasp2$^{GT/y}$ mutant males after 18 months. (C) Nuclear magnetic resonance spectroscopy (NMR) data showing a significant increase of body fat mass (lean mass/ fat mass) of five months old Gprasp2$^{GT/y}$ mutant males. (D) Organ weight after five months and (E) after 18 months showing an increase in liver and epididymal fat pad weight in Gprasp2$^{GT/y}$ mutant males. (F) LacZ expression of paraffin sections of three months old pancreata of heterozygous (Gprasp2$^{GT/x}$) female and hemizygous (Gprasp2$^{GT/y}$) male, showing restricted expression to the islets of Langerhans. (G) Paraffin sectioned liver and liver image (insert) of WT and Gprasp2$^{GT/y}$ mutant mice after 6 months, showing haematoxilin and eosin (H&E) staining and cryo-sectioned liver sections, showing Oil-Red-O staining and haematoxilin (Haemat.) counterstaining. (H) H&E staining of 6 months old pancreata, and insulin immunofluorescence staining, showing an increase in islet size in Gprasp2$^{GT/y}$ mutant mice. ($p < 0.05$, "*" is considered to be statistically relevant).

As previously discovered, *Gprasp2* is expressed in the pancreas, exclusively in the pancreatic islets (**Figure 36**D). In order to confirm these results in adult Gprasp2$^{GT/y}$ mutant mice, LacZ stainings were performed comparing Gprasp2$^{GT/x}$ heterozygous and Gprasp2$^{GT/y}$ hemizygous expression pattern (**Figure 37**F). In addition to previous findings, *Gprasp2* LacZ expression was exclusively found in pancreatic β-cells (**Figure 37**E). However, the exclusive Gprasp2 β-cell expression needs to be further confirmed by co-staining with a β-cell specific marker. Knowing the majority of cells in islets are β-cells, I speculate that Gprasp2 is also expressed in β-cells. Therefore we analyzed the islets of Gprasp2$^{GT/y}$ hemizygous males in more detail. This showed an increase in islet size in

Gprasp2$^{GT/y}$ hemizygous mice when compared to controls (**Figure 37**E). In summary, Gprasp2$^{GT/y}$ mutant mice develop obesity at around five month of age, accompanied by hepatosteatosis and extensive lipid storage in the epididymal fat pad, together with an increase in islet size. Whether the islet-size increase is due to a compensation for a peripheral insulin resistance, which manifests in lipid storage, remains to be elucidated.

2.2.6.3 Gprasp2 influence on islet architecture

In order to further investigate the increase in islet size in Gprasp2$^{GT/y}$ mutant mice, islet architecture was analyzed using various cell type specific marker combinations. CLSM analysis confirmed the increase in islet area in Gprasp2$^{GT/y}$ mutant males compared to WT controls at six months of age, on a cellular level (Figure 38A, B). Thus, in Gprasp2$^{GT/y}$ mutants I observed "super large" islets (Figure 38A). The quantification of different cell populations within the islets revealed that α- (glucagon), and δ- (somatostatin) cells were reduced in Gprasp2$^{GT/y}$ mutant males. The percentage of β-cells (NKX6.1) remained steady with expanding islet area (Figure 38C). Together with the fact, that the β-cell area did not increase, these results suggest an increased β-cell proliferation. In order to prove this, we plan to co-stain NKX6.1 with Ki-67, a proliferation marker. It was reported previously, that β-cell mass expansion is a mechanism by which obese mice compensate for insulin resistance (Davis et al. 2010). Obesity, hepatosteatosis and β-cell mass expansion of Gprasp2$^{GT/y}$ mutant mice, all point to a peripheral insulin defect and subsequent β-cell compensation, in order to prevent T2D.

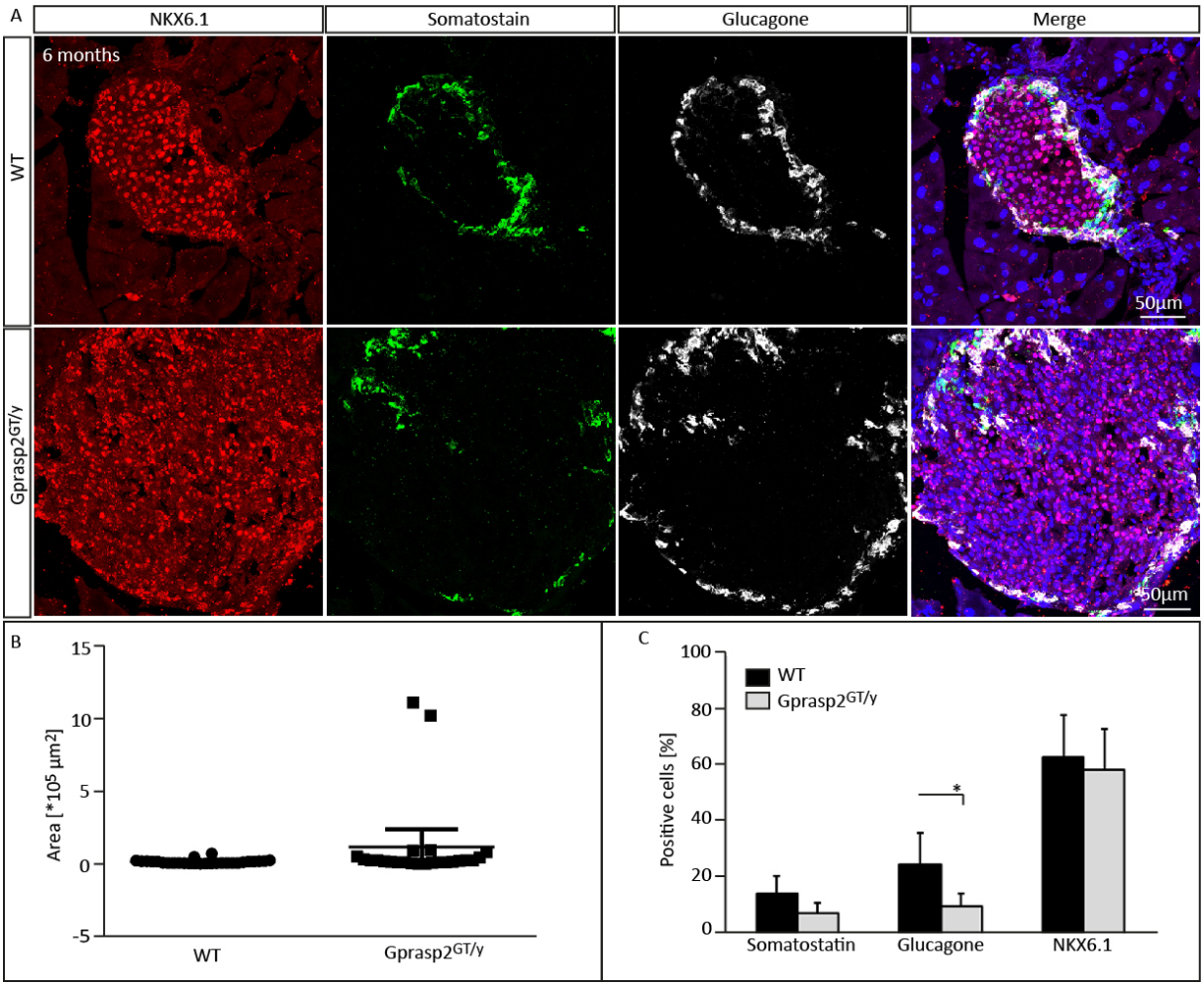

Figure 38 G-protein coupled associated sorting protein (Gprasp2) islet architecture. (A) Confocal laser scanning microscopy (CLSM) of six months old pancreatic cryo-sections of wild type (WT) and Gprasp2$^{GT/y}$ mutant male islets. 4', 6-diamidino-2-phenylindole (DAPI, blue) counter staining, NK6 homeobox 1 (NKX6.1, beta cell marker, red), somatostatin (δ-cell marker, green), and glucagone (α-cell marker, white) staining. (B) Quantification of islet area, showing an increase in Gprasp2$^{GT/y}$ mutant males and two super large islets, which were outside the 5 % quantil. (C) Marker quantification showing decrease in somatostatin and glucagone positive cells. NKX6.1 was imperceptible lower in Gprasp2$^{GT/y}$ mutant males. ($p < 0.05$, "*" is considered to be statistically relevant).

2.2.6.4 Gprasp2 metabolic influence

NAFLD is a hepatic complication of metabolic syndrome, characterized by obesity, concomitant with other metabolic abnormalities, such as reduced high-density lipoprotein levels, hypertriglyceridemia, and raised fasting glucose levels (Kennedy et al. 2010). In the previous chapter Gprasp2$^{GT/y}$ mutant mice were shown to exhibit obesity after five months of age, together with an increase in islet size and hepatosteatosis. In order to analyze the fat uptake and a possible metabolic effect further, I set Gprasp2$^{GT/y}$ mutant and WT cohorts on a HFD. The weight of WT and Gprasp$^{GT/y}$ mutant cohorts were not significant different, although the Gprasp$^{GT/y}$ mutant mice showed a tendency to be heavier (Figure 39A). Measuring the fat and lean mass via NMR, Gprasp$^{GT/y}$ mutant mice showed a higher fat content before HFD with four month of age (Figure 39B). However, no obvious difference in fat mass was observed in Gprasp$^{GT/y}$ mutant cohorts compared to WT, upon HFD feeding. When performing an ipGTT before HFD (Figure 39C) Gprasp$^{GT/y}$ mice showed higher glucose levels

after 120 minutes after glucose injection, suggesting a decreased glucose tolerance. Interestingly, when performing the same experiment after 12 weeks on HFD, the Gprasp$^{GT/y}$ mutant mice showed lower glucose level already after fasting (0 time point, Figure 39D).Thus, after glucose injection, Gprasp$^{GT/y}$ mice could not reach 350 mg/dl blood glucose levels, like the WT mice. After two hours both groups reached their basic value, which was again higher in the WT group. Simultaneously, the plasma insulin values were taken. They revealed no significant change in Gprasp$^{GT/y}$ mutant mice compared to WT, though a slight tendency of higher plasma insulin levels was found in Gprasp$^{GT/y}$ mutant mice (Figure 39F). Interestingly, analyzing the total insulin amount after HFD feeding, no change could be observed between the two groups (Figure 39K). However, comparing the total insulin amount (WT, Gprasp$^{GT/x}$, Gprasp$^{GT/GT}$, and Gprasp$^{GT/y}$) upon normal chow diet, Gprasp$^{GT/y}$ mutant males showed higher levels of insulin compared to WT controls (Figure 39E). Surprisingly, Gprasp$^{GT/y}$ hemizygous and Gprasp$^{GT/GT}$ homozygous total insulin amounts disclosed in opposite directions, as Gprasp$^{GT/GT}$ mutant females appeared to have lesser insulin amount, compared to Gprasp$^{GT/WT}$ heterozygous female, and WT male control. It is likely that the phenotypic difference between male and female could be due to the gender difference in hormone receptors (Parkin et al. 2005). Surprisingly, the liver steatosis, as well as the lipid storage in the epididymal fat pad was not significant in Gprasp$^{GT/y}$ mutant cohorts after HFD feeding anymore. Unexpectedly, the obese phenotype observed in Gprasp$^{GT/y}$ mutants under normal chow diet was not significant after HFD feeding anymore. The HFD food composition contains higher fat and lower carbohydrates. It is therefore likely that Gprasp$^{GT/y}$ mutants exhibit hyperphagia-like behavior under normal chow diet, which is not diet-induced. This would additionally suggest, that Gprasp2 plays a role in the carbohydrate metabolism. This will be further addressed by pair-feeding experiments, where the food intake or energy (calorie) intake is limited and equal between Gprasp$^{GT/y}$ mutant and WT cohorts. Next, I performed an *in vivo* experiment using glibenclamide an anti-diabetic drug, which leads to a constant closure of the Kir6.2 subunit, an activation of the PM, and a subsequent constant insulin secretion in order to distinguish the downstream effect of the glucose sensing at which the Gprasp$^{GT/y}$ mice develop a divergence. Although the glucose levels suggested that the mice were slightly stressed, Gprasp2$^{GT/y}$ mutant mice showed a significant drop in blood glucose levels (Figure 39I). When analyzing the plasma insulin levels, Gprasp2$^{GT/y}$ mutant mice showed significantly higher levels, which according to the lower blood glucose levels was expected (Figure 39J). This indicates that activating the plasma membrane leads to a constant insulin secretion which seems to be disturbed in Gprasp2$^{GT/y}$ mutant mice. This would also suggest that the Gprasp2$^{GT/y}$ mutant mice have a defect in the insulin secretion pathway at the level of the Kir6.2 channel, the Ca^{2+} influx, or the insulin efflux. In summary the HFD seemed not to strengthen the obesity phenotype of Gprasp2$^{GT/y}$ mutant mice, observed under normal diet conditions. This suggests that Gprasp2$^{GT/y}$ mutant mice exhibit no fat died-induced metabolic phenotype. The weight gain under normal diet conditins point to a role in carbohydrate metabolism, as in chow food, the carbohydrate portion is higher, compared to the HFD food. Thus, due to the previous found increase in islet cell mass, Gprasp2$^{GT/y}$ mutant mice rather face an islet proliferation phenotype. The higher total insulin amount, together with the results of the glibenclamide injection although suggest a defect in the insulin secretion pathway, which needs to be further elucidated.

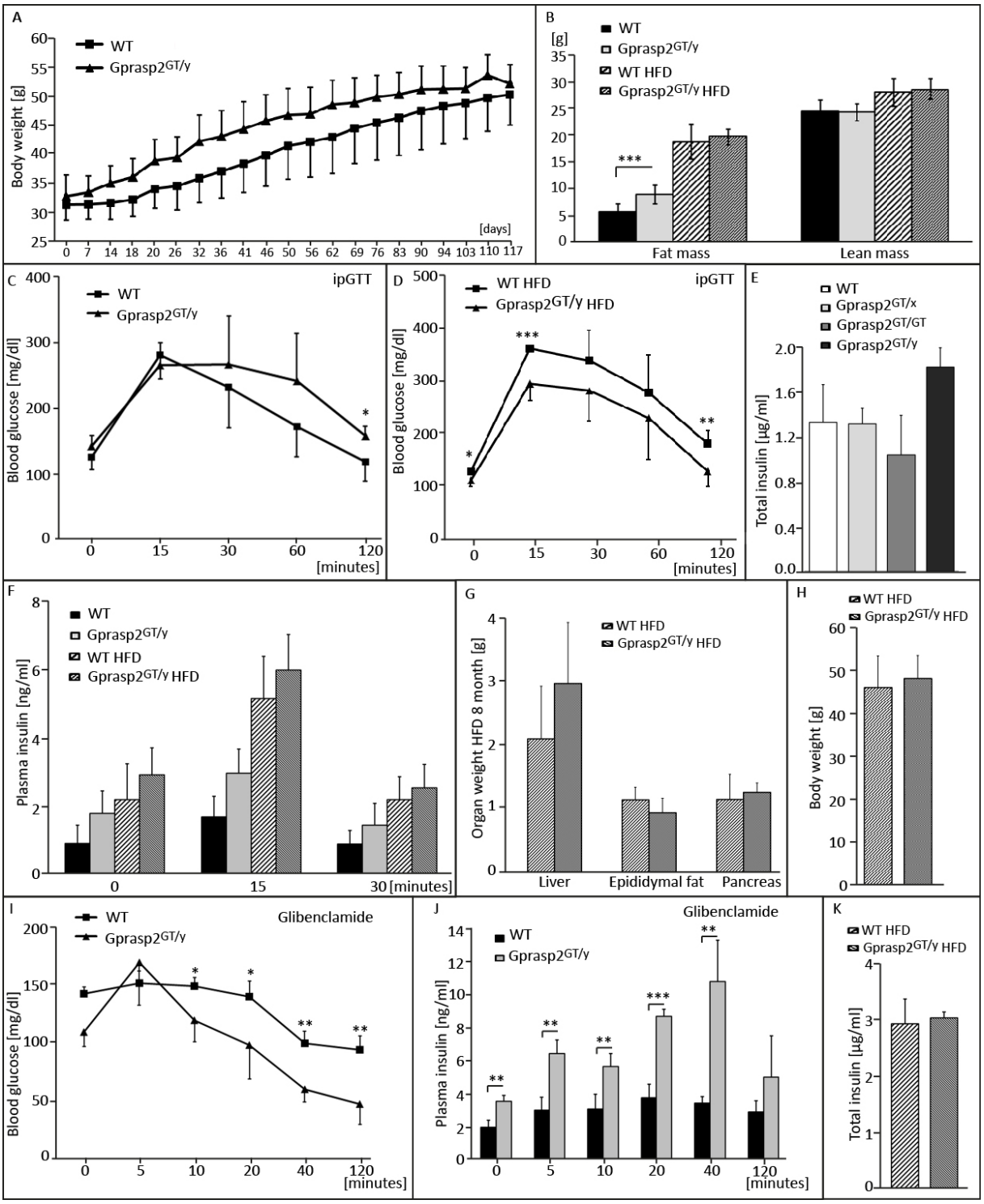

Figure 39 Metabolic influence of G-protein coupled associated sorting protein (Gprasp2) under high fat diet (HFD). (A) Body weight of wild type (WT) and Gprasp2$^{GT/y}$ mutant males over 117 days (~17 weeks). (B) Nuclear magnetic resonance spectroscopy (NMR) data showing lean and fat mass before (four month) and after the HFD. (C) Intraperitoneal (ip) glucose tolerance test (GTT) before HFD, and (D) after HFD. (E) Total pancreatic insulin comparing WT males, heterozygous (females, Gprasp$^{GT/x}$), homozygous (females, Gprasp$^{GT/GT}$), and hemizygous (males, Gprasp$^{GT/y}$) 3 – 4 month old mice. (F) Plasma insulin taken simultaneously to the glucose levels (ipGTT) from WT and Gprasp$^{GT/y}$ mutant males, before and after HFD. (G) Organ weigh and (H) body weight after HFD. (I) Blood glucose before (0 minutes) and after (5 – 120 minutes) glibenclamide ip injection, comparing WT and. Gprasp$^{GT/y}$ mutant mice cohorts (amount/ group = 4). (B) Plasma insulin was simultaneously measured. (K) Total pancreatic insulin after HFD. ($p < 0.05$, "*" is considered to be statistically relevant, $p < 0.01$, "**", is considered to be highly statistically relevant, and $p < 0.001$, "***", is considered to be extremely statistically relevant).

3 Discussion

3.1 Part I Development

In order to investigate the role of *Pifo* not only during development but also in adult tissues and organs we generated a conditional knock-out (KO) allele. Pifo$^{FD/FD}$ mutant mice were viable and fertile (Figure 5D). We found *Pifo* expression in particular in ciliated tissues such as the brain, lung, kidney, pancreas and testis (Figure 4G). By using Pifo$^{tm1e(KOMP)Wtsi}$ ES cells *Pifo* expression was shown in regions of high Shh activity, such as the NC and MN region, as well as in the AER of the LB at E 10.5 (Figure 6D-F). Together with previously described Shh phenotypes, that show reduction of *Ptch1* in the AER of the limb (Bouldin et al. 2010), the reduction of *Shh* in the FP of Pifo$^{FD/FD}$ mutant NT (**Figure 12**, **Figure 13**), implicated a function of *Pifo* in Shh signal transduction and target gene activation (Figure 12). Additionally, the Pifo H47 HPRT lacZ reporter revealed *Pifo* expression in the FP and the DRG of the NT at E 14.5 (Figure 7B, A´, B´, E´, G´). Deletion of the GTFBs in the cis-regulatory regions of Pifo, suggested that Shh regulates Pifo expression levels via GTFB sites, as the LacZ reporter expression levels and intensity was decreased in Pifo ΔHPRT (Figure 7B, C´, D´, F´, H´). Using the H47 and Tg(GBS-GFP) reporter we could further show a co-expression of Pifo in Shh regions (Figure 8). Thus, Pifo$^{FD/FD}$;Tg(GBS-GFP/+) mutant embryos showed a significant reduction of GBS-GFP reporter activity in the ventral NT (**Figure 15**), and subsequent neuronal marker analysis revealed that Olig2, was significantly reduced in Pifo$^{FD/FD}$ mutant NT at E10.5 (**Figure 16**, **Figure 3**). This was confirmed by quantitative mRNA analysis of Pifo$^{FD/FD}$ mutant NTs, with a reduction of Shh, Shh target genes, such as Ptch1, Gli1, and 2, and Shh signaling components, such as Sufu and Kif7 (**Figure 13**). *In vitro* PLC assays uncovered that Pifo is necessary for Smo translocation to the PC (**Figure 19**). We further identified Gprasp2 as Pifo interaction partner, which is co-expressed with Pifo in Shh high activity regions of the NT and LB (**Figure 25**, **Figure 21**, and **Figure 22**). We generated a Gprasp2 gene trap KO mouse line, which was viable and fertile (**Figure 20**C). *In vitro*, Gprasp2 was also necessary for Smo translocation to the PC (**Figure 24**). With the binding of Gprasp2 to 7TMR Smo, we have identified a heterotrimeric Pifo-Gprasp2-Smo complex, which forms upon Shh signaling (**Figure 26**).

3.1.1 Pifo a downstream target of Shh-Gli TF

Vertebrate Hh proteins, regulate diverse aspects of embryonic development and tissue homeostasis, while deregulated Hh signaling is associated with congenital defects, such as polydactyly, NT patterning defects, ataxia due to cerebellar hypoplasia and craniofacial defects (Goetz and Anderson 2010; Huangfu et al. 2003). In vertebrates the PC is the key-signaling center for the Hh pathway (Huangfu and Anderson 2006), but how PC integrate environmental signals to control tissue- and cell-type specific functions is still not well defined. In a microarray-based screen with the aim to identify novel mouse gastrula organizer genes during embryogenesis, *Pifo* was identified to be exclusively expressed in the embryonic node (Tamplin et al. 2008). Further functional studies showed that Pifo$^{LacZ/+}$ heterozygous mice die during development, due to L-R pattern formation defects leading to heart failure (Kinzel et al. 2010). The authors further showed that Pifo regulates the activity of mitotic kinase AurA that induces destabilization of PC axoneme and controls BB dislodging and centriole replication during cilia disassembly. In this study, *Pifo* expression was analyzed by LacZ reporter expression, using tetraploid (4n) embryo ↔ ES cell (Pifo$^{tm1e(KOMP)Wtsi}$) aggregations to generate completely ES cell-derived

embryos. *Pifo* LacZ expression was found in the AER of the LB, the FP, NC and MN region of the NT, where high Shh activity is reported (Cruz et al. 2010, Wong and Reiter 2008, **Figure 6**). In order to investigate the function of *Pifo* in more detail, our lab designed and generated a Pifo KO allele. The deletion results in a partial deletion of the ORF of the *Pifo* gene (deletion of exon 3-6, Figure 4). After removal of the neomycin selection cassette and deletion of the loxP sites by germ line transmission, and in contrast to the lethal $Pifo^{LacZ/+}$ allele, $Pifo^{FD/FD}$ mutant mice were viable and fertile (Figure 5D). The discrepancy between the two alleles could be due to the partial deletion of exon 3-6 which leaves a large portion of the ORF that is transcribed (**Figure 4**F) and likely translated. If this part of the protein has a function in Hh signaling by mediating e.g. interaction of Smo and Gprasp2, we would expect a hypomorph and not a loss-of-function phenotype, but there is currently no closing evidence for this hypothesis (see 3.1.3). The lethal phenotype of the $Pifo^{LacZ/+}$ mice, could be also due to the lack of GTFB sites in the intron 2 of the promoter region of the *Pifo* gene. Due to the only partial deletion of the ORF, these GTFB sites are present in the Pifo KO mouse model and might lead to an increased expression compared to the $Pifo^{LacZ/+}$ mouse model. Thus, it is likely that other cis-regulatory sides of the intron 2 are removed in the $Pifo^{LacZ/+}$ mouse model and might contribute to the enhanced Pifo reporter expression in the Pifo KO mouse model. The high frequency of GTFB sites in the cis-regulatory regions of Pifo and its expression in regions of Shh signaling, suggest that *Pifo* expression might be regulated by Gli TFs. Gli TFs are important in embryo development as they direct cell determination, specification, proliferation and cell death. *Gli2* and *Gli3* are required for patterning, whereas Gli1 was shown to be dispensable for development as $Gli1^{-/-}$ mutants are viable (Bowers et al. 2012). $Gli3^{-/-}$ embryos die due to NT defects and exhibit similar to $Pifo^{LacZ/+}$ haploinsufficient limbs, polydactyly due to an up-regulation of Gremlin and dHand normally repressed by Gli3 (Wong and Reiter 2008; Haycraft et al. 2005). The phenotypic difference between the two Pifo alleles could therefore be due to the deletion of the 11 GTFB sites of the intron region in $Pifo^{LacZ/+}$ mice. In fact, GTFBs are the main transcriptional regulators in Shh signaling, adapted to a PC in vertebrates. Thus, within this PhD thesis we showed *Pifo* expression in ciliated tissues such as the node, NT, brain, lung, kidney, testis and pancreas (Figure 4G). Taken together, expression analysis in combination with statistical reporter evaluation revealed Pifo expression in ciliated tissues and Shh regions, and further suggests a role for *Pifo* in Shh pathway mediated by GTFB sites.

3.1.2 Pifo-Gli expression in Shh regions

To analyze the transcriptional regulation of the Pifo gene, we established the H47 HPRT WT reporter, to analyze expression in regions of Hh signaling. This reporter enabled us to study Pifo LacZ expression pattern in the embryo, but also in the tissue and on cellular level. We showed that Pifo is expressed in the NT and the Chlx, where the Shh ligand is actively synthesized. The NT is a well-described Shh receiving tissue and specification of neuronal subpopulations depends on a Shh morphogen gradient. The Chlx functions as blood-cerebrospinal fluid barrier in the hindbrain and strongly expresses Shh (Huang et al. 2009). As cilia are highly required in the Chlx for the circulation of the fluid, cilia mutants show disruption of the fluid flow and subsequent holoprosencephaly formation (Banizs et al. 2005). Pifo likely does not play a role in cilia formation in the Chlx, as the mutants do not show holoposencephaly. This is consistent with its previous proposed role in cilia disassembly, rather than cilia assembly. The multi-ciliated cells of the Chlx are terminally differentiated and

do not re-enter the cell cycle anymore. Therefore, Pifo function for the Chlx is likely dispensable, but potentially it could regulated Shh signaling in these cells.

Comparing the HPRT WT reporter to the ΔHPRT reporter, we showed a slight decrease in *Pifo* LacZ reporter signal intensity in ΔHPRT embryonic NTs. Currently there is no evidence that *Pifo* is directly regulated via Gli TFs, but we can at least say that GTFB sites enhance *Pifo* expression, as deletion of GTFB sites reduces reporter expression. In order to clarify direct regulation of *Pifo* via GTFB sites, we will directly point mutate single GTFB sites and subsequent analyze *Pifo* LacZ reporter expression. Moreover, the HPRT system allows for direct selection of single copy insertions of expression constructs. Though, after homologous recombination into E14TG2a ES cells, which carry a deletion at the HPRT locus and subsequent embryo ↔ ES cell aggregation, no LacZ or Venus reporter activity was found before E14.5. We already showed early Pifo expression in the node (E 7.5), the NT and LB of E 10.5 embryos. It is therefore likely that important upstream cis-regulatory elements are missing in the promoter reporter constructs we have generated. However, with the HPRT WT reporter construct we have created a useful tool in studying Pifo expression and co-localization to Shh regions, regions at later embryonic stages and in adult organs that receive active Hh signaling, which was confirmed by immunohistochemistry. These results suggest that *Pifo* is a downstream target of Shh signaling, likely regulated by Gli TFs, which directly has to be tested by point mutation of these cis-regulatory elements in the future.

3.1.3 Pifo KO hypomorphism

Our previous analysis has shown that knock-in and knock-out of the *Pifo* gene by targeting exon 2 leads to embryonic lethality due to haploinsufficiency at E10.5-12.5 (Kinzel et al. 2010). Due to an annotated transcript in exon 2, we generated a Pifo KO allele to delete exon 3-6. Homozgyous KO mice of exon 3-6 of the *Pifo* gene are viable and fertile. Due to this observation, we further hypothesize that we have created a Pifo KO hypomorphic allele, which in contrast to the previously published $Pifo^{LacZ/+}$, does not lead to an embryonic lethal phenotype. Reasons for this idea are following: Additional deletion of several GTFB sites within the $Pifo^{LacZ/+}$ allele, and eventual deletion of cis-regulatory elements. Thus, we observed expression of Pifo mRNA of the remaining exons 1b and 2 in Pifo KO embryos, and therefore suggest a possible C-terminal truncated protein, with a calculated size of 12 kDa. Using monoclonal antibodies which were generated against different Pifo eptitopes, we are currently trying to confirm the existence of the N-terminal portion of the Pifo protein residue. Additionally, we currently investigate if the remaining N-terminal Pifo protein interacts with its known interaction partners Gprasp2 and Smo and might have a remaining function in Shh signaling. It is likely that these results will enable us to fully explain the differences between the two Pifo alleles. Hypomorphic alleles were already reported to overcome lethality, like shown for the Tg737 mutants. Loss-of-function of Tg737, results in severe malformation or absent cilia, midgastrulation lethality, L-R assymetry defects, NT defects, polydactyly and holoprosencephaly (Murcia et al. 2000). On the contrary, Tg737orpk homozygous survive to birth and exhibit phenotypes in many tissues such as the liver, kidney, skeleton and pancreas (Haycraft et al. 2005). The phenotypic differences between the two mutations suggest that the orpk mutation is a hypomorphic allele of the Tg737 gene. Taken together, we might have very likely created a hypomorphic Pifo KO allele, for which we still need to provide further evidence for the synthesis of the remaining protein. In

addition to this, we use a novel Crispr/Cas9 targeting technology to confirm the previously published haploinsufficient phenotype (Kinzel et al. 2010). With this technology we introduce small site-specific deletion on one or both alleles at the splice acceptor of Pifo exon 2. The resulting frameshift mutation has a similar deletion as the NLS-lacZ KO generated earlier.

3.1.4 Ptch1 downregulation in the AER as explanation for polydactyly

During vertebrate LB development, time and dose-dependent action of Shh is required for proper digit patterning (Harfe et al. 2004; Yang et al. 1997). Moreover, the growth of the LB is controlled by Shh signaling (Zhu et al. 2008). Using Pifo$^{tm1e(KOMP)Wtsi}$ ES cells I confirmed the *Pifo* expression in regions of high Shh activity, such as the NC and MN region, as well as in the AER of the LB as previously described by *Kinzel et al.* (**Figure 6**D-F, Kinzel et al. 2010). Expressions of Shh target genes were analyzed in Pifo$^{FD/FD}$ mutant compared to WT embryos, using whole-mount *in situ* hybridization technique, and *Ptch1* expression was reduced in the mesenchyme and in the AER of Pifo$^{FD/FD}$ mutant LB (**Figure 12**). It was previously shown that *Ptch1* and *Smo* are present in the AER and that Shh signaling is important in the AER, as deleting Smo precisely in the AER of the LB, led to a complete ablation of *Ptch1* in the AER and ventral ectoderm (Bouldin et al. 2010). The AER is responsible for proper LB development and elongates or reduces in according to the Shh gradient. In this regard Smo deletion led to subsequent extra cartilaginous condensations, suggesting a functional role of Shh signaling in the LB ectoderm. Comparing my results to our previous described Shh-like phenotype (Kinzel et al. 2010), the expression of *Pifo* in the AER and the reduction of the Shh target gene *Ptch1* suggests that *Pifo* functions in Shh signal transduction in the LB (**Figure 12**). As *Pifo* is exclusively expressed in the AER of the LB a possible change in elongation of this tissue could clarify an involvement of Pifo in the specification of the digit formation, which has to be further analyzed. Thus, taking the normal development of the Pifo$^{FD/FD}$ mutant limb into account, the reduction *Ptch1* might not affect the length of the AER, which could be further elucidated performing Fgf4 mRNA expression studies, as Fgf4 is exclusively expressed in the AER of the LB (**Figure 6**). Recently, GATA-binding factors 4 and 6 (GATA4 and 6) were found to be expressed in an A-P gradient, additional to the Shh gradient (Kozhemyakina, Ionescu, and Lassar 2014) and conditional deletion of Gata6 in the developing LB, revealed a normal Shh expression but a prolonged AER, leading to polydactyly. In summary, it is unlikely that a simple Shh gradient alone is crucial for the limb anatomy, as in Pifo$^{FD/FD}$ mutant limbs buds Shh signal is reduced without a consequence in development. Though, Shh target gene expression in the AER of Pifo$^{LacZ/+}$ haploinsufficient embryos could be interesting to analyze, taking into account, that they exhibit polydactyly. Interestingly, the IFT protein polaris (encoded by Tg737) is important in the murine LB specification, as deletion of Tg737 results in altered GliR processing and subsequent polydactyly (Haycraft et al. 2005). Thus, similar to Pifo$^{FD/FD}$ mutants, Tg737 mutants show a reduction of *Ptch1* and *Gli1* in the LB, compared to WT controls. Our results indicate once more that Pifo could be differentially involved in specific activities of the Gli proteins.

3.1.5 Pifo function in NT specification

Precise regulation of the Shh morphogen gradient is essential for proper NT and LB patterning and cell-type specification. The extracellular Shh concentration gradient in responding cells lead to regulation of target genes in a concentration dependent manner (Wolpert and Garcia-Bellido 1998). An obvious question is, if and how a

gradient can be precise enough to pattern a tissue (Balaskas et al. 2012), as tissue patterning can also proceed without a gradient of morphogen (Gregor et al. 2007; Kerszberg and Wolpert 2007). A Shh-Gli independent patterning of MN region was previously shown by phosphatase-activated TF and in Shh/Gli3 double mutant mice, which are able to generate all ventral neuronal subtypes (Krishnan et al. 1997; Litingtung et al. 2002).The precise regulation of NT patterning by Shh morphogen along the D-V axis is still unclear, even though the NT is one of the best-studied model systems for Shh-directed cell specification. We therefore studied Pifo function in more detail in the NT in a Shh-dependent manner. We showed *Pifo* expression in the MN region of the NT (**Figure 6**) and observed a reduction of Shh ligand expression in in $Pifo^{FD/FD}$ mutant NTs compared to WT (**Figure 12**, **Figure 13**). As MN were formed but reduced in the Olig2 domain in $Pifo^{FD/FD}$, we suggest a function for Pifo in Shh-dependend specification of the NT. TFs, like Olig2, Nkx2.2, and Isl1 were shown to identify distinct ventral progenitor domains, which are controlled by Shh signaling (Briscoe et al. 1999). The boundaries between these factors are regulated by Shh intensity and signal duration. Pifo is expressed in the ventral region and as a positive regulator of the Shh pathway might function to amplify the Shh signal for the differentiation of ventral neurons. The local amplification of a gradual signal might be important for boundary and pattern formation allowing the specification of neuronal subtype domains. Pifo deletion had no further impact on the development of the embryos, considering that the adult homozygous mice are viable and fertile. The reduced Shh ligand in $Pifo^{FD/FD}$ mutant NT might therefore still be enough in concentration and duration, for proper cell specification. A complete ablation of Shh signal on the other hand is accompanied with growth retardation, holoprocencephaly, cyclopia, and limb outgrowth defects, leading to an early death at around E12.5 of the $Shh^{-/-}$ mutant embryos (Bulgakov et al. 2004). $Smo^{-/-}$ mutants e.g. die during gastrulation due to growth arrestment, are unable to turn, and exhibit poor cranial development (Tran et al. 2008). Thus, $Shh^{-/-}$ and $Smo^{-/-}$ mutants lack most of the ventral fate including the FP, v3, and MN (Huangfu and Anderson 2006). The slight Shh reduction observed in $Pifo^{FD/FD}$ mutant NTs might be due to a deletion of downstream Shh targets, which negatively influence Shh morphogen in a feed-back loop. Thus, deletion of components of the Shh downstream signaling cascade like Gli proteins provide a wide range of phenotypes. $Gli1^{-/-}$ mutant mice are viable and fertile, and only show Shh defects in combination with Gli2 deletion (Park et al. 2000). Analysing the NT of $Gli2^{-/-}$ mutant mice revealed that the FP cells are absent and the v3 domain is reduced (Tuson, He, and Anderson 2011). Gli2 but not Gli1 was fund to be required for Shh activation. However, Gli1/2 double mutant studies (Park et al. 2000) and Gli2 replacement with Gli1 (Bai and Joyner 2001) revealed overlapping activating functions. Both single mutataions of Gli2 and Gli3 were found to be lethal at birth. It is therefore likely that the deletion of GTFB sites could influence Shh ligand secretion in feed-back loop, and subsequently affect the Shh receiving MN in $Pifo^{FD/FD}$ mutant NT. Though, the intensity of the signal is still enough to specify the MN region. This is supported by several reports about minor effects of single Gli mutations on the MN neuronal regions because of a functional redundancy of the Gli proteins (Ding et al. 1998; Matise et al. 1998; Park et al. 2000).

3.1.6 Pifo regulation during Shh activation *in vivo*

Pifo was initially identified as *Foxa2* target gene in a microarray-based screen. We further showed it`s expression in the FP, where also *Foxa2* and Shh are expressed. Moreover, we showed *Pifo* expression in the MN region of the NT and the reduction of MN Olig2 domain in $Pifo^{FD/FD}$ mutant embryos. These results are in

line with the previous noticed reduction of Shh in the NT, as a Shh gradient is responsible to specify neuronal subpopulations. We further confirmed Pifo-Shh co-expression, using a transgenic Shh-Gli reporter Tg(GBS-GFP) mouse line and Venus reporter gene expression (Balaskas et al. 2012). Intercrosses with Pifo KO mice in order to study $Pifo^{FD/FD}$;Tg(GBS-GFP/+) mutant embryos, enabled us to show a significant reduction of GBS-GFP reporter activity in the ventral NT (**Figure 15**). As this transgenic line reports Shh-Gli activity we could confirm the previous Shh reduction in MN region. This was done by quantitative mRNA analysis of dissected NT. Strikingly, Shh ligand and target genes such as *Gli1,2* and *Ptch1* were downregulated in $Pifo^{FD/FD}$ mutant NT (**Figure 13**), suggesting that *Pifo* functions in the Shh pathway. It was previously shown, that deletion of *Gli1* or *Gli3* had no apparent effects on the NT development (Park et al. 2000), but deletion of *Gli2* disrupted the development of the FP and Nkx2.2 ventral neuroepithelium (Matise et al. 1998; Ding et al. 1998). *Gli2* was found to be required for the initial production, but not the subsequent proliferation of oligodentrocyte progenitors (Qi et al. 2003). Thus, complete ablation of negative regulators likes *Ptch1* or *Rab23* result in D-V patterning defects (Goodrich et al. 1997; Eggenschwiler, Espinoza, and Anderson 2001). In $Pifo^{FD/FD}$ dissected mutant NTs, target genes were found to be decreased, but not totally deleted. This suggests compensation or a dose dependency of the Gli TFs and can explain the overall normal development in $Pifo^{FD/FD}$ mutant NT, when comparing to the non-viable Gli2 mutants. As already mentioned in *Park et al.*, due to compensatory effect of the Gli proteins, $Gli1^{-/-}$ mutant mice exhibit no developmental phenotype and mice are viable and fertile (Park et al. 2000). We discovered similar results for the Pifo KO mice. Although having tremendous Gli1 regulation defects *in vitro* and *in vivo*, $Pifo^{FD/FD}$ mutant mice exhibit no developmental deficits. Kif7 and Sufu are evolutionary conserved regulators of the Gli proteins. Kif7 and Sufu mRNA expression were both found to be downregulated in $Pifo^{FD/FD}$ mutant dissected NTs (**Figure 13**), whereas Gli3 on the other hand was unaltered when compared to WT dissected NT. Kif7 and Sufu are two conserved direct regulators of Gli proteins, as they regulate Gli processing (Barnfield et al. 2005; Chen et al. 2009). $Kif7^{-/-}$ mutant embryos exhibit an expansion of the MN domain, whereas $Sufu^{-/-}$ mutant embryos show a profoundly ventralized NT instead. *Law et al.* showed that Kif7 and Sufu possess cooperative as well as antagonistic functions and alter GliA/ GliR ratio to regulate intracellular Gli activity for the specification of ventral cell fates (Law et al. 2012). Pifo KO intercrosses with either Kif7 or Sufu mutant mouse lines, revealed no obvious phenotype differences to the already known single mutants (**Figure 17**). Although, these results are preliminarily they nevertheless suggest no direct genetic interaction between Pifo, Sufu and Kif7. However, it is likely for *Pifo* to have a function in GliA regulation. In summary, with different approaches we could show that *Pifo* is not only expressed in Shh regions, but also functions in the pathway in a Gli-mediated manner.

3.1.7 Pifo is a novel Shh target gene

In vertebrate the PC is essential for Hh signal transduction, as in the absence of Hh ligands Ptch1 localizes to the PC, where it prevents the localization of Smo (Rohatgi, Milenkovic, and Scott 2007). Hh binding to Ptch1 leads to its translocation out of the PC and subsequently Smo translocate to the PC (Chen et al. 2011). In this step other proteins such as GliA, Sufu and Kif7 (Barnfield et al. 2005) are involved in Shh-Smo dependent transcriptional activation of target genes. Here, we studied the involvement of *Pifo* function in Shh signaling and established an *in vitro* assay using PLCs. PLCs are cultured from LB, where *Pifo* was found to be weakly

expressed in the LB mesenchyme (**Figure 6**). We therefore established an *in vitro* cell system using PLCs, from control and mutant mice. PLCs are LB mesenchymal cells, which are Shh inducible and ciliated (**Figure 18**). PLCs are therefore a suitable system for studying cellular *Pifo* function in Shh signaling. This cell-based approach enabled us to show *Pifo* expression increase upon Shh pathway activation, similar to known target genes *Ptch1* and *Gli1* (**Figure 18**). Surprisingly, GliA/Gli1 regulation was already restricted and in Pifo heterozygous and almost absent in Pifo$^{FD/FD}$ mutant PLCs (**Figure 19**). Moreover, analysis of dynamic protein expression upon Shh stimulation over 48 hrs showed that GliA/Gli1 activation was not only decreased, but also delayed in Pifo$^{FD/FD}$ mutant PLCs. The PC links Gli activation to transcriptional activation, as upon pathway activation all Gli proteins were shown to translocate to the PC (Chen et al. 2009). It is likely that Kif7, which localizes to the base of the PC when the pathway is inactive, is responsible for the GliR processing, as at the BB the ubiquitin-proteasom system is enriched (Wigley et al. 1999). It was previously shown, that all three Gli TF possess a C-terminal transcriptional activation domain, whereas Gli2 and Gli3 also contain a N-terminal repression (Dai et al. 1999; Sasaki et al. 1999). In more detail: All three Gli TF contribute to GliA, but Gli3 and, to a lesser extent, Gli2 lead to GliR. In cell culture of Pifo$^{FD/FD}$ mutant PLCs, we have shown a clear deregulation of *Gli1*, though it had no influence *in vivo*. The overlapping activation and repressing functions of Gli TFs might compensate the impaired GliA/Gli1 regulation in Pifo$^{FD/FD}$ mutant PLCs, as e.g. GliR/Gli3 was unaltered. The main pathway for Gli regulation and processing is the Hh pathway. Though, increasing evidence suggests that non-canonical mechanisms independed of Hh signaling regulate Gli target gene expression. *Hu et al.* showed, in the developing embryonic kidey, where Hh signaling is absent, that Gli3 represses the transcription of Gli1 and Gli2 by binding to their promoters (Hu et al. 2006). It is therefore also possible that the Gli activation is a cross-talk mechanism with other than the Hh pathway involved. In summary, using this cell-based approach, we were able to show that *Pifo* is a novel Shh target gene, and also functions in the Shh pathway. We also showed that Pifo is necessary for activation of Hh signalling, as Pifo ablation caused a decreased and delayed Smo translocation with overall less ciliary Smo intensity at the PC (see further discussion 3.1.9).

3.1.8 Gprasp2 a novel Shh pathway member

In order to investigate the function of the Pifo protein in greater detail, we established the Pifo protein-protein interactome in cooperation with Prof. Marius Ueffing. Gprasp2 was found as one of the Pifo interacting proteins and has the potential to bind 7TMR, which immediately suggested to us that it might bridge a physical interaction to the 7TMR Smo (Moser et al. 2010). *Simonin et al.* identified Gprasp1 and -2 out of the 10 Gprasp X-linked gene family members to potentially interact with GPCR (Simonin et al. 2004). Gprasp1 has been associated with the sorting of 7TMR to the lysosome and subsequent receptor degradation after internalization. Beta arrestin target many 7TMR for internalization after phosphorylation of the 7TMR through GPCR kinase (Moser et al. 2010). One could speculate that Gprasp2 may interact with ß-arrestin for the receptor sorting to the lysosome or Gprasp2 might also be used to target 7TMR for internalization. Recently, *Bonert et al.* found a Gprasp family common protein-protein interaction motive which is important for the interaction with 7TMR C-tails (Bornert et al. 2013). Gprasp1 was shown to interact with the US28 GPCR, which following endocytosis is targeted to the lysosmes for degradation (Tschische et al. 2010). Endogenous Gprasp1 knock-down resulted in US28 signal impairment of the Galphaq/PLC/inositol phosphate accumulation and

decreased signal activation TF Nuclear Factor-kappaB and cyclic AMP responsive element binding protein. As literature provided evidence, that Gprasp proteins interact with 7TMRs, and Gprasp2 was found as Pifo interaction protein, we speculated that Gprasp2 might interact with Smo, which is a 7TMR. To test this hypothesis and to further analyze Gprasp2 function in Shh signaling we generated a GT mouse line to study the expression and function in Shh-dependent tissues. In this study I showed *Gprasp2* expression for the first time in the developing embryo using a gene trap mutant mouse line (**Figure 21**). *Gprasp2* is expressed in Shh-high regions such as the NC, the ventral NT, and the LB. As it is located on the X-chromosome, we observed a variety of expression patterns in the heterozygous female embryos, due to random X-linked inactivation. We found a variety of analogies between Pifo KO and Gprasp GT mutant mice: First, similar to $Pifo^{FD/FD}$ mutant NT analysis, Olig2 and Isl1 ventral neuronal regions were decreased in $Gprasp2^{GT/y}$ mutant NT, suggesting *Gprasp2* functions in the Shh signalling pathway. Second, *Gprasp2* followed the same induction kinetics when compared to known Shh target genes (**Figure 24**). When analyzing Shh or SAG induced $Gprasp2^{GT/y}$ mutant PLCs, Gli1/GliA was found to be dramatically reduced in $Gprasp2^{GT/y}$ mutant PLC after Shh or SAG induction. Protein kinetic experiments indeed showed a delay in Gli1 activation in $Gprasp2^{/y}$ mutant PLCs. These results already implicate that Gprasp2 functions in Shh signaling. Third, Pifo and Gprasp2 are co-expressed in Shh regions and moreover also physically interact with each other. Fourth, Gprasp2 is a novel regulator for the Smo translocation to the PC. In summary, we studied Pifo and Gprasp2 functions *in vitro* and *in vivo*, in well-understood Shh receiving tissues, the NT and the LB. Both genes were identified to be novel Shh target genes and function in the pathway.

3.1.9 Pifo-Gprasp2-Smo novel heterotrimeric complex

Pifo and Gprasp2 appear only within chordates and vertebrates, respectively (Kinzel et al. 2010), indicating that these genes are likely evolutionary adaptations to PC-dependent Hh signaling (Huangfu & Anderson, 2006). Mechanistically, both Pifo and Gprasp2 are functionally important components of the Smo ciliary targeting complex (**Figure 26**), as either lack of Pifo or Gprasp2 leads to failure of Smo ciliary translocation and Shh target gene activation in PLCs with structurally normal PC. How Smo is transported to the PC upon Hh signaling is still unclear. Interestingly, *Milenkovic et al.* showed three different ways of Hh-dependent Smo transport to the PC (Milenkovic, Scott, and Rohatgi 2009). First, MT-dependent directed transport of Smo intracellular vesicles from the Golgi to the base of the PC. Second, transport of PM-localized Smo laterally into the PC compartment breaking a diffusion barrier. Third, endocytosis and vesicular recycling of PM-localized Smo for translocation into the PC. These distinct transport mechanisms and the fast turnover rate of Smo imply that different molecular machineries are important for surface and intracellular Smo transport. Together with Dr. Bomi Jung, we identified the Hh-induced ciliary targeting heterotrimeric complex of Pifo-Gprasp2-Smo as one of these machineries involved in Hh-induced ciliary targeting (Jung et al. 2014, submitted). Without Shh pathway activation, Pifo and Gprasp2 proteins are presented in low quantities in the cells, and physically interact with MT subunits, but not with Smo. Upon Hh induction, Smo strongly increases it´s affinity to Pifo, Gprasp2 and βarr2 (Kovacs et al., 2008) for rapid translocation into the PC. By wich mechanism the affinity of Smo to the Gprasp2-Pifo-Kif3b complex is increased after Shh stimulation need to be elucidated. Interestingly, several studies indicate that phosphorylation mediated by CK1a and Grk2 induces a conformational change and

activation of Smo (Chen et al., 2004, 2011), which subsequently mediates βarr2-Kif3a (Kovacs et al., 2008). Arrestins 1 and -2 thereby mediate the Shh-dependent Smo transport to the PC, together with Kif3a, a motor subunit of kinesin II complex, which is involved in anterograde transport along the ciliary axoneme. Thus, we showed that the Pifo-Gprasp2-Smo heterotrimeric complex is associated with Kif3b, another motor transport unit, as Pifo interacts with Kif3b and Gprasp2 (**Figure 26**, Jung et al. 2014, submitted). We further conclude that the interaction of Pifo and Gprasp2 with anterograd MT-proteins (Kinzel et al., 2010; this study), results in intracellular transport of the Smo ciliary targeting complex to and into the PC. This suggests that with the Gprasp2-Pifo-Kif3b motor protein-driven anterograde transport of Smo into the PC, we have identified novel Smo transport machinery.

Although Smo is the central component of Hh pathway activation, the biochemical mechanism involved in Smo translocation to the PC is poorly understood. Interestingly, *in vitro* βarr1 and 2 (Kovacs et al., 2008) as well as Pifo and Gprasp2 are important for Smo transport to the PC, although the single KOs revealed no Hh-specific phenotype in mice (Bohn, Lefkowitz, and Caron 2002; Zhuang et al. 2011). This suggests that the Smo ciliary transport is secured by alternative ciliary targeting mechanism. Activated Smo is rapidly recruited to the PC upon Hh stimulation within an hour range (Milenkovics et al. 2009), which is consistent with the kinetics of Pifo and Gprasp2, showing expression kinetics and dynamics of immediate early Shh target genes. Gli proteins are the major effectors for Hh-dependent transcriptional regulation. Particularly, Gli1 functions as an amplifier of the activated state (Park et al., 2000). Although Gli2 and Gli3 can be found full-length activator form or proteolytically processed repressor form, Gli2 is mostly regarded as transcriptional activator and Gli3 acts as transcriptional repressor. We note that previous study showed Gli2 activation links Shh-dependent activation of Smo in the PC (Kim et al., 2009). Our observations also suggest that Gli2 activation possible depends on dynamic recruitment of ciliary Smo. Pifo and Gprasp2 appear to have a role in the ciliary Smo targeting complex formation consequently affecting Gli2 expression in Shh signaling pathway. However, it is still unclear how Smo activity in the PC influences gene expression.

3.1.10 Pifo-Gprasp2-Smo complex as therapeutic target

Hh signaling plays an important role not only during development but also in tissue homeostasis. Aberrant activation of Hh signaling has been implicated in various types of tumors and it strongly promotes tumorigenesis (Spivak-Kroizman et al. 2013). Constitutive Hh activation due to the loss of negative regulators, such as Ptch1 or Sufu or gain-of-function of the positive regulator Smo, results in direct target gene activation such as Gli1 and Gli2 that occurs in a Shh ligand-independent way (Scales and de Sauvage 2009; Di Marcotullio et al. 2004). Constitutively activated Gli2 was found in medullablsastomma where removal of cilia was important for the tumor growth (Han et al. 2009). Constitutive active Smo is also found in Hh mediated skin cancers (Gu et al. 2012), where almost all cells are ciliate. As SmoM2 mutation constitutively activates Smo along the PC, the heterotrimeric complex of Pifo-Gprasp2-Smo is a good target in preventing Smo ciliary translocation and pathway activation. Increased Hh signaling can occur through autocrine or paracrine Hh ligand secretion form tumor cells or peripheral cells, respectively. This is Shh ligand-dependent and is found especially in cancers of the gastrointestinal tract including the pancreas as well as in gallbladder-, breast-,

colon-, and prostate cancers (Onishi et al. 2011; Matsushita et al. 2014; Berman et al. 2003). Third, the increase in Hh signaling can cause the release of VEGF or EGF which further support tumor growth. Although altered Shh signaling can promote tumorigenesis, the mechanism underlying this process is poorly understood. It is also still not clear whether Shh signaling play a role in the normal pancreas, but it has been observed that upregulation of Shh expression in precursor lesions and primary pancreatic tumors (Kasperczyk et al. 2009; Morris, Wang, and Hebrok 2010). Taken together, there is growing evidence that impaired Shh activation is involved in the progression of various cancers, such as pancreatic tumors. With Pifo and Gprasp2 protein interaction and their expression in the pancreatic ß-cells, the heterotrimeric complex could be a novel therapeutic target site, in order to study Shh involvement in pancreatic cancers. Interestingly, Gprasp1 for example was already identified as a potential serum and tumor marker in breast cancer (Tuszynski et al. 2011). In all 107 cases of human ductal breast cancer samples, Gprasp1 overexpression was detected with WB and ISH, but absent in adjacent normal tissues. In summary, the overexpression of Hh targets in many tumors has led to the idea that these cancers might get treated with Shh antagonistic drugs. Thus, abnormal Shh pathway activation can also occur through receptor-induced signaling. Interestingly, *Reiter* and colleagues have recently reported on small molecule inhibitors of Smo that either disrupts slow intracellular trafficking or fast lateral PM entry of Smo into the PC (Wu, Chen, Arkin, & Reiter, 2012). Certainly, the identification of novel molecular machineries that regulate Smo translocation into the PC will be good drug targets for cancer therapy. In this regard, we currently search for drugs that prevent formation of the heterotrimeric Pifo-Gprasp2-Smo complex, which avoid ciliary translocation and target activation. We have to map interaction domains and currently screen for small molecules that prevent protein-protein interactions.

3.2 Part II Ciliopathies – Diabetes

3.2.1 PifoKO

Beside Pifo's expression and function in embryonic tissues, *Pifo* is also expressed in adult ciliated tissues, such as lung, kidney and pancreas (**Figure 4**). For this reason and due to the fact that we generated a mutant Pifo allele that overcame embryonic lethality, we analyzed Pifo's role in adult organogenesis in more detail, with specific focus on the pancreas. Briefly, Pifo is expressed in pancreatic islets at various ages shown by RT-, quantitative PCR and immunohitochemistry (**Figure 28**A), and is equally expressed in PLCs and WT islets (**Figure 28**C). As Shh had an influence on insulin mRNA expression, we analyzed GSIS in $Pifo^{FD/FD}$ mutant islets. Interestingly, 1.5 months old $Pifo^{FD/FD}$ mutant islets did not respond to the glucose exposure, compared to WT (**Figure 30**E). At three and nine months of age the insulin secretion was impaired in $Pifo^{FD/FD}$ mutant islets compared to WT. Shh stimulated *in vitro* islet assay on isolated islets showed Gli1, Smo and Kir6.2 upregulation and decreased Smo translocation in $Pifo^{FD/FD}$ mutant islets. In order to analyze environmental challenge, $Pifo^{FD/FD}$ mutant mice were fed a HFD. This revealed a died-induced glucose intolerance and β-cell-mass decline in $Pifo^{FD/FD}$ mutant mice, compared to controls. A proliferation defect was studied in a model of compensatory beta cell proliferation, where $Pifo^{FD/FD}$ mutant pregnant females showed a significant defect in compensating for the metabolic demand. The CDK4-pRB-E2F1 pathway has a role in insulin secretion and β-cell proliferation (Annicotte et al. 2009). In $Pifo^{FD/FD}$ mutant islets CDK4-pRB-E2F1 targets, E2F1, pRB, and CDK4 were found to be downregulated and Kir6.2 was found to be upregulated. In summary, the Pifo deletion led to died-induced glucose intolerance and proliferation decrease in pancreatic β-cells and an insulin secretion defect. We propose, that we have created a mouse model system to study predisposition and environmental factors in the context.

3.2.1.1 Pifo expression in β-cells

The endoderm-derived pancreas consists of an exocrine compartment, namely the duct and acinar cells, and an endocrine compartment, the islets of Langerhans. The islets can be further divided in different cell types, responsible for different hormone secretions. The principal sources for the hormone insulin are the pancreatic β-cells. Following the question whether Hh signaling has a function in the pancreas, I used the Pifo KO mouse model in order to study *Pifo* as Shh target gene and its role in pancreatic islets. Using WT islets, I observed *Pifo* expression in the pancreas, with a slight decrease in mRNA expression level over the age (**Figure 28**B, C, 3 – 18 months). Moreover, Pifo was expressed in the cytoplasm and along the PC in pancreatic islet cells (**Figure 28**A, D). Analyzing co-stainings, I found Pifo absent in α-cells. I concluded that the cytoplasmatic staining occurs in β-cells, as 80 % of the cell mass in islets consist of insulin producing cells. It is therefore likely, that being a Shh target gene *Pifo* might also have a function in the pancreatic β-cells. It is still controversially discussed, whether Hh signaling is important during pancreas development and/ or adult pancreas function. Though, loss- and gain of function studies in mice have shown that Shh signaling is required for proper pancreas development, as deregulated Shh signaling lead to changed pancreas morphogenesis and function (Lau, Kawahira, and Hebrok 2006). To determine whether PC regulate Hh signaling in the developing and postnatal pancreas, *Cervantes et al.* showed that a specific Gli2-activating mutation in combination with cilia ablation

resulted in stong Hh activation (Cervantes et al. 2010). As neither combination of GLI2-activating mutation with SmoM2 or Ptch1$^{lox/LacZ}$ mutant mice showed Hh activation, the authors suggest that PC regulate Hh activity downstream of Smo in the pancreas. As Pifo$^{FD/FD}$ mutant islets show no obvious cell-composition change (**Figure 30**), it is unlikely, that Pifo has a role in the pancreas development. But Hh signaling is likely functionally involved in adult pancreas, as the common receptors *Smo* and *Ptch1* are found to be expressed in the endocrine islets of Langerhans of the fully developed rat pancreas and in the β-cells line INS-1 (Thomas et al. 2000). In the adult pancreas, Shh signaling might also specify the mesenchyme, as inactivation of Smo in epithelial cells did not influence pancreas adenocarcinoma (PADC) formation, but deletion in the mesenchymal cells led to growth inhibition in pancreatic xenograft models (Nolan-Stevaux et al. 2009; Yauch et al. 2008). It is therefore likely that Pifo, which interacts with Smo, plays a role in the adult pancreas. It was shown, that altered Hh signaling is involved in pancreatic tumor progression. With regard to exocrine pancreatic tumors, *Friedrich et al.* showed, that ectopic Shh overexpression in acinar cells of murine adult pancreata resulted in an expansion of the periacinar mesenchymal compartment, rather then intraductal neoplasia, showing a paracrine epithelial-mesenchymal cross-talk (Fendrich et al. 2011). Ectopic expression of a constitutively activated Gli2 instead showed that epithelium-specific Hh signaling is sufficient to drive pancreatic neoplasia (Pasca di Magliano et al. 2006). Though, only in combination with Ras activation, the mice developed PDAC. Patients with PDAC show high Hh signaling (Li, Ma, et al. 2012) and in adult mice Hh was shown to promote cancer cell proliferation, to increase invasion and metastasis, and to protect against apoptosis (Xu et al. 2014). Very less is known about the influence of Hh singnaling on endocrine pancreatic tumors. A recent article established a link between endocrine neoplasia type 1, where the gene menin 1 (Men1) is mutated and Hh signaling (Gurung et al. 2013). The authors show that Men1, which normally regulates cell-cycle genes and represses cell proliferation, partially functions as suppressor for Hh signaling and subsequently Men1 mutants show altered Hh signaling. Thus, *Umeda et al.* reported, that exposure to proinflammatory cytokines (IL-1β and IFN-γ) increased Ihh expression in rat β-cells *in vitro* (Umeda et al. 2010). Shh overexpression on the other hand reduced cytokine-induced apoptosis with reducing the nuclear factor-kappa light chain enhancer promoter activity. This strongly suggests that Shh signaling is important for β-cells as it protects β-cells from cytokine-induced inflammation. In summary, *Pifo* is a novel Shh target gene and moreover expressed in β-cells. But, does *Pifo* as Shh target gene also play a role in pancreatic β-cell function?

3.2.1.2 Insulin secretion defect in Pifo$^{FD/FD}$ mutant mice

The main function of a β-cell is to produce insulin. In case of insulin resistance of e.g. the peripheral tissue the glucose cannot properly be cleared out of the blood system. This leads to a feedback, as the glucose receptor determines the β-cells to produce more insulin. The β-cells can adapt to this increased insulin production for a certain time. A subsequent insulin secretion defect can be measured *in vitro* via GSIS in mice. In order to analyze the effect of *Pifo* ablation on insulin secretion, we therefore compared WT to Pifo$^{FD/FD}$ mutant islets *in vitro*. Strikingly, an overall lower insulin secretion in Pifo$^{FD/FD}$ mutant islets was observed (**Figure 30**). I repeated this experiment including Pifo$^{FD/WT}$ mice and found, that at heterozygous stage despite of a lower total insulin amount, the overall insulin secretion is unaltered, compared to WT controls (**Figure 34**C, D). We concluded that Pifo$^{FD/FD}$ mutant mice develop an insulin secretion defect. *Thomas et al.* reported that Hh`s and their receptors,

which are expressed in the adult rat islets and INS-1 β-cell line, stimulate the insulin gene expression in β-cells (Thomas et al. 2000). With the application of Cyc, we found simultaneous inhibition of Hh signaling and reduced insulin promoter activity and subsequent endogenous insulin mRNA expression. The β-cells are targets of active Hh signaling as *Ptch1* and *insulin* are co-expressed. The authors propose that Hh signaling regulates the production of insulin and to consider defective Hh signaling as a considerable factor in the pathogenesis of T2D. In this regard, a recent article showed that the negative Hh regulator Gli3 is a risc gene for diabetes (Zung et al. 2011). The authors showed a link between Greig cephalopolysyndactyly syndrome (patients typically suffer from limb malformations and craniofacial developmental abnormalities) and MODY2, caused by mutations in the glucokinase gene (GCK), with the deletion of both genes, GCK and Gli3. The phenotype seen in $Pifo^{FD/FD}$ mutant islets supports the idea that Hh signaling regulates insulin production. In contrast, no major morphological changes in $Pifo^{FD/FD}$ mutant pancreatic islets were observed by cell-composition analysis (**Figure 30**), but an islet-mass decline was detected in aged $Pifo^{FD/FD}$ mutant mice. There are three possible explanations for the islet-mass decline: First, the Hh signaling pathway is a major pathway for autophagy in pancreatic cancers (Xu et al. 2014). It is therefore likely that it promotes apoptosis in $Pifo^{FD/FD}$ mutant islets. Second, the decrease in islet mass could be a consequence of the compensation for higher insulin demand, due to the secretion defect. As previously described partial insulin resistance of the peripheral tissue occurs before glucose intolerance is detectable and the still normal β-cells secrete more insulin in order to compensate for the higher demand (Martin et al. 1992). Afterwards a defect in insulin secretion occurs, where β-cells become unable to respond to glucose (Kahn 1994), which subsequently leads to a β-cell failure ensuing in T2D (Petersen and Shulman 2006). Third, Pifo was previously shown to colocalization with BB proteins in cilia dassembling cells (Kinzel et al 2010) and with motor subunits Kif3a (Kinzel et al. 2010) and Kif3b (**Figure 26**C), necessary for the PC transport. *Kinzel et al.* further showed high percentage of mitotic defects in $Pifo^{LacZ/+}$ mutant cells, Pifo accumulation at cell-cycle reentry in S-phase and declines during mitosis. The islet-mass decline, shown in $Pifo^{FD/FD}$ mutants, together with Pifo expression in β-cells, point to a cell-cycle control function for Pifo in pancreatic β-cells. But, how is Pifo precisely invoved in β-cell-cycle control?

3.2.1.3 Pifo involvement in cell-cycle mechanism

Environmental factors and prolonged metabolic stress induced by HFD or during pregnancy can increase the risk of T2D according to the genetic predisposition (Bonner-Weir 2000). In order to answer the question whether Pifo mutation predisposes for T2D, I studied the effect of metabolic stress on the pancreas and β-cells in $Pifo^{FD/FD}$ mutant mice. Under both metabolic changed conditions I found a slight insulin deficiency and decrease in β-cell proliferation rate in $Pifo^{FD/FD}$ mutant mice compared to WT mice. This suggests an important role for Pifo in the adaptation of a β-cell to metabolic changes to prevent the pathogenesis of T2D (under normal conditions). During HFD feeding or pregnancy the β-cells have to increase their proliferation due to the higher insulin demand. As I only observed decreased proliferation in $Pifo^{FD/FD}$ mutants under metabolic stress conditions it is likely that β-cells cannot adapt to these changes. This would further mean that $Pifo^{FD/FD}$ mutant β-cells are likely to have a cell proliferation defect. In the previously described Pifo protein-protein interaction experiment, we identified Cdk4 as potential interaction partner (Jung et al. 2014). Thus, the CDK4-pRB-E2F1 pathway was shown to mediate, pancreatic growth and β-cell proliferation, as well as insulin secretion

(Annicotte et al. 2009). Secreted insulin activates PI3 kinase, leading to an increase in Cdk4 activity, pRB phosphorylation and subsequent E2F1 transcriptional activity. CyclinD1 is expressed in most of the proliferating cells, is a further upstream regulator of Cdk4, and was reported to be regulated by Hh signaling (Locker et al. 2006). Whether or not Cdk4 is a Shh target is not known yet, but there is most likely a link between the Cdk4 and the Shh pathway. Cdk4 regulates G1 to S phase transition and it's kinase activity is dependent on its binding to one of the three D-type cyclins including cyclinD1. A recent study reports, that insulin activates cyclinD1-Cdk4 suppresses hepatic glucose production independently of cell-cycle progression (Lee et al. 2014). They further show that loss of cyclinD1 in the liver increases gluconeogenesis and hyperglycaemia. In $Pifo^{FD/FD}$ mutant islets I found target genes of both pathways the CDK4-pRB-E2F1 and Shh to be down regulated in $Pifo^{FD/FD}$ mutant islets (**Figure 34**). These results not only link Pifo to cell-cycle control, but also to glucose homeostasis and insulin secretion. Though the precise mechanism still needs to be elucidated, these results strongly suggest, that Pifo acts together with Cdk4 in controlling E2F1 transcripitonal regulation. We may have found a novel interplay between the Shh pathway and the β-cells proliferation and subsequent insulin secretion. Thus, in $Pifo^{FD/FD}$ mutant islets, Cdk4 was downregulated, suggesting a defect in cell-cycle reentry into S-phase. Together with the previous reported role in cilia disassembly, we might also have discovered a role for Pifo in cell-cycle regulation of pancreatic β-cells. Moreover, $Pifo^{FD/FD}$ mutant mice show a strong upregulation of the Kir6.2 subunit of the potassium channel. Upon glucose uptake through Glut2, ATP is produced which is necessary to close the channel and subsequently polarize the membrane to generate a Ca^{2+} influx. In case of $Pifo^{FD/FD}$ mutant mice the Kir6.2 subunit is more abundantly present, suggesting a higher ATP production. Although, target genes of the CDK4-pRB-E2F1 pathway are downregulated, the Kir6.2 subunit is upregulated in $Pifo^{FD/FD}$ mutant islets. This is in contrast to reported results, where Kir6.2 is described as a direct target of E2F1 transcription factor and downregulated in $E2F1^{-/-}$ mice (Annicotte et al. 2009). A defect in the Kir6.2 subunit in $Pifo^{FD/FD}$ mutant mice would also explain the elevated plama insulin levels found after the application of glibenclamide. Glibenclamide is an anti-diabetic drug, which leads to a constant closure of the potassium channel and a subsequent insulin efflux, regardless of ATP production. Thus, Kir6.2 is regulated either via the cell-cycle or the metabolism through phosphorylation of RB protein, which is downregulated in $Pifo^{FD/FD}$ mutant mice. It is likely, that $Pifo^{FD/FD}$ mutant defective insulin secretion can be compensated by β-cells with higher energy production in form of ATP, which would also explain the higher Kir6.2 expression. We previously identified p16ink4a as a Pifo interacting protein, which regulates cellular senescence (a process of aging) and the PI3K/ Akt pathway (Alimonti et al. 2010; Kennedy et al. 2011). P16ink4a binds to the Cdk4/ 6 complex, inhibiting the downstream phosphorylation of RB protein (Annicotte et al. 2009). The expression of p16ink4a increases remarkably with age accompanied with a decrease in proliferation capacity (Serrano, 1997; Krishnamurthy et al., 2004). *Zeng et al*. could show that Pten (phosphatase and tensin homologue deleted on chromosome 10) is also involved in cellular aging. It increases the expression of p16ink4a and thereby blocks the cell-cycle re-entry (Zeng et al. 2013). P16ink4a was shown to be involved in the CDK4-pRB-E2F1 β-cell proliferation pathway and deletion of either pathway target genes *Cdk4* or *cyclinD1*, lead to a decrease in β-cell mass (Kushner 2006). Due to the interaction of p16ink4a and Cdk4, and the interaction of Pifo with Cdk4 found in the interactom study, it is likely that the decrease in β-cell mass in aged $Pifo^{FD/FD}$ mutant mice arises from a change in the complex formation of these proteins. Thus, we previously published that like AurA, Pifo

accumulates at the basal body, which is important for cilia retraction and centriole liberation during cilia disassembly (Kinzel et al. 2010). Moreover, centriole retraction is controled by several kinases, like cyclinD2 (Bettencourt-Dias et al. 2004). Already within this study we raised the idea, that Pifo might regulate cell cycle-dependend kinases. The question of how Pifo acts in the CDK4-pRB-E2F1 pathway still remains. Thus, it is not clear if the deregulation is due to cell-cycle regulation or if the PI3K/ Akt pathway (which is important for the glucose driven phosphorylation of RB in order to upregulate cell-cycle transcription factor E2F1) is also affected in Pifo$^{FD/FD}$ mutant mice.

3.2.1.4 Pifo$^{FD/FD}$ mutants a novel mouse model to study T2D predisposition

T2D is thought to involve both, a first decline of insulin sensitivity and a decrease in β-cell function, although the order of events is not entirely clear, yet. This can be either due to diminished or inappropriate secretion of insulin or reduced β-cell mass (Prentki and Nolan 2006). Here we studied the influence of Pifo deletion on the adult pancreas and metabolism. But what role does Pifo as Shh target gene play in the adult pancreas and β-cell progression? Is Shh involved in the β-cell function or is Pifo in the pancreas regulated through other pathways? Applying the Pifo KO mouse line we were able to answere some of these questions. In summary, we showed that Pifo is expressed in β-cells and deletion of Pifo leds to an insulin secretion defect. Under normal chow conditions we were able to show that not only Shh pathway target genes, such as *Gli1* and *Ptch1* were downregulated and Smo translocation decreased, but we could also show, that β-cell G1 to S phase progression was affected. We observed a decrease in E2F1, pRB and Cdk4 in parallel with an increase in Kir6.2, suggesting a defect at the level of ATP production. Moreover, mutations in the potassium channel genes *KCNJ11* and *ABCC8* are associated with an increased risk in developing 2TD (Qiu et al. 2014; Takagi et al. 2013). We are one step closer develping a link between Shh signaling and the CDK4-pRB-E2F1 pathway, with the interaction of Pifo and cyclinD1-Cdk4. Thus, under challenged conditions of HFD feecing and pregnancy we could show that the β-cell proliferation is decreased, and moreover the β-cell mass declines upon HFD feeding. Pifo$^{FD/FD}$ mutant mice develop glucose intolerance on top of the insulin secretion defect upon HFD feeding. We might have have created a novel mouse model in order to study challenge induced predisposition to T2D. Encouraged by a human pre-diabetic cohort study, a PIFO SNP in the 3' UTR of the gene led to glucose intolerance and impaired insulin secretion. Thus, further human cohort studies show the effectiveness of lifestyle interventions to reduce the incidence of diabetes in people with impaired glucose tolerance (Wareham 2014). Patients in the combined lifestyle intervention groups had a 51 % lower incidence of T2D during the active intervention period. This study shows a novel link of Hh signaling and β-cell proliferation and offers a useful mouse line in order to study diet-induced genetic predisposition to T2D.

3.2.2 Gprasp2$^{GT/y}$

As described above, Gprasp2 was identified as Pifo interacting partner and forms a heterotrimeric Pifo-Gprasp2-Smo complex, which is required for Shh pathway activation *in vitro*. Using the Gprasp2 GT mouse line the adult phenotype was analyzed. Briefly, *Gprasp2* LacZ expression was found to be restricted to the β-cells of the islets of Langerhans in the adult pancreas. At approximately five months of age Gprasp2$^{GT/y}$ mutant males become obese (**Figure 37**A). The fat mass percentage of the Gprasp2$^{GT/y}$ mutant males was increased by two folds at the onset of obesity (**Figure 37**C). In fact, Gprasp2$^{GT/y}$ mutants showed higher lipid storage in the liver, and epididymal fat pad, already at the age of five months (**Figure 37**D). At the age of 18 months the phenotype is more distinct, as the liver weight is increased by almost three fold and the epididymal fad pad weight is increased four fold (**Figure 37**E). At five months of age the islet size is increased, by increased β-cell proliferation in Gprasp2$^{GT/y}$ mutant mice. Interestingly, upon HFD feeding the phenotype of the liver steatosis, as well as the lipid storage in the epididymal fat pad was not significant in Gprasp$^{GT/y}$ mutant cohorts anymore. Last, Gprasp2$^{GT/y}$ mutant mice showed significantly higher levels of plasma insulin after glibenclamide application (**Figure 39**J). We hypothesize that the Gprasp2 phenotype is due to a change in insulin demand consequent to an insulin resistance of the peripheral tissue like muscle and adipose tissue, leading to a subsequent increase in islet size.

3.2.2.1 What is known about the Gprasp gene family

Ten members of Gprasp2 gene family have been identified so far and all contain a 400 amino acid long conserved core domain at the C-terminus (Simonin et al. 2004). The C-terminal part of Gprasp1 e.g. has previously been shown to be responsible for binding 7TMR opioid receptor, in order to sort the receptor for lysosomal degradation (Whistler et al. 2002; Bartlett et al. 2005). Furthermore, Gprasp1-5 share a repeating 15 amino acid motif at the N-terminus, which is less conserved. In 2004 it was proposed that Gprasp1 (Heydorn et al. 2004) and Gprasp2 (Simonin et al. 2004) have the potential to bind 7TMR and it was further suggested that Gprasp proteins serve as adaptors for 7TMR turnover. In line with these reports, we found Gprasp2 to interact with a 7TMR as an adaptor protein for ciliary translocation of Smo in active Hh pathway. Moreover, Gprasp2 and other family members were found to be expressed in the CNS (Simonin et al. 2004) and to interact with huntingtin, a protein considered as a pathological hallmark of Huntington disease, suggesting that Gprasp2 might play a role in receptor trafficking (Horn et al. 2006). Consequently the protein interaction is involved in pathogenesis of the Huntington disease. In a case report of five generations of a Chinese family, the high prevalence of T2D and Huntington suggested a genetic link between these disorders (Hu, Liang, and Yu 2014). Thus, in a mouse model of Huntington disease, IRS2 increased mitochondrial dysfunction and oxidative stress, which are also associated with diabetes (Sadagurski et al. 2011). Gprasp1 and Gprasp2 were further involved in the Xq22.1 deletion syndrome, which is characterized by a deletion of a 350 kb region on the X-chromosome (Zhou et al. 2014). According to the study of *Zhou et al*., the Gprasp proteins together with Armcx5, and Bhlhb9 are responsible for the appearance of the syndrome, which manifests with epilepsy, mental retardation and various developmental defects including cleft palate in heterozygous female patients. It is still not clear whether the whole set of genes or a combination of single genes are responsible for the phenotypes. There is

some evidence to support the assertion that patients with intellectual and developmental disability are at higher risk to develop diabetes (McVilly et al. 2014). Mutations in Gprasp2 gene moreover were suggested to predispose patients to the mental diseases like schizophrenia (Piton et al. 2011). A study comparing 60 patients with a diagnosis of schizophrenia to the general population, revealed an increased risk for cardiovascular diseases, but also for metabolic syndrome, diabetes and obesity (Gladigau et al. 2014). It is therefore likely that Gprasp proteins, which were so far shown to be involved in 7TMR trafficking, degradation and mental disease, play also a role in metabolism and diabetes. For this reason, we used Gprasp2 GT mutant mice in order to study the Gprasp2 expression and influence in development, adult tissue homeostasis and metabolism.

3.2.2.2 Gprasp2$^{GT/y}$ mouse line as a model for obesity and carbohydrate metabolism

Mice that are hemizygous (Gprasp$^{GT/y}$) for Gprasp2 are males due to the location on the X chromosome. Females are either heterozygous or homozygous for Gprasp2 (Gprasp$^{GT/x}$ or Gprasp$^{GT/GT}$, respectively). All observed genotypes were born at expected Mendelian ratio and are viable. Analysis of Gprasp2 expression using the LacZ reporter showed that *Gprasp2* is highly expressed in lung and pancreas, with an exclusive expression in the islets (**Figure 36**). That was why we focused on studying Gprasp2 function in the pancreatic islets. According to the literature, Gprasp proteins are involved in mental diseases and there are some indications that patients suffering from Huntington disease, schizophrenia or mental retardation, develop susceptibility for metabolic diseases such as diabetes and obesity (3.2.2.1). But so far we did not analyze Gprasp2 expression in the CNS and the brain. As the CNS is a key regulator of the glucose homeostasis and consequently a central player in T2D and obesity (Malaguarnera and Belfiore 2014), it has to be considered for the phenotype analysis of Gprasp$^{GT/y}$ mutant mice. A first simple approach would be to analyze the *Gprasp2* LacZ expression in the brain and CNS of Gprasp$^{GT/y}$ mutant mice.

After approximately five months, the Gprasp$^{GT/y}$ males showed an increase in body weight. We indeed, identified tremendously increased pancreatic islet size, as well as liver and epididymal fat pad increase in Gprasp$^{GT/y}$ mutant males (**Figure 37**). Weight increase is referred to obesity and often studied in a well described mouse model, the ob/ob mice (Ingalls, Dickie, and Snell 1950). The gene affected in the ob/ob mice produces the hormone leptin, which is secreted in adipose tissue. As leptin negatively regulates the food intake and ob/ob mouse cannot produce leptin, their food intake is uncontrolled and the mice subsequently gain weight. This mouse line is mainly characterized by obesity and hyperinsulinemie (and hyperglycemia), both also observed in Gprasp$^{GT/y}$ mutant males (Lindstrom 2010). Compared to Gprasp2 mutants, the ob/ob mice increase their food intake (hyperphagia) and subsequently their weight already after weaning. The blood glucose levels reach a peak at three months in ob/ob mice, whereas Gprasp$^{GT/y}$ mutant males show no metabolic changes. Trans-differentiation experiments in hepatic stellate cells showed, that leptin activates Hh signaling, which was important in liver fibrosis and leptin-regulated processes, such as obesity (Choi et al. 2010). It is likely that with the Shh target gene Gprasp2 we have established a link between Hh signaling and obesity, which needs to be further elucidated. In this regard, *Suh et al.* showed a conserved mechanism for Hh signaling from fruit fly to mammalian models, in inhibiting fat formation eventually through induced expression of antiadipogenic transcription factors, such as Gata2 (Suh et al. 2006). As we have reduced Hh signaling

(**Figure 23**, **Figure 24**) in Gprasp$^{GT/y}$ mutant mice and literature provided evidence that there is a link between reduced Hh signaling and obesity, an interesting approach will be to follow leptin pathway components or antiadipogenic targets. Though, it is still not clearly described whether Shh target gene deletion leads to an obese phenotype in adult mice. Tamoxifen induced conditional deletion of ciliopathy gens *Kif3a* and *Tg737* in adult mice, resulted in hyperphagiy and subsequent obesity with elevated plasma levels of leptin, glucose and insulin (Davenport et al. 2007). Thus, the mutants developed slow onset of cystic kidney disease, which could be interesting to also analyze in Gprasp$^{GT/y}$ mutant mice. As Gprasp2 is also important in Shh signaling, the weight gain in Gprasp$^{GT/y}$ mutant mice could be due to hyperphagia. Hyperphagia can be addressed in pairfeeding experiments, were the food intake is monitored. As already mentioned earlier, in order to understand the Gpasp2 obese phenotype, we have to study the involvement of the brain. Oxytocin levels increase following a meal. Peripheral and hindbrain oxytocin receptors are responsible to limit food intake (Ho et al. 2014). Systemic KO study showed that IKK elipson may be a key inflammatory mediator in the hypothalamus of obese mice (Weissmann et al. 2014). When inhibited in the hypothalamus energy and glucose metabolism was improved. In summary, from literature we have a variety of propositions, serving us to direct the obese phenotype analysis of Gprasp2 GT mutants.

Obesity leads to the infiltration of fat in multiple organs including the heart, kidneys, liver, and pancreas, often accompanied with insulin resistance or T2D. Gprasp$^{GT/y}$ mutant males showed extensive lipid storage in the liver and WAT storage in the epididymal fad pad. It still needs to be clarified, whether the phenotype is due to a β-cell defect or a peripheral insulin resistance. But we hypothesize, that Gprasp$^{GT/y}$ mutant mice increase their islets size due to a possible insulin resistance of the peripheral tissue. This would implicate fist, the occurrence of an insulin resistance of the peripheral tissue, determining the higher insulin demand. Second, a response of the islets to the higher insulin demand with an increase in β-cell mass and subsequent islet size. Third, the body weight and liver fat increases in Gprasp$^{GT/y}$ mutant males, due to the continuous peripheral insulin resistance. In order to address this hypothesis, a time-resolved occurrence of β-cell mass increase, body weight gain, and liver fat increase is necessary. Thus, in order to address a possible insulin resistance effect of peripheral tissues and organs, an ipITT has to be performed. *Hebrock et al.* demonstrated that active Hh signaling within the pancreatic epithelium led to epithelial-specific Smo loss, which resulted in a reversible delay in β-cell morphogenesis, glucose intolerance and less insulin despite of increased β-cell mass (Lau and Hebrok 2010). In contrast, inhibition of Shh signaling by Cyc lead to an increase in islet size in chick embryos (Kim and Melton 1998). With deleting Gprasp2 we have reduced Hh signaling and increased islet size in Gprasp$^{GT/y}$ mutant males, which goes in line with the studies of chick embryos. Thus, several studies have shown that insulin resistance is a characteristic feature of NAFLD (Yki-Jarvinen 2010). Though, the mechanism which links intrahepatic triglyceride storage (liver steatosis), insulin resistance, and hypertriglyceridemia is not known so far. It might involve the redirection of the free-fatty acid (FFA) plasma uptake and intracellular triglyceride production form the adipose tissue depots to other tissues like the liver (Goldberg, Eckel, and Abumrad 2009). A gene controlling the FFA uptake is CD36. It is specific for the certain tissues like the skeletal muscle and adipose tissue, and therefore considered to be involved in the pathogenesis of triglyceride storage in the liver. As already mentioned, one possible explanation for the Gprasp2 phenotype could be a change in insulin demand,

consequent to an insulin resistance of peripheral tissues like muscle and adipose tissue, leading to a subsequent increase in islet size. Thus, it is possible that lack of Gprasp2 leads to depletion of triglycerides trafficking thereby allowing to store triglycerides in the liver and adipose tissue. The literature provides starting points which could redound to a better understanding of the uptake and trafficking of FFA and triglycerides and the possible connection with the liver. A recent study e.g. reports that hepatic overexpression of betatrophin (Angiopoietin-like protein, Angptl8) causes hypertriglyceridemia and increased insulin secretion (Quagliarini et al. 2012). Thus, Angptl3, a betatrophin interacting protein, inhibits lipoprotein lipase and cleaves FFA from triglycerides. *Wang et al.* further reported that triglycerides are delivered to skeletal muscle and heart or to adipose tissues during fasting or refeeding, respectively (Wang et al. 2013). This trafficking is not functioning in betatrophin mutant mice, which lead to storage failure of triglycerides in adipose tissue. Interestingly, there was no defect in glucose metabolism, which was similar to the phenotype observed in Gprasp$^{GT/y}$ mutant males. In summary, both proteins, Angptl3 and Angptl8, were reported to be responsible for the triglyceride trafficking, which is tissue specific according to the food intake. A possible connection between Gprasp2 mutants to betatrophin mutant mice should therefore be considered. Thus, taking a recent study into account, which reports that hepatic betatrophin overexpression promotes β-cell proliferation and insulin secretion (Yi, Park, and Melton 2013), we might also find a connection to the Pifo KO mutant phenotype, as Pifo KO mutants exhibit a diet-induced β-cell proliferation and an insulin secretion defect.

Phenotype analysis of homozygous females showed no weight gain and low levels of insulin, compared to hemizygous males (**Figure 39**). A possible explanation for the phenotypic difference between male and female could be due to the gender difference in hormone receptors. It was reported that e.g. the estrogen receptor exhibit a protective role in the progression of hepatocellular carcinoma (Parkin et al. 2005). Interestingly, Foxa1 and Foxa2 have been implicated their functions in liver development, as mice lacking either of these genes in the foregut endoderm, show no liver formation (Bochkis et al. 2008; Lee et al. 2005). Foxa2 is an interesting candidate to consider, as *Pifo* was found as Foxa2 target gene and Gprasp2 as an interaction partner of Pifo. It might be therefore important to follow this connection of Gprasp2 and Foxa2 with regard to triglyceride storage in the liver. It has been further shown that Foxa1 is necessary for sufficient recruitment and binding of the estrogen and androgen receptor to their targets. Foxa1 and Foxa2 are further important for liver pathogenesis, as liver specific KOs of either of these proteins led to hepatocellular carcinomas in male mice, but not in females due to the protective role of the estrogen receptor (Li, Tuteja, et al. 2012). The gender difference in insulin content observed in Gprasp2 gene trap mutant mice could therefore be of interest, but needs to be further analyzed. In the broader sense it would be important to follow the insulin secretion, weight gain and liver triglyceride storage in females and compare these results to the ones mentioned in hemizygous Gprasp$^{GT/y}$ males.

Genetics and environment are important factors in the development of obesity, with diet as *the* important environmental factor. Human studies have shown that increased fat intake leads to an increase in body weight, which can further lead to obesity and other metabolic disease. In order to understand the obese phenotype in more detail, we analyzed Gprasp$^{GT/y}$ mutant males on changed metabolic HFD conditions. Surprisingly, the

body weights as well as the fat and lean mass were unaltered in Gprasp$^{GT/y}$ mutant males compared to WT controls (**Figure 37**). Also the lipid and WAT storage in the liver and epididymal fad pad, respectively, was equal between the two groups. The unexpected moderate obese phenotype observed in Gprasp$^{GT/y}$ mutants after HFD feeding led us to the consumption that the phenotype is not HFD-diet induced. HFD food contains 58 % fat and 25.5 % carbohydrates, in comparison to normal chow diet which contains only 9 % fat and 61 % carbohydrates. In fact, the hyperphagia-like behavior, subsequent obesity and lipid storage is only observed under normal chow conditions. We therefore conclude that we have created a novel mouse model system in order to study carbohydrate metabolism.

3.3 Concluding remarks

With the discovery of being co-expressed in Shh regions in the developing mouse embryo and the regulation upon Shh signaling, *Pifo* and *Gprasp2* were identified to be novel Shh target genes. When either Pifo or Gprasp2 are absent, the translocation of Smo to the PC membrane fails. Mechanistically this study links Pifo and Gprasp2 for the first time with the IFT motor subunit and the core event in Shh pathway activation and therefore provides the basic mechanism for further studies of the pathway in diabetes and cancer. Gprasp2 thereby anchors Pifo to Smo and Kif3b when Shh signal is active. With the complex formation of Pifo-Gprasp2-Smo, we show a new Smo transport mechanism in Shh signaling and a potential therapeutic target, as skin and brain cancers show mutation in Smo activation and can be treated by Smo antagonists. Due to the restricted expression of Pifo to ciliated tissue and the previous observed ciliary phenotype (Kinzel et al. 2010), Pifo was suggested to be involved in ciliopathies, which have a broad range of phenotypes. Pifo deletion led to died-induced glucose intolerance and proliferation decrease in pancreatic β-cells and an insulin secretion defect. We provided a novel link between Shh signaling and CDK4-pRB-E2F1 pathway, which is involved in β-cell proliferation and insulin secretion. With the died-induction of the Pifo mutant phenotype, we have created a mouse model system to study predisposition and environmental factors in the context of T2D. Gprasp2 mutant mouse study, on the other hand encloses a model for obesity, and NAFLD in context of carbohydrate metabolism. Therefore, the analysis of Pifo and Gprasp2, two novel ciliary proteins, contribute to the better understanding of the Shh pathway in development, cancer and metabolic disease. This study provides further knowledge in the mechanism Smo translocation to the PC and provides a link how ciliopathy genes cause phenotypes, such as diabetes and obesity.

4 Material and methods

4.1 Material

4.1.1 Equipment

4.1.1.1 General

Shaking water bath	SWB25 (Thermo Fisher Scientific Inc., Langenselbold)
Thermomixer	Comfort 3152 SHR (Eppendorf AG, Wessling-Berzdorf)
Shaker	Shake'n'Stack (Thermo Fisher Scientific Inc., Waltham)
Vortexer	Vortexer (VWR international GmbH, Darmstadt)
Roller Mixer	SRT1 (Bibby Scientific, Staffordshire, GB)
Rotator/tumbler	VSR 23 (Grant BOEKEL, VWR international GmbH, Darmstadt)
Stirrer	STIR (VWR international GmbH, Darmstadt)
Microcentrifuge	Galaxy Mini C1200-RT (VWR International GmbH, Ismaning)
Centrifuges	5417 R, C and 5804 R (Eppendorf AG, Hamburg)
	Hettich Universal 30F (Andreas Hettich GmbH & Co. KG, Tuttlingen)
	1-14 (Sigma Laborzentrifugen GmbH, Osterode am Harz)
Microwave	700W (Severin Elektrogeräte GmbH, Sundern)
Freezer	-20°C (Liebherr Hausgeräte Ochsenhausen GmbH, Ochsenhausen)
Fridge	4°C (Liebherr Hausgeräte Ochsenhausen GmbH, Ochsenhausen)
Power supplier	Power Pack Basic (BioRad Laboratories, München)
Pumps	LABOPORT® (neoLab Migge, Laborbedarf Vertriebs GmbH, Heidelberg)
Pipettes	Eppendorf Research (Eppendorf AG, Hamburg)
Pipetboy	Accu jet® and accu jet® pro (Brand GmbH & Co. KG, Wertheim)
Glassware	Schott Duran (Schott AG, Mainz)
Plastic ware	(VITLAB GmbH, Grostheim)
Incubator	Shaking incubator, 37°C (Shel Lab, Sheldon Manufacturing)
	TH-30 and SM-30, 32°C (Edmund Buhler GmbH, Hechingen)
	Thermomixer comfort (Eppendorf AG, Hamburg)
Water purification system	Millipore Q-POD, 0.22µl filter (Merck Chemicals GmbH, Schwalbach)

4.1.1.2 Instrumentation

General

Photometer	BioPhotometer (Eppendorf)
	ND 1000 Spectrophotometer (NanoDrop, Thermo Fisher Scientific Inc., Waltham)
PH meter	pH211 Microprocessor pH Meter (HANNA Instrumentes Deutschland GmbH, Kehl am Rhein)
Electroporation system	BioRad Gene Pulser Xcell (BioRad Laboratories, München)

Cryostat	CM 3050S (Leica Mikrosysteme Vertrieb GmbH, Wetzlar)
Microplate reader	PHERAstar FS (BMG LABTECH GmbH, Ortenberg)
Microscopes and Cameras	
Microscopes	Axiovert 200M (Carl Zeiss AG, Göttingen)
	Lumar.V12 (Carl Zeiss AG, Göttingen)
	MS5 (Leica Microsystems GmbH, Wetzlar)
	TCS SP5 (Leica Microsystems GmbH, Wetzlar
Camera	AxioCam MRc5 (Carl Zeiss AG, Göttingen)
	AxioCam HRm (Carl Zeiss AG, Göttingen)
Primary and ES cell culture	
Cell culture hood	BDK (Luft-und Reinraumtechnik GmbH, Sonnenbühl-Genkingen)
Water bath	1003 (GFL - Gesellschaft für Labortechnik GmbH, Burgwedel)
Cell Incubator	KBF, (Binder GmbH, Tuttlingen-Möhringen)
Cell counting chamber	Neubauer (LO – Laboroptik GmbH, Friedrichsdorf)
Centrifuge	Rotanta 460R (Hettich AG, Bäch, CH)
Freezing boxes	CoolCell® Alcohol-Free (BioCision LLC, USA, CA)
	Freezing container, Nalgene® (Sigma-Aldrich Chemie Gmbh, München)
Seahorse	
Seahorse plates	XF24 Islet Capture Microplate (Seahorse Bioscience, USA, MA)
Seahorse inserts	XF24 Biosensor Cartridge (Seahorse Bioscience, USA, MA)
Media	XF Assay Medium, XF Calibrant Sulution (Seahorse Bioscience, USA, MA)
RT- and Real-time PCR	
PCR machines	Px2 ThermoHybaid (Thermo Fisher Scientific Inc., Waltham)
	PXE0.2 Thermo Cycler (Thermo Fisher Scientific Inc., Waltham)
Gel documentation system	UV – Transilluminator (Biorad, München)
	Gene Flash (Syngene Bio Imaging, Synoptics Ltd, Cambridge)
Electrophoresis chamber	Midi Horizontal (neoLab, Heidelberg)
Continuous fluorescence detection system	DNA Engine Opticon® (Genetic Technologies, Inc., Miami, FL)
Samplepreparation RNA/Protein	
Sonicator	Sonoplus HD2070 (Bandelin electronic GmbH&Co.KG, Berlin)
Disperser	Ultra Turrax® (IKA®-Werke GmbH&Co.KG, Staufen)
Westen Blot	
Gel chamber	Polyacrylamid, Mini Trans-Blot® Cell (BioRad GmbH, Heidelberg)
Semi-dry system	Trans-Blot® SD, Semi Dry Transfer cell, Mini-PROTEAN® Tetra Cell, Trans-Blot® Turbo™ Blotting System (Biorad, Heidelberg)
Developing machine	AGFA Curix 60 developing machine (AGFA HealthCare GmbH, Bonn)

Cro and Paraffin

Cryostat	CM1860 (Leica Mikrosysteme Vertrieb GmbH, Wetzlar)
Embedding station	EG1160 (Leica Mikrosysteme Vertrieb GmbH, Wetzlar)
Microm	HM 355 S (Thermo Fisher Scientific Inc., Waltham)
Water bath	WBL 793 (Vogel GmbH & Co. KG, Gieβen)
Heating plate	HI 1220 (Leica Mikrosysteme Vertrieb GmbH, Wetzlar)

Glucose and Insulin measurements

NMR	(EchoMRI LLC, Houston, TX, USA)
ELISA reader	PHERAastar FS (BMG Labtech GmbH, Ottenberg)
Seahorse	(Seahorse Bioscience, USA, MA)

4.1.2 Consumables

4.1.2.1 General

2 ml/ 1.5 ml tubes	Safe lock reaction tubes (Eppendorf AG, Hamburg)
50 ml/ 15 ml/ 14 ml tubes	BD Labware (Becton and Dickinson and Company, Heidelberg)
0.2 ml tubes	PCR tubes (Eppendorf AG, Hamburg)
0.5-10 µl/ 1-200 µl/ 100-1000 µl	Tips general (Omnitip™, Warsaw, P)
10 µl/ 200 µl/ 1000 µl	Filter tips (Tipone®, Hamburg)
50 ml/ 25 ml/ 10 ml/ 5 ml/ 2 ml/ 1 ml	Serological pipettes, plastic (Greiner Bio-One, Frickenhausen)
Pasteur pipettes	Plastic transfer pipettes (Carl Roth GmbH & Co. KG, Karlsruhe)
Parafilm	Parafilm (Pechiney Plastic Packaging, Menasha)
Surgical scalpel	Sterile (B|Braun, Tuttlingen)
Petridishes for bacteria	10 cm, BD FalconTM (Becton Dickinson GmbH, Heidelberg)
Cell strainer	1ea, 10 µl Nylon (BD Falcon™)
Cell scraper	(Sarstedt, Nümbrecht)
3 ml syringe	(Tyco Healthcare, Switzerland, CH)
5 ml syringe	(BD, Franklin Lakes, USA, NJ)
30 ml syringe	(B. Braun Melsungen AG, Melsungen)
30G1/2-G needle	(B. Braun Melsungen AG, Melsungen)
Steril filter	Rotilabo®-Spritzenfilter, 0.22 µm PVDF (Carl Roth GmbH, Karlsruhe)
Forceps	Dumount Inox #5 (11251-, 11252-20, Fine Science Tools GmbH, Heidelberg)
Scissors	(14088-10, Fine Science Tools GmbH, Heidelberg)
Clamp (pancreas)	Bulldog SerrefinE-– Straight 35 mm (Fine Science Tools GmbH, Heidelberg)

Cell culture dishes

15 cm/ 10 cm/ 6 cm dishes	Nunc (Thermo Scientific Fisher, Wiesbaden)
6-well/ 12-well/ 24-well/ 48-well/ 96-well plates	

(Straight or conical plates)	
Coverslips	round, ⌀ 12 mm (Carl-Roth GmbH, Karlsruhe)

RT-PCR and real time PCR

PCR tubes	
Real time PCR strips	Flat cap strips (BioRad,
Real time PCR tubes	low profile PCR tubes white (BioRad)

Western Blot

PVDF membrane	Immuno-Blot PVDF-Membrane (BioRad Laboratories, Hercules)
Nitrocellulose membrane	(GE Healthcare Buchler GmbH & Co. KG, München)
Blotting paper	Whatman paper (GE Healthcare Buchler GmbH & Co. KG, München)
Films	Kodak BioMax MS (Sigma-Aldrich GmbH, Hamburg)
	Hyperfilm ECL (GE Healthcare Buchler GmbH & Co. KG, München)
VivaSpin 500	centrifugal devices (Sartorius Stedim Biotech GmbH, Göttingen)

Cryo and Parafin

Embedding moulds	Peel-A-Way® (Carl Roth GmbH & Co. KG, Karlsruhe)
Embedding cassettes	Rotilabo® (Carl Roth GmbH & Co. KG, Karlsruhe)
Glas slides, histology	Menzel-glasses (Gerhard Menzel GmbH, Braunschweig)
Coverslips	24x50 mm, #1.5 and 24x60 mm #1 (Carl-Roth GmbH, Karlsruhe)
SecureSeal Imaging Spacer	SS8X9, 9 mm (Grace BioLabs, Bend, Oregon)

4.1.3 Cell lines and culture media

4.1.3.1 Cell culture solutions and media

1x PBS without Mg^{2+}/Ca^{2+}	D-PBS (Gibco, Invitrogen™ Cooperation, Carlsbad, CA),
1x trypsin-EDTA	0.05 % trypsin, 0.53 mM EDTA•4Na (Gibco, Invitrogen™ Cooperation, Carlsbad, CA)
Penicillin/streptomycin	pen/ strep (Gibco, Invitrogen™ Cooperation, Carlsbad, CA)
Antibiotic antimycotic solution	(Sigma, Hamburg, A5955)
FCS, primary cells and cell lines	PAA (Laboratories Gesellschaft GmbH, Pasching, Österreich)
FCS, ES cells	PAN (Biotech GmbH, Aidenbach)
L-glutamine	200 mM (Gibco; Invitrogen™ Cooperation, Carlsbad, CA)
1x MEM	non-essential amino acids, 100x (Gibco, Invitrogen™, Carlsbad, CA)
B-mercaptoethanol	50 mM (Gibco, Invitrogen™ Cooperation, Carlsbad, CA)
HEPES	200 mM (Gibco, Invitrogen™ Cooperation, Carlsbad, CA)
LIF	ESGRO® (Chemicon, Millipore, Schwalbach)
HBSS	Hank's balanced salt solution (Lonza Verviers, Belgium, BE10-508F)
Hepes	1 M (Lonza Verviers, Belgium)
Optiprep	Density gradient medium (Sigma, Hamburg, D1556-250ML)
Collagenase P	(Roche, Pensberg 11 213 865 001/11 213 873 001)

G-solution	HBSS supplemented with 1 % antibiotic antimycotic solution or pen/strep and 1 % BSA (5 g BSA sterile filtered)
40 % Optiprep	20 ml 60 % Optiprep, 9.7 ml D-BPS, 300 µl 1 M HEPES
15 % Optiprep	Supplement 5 ml 10 % RPMI 1640 in HBSS and add 3 ml 40% Optiprep
10 % RPMI	45 ml HBSS (with antibiotic antimycotic solution) supplemented with 5 ml cell culture medium
Colagenase P solution	6 mg Collagenase P (Col P) per mouse supplemented with 6 ml G-solution (1 mg/ml) under the cell culture hood and sterile filtrate, place on ice
10 x KRH buffer stock	1.200 mM NaCl, 48 mM KCl, 25 mM $CaCl_2.2H_2O$, 12 mM $MgCl_2$
KRH working solution	Final concentration: 120 mM NaCl, 4.8 mM KCl, 2.5 mM $CaCl_2.2H_2O$, 1.2 mM $MgCl_2$. For 200 ml (ph 7.4): 20 ml of 10 x KRB stock, 1 ml 1 M HEPES, 9.6 ml HCO_3 (0.5 M $NaHCO_3$) stock (1 M)

4.1.3.2 Cell lines, ES cells and primary cells

Primary limb bud cells	Primary murine LBs, abbreviated PLCs, derived from embryos at E10.5 isolated from the fore limbs of the embryo
Primary MEFs	Primary murine embryonic fibroblasts derived from E10.5 isolated from the body part around the fore limb of the embryo
Islets	Pancreatic islets were isolated at the particular age from adult mice and in general cultured prior to the experiments overnight
HEK293T	Human embryonic kidney cells stably expressing the T-large antigen of SV40 (Graham et al. 1977)
IMCD3 cells	Kidney, medulla/ collecting duct stable expressing the T-large antigen of SV40 (ATCC, USA, M)
865 cells	Fibroblast cells line, expression of SV40 large T antigen constitutively. A courtesy from Dr. Ralph Lange (Max Planck)
IDG3.2 ES cells	Murine ES cell line (F1); genetic background 129S6/SvEvTac x C57BL/6J (Hitz, Wurst, and Kuhn 2007)
Gprasp2 ES cells	ES cell clone in C57 BL/6 (IST12714A6, TIGM, College Station, TX)
$Pifo^{tm1e(KOMP)Wtsi}$	ES cell clone A7 (EUCOMM, KOMP institutions)
Feeder/MEFs	Primary murine embryonic fibroblasts isolated from E13.5 CD1 embryos
E14TG2A	Murine embryonic stem cell line derived from the blastocyst (ATCC, CRL-1821™, VA, USA)
BRL cells	Buffalo rat liver cell line

4.1.3.3 Cell culture media

Primary limb bud-/ MEFs/ 865-/ human embryonic kidney cells (Hek 293T)	D-MEM (Gibco, Invitrogen™ Cooperation, Carlsbad, CA) supplemented with 2 mM L-glutamine (Gibco), 10 % FCS (PAA, Laboratories Gesellschaft GmbH) and 1 % pen/strep (Gibco)

Islets	RPMI (Lonza Verviers, Bergium) supplemented with 10 % FCS (PAA, Laboratories Gesellschaft GmbH) and 1 % pen/strep (Gibco) or Antibiotic antimycotic solution (Sigma, Hamburg).
ES cells	D-MEM (Gibco) supplemented with 2 mM L-glutamine (Gibco), 15 % FCS (PAN, Biotech GmbH), 0.1 mM β-mercaptoethanol (Gibco), 1x MEM (Gibco), 2 mM HEPES, 107 U/ml ESGRO® (LIF, Chemicon, Millipore)
Gprasp2 ES cells	D-MEM (Gibco, #10829-018) supplemented with 92 ml FBS (Thermo Scientific™ HyClone™ #SH30070-30), 0.1 mM β-mercaptoethanol (Gibco), and 6.1 ml GPS: 100x Aino acid solution (Millipore, #TMS-001-C), 200 mM L-glutamine (Gibco, #25030-016), 5,000 U/ml Penicillin G, sodium salt. (Sigma, #P-3032), 5,000 µg/ml streptomycin sulfate (Life Technology, #11860-038)
Feeder/MEFs	D-MEM (Gibco) supplemented with 2 mM L-glutamine (Gibco), 15 % FCS (PAA, Laboratories Gesellschaft GmbH), 0.1 mM β-mercaptoethanol (Gibco), 1x MEM (Gibco), 2 mM HEPES (Gibco)
Freezing media	For freezing, cell culture media was supplemented with 20 % FCS, PAA or PAN, respectively and 10 %DMSO.
E14TG2A culture media	ES cell culture media supplemented with 10 % buffalo rat liver (BRL) cell supplemented media.
Immortalization medium	865 cell supernatant, expression of SV40 large T antigen constitutively

4.1.3.4 PLC assay supplements

Shh	Recombinant mouse Shh (C25II) N-Terminus (R&D Systems, Inc., Deubel, Minneapolis, MN)
SAG	Smoothened ligand (Alexis®Biochemicals, Lörrach)
Cyclopamine	Smootened ligand (Cyc, Sigma, Schnelldorf)

4.1.4 Mouse lines

C57BL/6NCrl	BL6 Mice were obtained from Charles River. This strain was used for the production of targeted mutation (knockout) mice. http://www.criver.com/en-US/ProdServ/ByType/ResModOver/ResMod/Pages/C57BL6Mouse.aspx
129S6/SvEvTac	129SVES6 Mice were obtained from Taconic. This strain was used for the production of targeted mutation (knockout) mice. http://www.taconic.com/wmspage.cfm?parm1=809
CD1	Outbred mouse strain (Helmholtz Zentrum München). This strain was used for LacZ analysis and Plug matings.
R26Cre	(Soriano 1999)
Flp-e	(Dymecki 1996)
Pifo flox/ flox	Mouse line generated from Ingo Burtscher and Doris Kinzel (BL6 background)
Pifo flox/ flox, RosaCre	Mouse line intercrosses of R26Cre and Pifo flox/ flox (BL6 background)
Pifo KO	Mouse line intercrosses of Pifo flox/ flox, RosaCre and BL6

Pifo KO129SVES6	Mouse line intercrosses of Pifo flox/ flox, Rosa Cre and 129SVES6
$Sufu^{-/-}$	(Lee et al. 2007)
$Kif7^{-/-}$	(Cheung et al. 2009)
Pifo Sufu	Mouse line intercrosses of Pifo KO and $Sufu^{-/-}$ (CD1, BL6 and 129SVES6 background)
Pifo Kif7	Mouse line intercrosses of Pifo KO and $Kif7^{-/-}$ (BL6 and 129SVES6 background)
Tg(GBS-GFP)	(Nikolaos Balaskas et al., Cell, 2012)
Pifo GBS-GFP	Mouse line crosses of Pifo KO and Tg(GBS-GFP) (BL6 background)
$Gprasp2^{GT/y}$	Mouse line generated in this thesis from gene trapped ES cells, which were obtained from Texas A&M Institute for Genomic Medicine. Chimeras were generated using diploid aggregation technique.
Pifo Gprasp2	Mouse line intercrosses of Pifo KO and $Gprasp2^{GT/y}$ (BL6 background)

4.1.5 Buffers and solutions

Transfection supplements

TransFectin	(Bio-Rad Laboratories GmbH, Munich)
PEI	25 kDa linear PEI (Polysciences Inc., Eppelheim)
PEI stock solution	final concentration 1 mg/ ml: 25 mM HEPES and 150 mM NaCl (pH 7.5)
Opti-MEM	(Life Technologies GmbH, Frankfurt)

Genomic DNA isolation (mouse tails)

Lysis buffer	100 mM Tris (pH 8.5), 5mM EDTA, 0.2 % SDS 200 mM Sodium chloride, 100 µg/ µl Proteinase K

EDU

Imaging Kit	Click-IT EDU Alexa Fluor 647 (#C10340, Life Technologies, Freiburg)
EdU	(#A10044, Life Technologies, Freiburg)

RNA

Trizol® reagent	(Gibco®, Invitrogen™ Cooperation, Karlsruhe)
QIAzol lysis reagent	(Quiagen GmbH, Hilden)
miRNeasy Mini Kit (50)	(Quiagen GmbH, Hilden)

cDNA

Random primer	(Promega Corporation, Madison, WI)
DTT	DL-Dithiothreitol (Thermo Scientific, St. Leon-Roth)
RNasin	Plus RNase Inhibitor (Promega GmbH, Mannheim)
dNTPs	dGTP, dCTP, dTTP, dATP 100 mM (Thermo Scientific, St. Leon-Roth)

Genotyping and RT-PCR

100 bp and 1 kb DNA marker	(New England Biolabs GmbH, Frankfurt am Main)
Nuclease free water	(Promega GmbH, Mannheim)
$MgCl_2$	25 mM (Thermo Scientific, St. Leon-Roth)

TaqBuffer $(NH_4)_2SO_4$-$MgCl_2$	10x Taq buffer with $(NH_4)_2SO_4$ (Thermo Scientific, St. Leon-Roth)
TaqBuffer KCl-$MgCl_2$	10x Taq buffer with KCl (Thermo Scientific, St. Leon-Roth)
Real-time qPCR	
SYBR® Green	(Bio-Rrad Laboratories, Herculess, CA)
TaqMan® MM	Fast Advanced Master Mix (Life Technologies GmbH, Darmstadt)
Agarose gel DNA/RNA	
50 x TAE buffer	2 M Tris, 50 mM Glacial acetic acid, 50 mM EDTA
Loading buffer DNA	100 mM EDTA, 2 % SDS, 60 % Glycerol, 0.2 % Bromine phenol blue
50x TAE buffer (RNA)	2 M Tris, 50 mM Glacial acetic acid, 50 mM EDTA, in DEPC-H_2O
Loading buffer RNA (2x):	95 % Formamide, 0.025 % SDS, 0.025 % Bromine phenol blue, 0.025 % Xylene cyanol FF, 0.025 % Ethidium bromide, 0.5 mM EDTA
Western Blot	
Protein quantification	Bradford Reagent (Sigma, Schnelldorf)
Bradford standard	BSA standard set (BioRad, München)
Sample lysisbuffer (RIPA)	50 mM Tris-HCl (pH 7.4), 150 mM sodium chloride, 0.5 % sodium deoxycholate, 0.1 % SDS, 1 % Nonidet P-40 (sterile filtrate)
4x SDS-loading-dye	200 mM Tris-HCl (pH 6.8), 8 % SDS, 0.4 % Bromophenol blue, 50 % Glycerol, 40 mM DTT
10x Tris-Glycine (running buffer)	1.0 % SDS, 0.25 M Tris, 1.92 M Glycine
Separation-/	4x Tris-HCl/SDS buffer 1.5 M Tris-HCl (pH 8.8), 0.4 % SDS
Collection gel buffer	4x Tris-HCl/SDS buffe 0.5 M Tris-HCl (pH 6.8)
APS	10 % APS
Anode buffer I	0.3 M Tris-HCl (pH 10.4), 10 % Methanol
Anode buffer II	25 mM Tris-HCl (pH 10.4), 10 % Methanol
Cathode buffer	25 mM Tris-HCl (pH 9.4), Methanol 10 %, Glycine 40 mM
10xTBST	100 mM Tris-HCl (pH 7.5), 1.5 M Sodium chloride;
1xTBST	+2% Tween20
Blocking solution	5 % milk (powder)/ 1x TBST
ECL-solution	Solution A and B mix: 1:1
SDS-polyacrylamide gel (4x)	6.5 %: 6.52 ml acrylamide (Carl Roth, Rotiphorese Gel 30; 30 % solution), 7.5ml separation buffer, 16 ml H_2O, 40 µl TEMED, 300 µl APS 10 % 7.5 %: 7.5 ml acrylamide, 7.5 ml separation buffer, 15 ml H_2O, 40 µl TEMED, 300 µl APS 10 % 10 %: 10 ml acrylamide, 7.5 ml separation buffer, 12.5 ml H_2O, 40 µl TEMED, 300 µl APS 10 % 12 %: 12 ml acrylamide, 7.5 ml separation buffer, 10.5 ml H_2O, 40 µl TEMED, 300 µl APS 10 %

	13 %:13.04 ml acrylamide, 7.5 ml separation buffer, 9.46 ml H_2O, 40 µl TEMED, 300 µl APS 10 % 15 %: 15 ml acrylamide, 7.5 ml separation buffer, 7.5 ml H_2O, 40 µl TEMED, 300 µl APS 10 %
Protein ladder	PageRuler™ Plus Prestained (Thermo Fisher Scientific, Rockford, IL)
Immuno-Prezipitation	
Sample lysisbuffer (strep-IP)	30 mM Tris-HCl (pH 7.4), 150 mM sodium chloride, 0.5 % Nonidet P-40
Washing buffer (strep-IP)	30 mM Tris-HCl (pH 7.4), 150 mM sodium chloride, 0.1 % Nonidet P-40
Elution buffer (strep-IP)	D-Desthiobiotin 10x concentrated Buffer E 25 ml (IBA GmbH, Göttingen)
Strep Tactin Superflow beads	Strep-Tactin Superflow 0.5 suspension 20 ml (IBA GmbH, Göttingen)
Southern Blot	
Depurinisation buffer	11 ml HCl in 989 ml H_2O
Depurination buffer	87.66 g NaCl, 20.00 g NaOH in 800 ml H_2O, filled up to 1 L
Neutralization buffer	87.66 g NaCl, 60.50 g Tris in 800 ml H_2O, filled up to 1 L
20x SSC stock solution	175.3 g NaCl, 88.2 g natrium citrat (pH 7.0)
20 5 SDS stock solution	200 g SDS in 1 l H_2O (under the hood)
Transfer, 20x SSC	88.23 g trinatrium citrat, 175.32 g NaCl in 800 ml H_2O, filled up to 1 L
Hybridisation buffer	29 g NaCl (final conc. 1 M), 25 ml 1 M Tris (pH 7.5, 50 mM), 50 g dextransulfate (10 %), 25 ml 20 % SDS, 12.5 ml salmon sepermidine DNA (250 µg/ µl)
100x Spermidine	S2626 (Sigma, Hamburg)
Klenow-Enzyme	DNA polymerase I large (Klenow) fragment (Promega GmbH, Ulm)
Primer Labeling Kit	Prime-It® RmT Random (# 300385, Stratagene AG Liquidation, CH, Basel)
Immuno-stainings	
DPBS	Dulbecco`s Phosphate-Buffered Saline (DPBS; Gibco®, Invitrogen™ Cooperation, Carlsbad, CA)
10xPBS	80 g NaCl, 2 gKCl, 11.5 g $Na_2HPO_4 \cdot 2H_2O$, 2 g KH_2PO_4 (pH 7.2-7.4)
PBST	PBS (pH 7.2-7.4), 0.1 % Triton-X 100
Permeabilization	0.1 M Glycine/PBST
Blocking solution	10 % FCS (heat inactivated, Gibco®, Invitrogen™ Cooperation, Karlsruhe), 3 % serum (donkey, goat), 0.1% BSA Gibco®, Invitrogen™ Cooperation, Carlsbad, CA)
DAPI	(Life Technologies GmbH, Invitrogen™ Cooperation, Darmstadt)
DAPI mounting medium	Prolong® Gold antifade reagend (Life Technologies GmbH, Invitrogen™ Cooperation, Darmstadt)
Labelling mouse IgG	Zenomn® mouse IgG labeling kit (Life Technologies GmbH, Invitrogen™ Cooperation, Darmstadt)
Cryo- and Parafin	

Tissue Freezing Medium	Jung embedding media (Leica Microsystems Nussloch GmbH, Nussloch)
Oil Red O	O0625 (Sigma-Aldrich, Taufkirchen)
Eosin Y solution, aqueous	HT110216 (Sigma, Hamburg)
Hematoxylin solution, Mayer´s	MHS1 (Sigma, Hamburg)
Nuclear fast red (NFR)	N3020 (Sigma, Hamburg)
Xylene mounting medium	Roti® Histokitt (Carl-Roth GmbH, Karlsruhe)

LacZ

Fixation buffer sterile	0.02 % NP-40, 5 mM EGTA pH 8.0, 2 mM $MgCl_2$ x $6H_2O$, 1 % Formaldehyde 0.2 % Glutaraldehyde/ PBS
Washing buffer	0.02 % NP-40/ PBS
Staining buffer sterile	0.02 % NP-40, 2 mM $MgCl_2$ x $6H_2O$, 5 mM $K_3[Fe(CN)_6]$, 5 mM $K_4[Fe(CN)_6]$ x $6H_2O$, 0.01 % Natriumdesoxycholat, 1 mg/ml X-Gal/ PBS

In-situ

PBT	0.1 % Tween-20/ PBS
PBT (pH 4.5)	0.1 % Tween-20/ PBS (pH 4.5 adjust with HCL)
Hybridisations buffer	50 % formamide, 5 x SSC pH 5.4, 1 % SDS, 50 µg/ ml yeast tRNA, 50 µg/ ml heparin
20 x SSC	175 g NaCl, 88.2 g Na citrate/ 1 l (pH 4.5 adjust with citric acid)
10 % SDS	10 g SDS in 100 ml DEPC H_2O
MAB	100 mM Maleic acid, 150 mM NaCl, 2 mM Levamisole, 0.1 % Tween-20 (pH 7.5 adjust with NaOH)
MAB/ blocking solution	2 % Boerhinger Manheim blocking reagent/ MAB
antibody solution	0.1 % embryo powder (v/v), 10 % MAB/Block, 1/100 Sheep serum, 1/5000 Anti-Dig Alkaline phosphatase
Solution I	50 % formamide, 5 x SSC pH 5.4, 1 % SDS
Solution II	50 % formamide, 2 x SSC pH5.4, 0.2 % SDS
TNT	10 mM Tris pH 7.5, 0.5 M NaCl, 0.1 % Tween-20
NTMT	100 mM Tris pH 9.5, 50 mM $MgCl_2$, 100 mM NaCl, 0.1 % Tween-20, 2 mM Levamisole

Plasmid preparation

P1 buffer	50 mM Tris-HCl (pH 8.0), 10 mM EDTA, 100 µg/ ml RNase A
P2 buffer	200 mM Sodium hydroxide, 1 % SDS
P3 buffer	3 M Potassium acetate (pH 5.5)
QBT buffer	750 mM Sodium chloride, 50 mM MOPS (pH 7.0), 15 % Isopropanol (v/v), 0.15 % Triton X-100 (v/v)
QC buffer	1 M Sodium chloride, 50 mM MOPS (pH 7.0), 15 % Isopropanol (v/v)
QF buffer	1.25 M Sodium chloride, 50 mM Tris HCl (pH 8.5), 15 % Isopropanol (v/v)
TE buffer	10 mM Tris-HCl (pH 8.0), 0.1 mM EDTA

EB buffer	10 mM Tris-HCl (pH 8.0)

Glucose and insulin measurements

Glibenclamide working solution	500 µg/ ml: 5 mg glibenclamide, 0.5ml DMSO (dissolve), 9.5 ml 0.9 % NaCl (milky solution), 0.1 ml 0.1M NaOH (clear solution)
Glucose working solution	0.3 mg/ µl: 2.1 g glucose, 7 ml 1x PBS without Mg^{2+}/Ca^{2+} (dissolve)

4.1.6 Transfection plasmids

AB30 pCAG-Strep-Flag-mPifo (Dr. Ingo Burtscher)

AB55 pCAG-Strep-Flag-hPifo (Dr. Ingo Burtscher)

AB21 pCDNA3.1-mShh (provided by Dr. Kay Grobe, Inst. F. Physiolog. Chemie und Pathobiochemie/ Münster)

AB19 pC107-Strep-His-mSmo-WT-Myc (Corbit et al. 2005, modified by Dr. Bomi Jung)

AB57 pTLHA1-HA-hGASP2-WT (provided by Dr. Erich Wanker, MPI, Germany)

AB54 pCAG-Strep-Flag (Dr. Ingo Burtscher)

4.1.7 Chemicals and Reagents

(Carl Roth GmbH & Co. KG, Karlsruhe; Merck KGaA, Darmstadt; Sigma-Aldrich GmbH, Hamburg)

A

Acetic acid
Acrylamide/bisacrylamide
Agarose (Biozym Scientific GmbH, Hess. Oldendorf)
Ammoniumpersulfat (APS)
Ampicillin
Antarctic phosphatase (NEB GmbH, Frankfurt a. M.)
Antimycin A

B

Bovine Serum Albumine (BSA)
BSA standard set (BioRad, München)
Bradford reagent
Bromophenol blue

C

Calcium chloride
Chloroform
CI (Chloroform-Isoamylalcohol: 24:1)
Cyclopamine (Cyc)

D

Dextransulfate
Diethylpyrocarbonate (DEPC), approx. 97 %
Dimethylsulfoxide (DMSO), >99.9 %
Dithiothreitol (DTT)
D-MEM (Gibco, Invitrogen™ Cooperation, Carlsbad, CA)
DNA Polymerase I, Large (Klenow) Fragment (NEB GmbH, Frankfurt a. M.)
D-PBS (Gibco, Invitrogen™ Cooperation, Carlsbad, CA)

E

Ethylenediaminetetraacetic acid (EDTA)
Ethanol, 96%
Ethidium bromide

F

Formaldehyde
Formamide

G

Gelatine
Glacial acetic acid
Glibenclamide
Glucose (D-)
Glutamine
Glutaraldehyde
Glycerol (Glycerin)
Glycine
G418 (Geneticin, 50mg/ml, Gibco, Invitrogen™ Cooperation, Carlsbad, CA)

H

HEPES (200mM, Gibco, Invitrogen™ Cooperation, Carlsbad, CA)
Hydrogen chloride (HCl)

I

Isopropanol, 100 %

K

Kanamycin

L

L-glutamine (200mM, Gibco, InvitrogenTM Cooperation, Carlsbad, CA)
Lif (ESGRO®, Chemicon, Millipore, Schwalbach)

M

Magnesium chloride
MEM non-essential amino acids (Gibco®, Invitrogen™ Cooperation, Karlsruhe)
Methanol, 100%
Milk powder (Becton Dickinson GmbH, Heidelberg)
Mitomycin C
3-(N-morpholino)propanesulfonic acid (MOPS; Qiagen,)
Mounting medium
β-mercaptoethanol (50mM, Gibco®, Invitrogen™ Cooperation, Karlsruhe)

N

Natrium citrate
Nitrogen(l)
Nuclear Fast Red
NP-40 nonylphenoxypolyethoxyethanol (Nonidet NP-40)

O

Orange G
Oligomycin

P

PAA (Laboratories Gesellschaft GmbH, Pasching, Österreich)
PAN (Biotech GmbH, Aidenbach)
Paraformaldehyde
Penicillin/Streptomycin (pen/strep, Gibco®, Invitrogen™ Cooperation, Karlsruhe)
Pfu DNA Polymerase (Stratagene, La Jolla, CA)
Phenol-Chloroform-Isoamylalcohol (PCl, Carl Roth GmbH&Co.KG, Karlsruhe)
Phosphate buffered saline (PBS, Gibco®, Invitrogen™ Cooperation, Karlsruhe)
Polyacrylamide
Polyethylenimine (PEI, Polysciences)

Potassium acetate
Proteinase inhibitors
Puromycin

Q

Q-Solution (Qiagen Holding, Hilden)

R

RNase (Promega GmbH, Mannheim)
RNase-free DNase I (Promega GmbH, Mannheim)
RNase inhibitors (Fermentas GmbH, St. Leon-Rot)
RNaseZAP
Rotenone
Rotihistol
RPMI (Lonza Verviers, Bergium)

S

SAG (Enzo Life Sciences, Lörrach)
Sodium chloride (NaCl)
Sodium dodecyl sulfate (SDS)
Sodium deoxycholate ($C_{24}H_{39}O_4Na$)
Sodium hydrogenic phosphate (Na_2HPO_4)
Sodium hydroxide
Sonic Hedgehog (Shh, R&D Systems, Wiesbaden-Nordenstadt)
Superscript II (Fermentas GmbH, St. Leon-Rot)

T

T4 DNA ligase (NEB GmbH, Frankfurt a. M., M0202)
T4 Polynucleotide Kinase (NEB GmbH, Frankfurt a. M.)
Taq DNA Polymerase recombinant (Fermentas GmbH, St. Leon-Rot)
Taq DNA Polymerase (Qiagen, Hilden; 201203;
Tetramethylethylenediamine (TEMED)
TWEEN 20
TransFectin (Bio-Rad, München)
Trinatrium citrate
Tris(hydroxymethyl)aminomethane
Triton X-100
Trizol Reagent (Gibco®, Invitrogen™ Cooperation, Karlsruhe)
Trypsin-EDTA (Gibco, Invitrogen™ Cooperation, Carlsbad, CA)

X

X-Gal (5-bromo-4-chloro-3-indolyl-beta-D-galacto-pyranoside, Fermentas)
Xylene
Xylene cyanole

4.1.8 Oligonucleotides and Primers

Primer for genotyping

Name/ EP nr.	Sequence	T [°C]	Cycles
Pifo			
EP 976	CTCTAAAGACTGAAGCCATTGGGATAC	55	35
EP 978	TCTGCACAACGCAGAGCTAAG		
EP 979	ACCAGAGAACTCATAAGCTCGAAAG		
Gprasp2			
EP 1194	ACCCAAGAGGGTGTTTACTG	55	35
EP 1195	TTCGCTTCTCGCTTCTGTTC		
EP 1196	ATGATGGCAGCAGCTTTGTG		
SRY			
EP 990	TGACTGGGATGCAGTAGTTC	54	30
EP 991	TGTGCTAGAGAGAAACCCTG		
GPS-GFP			
EP 1111	TGCAGTGCTTCAGCCGCTAC	58	30
EP 1112	CCAGCAGGACCATGTGATCG		
Kif7			
EP 963	CTATCCCCAATTCAAAGTAGAC	58	35
EP 964	CACCACCATGCCTGATAAAAC		
EP 965	CCAAATGTGTCAGTTTCATAGC		
EP 966	TTCTCACCCAAGCTCTTATCC		
Sufu			
EP 959	GCTGAATTCTTGACTCACTG	55	32
EP 960	CCTACCCTTTCCAGTGAAG		
EP 961	GCTGTTTGTACTCATGGTC		
EP 962	GTGTCAGTTTCATAGCCTG		
HPRT			
EP 992	GAAGGCACATGGCTGAATATCG	60	35
EP 127	GGTGGACCTGCTTCAGAACCTTGTACAC		
EP 671	CTCCTCGCCCTTGCTCACCA		

Table 4 Genotyping primer

Primer for RT-PCR

EP nr.	Name	Sense	Antisense	T [°C]	Cycles
142, 143	Actin	GACGAGGCCCAGAGCAAGAG	ATCTCCTTCTGCATCCTGTC	59	30
970, 971	Pifo	AGAAAGCATCGTAGCCGTGT	GGGTGACAATGAGACCCTGT	53	35
858, 859	Ptch1	GAAGGCGCTAATGTTCTGAC	TACCTAGGAGGTATGCTGTC	60	30
860, 861	Gli1	TGCCAGATATGCTTCAGCCA	TGTGGCGAATAGACAGAGGT	60	35
887,888	Gli2	ATCAAGAGGGAGCTACACGCAACA	TTGGGCATAGCTTCTGCTGTCTCT	56	35
885, 886	Gli3	TCTCATCCACCCTGCTCCAACATT	TTCCCAGTGGCAGTTTGTCTCGTA	56	35
889, 890	Shh	TACTCGCAGCAGCTGCTCTACCACATT	GTTTGCCTTCTGAAACGCAGGACA	60	30
883, 884	Smo	TTCCGGGACTATGTGCTATGCCAA	AGACAGTGTGCATGCTGAAGGAGA	56	35
	Pifo 1b-2	AGAGCAGACAGCAGAAGAAG	CTGTTGCTGCTGCATAACAC	57	35
	Pifo 2-3	CACAGGCCCTGGGTGTTATG	AGCTGTCCTGGCTCCAATAG	57	35
	Pifo 2-4	AACACGTCAAGCGAGGAAAC	TGATACATCCCTGGGTATGG	57	35

Table 5 RT-PCR primer

Real-time-PCR (qPCR): SYBR Green Primer

Name	Sense	Antisense
Pifo1-2	ACATCACTCATGGGAAGGTG	AAACCATTCCAATCTGTTGC
Pifo 5-6	CTCTAAAGGCTGAGCTGTCC	CCGAGGAACACAGAAATACA
Gprasp2 2-3	GACAGAGAACACCCAGGAATAG	TAAAGCAGGGCTCCAGAAATC
Gprasp2 3-4	CGGTGAGCATCTATAGACCAG	CCTTAAAGCAGGGCAATCTC
Ptch1	ATTCAACCAAACCTCTTGATG	AACCTTGACATCCACCATTC
Gli1	AGCTGCACTGAAGGATCTC	TACAGCGAGAGTTGATGAAAG
Gli2	GATGCCAACCAGAACAAG	TTGCTCCGCTTATGAATG
Gli3	CTCCATTACATGTGCCTTC	CAGTGGGATTACGGTGTG
Sufu	TCTTCCAGTCAGAGAACACC	ACCAACAATCTGGAGGAAAG
Kif7	CGGGAGAAAGGGAGATGAG	GTAGCCGCAGTTCTACCATC
Shh	CAGGTTTCGACTGGGTCTAC	ACGGAGTTCTCTGCTTTCAC

Table 6 Real-time PCR (qPCR)

Real-time PCR (qPCR): TaqMan probes

Number	Name	Ordernumber
001	KIF7	Mm01320525_m1
003	Gprasp2	Mm03992606_s1
005	Ins1	Mm01950294_s1
006	CDK4	Mm00726334_s2

Number	Name	Ordernumber
007	Smo	Mm01162710_m1
011	KLF-4	Mm00516104_m1
018	Ptch1	Mm00436026_m1
019	Cdkn2	Mm00494449_m1
027	Gprasp2	Mm03990556_g1
032	Pifo	Mm01307869_m1
033	Pifo	Mm01307871_m1
035	Gapdh	Hs-02758991_g1
038	Gli1	Mm00494651_m1
040	Ins2	Mm00731595_Gh
054	Shh	Mm00436528_m1
055	Sufu	Mm00489385_m1
074	Ki-67	Mm01278617_m1

Table 7 Real-time PCR (RT-PCR) primer

PifoVenus Targeting primer

EP 1232, Pifo Fusion Hom A Fwd, Hind III

NNN AAGCTT GCATGATAAACACCAGAGTATGATGTTC, Tm = 64^{o} C

EP 1233, Pifo Fusion Hom A Rev, Xba I

NNN TCTAGA CTGGTAATATAGGCTAAAGTAGGCCACAC, Tm = 66^{o} C

EP 1234, Pifo Fusion Hom B Fwd Not I, Asc I, Bam HI, Eco RI

NNN GCGGCCGC GGCGCGCC GGATCC GAATTCAATGTAGGCACTGTCTTCACGTGCTGTC, Tm = 70^{o} C

EP 1235, Pifo Fusion Hom B Rev, Mun I, Sac I

NNN GAGCTC AATT GGTTAGATAACCAACAGGGACAACTAGACC, Tm = 67^{o} C

Primer EP 1126: Not I, Xba I, Venus fwd. Tm = 74^{o} C

GCGGCCGCAGCCACCATG TCTAGAATGGTGAGCAAGGGCGAGGAGCTGTTC

EP 1236, Rev-Triple Flag

NNN GCGGCCGCTTGTCATCGTCATCCTTGTAATCGATGTC

4.1.9 Molecular weight markers

DNA ladder	100 bp ladder; 1 kb ladder (NEB GmbH, Frankfurt a. M.)
Protein ladder SeeBlueR Plus2	Pre-Stained Standard (Gibco, Invitrogen™ Cooperation, Carlsbad, CA)
RNA ladder	RNA ladder high range (Fermentas GmbH, St. Leon-Rot)

4.1.10 Kits

QIAquick PCR Purification-/	(Qiagen Holding, Hilden)
QIAquick Gel Extraction-/	

QIAgen Maxi-/ QIAgen Mini-	
RNeasy Mini Kit	
ECL Detection Kit	(Millipore Cooperation, Billerica, MA)
Insulin secretion Kit	Ultra Sensitive Mouse ELISA Kit (Crystal Chem INC., #90080, IL, USA)
SuperScript® VILO™	cDNA synthese Kit (Invitrogen, #11754-050, Carlsbad, CA)

4.1.11 Enzymes

Proteinase inhibitors	PI (Sigma-Aldrich GmbH, Seelze)
Superscript II	(Fermentas GmbH, St. Leon-Rot)
RNase inhibitors	(Fermentas GmbH, St. Leon-Rot)
Restriction enzymes	(NEB GmbH, Frankfurt a. M.; Fermentas GmbH, St. Leon-Rot)
DNA-Polymerases	DNA Polymerase I, Large (Klenow) Fragment (NEB GmbH, Frankfurt a. M.) M0210; Taq DNA Polymerase recombinant (Fermentas GmbH, St. Leon-Rot) EP0402; Taq DNA Polymerase (Qiagen, Hilden; 201203; Pfu DNA Polymerase (Stratagene, La Jolla, CA)
RNase	(Promega GmbH, Mannheim)
RNase-free DNase I	(Promega GmbH, Mannheim)
Ligase	(T4 DNA ligase; NEB GmbH, Frankfurt a. M.; M0202)
Phosphatase	(T4 Polynucleotide Kinase, NEB GmbH, Frankfurt a. M.; Antarctic phosphatase NEB GmbH, Frankfurt a. M.)

4.1.12 Vectors and BACs

Vectors

The PL-452 pBluescript vector contains a neo resistance gene flanked with loxP sites, under the control of a hybrid promoter consisting of the very efficient phosphoglycerate kinase (PGK). This allows expression in eukaryotic cells. It also contains EM7 promoter for prokaryotic expression, followed by the strong bovine growth hormone polyadenylation (bGHpA) signal. The L120 insert containing a NLS LacZ sequence was generated by Dr. Ingo Burtscher, as well as the 2A sequence.

BACs

RP23-306O20	(Kinzel et al. 2010)

4.1.13 Bacteria, culture media and reagents

Bacteria

E.coli K12	XL-1 Blue endA1 gyrA96(nalR) thi-1 recA1 relA1 lac glnV44 F`[:: Tn10 proAB + laclq Δ(lacZ)M15]hsdR17(rK-mK+) (Stratagene, LaJolla)
E.coli K12 DH5α	F-.lacl-recA1, endA1, D(lacZY A-argF), U169, F80dlacZDM15, supE44, thi-1, gyrA96, relA1 (Hanahan et al., 1985)
E.coli K12 EL250	(Lee et al. 2001)

Culture media

LB Medium	Lysogeny broth; (Bertani 1951)
LB Agar	Lysogeny broth; (Bertani 1951)
LB Agar conditioned	100 µg/ ml ampicillin (Roche Deutschland Holding GmbH, Grenzach-Wyhlen)
	25 µg/ ml kanamycin (Sigma-Aldrich Chemie Gmbh, Munich)
	12.5 µg/ ml chloramphenicol (Sigma-Aldrich Chemie Gmbh, Munich)
	X-Gal (Fisher Scientific - Germany GmbH, Schwerte)

4.1.14 Antibodies

4.1.14.1 Primary antibodies

ID	Name	Host species	Dilution	Company	Order nr.
1	Actin Ab-5	mouse	WB 1:5000	BD	612656
23	HNf-3β (Foxa2) M-20	goat	WB 1:800 IC 1:1000	Santa Cruz	sc-6554
25	Brachyury (N-19)	goat	WB 1:200 IC 1:1000	Santa Cruz	sc17743
29	anti-a tubulin	mouse	IF 1:250 WB 1:5000	Sigma	T6199
30	anti-Acetylated tubulin	mouse	IF 1:250	Sigma	T7451
35	Anti-KIF3A	mouse IgG1	WB 1:250 - 1:1000	BD	611508
42	Gli-3 (H-280)	rabbit	WB 1:1000 IC 1:500	Santa Cruz	sc-20688
45	Gli-3 (N-19)	goat	WB 1:1000 IC 1:50	Santa Cruz	sc-6155
47	KIF 3B	mouse	WB 1:250	BD	611534
48	chicken anti-GFP	chicken	WB 1:5000 IC 1:1000	Aves Labs	GFP-1020
54	anti-Centrin 1	rabbit	IC/IF 1:200 WB 1:2000	abcam	ab11257
55	Sox17 (H-130)	rabbit	WB 1:200-1000 IF 1:50	Santa Cruz	sc-20099
66	g tubulin	mouse	WB 1:1000, IF 1:250	Sigma	T5326
68	anti-beta-Tubulin	mouse	WB 1:1000, IF 1:200	Sigma	T4026
78	Human Insulin	guinea pig	WB 1:1000, IC 1:200	Millipore	AB3440
82	guinea pig anti-Glucagon	guinea pig.	IF 1:500	Millipore	4031-01F
83	Islet1 (39.4D5-c)	mouse	IC 1:250	DSHB Hybridoma	7B2
85	Nkx2.2 (74.5A5-c)	mouse	IF 1:500	DSHB Hybridoma	7G2
96	Anti-Gamma-Tubulin	rabbit	WB 1:250 IF 1:1000	Sigma	T5192
125	Ki67	rabbit	IC Paraffin 1:2000	Menarini/Novocastra	NCL-ki67p
129	alpha-Gli2	guinea pig.	WB 1:2000, IC 1:1000	Princeton University	*
135	GLI1	rabbit	WB 1:1000 IP 1:50	NEB	2553
141	Smoothened	rabbit	IHC 1:3000 WB 1:1000	abcam	ab38686
147	Gli1 (L42B10)	mouse	WB 1:1000, IP 1:50	NEB	2643
151	Olig2	rabbit	IHC 1:500 WB 1:2500	Millipore	AB9610
152	KIF3B (H-60)	rabbit	IHC 1:50 ,WB 1:500	Santa Cruz	sc-50456
153	Arl13B (L-15)	goat	IHC 1:50, WB 1:500	Santa Cruz	sc-102318
162	Sufu (C81H7)	rabbit	WB 1:1000 IP 1:50	NEB/Cell Signaling	2522

ID	Name	Host species	Dilution	Company	Order nr.
163	KIF7	rabbit	WB 1:2000 - 1:10.000	abcam	ab95884
171	anti-p16/INK4a	rabbit	WB 1:1000 IP 1:50	Millipore	04-239
173	Anti-Gamma-Tubulin	mouse	WB 1:10.000	abcam	ab11316
175	CDK4	mouse	WB 1:2000	NEB	2906
176	CDK2	rabbit	WB 1:1000	NEB	2546
177	CyclinD1	mouse	WB 1:2000	NEB	2926
190	SHH	goat	WB 1:1000	Santa Cruz	sc-1194
191	PAX6 (internal)	goat	IC 1:100	MYBioSource	MBS4210
193	anti-Insulin	guinea pig.	IF 1:250	Thermo Schientific	PAI26938
194	anti beta Tubulin	rabbit	1:500 in ALI	abcam	ab15568
195	anti -Insulin	rabbit	IC (Frozen) 1:1000	Thermo Schientific	PA118001
197	Pdx1 (D59H3)	rabbit	WB 1:1000 IF 1:300	NEB	5679
198	Nkx6.1 concentrated	mouse	IF 1:300	DSHB Hybridoma	F55A10
199	Anti-GLUT-2	rabbit	WB 1:500 - 1:1500	Millipore	07-1402
200	mouse GLI-2	goat		RD	AF3635
201	human/mouse GLI3	goat		RD	AF3690
202	Sufu	goat		Santa Cruz	sc-10933
203	patched (G-19)	goat		Santa Cruz	sc-6149
206	Anti-GAPDH	mouse	WB 1:6000	Merck Biosciences	CB1001
213	NKX 6.1	goat		BD	AF5857
214	Somatostatin (D-20)	goat	WB 1:200, IF 1:50	Santa Cruz	sc-7819
215	Nkx6.1	rabbit	WB 1:250, IC 1:200	Acris/Novus	NB182553
216	Ki-67	rabbit	WB 1µg/ml, IC-FR 1:200	abcam	15580
225	PAX6 a.a. 1-223	mouse	IF 1:250	DSHB Hybridoma	PAX6
228	Cdk4 (DCS-35)	mouse.	WB 1:1000, IF 1:50-500	Santa Cruz	sc-23896
256	GASP-2 (E14)	goat	WB 1:100- 1:1000	Santa Cruz	sc-162842
259	SYT13 N-terminal region	rabbit	WB 1:100, IC 1:50-100	Aviva Systems	OAAB0289

Table 8 Primary antibodies

4.1.14.2 Secondary antibodies

ID	Name	Host species	Dilution	Company	Order nr.
1	goat **anti-rabbit** IgG	HRP	WB 1:1000 IC 1:500	upstate/Millipore	12-348
2	rabbit **anti-goat** IgG	HRP	WB 1:5000 IC 1:500	Chemicon/Millipore	AP106P
3	goat **anti-mouse** IgG	HRP	WB 1:1000	upstate/Millipore	12-349
4	rabbit a**nti-goat** IgG **488**	Fluorescent	IC 1:800	Invitrogen	A-11078

ID	Name	Host species	Dilution	Company	Order nr.
5	rabbit **anti-goat** IgG **555**	Fluorescent	IC 1:800	Invitrogen	A-21431
5	rabbit **anti-goat** IgG **555**	Fluorescent	IC 1:800	Invitrogen	A-21431
6	goat **anti-rat** IgG	FITC		South. Biot.	3030-02
7	goat **anti-mouse** 488	Fluorescent	IC 1:800	Invitrogen	A11029
8	goat **anti-rabbit** 594	Fluorescent	IC 1:800	Invitrogen	A11037
9	goat **anti-rat** 594	Fluorescent	IC 1:800	Invitrogen	A11007
10	**goat-anti-guinea pig**	HRP	WB 1:10.000	Santa Cruz	sc2903
11	Alexa Fluor **546 phalloidin**	Fluorescent	IC 1:40	Invitrogen	A22283
12	goat **anti-mouse** IgG **546**	Fluorescent	IC 1:800	Invitrogen	A11030
13	goat **anti-rabbit** IgG **488**	Fluorescent	IC 1:800	Invitrogen	A11034
14	goat **anti-mouse** IgG **Cy3**	Fluorescent	IC 1:800	Dianova	115-165-003
15	goat **anti-mouse** IgG	HRP	WB 1:20.000 IC 1:500	Dianova	115-036-062
16	rabbit **anti-Goat** IgG	HRP	WB 1:20.000 IC 1:500	Dianova	305-035-045
17	goat **anti-mouse** IgG **405**	Fluorescent	IC 1:800	Invitrogen	A31553
18	donkey **anti-goat** IgG **633**	Fluorescent	IC 1:800	Invitrogen	A21082
19	goat **anti-rabbit** IgG	HRP	WB 1:20.000 IC 1:500	Dianova	111-036-045
20	donkey ***anti-chicken IgY***	**Cy5**	1:100 bis 1:800	Dianova	703-175-155
21	**LectinGS-II** Griff. Sim. **488**			Invitrogen	L-21415
22	goat **anti-rabbit** IgG **Fc**	HRP	WB 1:10.000-1:200.000	Dianova	111-035-046
23	donkey **anti-mouse** IgG **488**	Fluorescent	IC 1:800	Invitrogen	A21202
24	donkey **anti-rabbit** IgG **555**	Fluorescent	IC 1:800	Invitrogen	A31572
25	donkey **anti-goat** IgG **488**	Fluorescent	IC 1:800	Invitrogen	A11055
26	donkey **anti-rabbit** IgG **488**	Fluorescent	IC 1:800	Invitrogen	A21206
27	donkey ***anti-chicken IgY***	**Cy3**	1:100 bis 1:800	Dianova	703-165-155
28	donkey ***anti-chicken IgY***	**Cy2**	1:100 bis 1:800	Dianova	703-545-155
29	*goat* ***anti-rabbit IgG***	**Cy5**	1:100 bis 1:400	Dianova	111-175-144
30	goat ***anti-chicken IgY***	***488***	1:100 bis 1:800	Dianova	103-545-155
31	donkey **anti-chicken IgY**	HRP	1:15.000 WB	Dianova	703-035-155
32	donkey **anti-mouse** IgG **555**	Fluorescent	IC 1:800	Invitrogen	A31570
33	goat **anti-guinea pig** IgG **633**	Fluorescent	IC 1:800	Invitrogen	A21105
34	goat **anti-mouse** IgG **633**	Fluorescent	IC 1:800	Invitrogen	A21052
35	donkey **anti-goat** IgG **555**	Fluorescent	IC 1:800	Invitrogen	A21432
36	**anti-rat IgG2a** schwere Kette	HRP	WB 1:5000	"Kremmer" IMI	keine!
37	donkey **anti-mouse** IgG **647**	**Alexa Fluor**	IC 1:800	Dianova	715-605-151
38	**anti-rat IgG kappa** leichte Kette	HRP	WB 1:5000	"Kremmer" IMI	keine!
39	**anti-rat** kappa-HRP	HRP	WB 1:10.000	"Kremmer" IMI	keine!
40	goat **anti-Syrian Hamster**	***DyLight 549***	1:100 bis 1:800	Dianova	107-505-142

ID	Name	Host species	Dilution	Company	Order nr.
41	donkey **anti-rat** IgG **549**	***Cy3***	1:100 bis 1:800	Dianova	712-165-153
42	goat **anti-mouse** IgG1	HRP	WB 1:10000	abcam	ab97240
43	rabbit **anti-rat** IgG	HRP	WB 1:500	abcam	ab6734
44	donkey **anti-rabbit** IgG **649**	Fluorescent	1:50 bis 1:400	Dianova	711-605-152
45	donkey **anti-rat** IgG 649	***DyLight 649***	1:50 bis 1:400	Dianova	712-495-150
46	donkey **anti-guineapig** 649	***DyLight 649***	1:50 bis 1:400	Dianova	706-605-148
47	donkey **anti-rabbit** R-PE	R-PE	1:50 bis 1:200	Dianova	711-116-152
48	donkey **anti-mouse** DyLight	***DyLight 405***	1:50 bis 1:200	Dianova	715-475-150
49	donkey **anti-goat** APC	APC	1:50 bis 1:200	Dianova	705-136-147
53	Alexa Fluor **647 phalloidin**	Fluorescent	only for IC 1:200	Invitrogen	A22287

Table 9 Secondary antibodies

4.2 Methods

4.2.1 Cell culture

All cells used in this study were maintained at an appropriate temperature of 37° C and a gas mixture of 5 – 7 % CO_2 in an incubator. By use of trypsin (0.05 % trypsin, 0.53 mM EDTA), a serine protease located in the digestive system of most vertebrate, cells were detached from their culture dish and dissociated by protein hydrolysis. Prior to trypsin treatment cells were washed with PBS (- Mg^{2+}/ Ca^{2+}) to remove the serum containing trypsin inhibitors, magnesium and calcium. For preservation cell suspensions were transferred in cryvials, and placed in freezing boxes at - 80° C for two hours. For short term storage of two weeks cells were kept at - 80° C. In order to preserve cells longer they were further transferred in liquid nitrogen.

4.2.1.1 Embryonic stem cell culture

In order to prevent embryonic murine stem (ES) cells from spontaneous differentiation they are co-cultured on a murine embryonic feeder (MEF) cell layer supporting the ES cells by producing extra-cellular matrix like collagens and glycosaminoglycans.

4.2.1.1.1 Generation and treatment of MEFs

Generation of MEFs

MEFs are spindle-shaped cells which are generated from the corpus (after dissection of the head and inner organs) of CD1 embryos at day E14.5. They were expanded over three passages and kept at a high density of approx. 80 %. Depending on their proliferation rate they were split every three to five days on 15 cm plates by trypsinization. After a quick washing step with PBS trypsin-EDTA was added to the dish and incubated for four minutes at 37° C. Trypsin digestion was stopped by adding 10 ml of cell medium (4.1.3). The cell suspension was collected in a Falcon tube and eventual cells clusters were decollated by pipetting up and down. To dilute the trypsin concentration, cells were centrifuged for four minutes at 1.200 rpm (250 x g). The remaining medium was discarded and according to the further procedure the cell pellet was either resuspended using culture media or freezing medium.

Treatment of MEFs

In order to block the proliferation of the supportive MEF cell layer in the co-culture system and prevent them from getting over confluent, mitomycin C (MMC) a mitosis inhibitor was used. Therefore cells from five 15 cm plates were collected at passage three to four in a 50 ml Falcon in a total amount of 20 ml culture medium, treated with 200 µl MMC (1 mg/ ml) and incubated at 37° C for 45 min with a loose cap. Every 15 min the tube was inverted to prevent cell attachment. Subsequent, cells were centrifuged, the supernatant was discarded and cells further washed twice with PBS to remove the remaining MMC. These cells were either pelleted for further co-culture or frozen (4.2.1).

4.2.1.1.2 Culture of ES cells and MEFs

ES cell culture usually was performed in 6 cm plates. Therefore a monolayer of MMC treated MEFs was prepared. Frozen cryovials were thawed quickly in a water bath at 37° C, transferred in a Falcon tube containing ES cell medium and pelleted in order to eliminate the remaining EDTA from the freezing medium. The pellet was resuspended in ES cell medium and transferred to the monolayer dish. In order to prevent spontaneous differentiation, ES cells were passaged every second day depending on their proliferation rate (1:2 to 1:8) and the ES cell culture medium was changed every day.

4.2.1.1.3 TIGM Gprasp2 ES cells

Gprasp2 Lex3.13 ES cells were cultured as described earlier (4.2.1) with slide adaptions: D-MEM culture media (Gibco) was supplemented with a special FBS, that sets the industry standard for consistent quality and reliability (Thermo Scientific™ HyClone™ #SH30070-30). As described amino acids (Milipore), l-glutamine (Gibco), penicillin/streptomycin (Sigma) were added (4.1.3.1). In contrast to the other ES cell lines, Gprasp2 preferably was cultured under high confluence (80 %), passaged every second day and the medium was changed on daily basis. Harvesting was performed using trypsin/EDTA solution and cells were cryopreserved using a mixture of D-MEM/FBS/DMSO (2:2:1). As the cells were sticky the cell suspension was pipetted several times up and down, in order to separate the cell aggregations.

4.2.1.1.4 Transformation of ES cells using electroporation technique

The cellular uptake of targeting vectors (4.2.2.6.10) is achieved using an electrical current in order to temporarily permeabilize the cell membrane. Therefore ES cells were expanded on a 10 cm dish, the amount for one electroporation. Cells were trypsinized and pelleted as described before (4.2.1) and washed with PBS. The cell pellet was resuspended in 0.7 ml ice cold PBS, mixed with 100 µl vector (25 µg) and transferred into a pre-cooled cuvette. The electroporation was carried out using 220 V, a capacity of 500 µF and an infinite resistance. After electroporation the cuvette was kept on ice for additional five minutes and transferred into a pre-warmed 10 cm culture dish containing a feeder monolayer, supplemented with ES cell medium. After letting the cells recover for 24 hrs the selection was started using neomycin (G418; 300 µg/ ml). Six to eight days later ES cell colonies were formed and further expanded by picking single colonies. Therefore a conical 96 - well plate containing 60 µl PBS per well was used to disperse the picked colonies. Two further 96 -well plates were set, one for DNA preparation coated with gelatin (0.1 %) and one for further expansion of the colony coated with feeder cells, both containing ES cell media. The picking was carried out under a stereo microscope, whereby the medium of the 10 cm dish was exchanged to PBS. The clones were detached using a 100 µl pipette and transferred into one well of the prepared conical 96 -well. Colonies were trypsinized by adding 30 µl trypsin-EDTA per well and incubated at 37° C for 15 min. A single cell suspension was generated by pipetting up and down and further divided into the remaining 96 -wells plates.

4.2.1.1.5 The HPRT system

I used hypoxanthine-guanine-phoshoribosyltransferase, (HPRT, house-keeping gene) targeting technique to insert a single copy of either H44 or H47 reporter constructs (2.1.1.3, 4.2.1.1.5) in order to investigate whether

the subsequent sequence is sufficient to drive the Pifo expression (Alten et al. 2012). Therefore an HPRT locus deficient E14 ES cells line, E14TG2A was used (Hardy et al. 1990). Reporter constructs were introduced by homologous recombination into the genome of E14TG2a ES cells. The targeting vectors (pMP8) restores HPRT expression and HAT resistance, that after homologous recombination (4.2.1.1.5) the correctly targeted ES cells can be selected in HAT medium, containing hypocanthine, aminopterin and thymidine. Reporter constructs were introduced into pMP8 upstream of the HPTT locus by conventional cloning. The advantage, in theory is a single copy integration at a specific side. The Electroporation was carried out as described earlier (Hooper et al. 1987) using 300 V and a 2 ms pulse. This E14 ES cell line has been reported to high efficiently form germ line chimaeras after injection into blastocysts (Nagy et al. 1993). E14TG2A ES cells were cultured in buffalo rat liver (BRL) cell supplemented medium in order to prevent them from spontaneous differentiation, which occurs when cells are plated in the absence of supporting feeder cells.

4.2.1.2 Isolation of primary limb buds (PLCs)

Primary limb bud cells (PLC) were obtained from the forelimbs of E10.5 embryos. The explanted limbs were subjected to enzymatic treatment with 0.05 % trypsin-EDTA and subsequently mechanically dissociated by pipetting. PLCs were expanded according to their proliferation rate and either directly used (4.2.1.2.2) or further cultured. PLCs were in general passaged and preserved as mentioned earlier (4.2.1). Cell culture dishes ranged from 24 -well plates for immunostainings, 6 -well plates for WB and RNA analysis, to 10 cm plates for cell expansion and transfection. Cells were kept rather in high density of 80 %.

4.2.1.2.1 Generation and immortalization of PLCs

In order to gain a sufficient amount of material PLCs were immortalized. With the first method, cells were passaged every two to three days until they entered senescence phase, where they spontaneously restarted their proliferation after one to two weeks. With the second method PLC immortalization was induced using the supernatant of 865 cells. The viral oncogene SV40 T-large can inhibit senescence and induces immortalization with the inactivation of the tumor suppressor p53 and Rb pathways leading to cell growth extension for about 20–30 doublings (Shay, Wright, and Werbin 1991). The presence of T-large antigen, the telomerase catalytic unit, cells supplemented with the supernatant released from 865 cells can overcome senescence. Therefore cells were incubated for three passages with the T-large antigen supplemented supernatant, the culture medium was changed to normal PLC medium and after a further passaging, immortalized cells were expanded.

4.2.1.2.2 Shh assay

According to the desired confluency of 70 – 80 %, approx. 150.000 – 300.000 cells were seeded on a 6 -well plate. At the following day, cells were serum starved for 24 hrs and subsequently treated with 500 ng/ ml Shh ligand (R&D Systems), 1 µM chlorobenzothiophene-containing Hh pathway agonist (SAG, Enzo Life Sciences) a Shh agonist (acting on Smo level in the signaling cascade), or 10 µM cyclopamine (Cyc, Sigma) a Shh antagonist (acting on Smo level in the signaling cascade) for the indicated time points.

4.2.1.2.3 Transient transfection

HEK 293T cells

Human embryonic kidney cells (HEK293T) cells were transiently transfected using PEI (polyethylenimine, Polysciences). Cells were grown to 80 – 90 % confluency and 8 µg of plasmid DNA (4.1.6) were mixed with 1 ml PEI. After 15 min incubation at room temperature the PEI mixture was dropped on to the 10 cm dish filled with normal culture. The medium was changed the next day to serum free conditions in order to let cells exit the cell cycle (G0 phase). Adjacent cells were incubated with either Shh or SAG for further 6 – 24 hrs.

PLC transfection

Transfection of PLCs was performed using TransFectin (Bio-Rad). TransFectin is a lipid reagent consisting of a cationic compound and a co-lipid DOPE (1,2-dioleoyl-sn-glycero-3-phosphoethanolamine). It is widely used for plasmid delivery in a variety of cells. The transfection was carried out using 8 µl of plasmid DNA, mixed with 1 ml Opti-MEM. In parallel 15 µl TransFectin were mixed with Opti-MEM and subsequently mixed together. After 20 min incubation the TransFectin mixture was dropped onto the 10 dish. PLCs were equally preceded as HEK 293T cells.

4.2.1.2.4 Down-regulation siRNA in PLCs

PLCs were maintained in standard culture medium (4.1.3.3). Down-regulation of the particular gene was performed in a 10 cm of PLCs using si-RNA and TransFectin as described in as described in the previous chapter. Prior to the Shh or SAG incubation for 24 hrs, cells were serum starved overnight.

4.2.1.3 Islet cell culture

4.2.1.3.1 Islet isolation

Pancreatic islets were isolated from adult mice by initially perfusing the pancreas with 1 mg/ ml Collagenase P (Col P) solution which is the key step in the islet isolation protocol. The dead mice were quickly processed as according to its nature the pancreas produces digestive enzyme, which makes the whole procedure time-sensitive towards the isolation. Therefore the mouse was placed under the microscope, the abdomen opened and the common bile duct was clamped at its connection with the gut in order to ensure the influx of collagenase exclusively in the pancreas. This connection forms a characteristic triangle-shaped white-milky area on the surface of the duodenum, called ampulla. The needle containing the Col P solution was inserted in the common bile duct and the Col P was very slowly injected. The inflated pancreas was dissected and placed in 2 ml remaining Col P on ice. After seven minutes the homogenate was briefly shaken and the enzymatic digestion was terminated with the addition of 12 ml G - solution after 15 min of incubation at 37^{o} C. After a centrifugation step (2 min, 1.620 rpm or 290 x g) the supernatant was discarded and the tissue was resuspended and washed in 12 ml G - solution. The next step was the phase separation. Therefore the pellet was resuspended in 5.5 ml 15 % Optiprep and pipetted on the remaining 2.5 ml 15 % Optiprep very carefully. 6 ml of G - solution was very slowly stocked on top of the two phases. After 10 min incubation at room

temperature and a centrifugation step (10 min, 1.700 rpm, brake = 0 , acceleration = 5), the separation of the three phases became visible and most of the islets remained in the upper interphase.

4.2.1.3.2 Islet picking and culture

For the picking of the islets the previous described phase separation was performed, in which the most islets are located to the upper interphase. For further culture, assays or immunohistochemistry, islets were picked from this phase. Prior to the picking the interphase was collected in the G - solution. The islets were individually picked under a stereomicroscope and either directly used or further cultured in islet culture media.

4.2.1.3.3 Shh assay on islets

Overnight cultured islets were serum starved for four to six hours and incubated with Shh, SAG or Cyc in 6 -well plates as described previously (4.2.1.2.2).

4.2.1.3.4 Seahorse

Seahorse was performed in order to measure the mitochondrial respiration and energy consumption in real-time. The experiment was performed using isolated islets, which were cultured O/N in normal media (RPMI), together with the XF sensor, which was cultured O/N at 37^{o} C but without O_2. Next day the components were prepared: D-Glucose (200 mM), Oligomycin (50 µg/ ml), and Rotenone (10 µM), and Antimycin A (10 µM). The screens were added to a Petri dish, containing MA media, and incubated at 37^{o} C, without O_2. The islets were washed in MA media and 30 islets were than seeded in the depressed chamber under a dissecting microscope. The islet capture screens were carefully placed on top of the islets, using forceps. The islets were incubated for one hour at 37^{o} C in order to equilibrate temperature and to adjust the islet metabolism to 3 mM glucose. Meanwhile the cartridge with the desired components was prepared.

4.2.1.3.5 Destination of Insulin in Islet cells

Glucose Stimulated Insulin Secretion (GSIS)

After letting the isolated islets recover overnight, triplicates of batches of 10 similarly sized islets were collected in a conical 96 -well plate in 0.5 % albumin-Kreps-Ringer HEPES-buffered (KRH) saline, containing low glucose concentrations (2.8 mM) and incubated for one hour at 37^{o} C. From the in total 90 µl volume in each well 80 µl were collected and placed in PCR tubes on ice. The 80 µl were refilled with KRH buffer containing high glucose concentrations (16.8 mM) and incubated for another hour. For insulin determination 80 µl were again collected. The remaining islets were lysed with 80 µl of protein lysis buffer. All samples were stored at -20^{o} C until the insulin levels were assayed using the Insulin ELISA Kit (Crystal Chem INC.).

Insulin ELISA Kit

For the quantitative determination of insulin in mouse plasma (4.2.9.2), islet cell lysates or whole pancreata (4.2.9.1), the Ultra Sensitive Mouse Insulin ELISA kit (Crystal Chem INC.) was used. It uses sandwich antibody detection with insulin antibody - coated 96 -well microplate modules. A standard row of defined insulin amount (12.8 µg/ µl – 0.2 µg/ µl) as well as the sample plasma (5 µl) was added to the wells together with 95 µl

G - solution (diluent). In a first reaction step the mouse insulin from the sample is bound to the guinea pig anti-insulin antibody coated on the microplate well. After a washing step with G - solution the unbound material is removed. The second reaction is based on the horse radish peroxidase (POD)-conjugated anti-insulin antibody (100 µl of solution C and D, 1:2), which binds to the guinea pig anti-insulin antibody bound to the mouse insulin complex immobilized to the microplate well. After a further washing the excess POD-conjugate is removed. The bound POD conjugate in the microplate well is detected by the addition of the 3, 3', 5, 5'-tetramethylbenzidine (TMB) enzyme substrate solution, E. In order to stop the enzymatic reaction an acid stop solution is applied (solution F, 1 N sulfuric acid) which gives a yellowish color change, which can be measured using an ELISA reader.

4.2.2 Molecular Biology

4.2.2.1 DNA extraction

4.2.2.1.1 Plasmid and BAC preparation

Plasmid DNA preparation was performed according to the Quiagen Plasmid Kit. In order to isolate plasmid DNA from a bacterial suspension the first step was to separate the bacterial cells from the medium by centrifugation (6.000 x g) for 15 min at 4^{o} C. Bacteria were resuspended in lysis buffer, P1 until the pellet was completely dissolved. The addition of detergents (buffer P2) lyses the cells. DNA denaturing solutions (buffer P3) are added according to the protocol, subsequently. Afterwards, the medium was neutralized and RNases were added in order to renaturate the RNA. Plasmid DNA is now precipitated by adding isopropanol, washed with ethanol, and resuspended in water. For long term storage the DNA can be resuspended in TE (Tris, EDTA) buffer and stored at - 20^{o} C.

4.2.2.1.2 BAC mini preparation according to Copeland

The BAC DNA preparation protocol is adopted from an already published protocol (Warming et al. 2005). The obtained yield of BAC DNA lies at approx. 1 – 1.5 µg. 5 ml of a bacterial overnight culture medium supplemented with 25 µg/ ml chloramphenicol were centrifuged at 5.000 rpm in a 15 ml Falcon tube for 5 min. The supernatant was discarded, the pellet resuspended in 250 µl P1 buffer, and transferred to an Eppendorf tube. 250 µl of P2 buffer were added and the reaction tube was carefully inverted. Afterwards, the suspension was incubated at room temperature for another 5 min. 250 µl of P3 buffer were added and the tube was subsequently incubated for 5 min on ice. The protein precipitate was collected by centrifugation (13.500 rpm) for 5 min and the DNA containing supernatant was transferred to a new Eppendorf reaction tube. This procedure was repeated to completely eliminate the precipitate. To precipitate the BAC DNA 750 µl of isopropanol were added to the clean supernatant, mixed, and incubated on ice for 10 min. After the incubation the DNA was pelleted for 10 min, the supernatant was removed, and the DNA pellet was washed using 1 ml 70 % ethanol. Following this step, the DNA was centrifuged again for 5 min. The ethanol was removed carefully; the pellet was air-dried and dissolved in 50 µl TE while incubating at 37^{o} C under constant shaking (500 rpm) for one hour. Subsequent restriction digests were carried out in a volume of at least 60 µl.

4.2.2.1.3 Isolation of genomic DNA form cells and tissues

Isolation of DNA from cells in 96 - well plates

The picked ES cell clones were expanded until they reached confluency for 2 - 3 days. Proteinase K was freshly added to the lysis buffer in a concentration of 100 µg/ ml to avoid self-digestion. Prior to the lysis buffer cells were washed two times with PBS to remove medium residual. Containing 50 µl lysis buffer/ well the 96 - well plate was sealed with parafilm and incubated at 55^{o} C overnight in a humid chamber. The next day 150 µl sodium chloride (5 M) were mixed with 10 ml 100 % ice-cold ethanol and added to each well (100 µl) for precipitation. The plate was incubated at room temperature without moving. After for 30 min the plate was inverted carefully and placed slowly on a paper towel to decant the liquid. Repeating the decanting the DNA pellet was washed three times in 150 µl 70 % ice-cold ethanol. The DNA can be stored in 70% ethanol at - 20^{o} C. After the last washing step the DNA was dried at room temperature for 10 - 15 min. To dissolve the pellet 25 µl TE buffer or autoclaved water were added to the pellet and it was dissolved at 4^{o} C overnight or shaking at 37^{o} C for one hour in a humid chamber.

Isolation of DNA from cells in culture dishes

Prior to applying the lysis buffer (4.2.2.1) cells were washed two times with PBS. After removing the remaining PBS 5 ml of lysis buffer were added to a 10 cm plate. The cells were detached using a cell scraper and subsequently transferred into a 50 ml Falcon tube and incubated at 55^{o} C overnight. On the next day Phenolchloroform- isoamylalcohol (PCI, 25:24:1) was added 1:1 to the cell solution and was mixed by vortexing. The phases were separated by centrifugation (4.500 x g) for 10 min at room temperature. The upper phase was removed without the protein-containing interphase and mixed 1:1 with PCI. After a centrifugation step the upper phase was transferred to a new tube and the DNA precipitated by adding 10 ml EtOH : sodium-acetate (25:1). A further centrifugation step was applied in order to pellet the DNA. The pellet was washed with 7.5 ml of 70 % ice-cold EtOH. The DNA pellet was dried at room temperature and dissolved in a suitable volume TE buffer at 4^{o} C overnight or shaking at 37^{o} C for one hour. The DNA can be stored at 4°C.

Isolation of genomic DNA

With the following protocol mostly the genotyping of mice was carried out, but also DNA from cultured cells was isolated. The mouse tail clip biopsies were placed in an Eppendorf tube and according to the size 300 – 500 µl lysis buffer was added overnight at 55^{o} C. If the tail clip biopsies were not lysed the same day, they were stored at - 20^{o} C. On the next day the digested explants were vortexed and centrifuged at 14.000 rpm for 10 min to pellet the hair and other insoluble fragments. The supernatant, containing the genomic DNA was transferred into a new tube and the DNA was precipitate using isopropanol (300 – 500 µl, as much as lysis buffer) and in order to properly mix, vortexed. After a centrifugation step of 10 min the supernatant was discarded and the pellet washed with 700 µl 70 % EtOH for 5 min. The pellet was air-dried and resuspended in 300 – 500 µl H_2O. Usually 1 µl was used for genotyping of mouse lines.

Hot-Shot-Method for isolation of genomic DNA from mouse tail biopsy

This very quick and "dirty" method of isolating genomic DNA was used for genotyping mice. Therefore mouse tail clip biopsies were covered with 100 µl NaOH (50 mM), boiled 20 min at 98° C, cooled down on ice for 5 min, and then neutralized by adding 30 µl of Tris (pH 7.5).

4.2.2.2 DNA sequencing

To determine the exact order of nucleotides of a specific part of the DNA, the four dideoxynucleotides (adenosine, cytosine, guanine and thymidine) were coupled with a unique fluorescence dyes. A PCR reaction was used with only one primer (sense/ antisense, (n) bp/ 100 = x ng) per reaction and the integration of one of these labeled bases into the elongating DNA strand stops the elongation reaction. DNA strands of all possible length with the last base being a fluorescent tagged dideoxynucleotide are generated. Subsequent DNA precipitation was performed using 0.5 µl of 125 mM EDTA, 2.0 µl 3 M NaAC, and 50 µl 100 % EtOH and incubated at room temperature for 15 min. After a centrifugation step (15.000 pm, 4° C, 30 min) the DNA was washed with 70 % EtOH and air-dried. The DNA was resuspended in 25 µl water. The following master mix was used.

0.5 µl BigDye
2.0 µl BigDye-buffer
10 pM Primer
Σ 5,0 µl

The PCR program used to amplify the sequencing products:

96° C 1 min
96° C 10 sec
50° C 5 sec
60° C 4 min } 35 x
16° C ∞

4.2.2.3 RNA and reverse Transcription

It is of importance to create an RNase free environment while working with RNA. To ensure success gloves are indispensable and for a clean working space and instruments, RNase inhibitors like RNaseZAP are used. Solutions should be prepared with diethyl pyrocarbonate (DEPC) an RNase inactivator.

4.2.2.3.1 RNA preparation

Conventional RNA preparation method

In order to prepare RNA and later complementary DNA (cDNA) for room temperature PCR the following conventional RNA preparation method was used. To isolate RNA from cells 750 µl Trizol was used for RNA

isolation from embryonic or adult tissue 1 ml Trizol/ 100 mg tissue was used. To better de-touch cells from the cell culture dish, a cell scraper was used. The cells and embryonic tissue was homogenized with the help of a pipet tip and a vortexer, whereas adult tissue and organs were homogenized using a tissue homogenizer and subsequent sonicator and incubated five minutes at room temperature. In a next step chloroform was added (140 µl) and the tube 15 sec vigorously shaken. To separate the phases the tube was centrifuged at 14.000 rpm for 10 min at 4^{o} C. The RNA containing upper phase was transferred into a new sterile reaction tube. For RNA precipitation 400 µl isopropanol were added and centrifuged. The pellet was washed with 70 % EtOH. The pellet was dried shortly and resuspended in 10 – 50 µl of DEPC water. When not immediately used the RNA was stored it at - 80^{o} C.

RNA preparation using Quiagen miRNeasy mini Kit

To isolate RNA from cells or islets for further real time quantitative PCR analysis miRNeasy mini Kit was used. In order to disrupt the cells 700 µl of QIAzol Reagent was added to the samples and vortexed for one minute and further incubated for five minutes at room temperature. 140 µl chloroform were added to the homogenate and as earlier mentioned shacked for 15 sec for proper phase separation. After 2 – 3 min incubation at room temperature the homogenate was centrifuged at 14.000 rpm at 4^{o} C for 15 min. The upper aqueous phase (approx. 350 µl) was transferred into a new collection tube, provided and 1.5 x of the volume of the upper phase (approx. 525 µl) of 100 % EtOH were added and mixed by pipetting. In contrast to the conventional RNA isolation method the QIAgen miRNeasy mini Kit uses a column to purify RNA, which is able to contain 700 µl total volumes. After a centrifugation step (15 sec at 12.000 rpm) through the column the total RNA as well as miRNA was bound on it and the flow through was discarded. After a quick washing step a DNase I digestion was performed directly on the column according to the protocol. Following, several washing steps are applied and to elute the RNA from the column RNAse free water 10 – 20 µl was pipetted on the column, incubated for one minute and centrifuged in a new collection tube.

4.2.2.3.2 Reverse Transcription – cDNA preparation

Conventional method for cDNA synthesis

Reverse transcription is a process by which RNA is transcribed into cDNA. Before the reverse transcription can start, DNA has to be removed from the RNA sample by DNase digestion. After the digestion the RNA solution proteins and chemicals have to be removed by LiCl precipitation. For cDNA preparation the following mixture was used:

1 -2.5 µg RNA
1.0 µl Oligo-dT-primer or Random Primer (500 ng/ µl)
11.0 µl filled up with DEPC-treated H_2O

Denaturation of the RNA was performed by incubation the mixture at 70^{o} C for 10 min in order to allow the annealing of the primers. Afterwards, the mixture was placed on ice and the following components were added:

4.0 µl 5x transcriptase buffer

2.0 µl DTT (0.1 M > 10 mM)

1.0 µl dNTPs (10 mM > 0.8 mM each)

1.0 µl RNA inhibitor (40 U/µl > 40 U)

The mixture was incubated for two minutes at 37° C. Afterwards 200 U SuperScript (200 U/ µl > 1 µl) was added and subsequently incubated at 42° C for 50 min. To stop the reaction the enzyme was inactivated at 95° C for 5 min. The cDNA was stored at - 20°C.

Reverse transcription using VILO cDNA Synthese Kit

In order to transcribe RNA in complementary DNA (cDNA), 1.0 – 2.5 µg RNA were used and the master mix for one reaction mixed as followed, prior to an incubation step at room temperature for 10 min and inactivation at 85° C for five minutes:

5 x VILO Reaction Mix 4 µl

10 x SS Enzyme Mix 2 µl

DEPC or RNAse free water filled up to 20 µl

4.2.2.3.3 Determination of RNA and DNA concentrations

The concentration of RNA (or DNA) in solution can be determined by measuring the extinction at 260 nm with a photometer (NanoDrop). The quotient E260 nm/ E280 nm should be between 1.9 – 2.0 for clean RNA solutions and between 1.8 – 1.9 for clean DNA solutions.

4.2.2.4 PCR techniques and protocols

4.2.2.4.1 Genotyping of mice and embryos

Tail clip biopsies from mice at a weaning age of one month were used for genotyping using previous described DNA extraction method (4.2.2.1). For embryos the Hot-Shot-Method was also used (4.2.2.1.3). Usually 1 – 3 µl of the DNA were used for further PCR reaction.

Genotyping of Pifo intercrossed mouse lines

Genotyping of all mouse lines intercrossed with Pifo KO (Pifo KO, Pifo RC, Pifo KO 129SVES6, Pifo flox/ flox) was performed using a forward primer (EP 967) which is located before the lox P site of exon three in combination with a reverse primer (EP 968) which is located after the lox P site of exon three, in order to detect and/ or distinguish the WT allele (203 bp) from the floxed allele (272 bp). To detect the deletion of exon three to six the same forward primer (EP 967) was used together with a reverse primer (EP 969) which is located after the lox P site of exon six. This primer pair combination only gives a band (324 bp) if the lox P sites are recombined. All three primers were used together in one reaction mix with 35 cycles and an annealing temperature of 55° C.

Genotyping of Gprasp2 GT/y mouse line

Genotyping of Gprasp2 and intercrosses (Pifo KO/ Gprasp2$^{GT/y}$) was performed using a forward primer located before the trapped exon 4 (EP 1194) in combination with a reverse primer after exon 4 (EP 1196) in order to genotype the WT allele (287 bp) and in combination with a reverse primer located in the lacZ reporter (EP 1195) in order to genotype the gene trap construct (338 bp). The PCR was carried out with all primers in one reaction using 35 cycles and an annealing temperature of 55^{o} C.

Genotyping of Tg(GBS-GFP) mouse line

Genotyping of the transgenic GBS-GFP mouse line and intercrosses (Pifo GBS-GFP) was performed using a forward (EP 1111) and a reverse primer (EP 1112) recognizing the sequence of the eight concatemerized fragments of Gli binding sites (GBS; TTATGACGGAGGCTAACAAGCAGGGAACACCCAAGTAGAAGCTGGCTGTC) (Sasaki et al. 1997). Using 30 cycles and an annealing of 58^{o} C both primers result in a fragment of 450 bps, when positive for GBS-GFP.

Genotyping in order to identify the sex of embryos

In order to identify the sex of the embryos a primer pair (EP 990, EP 991) located on the sex-determination region Y (SRY) on the Y chromosome where used and a male specific band at 239 bp was detected.

Genotyping of Kif7 mouse line

Genotyping of the Kif7$^{-/-}$ mouse line and intercrosses (Pifo Kif7) was performed using two forward (EP 963 and EP 965) and two reverse primers (EP 964 and EP 966), respectively in order to identify a wild type band with ~ 300 bp and a mutant band with ~ 500 bp.

Genotyping of Sufu mouse line

Genotyping of the Sufu$^{-/-}$ mouse line and intercrosses (Pifo Sufu) was performed using two forward (EP 960 and EP 962) and two reverse primers (EP 959 and EP 961), respectively in order to identify a wild type band with ~ 290 bp and a mutant band with ~ 400 bp.

4.2.2.4.2 PCR programs for genotyping

Pifo KO, Gprasp2 GT/y and Sufu$^{-/-}$ PCR program

94^{o} C 5 min
94^{o} C 45 sec
55^{o} C 45 sec
72^{o} C 1 min } 35 x
72^{o} C 10 min
16^{o} C ∞

Tg(GBS-GFP) and Kif7$^{-/-}$ PCR program

94° C 5 min		
94° C 30 sec	}	35 x
58° C 45 sec		
72° C 1 min		
72° C 10 min		
16° C ∞		

SRY PCR program

94° C 4 min		
94° C 1 min	}	30 x
54° C 45 sec		
72° C 45 min		
72° C 10 min		
16° C ∞		

4.2.2.4.3 RT-PCR

Reverse transcription polymerase chain reaction (RT-PCR) is used to detect gene expression through creation of cDNA from former RNA (4.2.2.3). The PCR is carried out in a thermal cycler, with the ability to rapidly repeat heating and chilling steps. The composition of the master mix was similar to the one used for genotyping of mice and included:

cDNA	1 – 3 µl
polymerase buffer/	
KCl (-$MgCl_2$)	2 µl
$MgCl_2$	2 µl
Primer (sense/ antisense)	1 µl each
Nucleotides (dNTPs)	1 µl
DNA polymerase/ Taq	0.3 µl
H_20	filled up to 20 µl

4.2.2.4.4 Quantitative real-time PCR

Quantitative real-time PCR (qPCR) is used to quantitatively measure the amplification of DNA using fluorescent dyes (SYBR green) or fluorescent probes (TaqMan). The PCR is carried out in a thermal cycler, which can also illuminate the each sample with a certain wave length and measure the excitation of the fluorescent dye or probe. After each cycle the excitation is measured until it reaches saturation, thereby every sample is normalized to a house keeping gene (Actin, GAPDH, and HPRT).

SYBR green

SYBR green binds double-stranded DNA and thereby emits fluorescence. The composition of the master mix was calculated as followed:

cDNA (1:3 dilution)	1 – 3 µl
SYBR green mix	12.5 µl
Primer (sense/ antisense)	1.0 µl each
H_2O	filled up to 25 µl

TaqMan

The TaqMan probe consists of a fluorophore at the 5`end and a so called quencher at the 3`end. As long as the quencher is attached to the flourophore it inhibits the emittion of the fluorescence. When annealing to the DNA, the TaqMan probe is degraded by the polymerase, which elongates the primers and sets the flourophore free. This fluorescence is detected by the thermal cycler. The composition of the master mix was calculated as followed:

cDNA (1:3 dilution)	1 – 3 µl
TaqMan fast advanced MM	5.0 µl
TaqMan probe	0.5 µl
H_2O	filled up to 10 µl

4.2.2.5 Gelelectrophoresis

Gelelectrophoresis is a method to separate RNA, DNA or their fragments by the size of the molecule due to their negative charge. With the application of an electric field the molecule or fragment can be moved through the agarose gel matrix, whereas small fragments move faster than large ones. According to the size of the PCR product or fragment a 0.8 – 2 % agarose/ TAE (Tris-acetate, EDTA) gel was prepared, by heating the solution in the microwave, subsequent cooling and adding of 5 – 10 µl (1:20.000) ethidium bromide (EtBr). The agarose solution was poured in a gel tray and in order to form the pockets, a camp was applied. Prior to the sample loading, the hardened agarose gel was placed in a chamber and covered with TAE buffer. Because of the intercalation between the base pairs of the helix and its UV absorbance (300 – 360 nm) EtBr is used to visualize the separated fragments with the help of a UV lamp. In order to prevent the degradation of RNA, prior to the usage all supplies were cleaned with NaHO pellets and RNAZap and the running time was shortened.

4.2.2.6 Cloning and Targeting

4.2.2.6.1 Restriction analysis of DNA

With the help of bacterial derived enzymes (restriction endonucleases) and their ability to cut DNA at specific recognition sites of the nucleotide sequence the desired DNA fragment can be isolated. The digest was incubated at 25° C or 37° C for 1.5 h and the restriction digest of plasmid or BAC DNA was composed of following ingredients:

DNA (mini prep, 100 – 500 ng)	5.0 µl
10 x buffer	2.0 µl
10 x BSA (optional)	2.0 µl
enzyme (5.000 U)	0.5 µl
H_2O	filled up to 20 µl

4.2.2.6.2 High-fidelity DNA synthesis using Pfu polymerase

Compared to the Taq (0.5 – 1.0 min/ kb) the error rate of the Pfu (1 – 2 min/ kb) is more than 6 times lesser, according to the manufactures description. Therefore Pfu polymerase was used in order to amplify large products from a plasmid DNA. A typical mix was carried out as follows:

10 x PFU-buffer	2.0 µl
$MgSO_4$ (25 mM)	2.0 µl
dNTPs (10 mM)	2.0 µl
Primer (sense/ antisense)	1.0 µl each
Pfu polymerase (2.5 – 5.0 U)	0.25 µl
H_2O	filled up to 20 µl

4.2.2.6.3 Dephosphorylation of DNA

In order to improve the percentage of clones containing the insert, a phosphatase treatment is applied. This minimizes the self-ligation of the vector by removing the 5' phosphates necessary for the ligation. Therefore, 3 µl artic phosphatase were added to the digest and incubated for 30 min at 37° C. To inactivate the phosphatase the digest was incubated for five minutes at 65° C. A typical mix for a linearized DNA fragment was carried out as follows:

DNA 1 µg	
10x enzyme buffer	1.0 µl
alcaline phosphatase (1 U/ µl)	1.0 µl
H_2O	filled up to 10 µl

4.2.2.6.4 DNA purification

The purification of single- or double-stranded DNA fragments from PCR and other enzymatic reactions was carried out using the QIAquick PCR Purification Kit50 (CaNo #28104) according to the manufacturer's protocol: After the extraction of the desired fragment from a agarose gel, the gel is dissolved adding five times its volume. The purification is performed using a column (100 bp – 10 kb). After a quick centrifugation step (1 min, 14.000 rpm) the supernatant is discarded and the DNA eluted with the provided EB buffer (30 – 50 µl). The proper size was further checked on an agarose gel (1 µl DNA, 9 µl H_2O and 3 µl Orange G).

4.2.2.6.5 Ligation

The term ligation is used to declare the enzymatic assignment of two DNA or RNA fragments on their ends (blunt or 3' – 5' overhang). In our case we used T4 ligase it to assign the insert with the vector DNA. In order to

find the right ratio between vector and insert, we used the empirical value of 200 ng vector per 10 µl volume and 1:2.5 ratio of vector : insert. The ligation was performed in a total volume of 10 µl in 16^{o} C overnight.

4.2.2.6.6 Plasmid preparation

Plasmid DNA isolation - conventional method

In a first step the 4 ml of the overnight culture are pelleted (1 min, 8.000 rpm) using an Eppendorf tube and lysed with 350 µl P1 alkaline lysis buffer. After dissolving the cell pellet 350 µl of P2 neutralization buffer are added an inverted for 6 – 8 times prior to a five minutes incubation step at room temperature. With the addition of buffer P3 the tube was inverted several times again and spined down (10 min, 14.000 rpm). The clean supernatant was transferred in a new Eppendorf tube and 500 µl isopropanol was applied and properly mixed. After pelleting the DNA a 70 % EtOH washing step was applied and the dried pellet was dissolved in 50 µl TE buffer. This conventional method was used in order to screen several Minis for further analysis or cloning.

Plasmid DNA isolation using QIAgen Mini-/ Maxi Kit

For the isolation of plasmid DNA the QIAgen Mini Kit was used for Mini preps (see plasmidprep) or the QIAgen Maxi Kit for larger amount of plasmid isolation. The bacterial pellets were lysed under alkaline conditions and subsequently neutralized and adjusted to high-salt binding conditions with the provided buffers of the kit. After clearing the solution it was purified using QIAprep silica membrane.

4.2.2.6.7 Transformation of bacteria

Two methods were used to introduce DNA into bacterial cells, namely the transformation by using electroporation and using heat shock.

Transformation and using heat shock

In order to amplify plasmid DNA (retransformation) or DNA fragments a method called transformation is used. Thereby 50 – 100 µl of RbCl-competent DHα5F'4x bacteria are thawed on ice and 1 – 3 µl of DNA is added. After 30 min incubation step on ice the bacteria are heat shocked exactly 90 sec at 42^{o} C. Bacterial cells are kept for further five minutes on ice and for 60 min shacked at 37^{o} C with the addition of 900 µl LB medium without ampicillin resistance. If a blue - white selection is possible 100 µl X - gal are streaked on ampicillin conditioned plates together with the pelleted bacteria and incubated upside down overnight at 37^{o} C degree. The next day white colonies are further picked and grown in 6 ml conditioned LB medium overnight (Minis).

Transformation of bacteria using electroporation

After thawing the competent bacteria on ice and adding 1 – 3 µl of DNA the bacteria were transferred in a pre-cooled electroporation cuvette (0.1 cm). After the puls (U = 2.5 kV) the bacterial cells were immediately transferred in a 1.5 ml Eppendorf tube and 1 ml LB medium was added for 60 min shacked at 37^{o} C. As described before (4.2.2.1.2) bacteria were streaked out on conditioned plates and incubated overnight.

4.2.2.6.8 Bacterial homologous recombination

EL250 bacteria were grown in 7 ml LB medium at 32° C overnight. The bacteria were inoculated 1:25, 1:50, 1:100 in 100 ml volume and grown until they reached a density of OD = 0.6, which was measured by a photometer. The culture was split 1:1, whereas 50 ml were kept on ice (recombineering control). The other 50 ml were centrifuged for 5 – 10 min (4° C, 5.000 rpm), the pellet was resuspended in 1.8 ml ice - cold 10 % glycerol for four times (5.000 rpm) in in order to remove the residual salt. After the last washing the bacteria were centrifuged at 11.000 rpm for 30 sec and the pellet resuspended in 200 µl 10 %. 50 µl were used for one each electroporation and incubated with 7 – 15 ng the Pifo Venus targeting Vector L416, prior to the electroporation (1.700 V, 25 µF, 200 Ω).

4.2.2.6.9 Generation of Pifo conditional allele

The Pifo gene consists of six exons and the open reading frame lies within exon three to exon six. In order to analyze Pifo function Dr. Ingo Burtscher electroporated IDG3.2-F1 (C57BL/6J x 129S6/SvEvTac) ES cells (Hitz, Wurst, and Kuhn 2007) with the linearized (AscI) Pifo targeting vector and selected neomycin resistance (of G418, 300 µg/ml, Invitrogen) clones. After one week of selection ES cell clones were picked under a stereo microscope. From these clones DNA was prepared for confirmation of the homologous recombination by further Southern blot analysis. Hereby the complete open reading frame was flanked by loxP sites. Mouse ES cells were cultured as previously described under chapter (4.2.1). Homologous recombination at the Pifo locus was confirmed by Southern blot analysis using BamHI and ASEI digested genomic DNA and a Pifo 3' Southern probe. The wild-type (WT) band for BamHI and ASEI digestion revealed 9782 bp and 8349 bp, respectively. The recombination band for the ΔNeo digested with BamHI was at 9145 bp and the size of the flox deleted (conditioned allele) band is 11525 bp. Homologous recombined clone were aggregated with CD1 morula to obtain chimeras and the FRT-flanked PGK-gb2-neo cassette was then removed in the germline by intercrossing the Flp-e expressing mice. To generate Pifo CKO mice they were further intercrossed with Rosa Cre expressing mice. Pifo FD/ WT/RosaCre+ mice were intercrossed with BL6/J and 129SVES6 and RosaCre negative mice were selected (Pifo FD/ WT) for further intercrossings.

4.2.2.6.10 Targeting PifoVenus2ALacZ

In order to study the expression of Pifo, a targeting construct was designed which includes a LacZ and a Venus reporter. The containing T2A sequence, a small peptide linker sequences derived from viral genomes, allows efficient production of both reporters as it makes it possible two express two independent proteins from a single transcript (Szymczak et al. 2004). Additionally a triple FLAG tag sequence was introduced upstream of the T2A sequence.

PifoVenus Targeting strategy

L411 pCAG-2A-NLS-lacZ

Plasmid L120 (5 µg) was cut with Not I, dephosphorylated with arctic phosphatase and PCR purified. As insert 2A annealing primer were used. The ligation was set using 200 ng vector, 2 µl and 5 µl 2A peptide in a volume of 10 µl. The orientation of the 2A peptide was controlled using plasmid DNA from Minis and a double digest

with Bam HI and Not I enzymes (correct size: 7431, 1764, 337, 17 bp; wrong size/ orientation: 7431, 1832, 337, 105 bp). Additionally at least three correct orientated Minis were sequenced.

L412 pKS – Pifo homology A

PKS E001 was digested with Hind III and Xba I (2916 bp and 42 bp) and PCR purified (2916 bp vector). Primer EP 1232 and EP 1233 were used to amplify the first homology arm from the BAC DNA of Pifo with Pfu proof reading enzyme. The product was PCR purified (269 bp) and further digested with Hind III and Xba I and gel purified (263 bp product). The ligation was set and plated on amp/ X-gal conditioned plates for blue-white selection.

L413 pKS – Pifo homology A&B

L412 was digested with Not I and Sac I (3166 bp and 13 bp) and PCR purified (3166 bp vector). Primer EP 1234 and EP 1235 were used to amplify the second homology arm from the BAC DNA of Pifo with Pfu proof reading enzyme. The product (266 bp) was PCR purified and digested with Not I and Sac I and gel purified (260 bp product). The ligation was set and plated on amp conditioned plates.

L414 pKS – Pifo homology A&B, Venus

L413 was digested with Xba I, Not I (3411 bp and 7 bp) and PCR purified (3407 bp vector). As insert a PCR was performed using EP 1126 and Rev tripple FLAG EP 1236 primers and L393 as template with Pfu proof reading enzyme (817 bp product). The product was PCR purified and digested with Xba I and Not I and gel purified (789 bp product). The ligation was set and plated on amp conditioned plates.

L415 pKS – Pifo homology A&B, Venus, Neo

L414 was digested with Bam HI and Eco RI (4194 bp and 6 bp) and PCR purified (4190 bp vector). As insert E007 was cut with Bam HI and Eco RI (2934 bp and 1889 bp) and gel purified (1889 bp insert). The ligation was set and plated on kan conditioned plates.

L416 pKS – Pifo homology A&B, Venus 2A lacZ, Neo

L415 was digested with Not I and Asc I (6075 bp and 8 bp) and PCR purified (6071 bp vector). As insert L411 was cut with Not I and Asc I (6479 bp and 3226 bp) and gel purified (3226 bp cassette). The ligation was set and plated on kan conditioned plates.

H47-Pifo Venus 2A LacZ Fusion Targeting vector (S)

L416 cassette was digested with Hind III and Mun I (6404 bp and 2897 bp) and gel purified (6404 bp insert). For the electroporation EL250 containing H30 vector bacteria were grown overnight and proceeded as described earlier (4.2.2.1.1). After the electroporation the bacteria were plated at various dilutions on kan conditioned plates (1:5, 1:50, 1:1.000) and to further grow the culture in 50 ml kan conditioned LB medium overnight at 32^{o} C. If the liquid culture grew, Minis were prepared of 4 ml culture and a retransformation in DH5α was performed using heat shock and 1 µl of Mini DNA. The pellet was streaked out on kan conditioned plates and three colonies were picked (“pure” clones). If the liquid culture did not grow, the Minis were inoculated from four colonies of “mixed clones” from the plate and plasmid DNA was prepared and heat shocked in DH5α

bacteria and again plated on kan condidioned plates. From each plate only one colony was picked (“pure” clones)

4.2.2.6.11 Southern blot

Southern blotting is a relatively fast method with which one can analyze gene sequences in the genome without having to decode the whole sequence. We used it to confirm the proper integration of a targeted vector into the genome. First the DNA was fragmented with the help of enzymes (4.1.11) and loaded on an agarose gel in order to separate them by size. After the DNA is blotted to a membrane and marked by a radioactive labeled probe.

Gelelectrophoresis

A 0.8 % agarose gel was prepared and the digested DNA separated (30 V) overnight. The next day the agarose gel was documented with a size indication of the DNA ladder (ruler) in order to have a reference length.

Blot

Incubating the gel in 11 ml HCl (conc.) in 989 ml H_2O for 15 – 20 min while shaking, led to a separation of the purin bases (depurination). It was followed by a denaturation step in 0.4 M sodium hydroxide and 0.6 M sodium chloride for 30 min while shaking. In order to neutralize the gel, it was incubated in 0.5 M Tris and 1 M sodium chloride (pH 7.2) for another 30 min while shaking. Finally, the blot was built up and the transfer was carried out overnight. Therefore four sheets of 20x SSC wetted blotting paper were placed on a glass plate with a contact to a 20x SSC reservoir and on top of them four additional 20x SSC blotting papers with perfect size of the gel were placed. Next the gel was positioned on the top upside down to the blot and covered with a nitrocellulose membrane. A transparent foil was used to cover the gel pockets and the margins of the gel. A few layers of blotting paper and paper towels covered the blot. The next day, the gel pockets were marked on the membrane with a pen and the membrane was dried and cross-linked for 30 min at 80^{o} C.

Prehybridization

The binding of the probe to the DNA involves three hybridization steps. The first one is the prehybridization which is applied in order to reduce background. Therefore 30 ml hybridization buffer were preheated to 65^{o} C in a water bath and added to a glass tube including the membrane. This was incubated at 65^{o} C on a roller for three hours.

Radioactive labeling

Briefly, 25 ng of the linearized DNA probe was diluted in H_2O to a final volume of 24 µl in an Eppendorf tube. Then, 10 µl random primers were added and the mix was denaturized for 5 min at 100^{o} C. After a centrifugation step 10 µl 5x buffer (d*CTP-buffer for 32P labeled CTP) was added. From here on the radioactive labeling was carried out in the radioactive lab, with the addition of 5 µl radioactive labeled dCTP (50 Cu) and 1 µl of 5 U Klenow-enzyme. After a brief mix and centrifugation step the probe was labeled for 30 min at room temperature. In order to stop the reaction 2 µl STOPmix were added. For the purification the reaction mixture

was loaded on a prepared column and centrifuged at 3000 rpm for one minute. To measure the activity of the sample 1 µl was used. For denaturation of the probe 500 µl salmon sperm DNA (10 mg/ml) were boiled for 10 min at 100° C, placed in a 50 ml Falcon tube, and stored on ice. The labeled probe was added (1 x 10^6 counts/ 1 ml hybridization buffer) and denaturized by pipetting 50 µl 10 N sodium hydroxyl drop wise to the sample. For neutralization 300 µl 2 M Tris (pH 8.0), and subsequently 475 µl 1 M HCl were pipetted drop wise into the tube.

Hybridization

For the actual hybridization of the DNA and the probe and fist the 10 ml hybridization buffer were discarded and the radioactive-labeled DNA probe was added. The tube was incubated at 65° C for 12 – 24 hrs, rotating. Next day, the membrane was washed with 2x SSC/ 0.5 % SDS for five minutes, and the second time the washing buffer was preheated to 65° C and the membrane washed for 30 min. With a signal of approximately 3.500 counts, the membrane was wrapped tightly in saran wrap and fixed in a film cassette. In order to develop the film, it was stored at - 80° C up to three days and developed using a Kodak film.

4.2.3 Protein biochemistry

To prevent proteins from degrading low temperature is required. Therefore the lysates where kept on ice during the procedure and proteinase inhibitors were used.

4.2.3.1 Protein alignment with EBI-ClustalW

The program EBI-ClustalW (freeware; http://www.ebi.ac.uk/Tools/msa/clustalw2/) was used for multiple sequence alignments for visualization of conserved Pifo domains. Given that Pifo appears with chordates the human protein sequence was aligned with different chordate species: gorilla, namascus leucogenys (northern white-cheeked gibbon), Odobenus (walrus), Felis catus (domestic cat), Ceratotherium (white rhinoceros or square-lipped rhinoceros), Bos taurus (Cattle or colloquially cows), Trichechus manatus latirostris (West Indian manatee) and Mus musculus (mouse). Protein sequences were taken from the NCBI protein data base (FASTA).

4.2.3.2 Generation of Pifo Antibodies

Rabbit and rat polyclonal antibodies against mouse Pifo were generated as previously described (Gordon I/II rabbit, Pifo6E6 rat, Kinzel et al., 2010). All monoclonal Pifo antibodies used in this study were generated in the Dr. Kremmer laboratory (Institute for Molecular Immunology). Therefore they synthesized a peptide comprising 14 amino acid (mouse Pifo protein, RKHRSRVAYFSLYY) and coupled it to BSA and OVA (PSL, Heidelberg, Germany). Rats were immunized subcutaneously and intraperitoneally with a mixture of 50 µg peptide-OVA, 5 nmol CPG oligonucleotide (Tib Molbiol, Berlin), 500 µl PBS and 500 µl incomplete Freund's adjuvant. Six weeks after the primary injection a boost without adjuvant was applied. Fusion was performed using standard procedures. Supernatants were tested in a differential ELISA with the Pifo peptide coupled to BSA and irrelevant peptides coupled to the same carrier. Monoclonal antibodies that reacted specifically with the Pifo peptide were further analyzed in immunostaining. I further tested the specificity of these antibodies on Western blot and in immunostaining using HEK293T cells, which overexpressed mPifo (4.1.6). For Western blot

analysis 30 – 100 µg lysates were used. Antibodies positive for either experiment, were further tested on Western blot using 50 – 300 µg WT and Pifo$^{FD/FD}$ testis lysates (**Table 2**).

4.2.3.3 Protein extraction

For western blot analysis either cells or organs were lysed in RIPA buffer. After a quick D-PBS washing step, cells were shared using a cell scraper. Organs and embryos were chopped using at first step a dispenser and at a second step, in order to further chop the tissue a sonicator. Samples were than centrifuged at full speed (14.000 rpm) for 10 min at 4^{o} C and the supernatant was collected. For longer storage protein lysates were frozen at - 80^{o} C.

4.2.3.4 Determination of protein concentration

The protein concentration was determined using the Bradford reagent with a BSA standard set. The method is based on the complex formation of Brilliant G, a member of the comassie-brilliant blue family and proteins in solution. The dye-protein formation results in a shift in the maximum of the absorbance spectrum from 465 nm to 595 nm which can be measured with a standard photometer. The proportion of the color reaction depends on the amount of protein in solution in that way, that the more protein content is present, the more the color shifts towards a violet tone. In this account in order to obtain the particular concentration of the protein solution a calibration is required. Therefor a BSA based protein standard was used with known concentrations from 0.125 mg/ ml – 2 mg/ ml. The dilution factor for the samples was 1:10 in a total amount of 1 ml Breadford reagent, which was incubated for 10 min prior to the photometric measurement.

4.2.3.5 Western blot

With this technique proteins can be separated by size on a denaturing Sodium dodecyl sulfate (SDS) - polyacrylamide gel electrophoreses (SDS-PAGE). SDS thereby gives the proteins a negative charge, that they can be separated via electrophoresis. Proteins in the SDS-PAGE are than blotted on a membrane using a semi-dry blot. Proteins bound on that membrane can be detected by specific antibodies, whereas the primary antibodies are recognized by secondary antibodies bound to the enzyme horseradish peroxidase (HRP). HRP catalyzes the reaction of a substrate into a fluorescent product that can be exposed to a film. Unspecific binding sides are blocked with 5 % milk/ TBST.

4.2.3.5.1 Denaturing SDS-polyacrylamide gel electrophorese (SDS-PAGE)

Acrylamide gel preparation

For protein detection, samples were resolved on 6.5 % (57 – 212 kDa), 7 % (36 – 94 kDa), 10 % (16 – 68 kDa), 12 – 13 % (18 – 68 kDa), and 15 % (12 – 43 kDa) acrylamide gels. In order to prepare the gel, glass plates (1 mm or 1.5 mm) were mounted in the casting frames on the casting stands. For four 1 mm thick separation gels the following mixture was used:

4x 1 mm	6.5 %	7 %	10 %	13 %	15 %
Acrylamide	6.0 ml	7.5 ml	10 ml	13 ml	15 ml
Separation buffer	7.5 ml	7.5 ml	7.5 ml	7.5 ml	7.5 ml
H_2O	16.5 ml	15 ml	12.5 ml	9.5 ml	7.5 ml
TEMED	40 µl	40 µl	40 µl	40 µl	40 µl
APS 10 %	300 µl	300 µl	300 µl	300 µl	300 µl

Table 10 Separation gel mixture

The separation buffer was immediately filled between the two glass plates until the lower border of the casting frames was reached. The rest of the space was filled up with 70 % isopropanol in order to gain a sharp and straight border. After polymerization the isopropanol was decanted and completely sucked off with a paper towel. The collecting gel for four 1 mm thick gels was mixed as following:

4x 1 mm	15 %
Acrylamide	1.3 ml
Separation buffer	2.5 ml
H_2O	6.2 ml
TEMED	20 µl
APS 10 %	100 µl

Table 11 Collecting gel mixture

It was pipetted until it filled the remaining space of the glass plates and comps were inserted.

Sample preparation

The protein samples were mixed with 1:3 4x SDS/ dithiothreitol (DTT) loading buffer and denaturated at 95^{o} C for five minutes and immediately put on ice. After a quick centrifugation step (14.000 rpm, 4 min) the samples were loaded on the gel, which was placed in the running chamber and filled up with 1x Tris glycine running buffer. The proteins were separated with a running speed of 80 – 100 V for 1.5 – 3.0 hrs.

4.2.3.5.2 Semi-dry immunoblot

After the protein separation the gel was placed in KP buffer. Meanwhile the PVDF membrane was rinsed in 100 % methanol due to their highly hydrophobic surface and incubated two minutes in APII buffer. The blot was built from anode (bottom) to cathode (top) as following:

blotting paper rinsed in API (2x)

blotting paper rinsed in APII (1x)

PVDF membrane rinsed in APII

Acrylamide gel rinsed in KP

Blotting paper rinsed in KP (1x)

The blotting was performed using a Trans Blot® SD or Trans - Blot® Turbo™ blotting machine with a constant current of 0.22 A for one blot per chamber (0.44 A for two blots per chamber) with 25 V for 30 min. In order to confirm the successful protein separation, the blotted PVDV membrane was optionally incubated with Ponceau - S solution.

4.2.3.6 Affinity purification of protein complexes

For semi-endogenous immunoprecipitation (IP) experiments, HEK293T cells were transiently transfected (4.1.6) with Strep-FLAG-TAP (Strep-Tactin sepharose FLAG-TAP, SF-TAP) tagged mouse Pifo (mPifo) and incubated for 24 hrs with SAG. For co-IP experiments HEK293T cells were transiently transfected with Strep-His-TAP (SH-TAP) tagged mouse Smo (mSmo) and incubated for 24 hrs with SAG. The cells were subsequently lysed in Strep-IP lysis buffer containing 0.5% Nonidet-P40 protease inhibitor cocktail (Roche) with freshly added proteinase inhibitor (1:200) in TBS (30 mM Tris-HCl, pH 7.4, 150 mM NaCl), and incubated for 20 min at 4° C. After sedimentation at 14.000 rpm for 10 min, the protein concentration was determined by a Bradford assay and equal amounts of each lysate were transferred to Strep-Tactin-Superflow beads (IBA) and incubated for one hour. The resin was washed three times with washing buffer and incubated for 10 min in Strep-elution buffer (IBA). For semi-endogenous IP experiments the beads were subjected to PLC lysates for 24 hrs (rotating at 4°C), which before were incubated for 24 hrs with SAG. Similar for co-IP experiments the beats were incubated with PLC lysates, which before were transiently transfected with HA tagged human Gprasp2 (hGprasp2), and also incubated for 24 hrs with SAG. After another three washing steps, the samples were mixed with 1:3 4x SDS/ dithiothreitol (DTT) loading buffer and denaturated at 95° C, and subsequently loaded on a SDS-PAGE or further concentrated using 10 kDa cut-off VivaSpin 500 centrifugal devices.

4.2.3.6.1 **Immunostaining and detection**

After the transfer, membranes were blocked for one hour in TBST/ 5 % milk at room temperature and incubated with the primary antibody (4.1.14.1) in TBST/ 5 % milk overnight at 4° C. The membranes were then washed three times with 1x TBST and incubated with the secondary antibody (4.1.14.2) for one hour at room temperature. After further washing steps (3x 10 min, shaking) with 1x TBST the membrane was incubated one minute with enzymatic ECL (enhanced chemiluminescence) solution and wrapped in foil. In the dark room it was exposed to a film (1 sec – 10 min) and subsequently developed.

4.2.4 Embryology

For analysis of embryos, mice were plug checked every day, whereas the actual day of the plug was counted as embryonic day (E) 0.5. Embryos were dissected according to Nagy and Behringer („Manipulating the mouse embryo: a laboratory manual") and staged according to Downs and Davis (Downs and Davies 1993).

4.2.5 Cryo-preservation

The dissected embryo or tissue were first preserved from decay using 4 % PFA fixation. Embryos at the stage of E7.5 were fixed up to half an hour; embryos at the stage of E9.5 were fixed for one hour. From E12.5 onwards the embryo was no longer fixed as whole mount, instead the organs were dissected and fixed for two hours. Adult tissue was also fixed for at least two hours. After the fixation a sucrose gradient was applied. The gradient was performed as following: 10 % sucrose overnight at 4° C, 15 % sucrose for 2 hours and 30 % sucrose overnight. The next day the tissue was incubated for at least two hours in (1:1) 50 % sucrose and Tissue Freezing Medium (shaking or rolling) and embedded in Tissue Freezing Medium subsequently using dry ice. Samples were further preceded using a Cryostat and usually cut at 14 µm thickness.

4.2.6 Immunohistochemistry

4.2.6.1 Cell culture

Cells were grown overnight on clean and sterile glass slides in 24 well plates to a confluency of 80 %. The next day cells were washed twice with PBS and fixed with 4 % PFA for 15 min at room temperature. After a brief washing step cell membranes were permeabilized with PBST (0.1 % Triton X-100) for 10 min at room temperature. Cells were further incubated in blocking solution (10 % FCS, 3 % donkey serum, 0.1 % BSA in PBST) for one hour and incubated with the primary antibody overnight at 4° C in a humid chamber. The next day the slides were briefly washed with PBS and incubated with the secondary antibody in PBST for 1 – 2 hours at room temperature, washed with PBS and either stained for 4',6-diamidino-2-phenylindole, dihydrochloride (DAPI, 1:500) or mounted with DAPI mounting medium.

4.2.6.2 Whole mount E7.5 embryos

Immunostainig on E7.5 embryos was performed as previously reported (Nakaya et al. 2005). Therefore embryos were fixed with 4 % PFA for 20 min, permeabilized in 0.1 % Triton X-100, 0.1 M glycine (pH 8.0) for 15 min and subsequently incubated in blocking solution (10 % FCS, 3 % donkey serum, 0.1 % BSA in 0.1 % Tween 20) for two hours prior to the antibody labeling (4° C, overnight, in blocking solution). The next day embryos were washed in PBS and incubated with the secondary antibody for two hours and subsequently washed and mounted between coverslips using SecureSeal spacer and DAPI mounting medium.

4.2.6.3 Cryosections

Immunostaining of crosectioned embryos or organs was carried out as following: Frozen sections were dried for five minutes at room temperature prior to a 10 min permeabilization (0.1 % Triton X-100) step. Slides were permeabilized another 30 min using PBST (0.1 % Tween 20) and further blocked (10 % FCS, 3 % donkey serum, 0.1 % BSA in 0.1 % Tween 20) for one hour at room temperature in a humid chamber. As described earlier the first antibody was applied overnight and the second antibody the following day, and nuclei were stained with DAPI.

4.2.6.4 EdU labelling of islets

This assay was uses to measure the proliferation of islets. It is based on the incorporation of the modified thymidine analogue EdU, into newly synthesized DNA. Thereby it is fluorescently labeled with a bright, photostable Alexa Fluor® dye in a click reaction. Mice were incected with 10 mg/ ml PBS; 10 µl/ g body weight (=100 µg/ g) EDU solution and sacrificed 24 hrs after the injection in order to gain one percent labelled proliferating cells.

4.2.6.5 Islets

In order to not suck the islets up during washing, conical 96-well plates were use. Per well 10 – 20 islets were collected and fixed with 200 µl of 2 % PFA for 30 min on a shaker at room temperature. After a washing step with PBS islets were permeabilized with 200 µl of 0.1 % Triton X-100 in PBS for 30 min, washed with PBS and incubated in blocking solution (10 % FCS, 3 % donkey serum, 0.1 % BSA in 0.1 % Tween 20). As described earlier (4.2.6) the first antibody was applied overnight and the second antibody the following day, and nuclei were stained with DAPI. As described for the embryos, islets were mounted in-between spacer.

4.2.7 Whole mount *in situ* hybridization

In order to analyze gene expression patterns, whole mount *in situ* hybridization was performed on embryos (E7.5 – 12.5). Thereby the digoxygenin labeled complementary RNA is recognized by an antibody and visualized via an enzymatic reaction using BM-purple. Due to RNase driven RNA degradation embryos had to be dissected under sterile conditions. They were further fixed with 4 % PFA and dehydrated in a methanol increasing row. Thereby the protocol was carried out over four to five days, depending on the intensity of the probe and the gene expression.

First day

Embryos were rehydrated in an increasing methanol/ PBT (0.1 % Tween 20) row with five minutes of incubation at each step and subsequently washed in PBT for 10 min. They were further bleached with 3 % H_2O_2/ PBT for 20 min and washed three times with PBT prior to a fixation step with 4 %PFA/ 0.2 % glutaraldehyde for 20 min. After washing three times with PBT the prehybridization buffer was added for two hours before the embryos were incubated overnight at 70^{o} C in the actual hybridization buffer including the probe (500 ng – 1 µg RNA/ ml).

Second day

After a quick washing step in prewarmed (70^{o} C) hybridization buffer, additional three 30 min washing steps at 70^{o} C with solution I were applied. Embryos were treated with 100 µg/ ml RNase/ TNT at 37^{o} C for 60 min, quickly washed in TNT/ solution II (1:1) for five minutes, then three times (30 min) washed with solution II at 65^{o} C, and prior to the two hour long preblocking in MAB/ 2 % blocking reagent including 10 % seep, washed three times in MAB. The antibody solution was applied at 4^{o} C overnight while gently rocking the samples.

Third day

The third day is the washing day, as the embryos were first washed three times in MAB for 10 min, then hourly the MAB was changed and incubated overnight.

Fourth day

Three washing steps of 10 min in NTMT were followed by the BM-purple staining at room temperature until the desired staining appeared. Samples could be stained further overnight at 4^{o} C or even room temperature due to the probe and gene expression. The chromogenic reaction could be stopped by washing three times in PBT and subsequent fixation in 4 % PFA/ 0.1 % glutaraldehyde for one hour.

4.2.8 Histology

4.2.8.1 Paraffin embedding

Embryos and tissues or in situ proceeded or LacZ stained samples were dehydrated in a methanol row (25 – 100 %) for 10 min per step. In order to gain a more transparent tissue, the samples were treated with xylol for 5 – 10 min (depending on the sample thickness). Prior to the paraffin embedding, the samples were incubated overnight in 65^{o} C paraffin. The next day samples were further embedded in a mold, were they were mounted on a grid, sectioned with a microtome (6 – 14 µm) and gathered on glass slides. The slides were dewaxed using xylol (2x 15 min), fixed with mounting medium and covered with a cover slip.

4.2.8.2 Mayer`s solution for hematoxylin and eosin staining

The combination of hematoxylin and eosin (H&E) is a standard procedure in to first describe the pathology of a given tissue section. Therefore mainly paraffin sections were used, but also cryosections were preceded. For the paraffin sections five minutes xylene were applied. Then, an EtOH row (100 – 70 %) was used to dehydrate the sample. Removing the slides from a quick water step, they were stained with freshly prepared Mayer´s solution for up to eight minutes, depending on the strength of staining. Subsequent an eosin counterstaining was applied. After a quick washing step in water the samples were incubated two minutes in 95 % EtOH and 10 min in 100 % EtOH before they were brought to xylene again and mounted with a xylene mounting medium. Cryosections were rehydrated in PBS for 10 min and H_2O for five minutes prior to the staining, which was similar to the already mentioned paraffin sections.

4.2.8.3 Oil Red O and counterstaining

In order to stain triglyceride and lipids cryosections were stained with Oil Red O staining solution. Therefore the frozen slides were dried for five minutes at room temperature and prefixed using 4 % PFA for 10 min. After a quick washing step with H_2O the slides were incubated with 60 % isopropanol for 10 min. The staining was proceeded using red oil working solution for 10 min. Thereafter the slides were washed H_2O until the red staining disappears in the water and subsequently counter stained using either hematoxylin for up to two minutes or nuclear fast red (NFR) for up to five minutes, depending on the desired intensity. After a quick washing step with H_2O, cryosections were mounted using glycerol.

4.2.8.4 X - gal (5-bromo-4-chloro-3-indolyl β-D-galactosidase) staining

Betagalactosidase (β-gal) staining of whole-mount embryos and organs were performed as previously described (Liao et al. 2009). Briefly, the tissue was fixed using a fixation buffer composed of a mixture of

formaldehyde and glutaraldehyde, washed with PBS and subsequently stained with a staining buffer including x-gal. Some tissues were processed further (see next chapter).

4.2.8.5 Tissue clearing with BABB

Tissues and embryos were dehydrated using a methanol/ H_2O series (25 %, 50 %, 75 %, and 100 %) for several hours at each step. Finally the tissue was transferred to a clearing solution (1:2, benzyl alcohol : benzyl benzoate, BABB).

4.2.9 Insulin and glucose determination

4.2.9.1 Total pancreatic insulin amount

The dissected pancreata were placed on ice, covered with 5 ml 0.2 M HCl in 70 % EtOH, and homogenized. After an incubation step at - 20° C additional 5 ml of 0.2 M HCl in 70 % EtOH were added, mixed, and stored in the freezer overnight. The next day the homogenate was pelleted (> 1.000 g) for five minutes at 4° C. The supernatant was subsequently transferred to a new 15 ml Falcon tube and 100 µl acid-EtOH extract were neutralized with the same amount of 1 M Tris (pH 7.5). For the insulin determination the Elisa Kit (4.2.1.3.5) was used with sample dilutions of 1:500 and 1:1.000. The protein amount was determined using 20 µl of the neutralized solution. The total pancreatic insulin was calculated with consideration of the dilution factor and as ng of insulin per µg protein.

4.2.9.2 Glucose Tolerance Test (GTT)

Mice were housed at an ambient temperature of 23° C in a constant humidity with a 12 hrs light - dark cycle. They were fed with high fat diet (HFD) with a metabolic energy content of 23 MJ/ kg, containing 58 % fat, 16.4 % protein and 25.5% carbohydrate, and no fibers. A cohort of at least six animals per group was collected and for the GTT starved for 12 hrs. Body fat and lean tissue mass was assessed using the EchoMRI. For first and second phase of glucose and insulin measurement prior to the glucose injection (1.5 mg glucose/ g body weight), the blood insulin as well as blood glucose values were taken from the tail vein blood at various time points 15 – 120 min. GTT was performed twice on each cohort, before and after the HFD of 12 – 16 weeks.

4.2.9.3 Glibenclamide

Glibenclamide, binds the sulfonylurea receptor 1 (SUR1), a pancreatic beta cells regulatory subunit of the ATP-sensitive potassium channels. This causes a constant depolarization of the membrane, which results in an constant opening of the voltage-dependent calcium channel. As a result calcium enters the beta cell and leads to an insulin release, which is measured by applying the GTT experiment. Instead of glucose, 10 µg/ g mouse glibenclamide (500 µg/ ml) were injected intraperitoneal and blood was taken for insulin and glucose measurement like described in the previous chapter (4.2.9.2).

5 Suplemental

5.1 Abbreviations

AER	apical ectodermal ridge
AKT	protein kinase B
A-P	anterior-posterior
AurA	Aurora A
AVE	anterior visceral endoderm
β-cell	beta cell
BAC	bacterial artificial chromosome
BADJ	broncho-alveolar-duct junction
BB	basal body
BBS	Bardet-Biedl syndrome
BCA	Bicinchoninic acid
β-gal	β-galactosidase
BMP	bone morphogenetic protein
bp	base pair
BSA	bovine serum albumin
C	Celsius
Cdk4	cyclin debendent kinase 4
CEP	centrosomal protein
Chlx	choroid plexus
Cis	cubicus interruptus
CLSM	confocal laser scanning microscopy
Chlx	choroid plexus
CNS	central nervous system
Cyc	cyclopamine
DE	definitive endoderm
DNA	deoxyribonucleic acid
DKO	double knock-out
DRG	dorsal root ganglia
DTT	Dithiothreitol
D-V	dorsal-ventral
E	embryonic day
EB	elution buffer
ECL	enhanced chemiluminescence
evC	ellis-van Creveld
eGFP	enhanced green fluorescent protein

EMT	epithelial-mesenchymal transition
ES	embryonic stem
FBS	fetal bovine serum
FFA	free fatty acids
FGF	fibroblast growth factor
Flp-e	enhanced flippase
Foxa2	forkhead box transcription factor a 2
FP	floorplate
FRT	Flp recombination target
G	generation
Gli	glioma
GLP1	glucagone-like peptide 1
GLUT2	glucose transporter 2
Gprasp2	G protein-coupled associated sorting protein 2
GSIS	glucose stimulated insulin secretion
GTFBS	gli transcriptionfactor binding site
GTT	glucose tolerance test
HEF1	human enhancer filament 1
HEK	human embryonic kidney
HFD	high fat diet
Hh	hedgehog
Hnf1a	hepatocyte nuclear factor 1 homeobox A
HR	homology regions
HRP	horseradish peroxidase
ICM	inner cell mass
iCre	improved Cre recombinase
IFT	intraflagellar transport
IR	insulin receptor
IRS	insulin receptor substrate
IP	immunoprecipitation
kb	kilo base
KIF3b/ 7	kinesin like protein 3b/ 7
KO	knock-out
LB	limb bud
LIF	leukemia inhibitory factor
L-R	left-reight
LyB	lysogeny broth
MEF	murine embryonic fibroblast
MKS	meckel gruber syndrome

MMC	mitomycin C
MN	motoneuron
MODY	maturity onset diabetes of the young
mTor	mechanistic target of rapamycin
MT	microtubule
NAFL	non alcoholic fatty liver
NC	notochord
Neo	neomycin
NFR	nuclear fast red
NT	neural tube
OFD1	oral-facial-digital syndrome 1
ON	over night
ORF	open reading frame
P	postnatal day
P16ink4a	cycline dependent kinase inhibitor 2A
pBKS	pBluescriptKS
PBS	phosphate buffered saline
PCR	polymerase chain reaction
PDGFR	platelet derived growth factor receptor
Pdx1	pancreas and duodenum homeobox protein1
PE	primitive endoderm
PFA	paraformaldehyde
PGK	phospho-glycerate kinase
Pifo	Pitchfork
PKD	polycystic kidney disease
PLC	primary limb bud cells
PM	plasma membrane
Pr-Di	proximal-distal
PS	primitive streak
Ptch1	Patched1
R26R	ROSA26 reporter
RT	room temperature
SAG	Shh agonist
Shh	sonic hedgehog
Smo	Smoothened
Sufu	suppressor of fused
SUR1	sulfonylurea receptor 1
TR	transcription factor
7TMR	seven transmembrane receptor

SV40pA	Simian Virus 40 polyadenylation signal sequence
T	brachyury
T1/ 2D	type 1/ 2 diabetes
TAE	Tris-acetate, EDTA
TE	trophectoderm
TSS	transcriptional start site
VE	visceral endoderm
WB	Western Blot
WT	wild type
YFP	yellow fluorescent protein
ZPA	zone of polarizing activity

5.2 Figures

6 References

Ahlgren, U., J. Jonsson, and H. Edlund. 1996. The morphogenesis of the pancreatic mesenchyme is uncoupled from that of the pancreatic epithelium in IPF1/PDX1-deficient mice. *Development* 122 (5):1409-16.

Alimonti, A., C. Nardella, Z. Chen, J. G. Clohessy, A. Carracedo, L. C. Trotman, K. Cheng, S. Varmeh, S. C. Kozma, G. Thomas, E. Rosivatz, R. Woscholski, F. Cognetti, H. I. Scher, and P. P. Pandolfi. 2010. A novel type of cellular senescence that can be enhanced in mouse models and human tumor xenografts to suppress prostate tumorigenesis. *J Clin Invest* 120 (3):681-93.

Alten, L., K. Schuster-Gossler, M. P. Eichenlaub, B. Wittbrodt, J. Wittbrodt, and A. Gossler. 2012. A novel mammal-specific three partite enhancer element regulates node and notochord-specific Noto expression. *PLoS One* 7 (10):e47785.

Anderson, E., S. Peluso, L. A. Lettice, and R. E. Hill. 2012. Human limb abnormalities caused by disruption of hedgehog signaling. *Trends Genet* 28 (8):364-73.

Ang, S. L., and J. Rossant. 1994. HNF-3 beta is essential for node and notochord formation in mouse development. *Cell* 78 (4):561-74.

Annicotte, J. S., E. Blanchet, C. Chavey, I. Iankova, S. Costes, S. Assou, J. Teyssier, S. Dalle, C. Sardet, and L. Fajas. 2009. The CDK4-pRB-E2F1 pathway controls insulin secretion. *Nat Cell Biol* 11 (8):1017-23.

Araki, E., M. A. Lipes, M. E. Patti, J. C. Bruning, B. Haag, 3rd, R. S. Johnson, and C. R. Kahn. 1994. Alternative pathway of insulin signalling in mice with targeted disruption of the IRS-1 gene. *Nature* 372 (6502):186-90.

Arsov, T., D. G. Silva, M. K. O'Bryan, A. Sainsbury, N. J. Lee, C. Kennedy, S. S. Manji, K. Nelms, C. Liu, C. G. Vinuesa, D. M. de Kretser, C. C. Goodnow, and N. Petrovsky. 2006. Fat aussie--a new Alstrom syndrome mouse showing a critical role for ALMS1 in obesity, diabetes, and spermatogenesis. *Mol Endocrinol* 20 (7):1610-22.

Assefa, Z., A. Lavens, C. Steyaert, G. Stange, G. A. Martens, Z. Ling, K. Hellemans, and D. Pipeleers. 2014. Glucose Regulates Rat Beta Cell Number through Age-Dependent Effects on Beta Cell Survival and Proliferation. *PLoS One* 9 (1):e85174.

Bai, C. B., and A. L. Joyner. 2001. Gli1 can rescue the in vivo function of Gli2. *Development* 128 (24):5161-72.

Bai, C. B., D. Stephen, and A. L. Joyner. 2004. All mouse ventral spinal cord patterning by hedgehog is Gli dependent and involves an activator function of Gli3. *Dev Cell* 6 (1):103-15.

Balaskas, N., A. Ribeiro, J. Panovska, E. Dessaud, N. Sasai, K. M. Page, J. Briscoe, and V. Ribes. 2012. Gene regulatory logic for reading the Sonic Hedgehog signaling gradient in the vertebrate neural tube. *Cell* 148 (1-2):273-84.

Banizs, B., M. M. Pike, C. L. Millican, W. B. Ferguson, P. Komlosi, J. Sheetz, P. D. Bell, E. M. Schwiebert, and B. K. Yoder. 2005. Dysfunctional cilia lead to altered ependyma and choroid plexus function, and result in the formation of hydrocephalus. *Development* 132 (23):5329-39.

Barnes, B. G. 1961. Ciliated secretory cells in the pars distalis of the mouse hypophysis. *J Ultrastruct Res* 5:453-67.

Barnfield, P. C., X. Zhang, V. Thanabalasingham, M. Yoshida, and C. C. Hui. 2005. Negative regulation of Gli1 and Gli2 activator function by Suppressor of fused through multiple mechanisms. *Differentiation* 73 (8):397-405.

Bartlett, S. E., J. Enquist, F. W. Hopf, J. H. Lee, F. Gladher, V. Kharazia, M. Waldhoer, W. S. Mailliard, R. Armstrong, A. Bonci, and J. L. Whistler. 2005. Dopamine responsiveness is regulated by targeted sorting of D2 receptors. *Proc Natl Acad Sci U S A* 102 (32):11521-6.

Beddington, R. S. 1994. Induction of a second neural axis by the mouse node. *Development* 120 (3):613-20.

Berman, D. M., S. S. Karhadkar, A. Maitra, R. Montes De Oca, M. R. Gerstenblith, K. Briggs, A. R. Parker, Y. Shimada, J. R. Eshleman, D. N. Watkins, and P. A. Beachy. 2003. Widespread requirement for Hedgehog ligand stimulation in growth of digestive tract tumours. *Nature* 425 (6960):846-51.

Bertani, G. 1951. A Method for Detection of Mutations, Using Streptomycin Dependence in Escherichia Coli. *Genetics* 36 (6):598-611.

Bettencourt-Dias, M., R. Giet, R. Sinka, A. Mazumdar, W. G. Lock, F. Balloux, P. J. Zafiropoulos, S. Yamaguchi, S. Winter, R. W. Carthew, M. Cooper, D. Jones, L. Frenz, and D. M. Glover. 2004. Genome-wide survey of protein kinases required for cell cycle progression. *Nature* 432 (7020):980-7.

Bialas, N. J., P. N. Inglis, C. Li, J. F. Robinson, J. D. Parker, M. P. Healey, E. E. Davis, C. D. Inglis, T. Toivonen, D. C. Cottell, O. E. Blacque, L. M. Quarmby, N. Katsanis, and M. R. Leroux. 2009. Functional interactions between the ciliopathy-associated Meckel syndrome 1 (MKS1) protein and two novel MKS1-related (MKSR) proteins. *J Cell Sci* 122 (Pt 5):611-24.

Bielas, S. L., J. L. Silhavy, F. Brancati, M. V. Kisseleva, L. Al-Gazali, L. Sztriha, R. A. Bayoumi, M. S. Zaki, A. Abdel-Aleem, R. O. Rosti, H. Kayserili, D. Swistun, L. C. Scott, E. Bertini, E. Boltshauser, E. Fazzi, L. Travaglini, S. J. Field, S. Gayral, M. Jacoby, S. Schurmans, B. Dallapiccola, P. W. Majerus, E. M. Valente, and J. G. Gleeson. 2009. Mutations in INPP5E, encoding inositol polyphosphate-5-phosphatase E, link phosphatidyl inositol signaling to the ciliopathies. *Nat Genet* 41 (9):1032-6.

Birkenfeld, A. L., and G. I. Shulman. 2014. Nonalcoholic fatty liver disease, hepatic insulin resistance, and type 2 diabetes. *Hepatology* 59 (2):713-23.

Bochkis, I. M., N. E. Rubins, P. White, E. E. Furth, J. R. Friedman, and K. H. Kaestner. 2008. Hepatocyte-specific ablation of Foxa2 alters bile acid homeostasis and results in endoplasmic reticulum stress. *Nat Med* 14 (8):828-36.

Bohn, L. M., R. J. Lefkowitz, and M. G. Caron. 2002. Differential mechanisms of morphine antinociceptive tolerance revealed in (beta)arrestin-2 knock-out mice. *J Neurosci* 22 (23):10494-500.

Boldt, K., J. van Reeuwijk, C. J. Gloeckner, M. Ueffing, and R. Roepman. 2009. Tandem affinity purification of ciliopathy-associated protein complexes. *Methods Cell Biol* 91:143-60.

Bonner-Weir, S. 2000. Perspective: Postnatal pancreatic beta cell growth. *Endocrinology* 141 (6):1926-9.

Borge, P. D., J. Moibi, S. R. Greene, M. Trucco, R. A. Young, Z. Gao, and B. A. Wolf. 2002. Insulin receptor signaling and sarco/endoplasmic reticulum calcium ATPase in beta-cells. *Diabetes* 51 Suppl 3:S427-33.

Bornert, O., T. C. Moller, J. Boeuf, M. P. Candusso, R. Wagner, K. L. Martinez, and F. Simonin. 2013. Identification of a novel protein-protein interaction motif mediating interaction of GPCR-associated sorting proteins with G protein-coupled receptors. *PLoS One* 8 (2):e56336.

Bosco, D., M. Armanet, P. Morel, N. Niclauss, A. Sgroi, Y. D. Muller, L. Giovannoni, G. Parnaud, and T. Berney. 2010. Unique arrangement of alpha- and beta-cells in human islets of Langerhans. *Diabetes* 59 (5):1202-10.

Bouldin, C. M., A. Gritli-Linde, S. Ahn, and B. D. Harfe. 2010. Shh pathway activation is present and required within the vertebrate limb bud apical ectodermal ridge for normal autopod patterning. *Proc Natl Acad Sci U S A* 107 (12):5489-94.

Bowers, M., L. Eng, Z. Lao, R. K. Turnbull, X. Bao, E. Riedel, S. Mackem, and A. L. Joyner. 2012. Limb anterior-posterior polarity integrates activator and repressor functions of GLI2 as well as GLI3. *Dev Biol* 370 (1):110-24.

Briscoe, J., L. Sussel, P. Serup, D. Hartigan-O'Connor, T. M. Jessell, J. L. Rubenstein, and J. Ericson. 1999. Homeobox gene Nkx2.2 and specification of neuronal identity by graded Sonic hedgehog signalling. *Nature* 398 (6728):622-7.

Brunham, L. R., J. K. Kruit, T. D. Pape, J. M. Timmins, A. Q. Reuwer, Z. Vasanji, B. J. Marsh, B. Rodrigues, J. D. Johnson, J. S. Parks, C. B. Verchere, and M. R. Hayden. 2007. Beta-cell ABCA1 influences insulin secretion, glucose homeostasis and response to thiazolidinedione treatment. *Nat Med* 13 (3):340-7.

Bulgakov, O. V., J. T. Eggenschwiler, D. H. Hong, K. V. Anderson, and T. Li. 2004. FKBP8 is a negative regulator of mouse sonic hedgehog signaling in neural tissues. *Development* 131 (9):2149-59.

Burtscher, I., and H. Lickert. 2009. Foxa2 regulates polarity and epithelialization in the endoderm germ layer of the mouse embryo. *Development* 136 (6):1029-38.

Butler, A. E., J. Janson, S. Bonner-Weir, R. Ritzel, R. A. Rizza, and P. C. Butler. 2003. Beta-cell deficit and increased beta-cell apoptosis in humans with type 2 diabetes. *Diabetes* 52 (1):102-10.

Cabrera, O., D. M. Berman, N. S. Kenyon, C. Ricordi, P. O. Berggren, and A. Caicedo. 2006. The unique cytoarchitecture of human pancreatic islets has implications for islet cell function. *Proc Natl Acad Sci U S A* 103 (7):2334-9.

Cardenas-Rodriguez, M., and J. L. Badano. 2009. Ciliary biology: understanding the cellular and genetic basis of human ciliopathies. *Am J Med Genet C Semin Med Genet* 151C (4):263-80.

Cerasi, E., and R. Luft. 1967. "What is inherited--what is added" hypothesis for the pathogenesis of diabetes mellitus. *Diabetes* 16 (9):615-27.

Cervantes, S., J. Lau, D. A. Cano, C. Borromeo-Austin, and M. Hebrok. 2010. Primary cilia regulate Gli/Hedgehog activation in pancreas. *Proc Natl Acad Sci U S A* 107 (22):10109-14.

Chakravarthy, M. V., and C. F. Semenkovich. 2007. The ABCs of beta-cell dysfunction in type 2 diabetes. *Nat Med* 13 (3):241-2.

Chen, M. H., C. W. Wilson, Y. J. Li, K. K. Law, C. S. Lu, R. Gacayan, X. Zhang, C. C. Hui, and P. T. Chuang. 2009. Cilium-independent regulation of Gli protein function by Sufu in Hedgehog signaling is evolutionarily conserved. *Genes Dev* 23 (16):1910-28.

Chen, W., X. R. Ren, C. D. Nelson, L. S. Barak, J. K. Chen, P. A. Beachy, F. de Sauvage, and R. J. Lefkowitz. 2004. Activity-dependent internalization of smoothened mediated by beta-arrestin 2 and GRK2. *Science* 306 (5705):2257-60.

Chen, Y., N. Sasai, G. Ma, T. Yue, J. Jia, J. Briscoe, and J. Jiang. 2011. Sonic Hedgehog dependent phosphorylation by CK1alpha and GRK2 is required for ciliary accumulation and activation of smoothened. *PLoS Biol* 9 (6):e1001083.

Cheung, H. O., X. Zhang, A. Ribeiro, R. Mo, S. Makino, V. Puviindran, K. K. Law, J. Briscoe, and C. C. Hui. 2009. The kinesin protein Kif7 is a critical regulator of Gli transcription factors in mammalian hedgehog signaling. *Sci Signal* 2 (76):ra29.

Chiang, C., Y. Litingtung, E. Lee, K. E. Young, J. L. Corden, H. Westphal, and P. A. Beachy. 1996. Cyclopia and defective axial patterning in mice lacking Sonic hedgehog gene function. *Nature* 383 (6599):407-13.

Choi, S. S., W. K. Syn, G. F. Karaca, A. Omenetti, C. A. Moylan, R. P. Witek, K. M. Agboola, Y. Jung, G. A. Michelotti, and A. M. Diehl. 2010. Leptin promotes the myofibroblastic phenotype in hepatic stellate cells by activating the hedgehog pathway. *J Biol Chem* 285 (47):36551-60.

Corbit, K. C., P. Aanstad, V. Singla, A. R. Norman, D. Y. Stainier, and J. F. Reiter. 2005. Vertebrate Smoothened functions at the primary cilium. *Nature* 437 (7061):1018-21.

Cruz, C., V. Ribes, E. Kutejova, J. Cayuso, V. Lawson, D. Norris, J. Stevens, M. Davey, K. Blight, F. Bangs, A. Mynett, E. Hirst, R. Chung, N. Balaskas, S. L. Brody, E. Marti, and J. Briscoe. 2010. Foxj1 regulates floor plate cilia architecture and modifies the response of cells to sonic hedgehog signalling. *Development* 137 (24):4271-82.

Cui, C., B. Chatterjee, D. Francis, Q. Yu, J. T. SanAgustin, R. Francis, T. Tansey, C. Henry, B. Wang, B. Lemley, G. J. Pazour, and C. W. Lo. 2011. Disruption of Mks1 localization to the mother centriole causes cilia defects and developmental malformations in Meckel-Gruber syndrome. *Dis Model Mech* 4 (1):43-56.

Cuthbertson, D. J., A. Irwin, C. J. Pugh, H. Jones, V. S. Sprung, C. Daousi, V. L. Adams, W. E. Bimson, F. Shojaee-Moradie, A. M. Umpleby, J. P. Wilding, and G. J. Kemp. 2014. Ectopic lipid storage in Non-Alcoholic Fatty Liver Disease is not mediated by impaired mitochondrial oxidative capacity in skeletal muscle. *Clin Sci (Lond)*.

Dai, P., H. Akimaru, Y. Tanaka, T. Maekawa, M. Nakafuku, and S. Ishii. 1999. Sonic Hedgehog-induced activation of the Gli1 promoter is mediated by GLI3. *J Biol Chem* 274 (12):8143-52.

Davenport, J. R., A. J. Watts, V. C. Roper, M. J. Croyle, T. van Groen, J. M. Wyss, T. R. Nagy, R. A. Kesterson, and B. K. Yoder. 2007. Disruption of intraflagellar transport in adult mice leads to obesity and slow-onset cystic kidney disease. *Curr Biol* 17 (18):1586-94.

Davis, D. B., J. A. Lavine, J. I. Suhonen, K. A. Krautkramer, M. E. Rabaglia, J. M. Sperger, L. A. Fernandez, B. S. Yandell, M. P. Keller, I. M. Wang, E. E. Schadt, and A. D. Attie. 2010. FoxM1 is up-regulated by obesity and stimulates beta-cell proliferation. *Mol Endocrinol* 24 (9):1822-34.

De Robertis, E., and C. M. Franchi. 1956. Electron microscope observations on synaptic vesicles in synapses of the retinal rods and cones. *J Biophys Biochem Cytol* 2 (3):307-18.

Delous, M., L. Baala, R. Salomon, C. Laclef, J. Vierkotten, K. Tory, C. Golzio, T. Lacoste, L. Besse, C. Ozilou, I. Moutkine, N. E. Hellman, I. Anselme, F. Silbermann, C. Vesque, C. Gerhardt, E. Rattenberry, M. T. Wolf, M. C. Gubler, J. Martinovic, F. Encha-Razavi, N. Boddaert, M. Gonzales, M. A. Macher, H. Nivet, G. Champion, J. P. Bertheleme, P. Niaudet, F. McDonald, F. Hildebrandt, C. A. Johnson, M. Vekemans, C. Antignac, U. Ruther, S. Schneider-Maunoury, T. Attie-Bitach, and S. Saunier. 2007. The ciliary gene RPGRIP1L is mutated in cerebello-oculo-renal syndrome (Joubert syndrome type B) and Meckel syndrome. *Nat Genet* 39 (7):875-81.

Dessaud, E., A. P. McMahon, and J. Briscoe. 2008. Pattern formation in the vertebrate neural tube: a sonic hedgehog morphogen-regulated transcriptional network. *Development* 135 (15):2489-503.

Di Marcotullio, L., E. Ferretti, E. De Smaele, B. Argenti, C. Mincione, F. Zazzeroni, R. Gallo, L. Masuelli, M. Napolitano, M. Maroder, A. Modesti, F. Giangaspero, I. Screpanti, E. Alesse, and A. Gulino. 2004. REN(KCTD11) is a suppressor of Hedgehog signaling and is deleted in human medulloblastoma. *Proc Natl Acad Sci U S A* 101 (29):10833-8.

Dietrich, J. E., and T. Hiiragi. 2007. Stochastic patterning in the mouse pre-implantation embryo. *Development* 134 (23):4219-31.

Ding, J., F. Yuan, J. Y. Guo, H. Chen, and H. L. Tian. 2013. Influence of glibenclamide on outcome in patients with type 2 diabetes and traumatic brain injury. *Clin Neurol Neurosurg* 115 (10):2166-9.

Ding, Q., J. Motoyama, S. Gasca, R. Mo, H. Sasaki, J. Rossant, and C. C. Hui. 1998. Diminished Sonic hedgehog signaling and lack of floor plate differentiation in Gli2 mutant mice. *Development* 125 (14):2533-43.

Downs, K. M., and T. Davies. 1993. Staging of gastrulating mouse embryos by morphological landmarks in the dissecting microscope. *Development* 118 (4):1255-66.

Dymecki, S. M. 1996. Flp recombinase promotes site-specific DNA recombination in embryonic stem cells and transgenic mice. *Proc Natl Acad Sci U S A* 93 (12):6191-6.

Ede, D. A., and W. A. Kelly. 1964. Developmental Abnormalities in the Trunk and Limbs of the Talpid3 Mutant of the Fowl. *J Embryol Exp Morphol* 12:339-56.

Eggenschwiler, J. T., E. Espinoza, and K. V. Anderson. 2001. Rab23 is an essential negative regulator of the mouse Sonic hedgehog signalling pathway. *Nature* 412 (6843):194-8.

Fajans, S. S., G. I. Bell, and K. S. Polonsky. 2001. Molecular mechanisms and clinical pathophysiology of maturity-onset diabetes of the young. *N Engl J Med* 345 (13):971-80.

Fajas, L., J. S. Annicotte, S. Miard, D. Sarruf, M. Watanabe, and J. Auwerx. 2004. Impaired pancreatic growth, beta cell mass, and beta cell function in E2F1 (-/-)mice. *J Clin Invest* 113 (9):1288-95.

Fawcett, D. W. 1954. The study of epithelial cilia and sperm flagella with the electron microscope. *Laryngoscope* 64 (7):557-67.

Fendrich, V., E. Oh, S. Bang, C. Karikari, N. Ottenhof, S. Bisht, M. Lauth, P. Brossart, N. Katsanis, A. Maitra, and G. Feldmann. 2011. Ectopic overexpression of Sonic Hedgehog (Shh) induces stromal expansion and metaplasia in the adult murine pancreas. *Neoplasia* 13 (10):923-30.

Ferrante, M. I., A. Zullo, A. Barra, S. Bimonte, N. Messaddeq, M. Studer, P. Dolle, and B. Franco. 2006. Oral-facial-digital type I protein is required for primary cilia formation and left-right axis specification. *Nat Genet* 38 (1):112-7.

Franks, P. W., E. Pearson, and J. C. Florez. 2013. Gene-environment and gene-treatment interactions in type 2 diabetes: progress, pitfalls, and prospects. *Diabetes Care* 36 (5):1413-21.

Fraulob, J. C., R. Ogg-Diamantino, C. Fernandes-Santos, M. B. Aguila, and C. A. Mandarim-de-Lacerda. 2010. A Mouse Model of Metabolic Syndrome: Insulin Resistance, Fatty Liver and Non-Alcoholic Fatty Pancreas Disease (NAFPD) in C57BL/6 Mice Fed a High Fat Diet. *J Clin Biochem Nutr* 46 (3):212-23.

Gerdes, J. M., E. E. Davis, and N. Katsanis. 2009. The vertebrate primary cilium in development, homeostasis, and disease. *Cell* 137 (1):32-45.

Girard, D., and N. Petrovsky. 2011. Alstrom syndrome: insights into the pathogenesis of metabolic disorders. *Nat Rev Endocrinol* 7 (2):77-88.

Gladigau, E. L., T. N. Fazio, J. P. Hannam, L. M. Dawson, and S. G. Jones. 2014. Increased cardiovascular risk in patients with severe mental illness. *Intern Med J* 44 (1):65-9.

Glinka, A., W. Wu, H. Delius, A. P. Monaghan, C. Blumenstock, and C. Niehrs. 1998. Dickkopf-1 is a member of a new family of secreted proteins and functions in head induction. *Nature* 391 (6665):357-62.

Goetz, S. C., and K. V. Anderson. 2010. The primary cilium: a signalling centre during vertebrate development. *Nat Rev Genet* 11 (5):331-44.

Goetz, S. C., P. J. Ocbina, and K. V. Anderson. 2009. The primary cilium as a Hedgehog signal transduction machine. *Methods Cell Biol* 94:199-222.

Goldberg, I. J., R. H. Eckel, and N. A. Abumrad. 2009. Regulation of fatty acid uptake into tissues: lipoprotein lipase- and CD36-mediated pathways. *J Lipid Res* 50 Suppl:S86-90.

Goodrich, L. V., L. Milenkovic, K. M. Higgins, and M. P. Scott. 1997. Altered neural cell fates and medulloblastoma in mouse patched mutants. *Science* 277 (5329):1109-13.

Graham, F. L., J. Smiley, W. C. Russell, and R. Nairn. 1977. Characteristics of a human cell line transformed by DNA from human adenovirus type 5. *J Gen Virol* 36 (1):59-74.

Grayson, B. E., R. J. Seeley, and D. A. Sandoval. 2013. Wired on sugar: the role of the CNS in the regulation of glucose homeostasis. *Nat Rev Neurosci* 14 (1):24-37.

Gregor, T., D. W. Tank, E. F. Wieschaus, and W. Bialek. 2007. Probing the limits to positional information. *Cell* 130 (1):153-64.

Grillo, M. A., and S. L. Palay. 1963. Ciliated Schwann cells in the autonomic nervous system of the adult rat. *J Cell Biol* 16:430-6.

Gu, D., Q. Fan, X. Zhang, and J. Xie. 2012. A role for transcription factor STAT3 signaling in oncogene smoothened-driven carcinogenesis. *J Biol Chem* 287 (45):38356-66.

Guo, D. F., and K. Rahmouni. 2011. Molecular basis of the obesity associated with Bardet-Biedl syndrome. *Trends Endocrinol Metab* 22 (7):286-93.

Gurung, B., Z. Feng, D. V. Iwamoto, A. Thiel, G. Jin, C. M. Fan, J. M. Ng, T. Curran, and X. Hua. 2013. Menin epigenetically represses Hedgehog signaling in MEN1 tumor syndrome. *Cancer Res* 73 (8):2650-8.

Hadjantonakis, A. K., S. Macmaster, and A. Nagy. 2002. Embryonic stem cells and mice expressing different GFP variants for multiple non-invasive reporter usage within a single animal. *BMC Biotechnol* 2:11.

Han, Y. G., H. J. Kim, A. A. Dlugosz, D. W. Ellison, R. J. Gilbertson, and A. Alvarez-Buylla. 2009. Dual and opposing roles of primary cilia in medulloblastoma development. *Nat Med* 15 (9):1062-5.

Hardy, K., P. Carthew, A. H. Handyside, and M. L. Hooper. 1990. Extragonadal teratocarcinoma derived from embryonal stem cells in chimaeric mice. *J Pathol* 160 (1):71-6.

Harfe, B. D., P. J. Scherz, S. Nissim, H. Tian, A. P. McMahon, and C. J. Tabin. 2004. Evidence for an expansion-based temporal Shh gradient in specifying vertebrate digit identities. *Cell* 118 (4):517-28.

Haycraft, C. J., B. Banizs, Y. Aydin-Son, Q. Zhang, E. J. Michaud, and B. K. Yoder. 2005. Gli2 and Gli3 localize to cilia and require the intraflagellar transport protein polaris for processing and function. *PLoS Genet* 1 (4):e53.

Heydorn, A., B. P. Sondergaard, B. Ersboll, B. Holst, F. C. Nielsen, C. R. Haft, J. Whistler, and T. W. Schwartz. 2004. A library of 7TM receptor C-terminal tails. Interactions with the proposed post-endocytic sorting proteins ERM-binding phosphoprotein 50 (EBP50), N-ethylmaleimide-sensitive factor (NSF), sorting nexin 1 (SNX1), and G protein-coupled receptor-associated sorting protein (GASP). *J Biol Chem* 279 (52):54291-303.

Hinchcliffe, E. H., C. Li, E. A. Thompson, J. L. Maller, and G. Sluder. 1999. Requirement of Cdk2-cyclin E activity for repeated centrosome reproduction in Xenopus egg extracts. *Science* 283 (5403):851-4.

Hirokawa, N., Y. Tanaka, Y. Okada, and S. Takeda. 2006. Nodal flow and the generation of left-right asymmetry. *Cell* 125 (1):33-45.

Hitz, C., W. Wurst, and R. Kuhn. 2007. Conditional brain-specific knockdown of MAPK using Cre/loxP regulated RNA interference. *Nucleic Acids Res* 35 (12):e90.

Ho, J. M., V. T. Anekonda, B. W. Thompson, M. Zhu, R. W. Curry, B. H. Hwang, G. J. Morton, M. W. Schwartz, D. G. Baskin, S. M. Appleyard, and J. E. Blevins. 2014. Hindbrain oxytocin receptors contribute to the effects of circulating oxytocin on food intake in male rats. *Endocrinology*:en20141148.

Hooper, M., K. Hardy, A. Handyside, S. Hunter, and M. Monk. 1987. HPRT-deficient (Lesch-Nyhan) mouse embryos derived from germline colonization by cultured cells. *Nature* 326 (6110):292-5.

Horn, S. C., M. Lalowski, H. Goehler, A. Droge, E. E. Wanker, and U. Stelzl. 2006. Huntingtin interacts with the receptor sorting family protein GASP2. *J Neural Transm* 113 (8):1081-90.

Houde, C., R. J. Dickinson, V. M. Houtzager, R. Cullum, R. Montpetit, M. Metzler, E. M. Simpson, S. Roy, M. R. Hayden, P. A. Hoodless, and D. W. Nicholson. 2006. Hippi is essential for node cilia assembly and Sonic hedgehog signaling. *Dev Biol* 300 (2):523-33.

Hu, Y., J. Liang, and S. Yu. 2014. High Prevalence of Diabetes Mellitus in a Five-Generation Chinese Family with Huntington's Disease. *J Alzheimers Dis* 40 (4):863-8.

Huang, X., T. Ketova, J. T. Fleming, H. Wang, S. K. Dey, Y. Litingtung, and C. Chiang. 2009. Sonic hedgehog signaling regulates a novel epithelial progenitor domain of the hindbrain choroid plexus. *Development* 136 (15):2535-43.

Huangfu, D., and K. V. Anderson. 2005. Cilia and Hedgehog responsiveness in the mouse. *Proc Natl Acad Sci U S A* 102 (32):11325-30.

———. 2006. Signaling from Smo to Ci/Gli: conservation and divergence of Hedgehog pathways from Drosophila to vertebrates. *Development* 133 (1):3-14.

Huangfu, D., A. Liu, A. S. Rakeman, N. S. Murcia, L. Niswander, and K. V. Anderson. 2003. Hedgehog signalling in the mouse requires intraflagellar transport proteins. *Nature* 426 (6962):83-7.

Hui, C. C., and S. Angers. 2011. Gli proteins in development and disease. *Annu Rev Cell Dev Biol* 27:513-37.

Inagaki, N., T. Gonoi, J. P. th Clement, N. Namba, J. Inazawa, G. Gonzalez, L. Aguilar-Bryan, S. Seino, and J. Bryan. 1995. Reconstitution of IKATP: an inward rectifier subunit plus the sulfonylurea receptor. *Science* 270 (5239):1166-70.

Ingalls, A. M., M. M. Dickie, and G. D. Snell. 1950. Obese, a new mutation in the house mouse. *J Hered* 41 (12):317-8.

Jonsson, J., L. Carlsson, T. Edlund, and H. Edlund. 1994. Insulin-promoter-factor 1 is required for pancreas development in mice. *Nature* 371 (6498):606-9.

Kaestner, K. H. 2010. The FoxA factors in organogenesis and differentiation. *Curr Opin Genet Dev* 20 (5):527-32.

Kahn, C. R. 1994. Banting Lecture. Insulin action, diabetogenes, and the cause of type II diabetes. *Diabetes* 43 (8):1066-84.

Kahn, C. R., D. Vicent, and A. Doria. 1996. Genetics of non-insulin-dependent (type-II) diabetes mellitus. *Annu Rev Med* 47:509-31.

Kardon, J. R., and R. D. Vale. 2009. Regulators of the cytoplasmic dynein motor. *Nat Rev Mol Cell Biol* 10 (12):854-65.

Kasperczyk, H., B. Baumann, K. M. Debatin, and S. Fulda. 2009. Characterization of sonic hedgehog as a novel NF-kappaB target gene that promotes NF-kappaB-mediated apoptosis resistance and tumor growth in vivo. *FASEB J* 23 (1):21-33.

Kennedy, A. J., K. L. Ellacott, V. L. King, and A. H. Hasty. 2010. Mouse models of the metabolic syndrome. *Dis Model Mech* 3 (3-4):156-66.

Kennedy, A. L., J. P. Morton, I. Manoharan, D. M. Nelson, N. B. Jamieson, J. S. Pawlikowski, T. McBryan, B. Doyle, C. McKay, K. A. Oien, G. H. Enders, R. Zhang, O. J. Sansom, and P. D. Adams. 2011. Activation of the PIK3CA/AKT pathway suppresses senescence induced by an activated RAS oncogene to promote tumorigenesis. *Mol Cell* 42 (1):36-49.

Kenney, A. M., and D. H. Rowitch. 2000. Sonic hedgehog promotes G(1) cyclin expression and sustained cell cycle progression in mammalian neuronal precursors. *Mol Cell Biol* 20 (23):9055-67.

Kerszberg, M., and L. Wolpert. 2007. Specifying positional information in the embryo: looking beyond morphogens. *Cell* 130 (2):205-9.

Khanna, H., T. W. Hurd, C. Lillo, X. Shu, S. K. Parapuram, S. He, M. Akimoto, A. F. Wright, B. Margolis, D. S. Williams, and A. Swaroop. 2005. RPGR-ORF15, which is mutated in retinitis pigmentosa, associates with SMC1, SMC3, and microtubule transport proteins. *J Biol Chem* 280 (39):33580-7.

Kilimnik, G., A. Kim, D. F. Steiner, T. C. Friedman, and M. Hara. 2010. Intraislet production of GLP-1 by activation of prohormone convertase 1/3 in pancreatic alpha-cells in mouse models of ss-cell regeneration. *Islets* 2 (3):149-55.

Kim, S. K., and D. A. Melton. 1998. Pancreas development is promoted by cyclopamine, a hedgehog signaling inhibitor. *Proc Natl Acad Sci U S A* 95 (22):13036-41.

Kinder, S. J., T. E. Tsang, M. Wakamiya, H. Sasaki, R. R. Behringer, A. Nagy, and P. P. Tam. 2001. The organizer of the mouse gastrula is composed of a dynamic population of progenitor cells for the axial mesoderm. *Development* 128 (18):3623-34.

Kinzel, D., K. Boldt, E. E. Davis, I. Burtscher, D. Trumbach, B. Diplas, T. Attie-Bitach, W. Wurst, N. Katsanis, M. Ueffing, and H. Lickert. 2010. Pitchfork regulates primary cilia disassembly and left-right asymmetry. *Dev Cell* 19 (1):66-77.

Kise, Y., A. Morinaka, S. Teglund, and H. Miki. 2009. Sufu recruits GSK3beta for efficient processing of Gli3. *Biochem Biophys Res Commun* 387 (3):569-74.

Kloppel, G., M. Lohr, K. Habich, M. Oberholzer, and P. U. Heitz. 1985. Islet pathology and the pathogenesis of type 1 and type 2 diabetes mellitus revisited. *Surv Synth Pathol Res* 4 (2):110-25.

Konner, A. C., R. Janoschek, L. Plum, S. D. Jordan, E. Rother, X. Ma, C. Xu, P. Enriori, B. Hampel, G. S. Barsh, C. R. Kahn, M. A. Cowley, F. M. Ashcroft, and J. C. Bruning. 2007. Insulin action in AgRP-expressing neurons is required for suppression of hepatic glucose production. *Cell Metab* 5 (6):438-49.

Kovacs, J. J., E. J. Whalen, R. Liu, K. Xiao, J. Kim, M. Chen, J. Wang, W. Chen, and R. J. Lefkowitz. 2008. Beta-arrestin-mediated localization of smoothened to the primary cilium. *Science* 320 (5884):1777-81.

Kozhemyakina, E., A. Ionescu, and A. B. Lassar. 2014. GATA6 is a crucial regulator of Shh in the limb bud. *PLoS Genet* 10 (1):e1004072.

Krishnan, V., F. A. Pereira, Y. Qiu, C. H. Chen, P. A. Beachy, S. Y. Tsai, and M. J. Tsai. 1997. Mediation of Sonic hedgehog-induced expression of COUP-TFII by a protein phosphatase. *Science* 278 (5345):1947-50.

Kushner, J. A. 2006. Beta-cell growth: an unusual paradigm of organogenesis that is cyclin D2/Cdk4 dependent. *Cell Cycle* 5 (3):234-7.

Landsman, L., A. Parent, and M. Hebrok. 2011. Elevated Hedgehog/Gli signaling causes beta-cell dedifferentiation in mice. *Proc Natl Acad Sci U S A* 108 (41):17010-5.

Lau, J., and M. Hebrok. 2010. Hedgehog signaling in pancreas epithelium regulates embryonic organ formation and adult beta-cell function. *Diabetes* 59 (5):1211-21.

Lau, J., H. Kawahira, and M. Hebrok. 2006. Hedgehog signaling in pancreas development and disease. *Cell Mol Life Sci* 63 (6):642-52.

Law, K. K., S. Makino, R. Mo, X. Zhang, V. Puviindran, and C. C. Hui. 2012. Antagonistic and cooperative actions of Kif7 and Sufu define graded intracellular Gli activities in Hedgehog signaling. *PLoS One* 7 (11):e50193.

Lee, C. S., J. R. Friedman, J. T. Fulmer, and K. H. Kaestner. 2005. The initiation of liver development is dependent on Foxa transcription factors. *Nature* 435 (7044):944-7.

Lee, E. C., D. Yu, J. Martinez de Velasco, L. Tessarollo, D. A. Swing, D. L. Court, N. A. Jenkins, and N. G. Copeland. 2001. A highly efficient Escherichia coli-based chromosome engineering system adapted for recombinogenic targeting and subcloning of BAC DNA. *Genomics* 73 (1):56-65.

Lee, Y., J. E. Dominy, Y. J. Choi, M. Jurczak, N. Tolliday, J. P. Camporez, H. Chim, J. H. Lim, H. B. Ruan, X. Yang, F. Vazquez, P. Sicinski, G. I. Shulman, and P. Puigserver. 2014. Cyclin D1-Cdk4 controls glucose metabolism independently of cell cycle progression. *Nature*.

Lee, Y., R. Kawagoe, K. Sasai, Y. Li, H. R. Russell, T. Curran, and P. J. McKinnon. 2007. Loss of suppressor-of-fused function promotes tumorigenesis. *Oncogene* 26 (44):6442-7.

Lewis, S. L., and P. P. Tam. 2006. Definitive endoderm of the mouse embryo: formation, cell fates, and morphogenetic function. *Dev Dyn* 235 (9):2315-29.

Li, A., M. Saito, J. Z. Chuang, Y. Y. Tseng, C. Dedesma, K. Tomizawa, T. Kaitsuka, and C. H. Sung. 2011. Ciliary transition zone activation of phosphorylated Tctex-1 controls ciliary resorption, S-phase entry and fate of neural progenitors. *Nat Cell Biol* 13 (4):402-11.

Li, X., Q. Ma, W. Duan, H. Liu, H. Xu, and E. Wu. 2012. Paracrine sonic hedgehog signaling derived from tumor epithelial cells: a key regulator in the pancreatic tumor microenvironment. *Crit Rev Eukaryot Gene Expr* 22 (2):97-108.

Li, Z. J., E. Nieuwenhuis, W. Nien, X. Zhang, J. Zhang, V. Puviindran, B. J. Wainwright, P. C. Kim, and C. C. Hui. 2012. Kif7 regulates Gli2 through Sufu-dependent and -independent functions during skin development and tumorigenesis. *Development* 139 (22):4152-61.

Li, Z., G. Tuteja, J. Schug, and K. H. Kaestner. 2012. Foxa1 and Foxa2 are essential for sexual dimorphism in liver cancer. *Cell* 148 (1-2):72-83.

Li, Z., P. White, G. Tuteja, N. Rubins, S. Sackett, and K. H. Kaestner. 2009. Foxa1 and Foxa2 regulate bile duct development in mice. *J Clin Invest* 119 (6):1537-45.

Liao, W. P., L. Uetzmann, I. Burtscher, and H. Lickert. 2009. Generation of a mouse line expressing Sox17-driven Cre recombinase with specific activity in arteries. *Genesis* 47 (7):476-83.

Lindstrom, P. 2010. beta-cell function in obese-hyperglycemic mice [ob/ob Mice]. *Adv Exp Med Biol* 654:463-77.

Litingtung, Y., R. D. Dahn, Y. Li, J. F. Fallon, and C. Chiang. 2002. Shh and Gli3 are dispensable for limb skeleton formation but regulate digit number and identity. *Nature* 418 (6901):979-83.

Liu, A., B. Wang, and L. A. Niswander. 2005. Mouse intraflagellar transport proteins regulate both the activator and repressor functions of Gli transcription factors. *Development* 132 (13):3103-11.

Liu, Q., G. Tan, N. Levenkova, T. Li, E. N. Pugh, Jr., J. J. Rux, D. W. Speicher, and E. A. Pierce. 2007. The proteome of the mouse photoreceptor sensory cilium complex. *Mol Cell Proteomics* 6 (8):1299-317.

Locker, M., M. Agathocleous, M. A. Amato, K. Parain, W. A. Harris, and M. Perron. 2006. Hedgehog signaling and the retina: insights into the mechanisms controlling the proliferative properties of neural precursors. *Genes Dev* 20 (21):3036-48.

Loges, N. T., H. Olbrich, L. Fenske, H. Mussaffi, J. Horvath, M. Fliegauf, H. Kuhl, G. Baktai, E. Peterffy, R. Chodhari, E. M. Chung, A. Rutman, C. O'Callaghan, H. Blau, L. Tiszlavicz, K. Voelkel, M. Witt, E. Zietkiewicz, J. Neesen, R. Reinhardt, H. M. Mitchison, and H. Omran. 2008. DNAI2 mutations cause primary ciliary dyskinesia with defects in the outer dynein arm. *Am J Hum Genet* 83 (5):547-58.

Luders, J., and T. Stearns. 2007. Microtubule-organizing centres: a re-evaluation. *Nat Rev Mol Cell Biol* 8 (2):161-7.

Malaguarnera, R., and A. Belfiore. 2014. The Emerging Role of Insulin and Insulin-Like Growth Factor Signaling in Cancer Stem Cells. *Front Endocrinol (Lausanne)* 5:10.

Marshall, J. D., R. T. Bronson, G. B. Collin, A. D. Nordstrom, P. Maffei, R. B. Paisey, C. Carey, S. Macdermott, I. Russell-Eggitt, S. E. Shea, J. Davis, S. Beck, G. Shatirishvili, C. M. Mihai, M. Hoeltzenbein, G. B. Pozzan, I. Hopkinson, N. Sicolo, J. K. Naggert, and P. M. Nishina. 2005. New Alstrom syndrome phenotypes based on the evaluation of 182 cases. *Arch Intern Med* 165 (6):675-83.

Martin, B. C., J. H. Warram, A. S. Krolewski, R. N. Bergman, J. S. Soeldner, and C. R. Kahn. 1992. Role of glucose and insulin resistance in development of type 2 diabetes mellitus: results of a 25-year follow-up study. *Lancet* 340 (8825):925-9.

Martin, G. R. 1981. Isolation of a pluripotent cell line from early mouse embryos cultured in medium conditioned by teratocarcinoma stem cells. *Proc Natl Acad Sci U S A* 78 (12):7634-8.

Matise, M. P., D. J. Epstein, H. L. Park, K. A. Platt, and A. L. Joyner. 1998. Gli2 is required for induction of floor plate and adjacent cells, but not most ventral neurons in the mouse central nervous system. *Development* 125 (15):2759-70.

Matsushita, S., H. Onishi, K. Nakano, I. Nagamatsu, A. Imaizumi, M. Hattori, Y. Oda, M. Tanaka, and M. Katano. 2014. Hedgehog signaling pathway is a potential therapeutic target for gallbladder cancer. *Cancer Sci* 105 (3):272-80.

May, S. R., A. M. Ashique, M. Karlen, B. Wang, Y. Shen, K. Zarbalis, J. Reiter, J. Ericson, and A. S. Peterson. 2005. Loss of the retrograde motor for IFT disrupts localization of Smo to cilia and prevents the expression of both activator and repressor functions of Gli. *Dev Biol* 287 (2):378-89.

McVilly, K., J. McGillivray, A. Curtis, J. Lehmann, L. Morrish, and J. Speight. 2014. Diabetes in people with an intellectual disability: a systematic review of prevalence, incidence and impact. *Diabet Med*.

Methot, N., and K. Basler. 2000. Suppressor of fused opposes hedgehog signal transduction by impeding nuclear accumulation of the activator form of Cubitus interruptus. *Development* 127 (18):4001-10.

Michaud, E. J., and B. K. Yoder. 2006. The primary cilium in cell signaling and cancer. *Cancer Res* 66 (13):6463-7.

Milenkovic, L., M. P. Scott, and R. Rohatgi. 2009. Lateral transport of Smoothened from the plasma membrane to the membrane of the cilium. *J Cell Biol* 187 (3):365-74.

Moore, A., E. Escudier, G. Roger, A. Tamalet, B. Pelosse, S. Marlin, A. Clement, M. Geremek, B. Delaisi, A. M. Bridoux, A. Coste, M. Witt, B. Duriez, and S. Amselem. 2006. RPGR is mutated in patients with a complex X linked phenotype combining primary ciliary dyskinesia and retinitis pigmentosa. *J Med Genet* 43 (4):326-33.

Morris, J. P. th, S. C. Wang, and M. Hebrok. 2010. KRAS, Hedgehog, Wnt and the twisted developmental biology of pancreatic ductal adenocarcinoma. *Nat Rev Cancer* 10 (10):683-95.

Moser, E., J. Kargl, J. L. Whistler, M. Waldhoer, and P. Tschische. 2010. G protein-coupled receptor-associated sorting protein 1 regulates the postendocytic sorting of seven-transmembrane-spanning G protein-coupled receptors. *Pharmacology* 86 (1):22-9.

Motoyama, J., L. Milenkovic, M. Iwama, Y. Shikata, M. P. Scott, and C. C. Hui. 2003. Differential requirement for Gli2 and Gli3 in ventral neural cell fate specification. *Dev Biol* 259 (1):150-61.

Murcia, N. S., W. G. Richards, B. K. Yoder, M. L. Mucenski, J. R. Dunlap, and R. P. Woychik. 2000. The Oak Ridge Polycystic Kidney (orpk) disease gene is required for left-right axis determination. *Development* 127 (11):2347-55.

Murdoch, J. N., and A. J. Copp. 2010. The relationship between sonic Hedgehog signaling, cilia, and neural tube defects. *Birth Defects Res A Clin Mol Teratol* 88 (8):633-52.

Nagy, A., J. Rossant, R. Nagy, W. Abramow-Newerly, and J. C. Roder. 1993. Derivation of completely cell culture-derived mice from early-passage embryonic stem cells. *Proc Natl Acad Sci U S A* 90 (18):8424-8.

Nakaya, M. A., K. Biris, T. Tsukiyama, S. Jaime, J. A. Rawls, and T. P. Yamaguchi. 2005. Wnt3a links left-right determination with segmentation and anteroposterior axis elongation. *Development* 132 (24):5425-36.

Nakayama, S., M. Arakawa, T. Uchida, T. Ogihara, R. Kanno, F. Ikeda, K. Azuma, T. Hirose, R. Kawamori, Y. Fujitani, and H. Watada. 2008. Dose-dependent requirement of patched homologue 1 in mouse pancreatic beta cell mass. *Diabetologia* 51 (10):1883-92.

Niswander, L. 2003. Pattern formation: old models out on a limb. *Nat Rev Genet* 4 (2):133-43.

Niwa, H., Y. Toyooka, D. Shimosato, D. Strumpf, K. Takahashi, R. Yagi, and J. Rossant. 2005. Interaction between Oct3/4 and Cdx2 determines trophectoderm differentiation. *Cell* 123 (5):917-29.

Noble, J. A., A. Martin, A. M. Valdes, J. A. Lane, A. Galgani, A. Petrone, R. Lorini, P. Pozzilli, R. Buzzetti, and H. A. Erlich. 2008. Type 1 diabetes risk for human leukocyte antigen (HLA)-DR3 haplotypes depends on genotypic context: association of DPB1 and HLA class I loci among DR3- and DR4-matched Italian patients and controls. *Hum Immunol* 69 (4-5):291-300.

Nolan-Stevaux, O., J. Lau, M. L. Truitt, G. C. Chu, M. Hebrok, M. E. Fernandez-Zapico, and D. Hanahan. 2009. GLI1 is regulated through Smoothened-independent mechanisms in neoplastic pancreatic ducts and mediates PDAC cell survival and transformation. *Genes Dev* 23 (1):24-36.

Nonaka, S., S. Yoshiba, D. Watanabe, S. Ikeuchi, T. Goto, W. F. Marshall, and H. Hamada. 2005. De novo formation of left-right asymmetry by posterior tilt of nodal cilia. *PLoS Biol* 3 (8):e268.

Nusslein-Volhard, C., and E. Wieschaus. 1980. Mutations affecting segment number and polarity in Drosophila. *Nature* 287 (5785):795-801.

Obici, S., Z. Feng, G. Karkanias, D. G. Baskin, and L. Rossetti. 2002. Decreasing hypothalamic insulin receptors causes hyperphagia and insulin resistance in rats. *Nat Neurosci* 5 (6):566-72.

Ocbina, P. J., J. T. Eggenschwiler, I. Moskowitz, and K. V. Anderson. 2011. Complex interactions between genes controlling trafficking in primary cilia. *Nat Genet* 43 (6):547-53.

Ohtsubo, K., M. Z. Chen, J. M. Olefsky, and J. D. Marth. 2011. Pathway to diabetes through attenuation of pancreatic beta cell glycosylation and glucose transport. *Nat Med* 17 (9):1067-75.

Onishi, H., M. Kai, S. Odate, H. Iwasaki, Y. Morifuji, T. Ogino, T. Morisaki, Y. Nakashima, and M. Katano. 2011. Hypoxia activates the hedgehog signaling pathway in a ligand-independent manner by upregulation of Smo transcription in pancreatic cancer. *Cancer Sci* 102 (6):1144-50.

Pan, F. C., and C. Wright. 2011. Pancreas organogenesis: from bud to plexus to gland. *Dev Dyn* 240 (3):530-65.

Park, H. L., C. Bai, K. A. Platt, M. P. Matise, A. Beeghly, C. C. Hui, M. Nakashima, and A. L. Joyner. 2000. Mouse Gli1 mutants are viable but have defects in SHH signaling in combination with a Gli2 mutation. *Development* 127 (8):1593-605.

Parkin, D. M., F. Bray, J. Ferlay, and P. Pisani. 2005. Global cancer statistics, 2002. *CA Cancer J Clin* 55 (2):74-108.

Pasca di Magliano, M., S. Sekine, A. Ermilov, J. Ferris, A. A. Dlugosz, and M. Hebrok. 2006. Hedgehog/Ras interactions regulate early stages of pancreatic cancer. *Genes Dev* 20 (22):3161-73.

Pazour, G. J., B. L. Dickert, Y. Vucica, E. S. Seeley, J. L. Rosenbaum, G. B. Witman, and D. G. Cole. 2000. Chlamydomonas IFT88 and its mouse homologue, polycystic kidney disease gene tg737, are required for assembly of cilia and flagella. *J Cell Biol* 151 (3):709-18.

Perea-Gomez, A., F. D. Vella, W. Shawlot, M. Oulad-Abdelghani, C. Chazaud, C. Meno, V. Pfister, L. Chen, E. Robertson, H. Hamada, R. R. Behringer, and S. L. Ang. 2002. Nodal antagonists in the anterior visceral endoderm prevent the formation of multiple primitive streaks. *Dev Cell* 3 (5):745-56.

Petersen, K. F., and G. I. Shulman. 2006. Etiology of insulin resistance. *Am J Med* 119 (5 Suppl 1):S10-6.

Piccolo, S., E. Agius, L. Leyns, S. Bhattacharyya, H. Grunz, T. Bouwmeester, and E. M. De Robertis. 1999. The head inducer Cerberus is a multifunctional antagonist of Nodal, BMP and Wnt signals. *Nature* 397 (6721):707-10.

Piton, A., J. Gauthier, F. F. Hamdan, R. G. Lafreniere, Y. Yang, E. Henrion, S. Laurent, A. Noreau, P. Thibodeau, L. Karemera, D. Spiegelman, F. Kuku, J. Duguay, L. Destroismaisons, P. Jolivet, M. Cote, K. Lachapelle, O. Diallo, A. Raymond, C. Marineau, N. Champagne, L. Xiong, C. Gaspar, J. B. Riviere, J. Tarabeux, P. Cossette, M. O. Krebs, J. L. Rapoport, A. Addington, L. E. Delisi, L. Mottron, R. Joober, E. Fombonne, P. Drapeau, and G. A. Rouleau. 2011. Systematic resequencing of X-chromosome synaptic genes in autism spectrum disorder and schizophrenia. *Mol Psychiatry* 16 (8):867-80.

Prentki, M., and C. J. Nolan. 2006. Islet beta cell failure in type 2 diabetes. *J Clin Invest* 116 (7):1802-12.

Pugacheva, E. N., S. A. Jablonski, T. R. Hartman, E. P. Henske, and E. A. Golemis. 2007. HEF1-dependent Aurora A activation induces disassembly of the primary cilium. *Cell* 129 (7):1351-63.

Qi, Y., M. Tan, C. C. Hui, and M. Qiu. 2003. Gli2 is required for normal Shh signaling and oligodendrocyte development in the spinal cord. *Mol Cell Neurosci* 23 (3):440-50.

Qiu, L., R. Na, R. Xu, S. Wang, H. Sheng, W. Wu, and Y. Qu. 2014. Quantitative Assessment of the Effect of KCNJ11 Gene Polymorphism on the Risk of Type 2 Diabetes. *PLoS One* 9 (4):e93961.

Quagliarini, F., Y. Wang, J. Kozlitina, N. V. Grishin, R. Hyde, E. Boerwinkle, D. M. Valenzuela, A. J. Murphy, J. C. Cohen, and H. H. Hobbs. 2012. Atypical angiopoietin-like protein that regulates ANGPTL3. *Proc Natl Acad Sci U S A* 109 (48):19751-6.

Rhodes, C. J. 2005. Type 2 diabetes-a matter of beta-cell life and death? *Science* 307 (5708):380-4.

Ribes, V., and J. Briscoe. 2009. Establishing and interpreting graded Sonic Hedgehog signaling during vertebrate neural tube patterning: the role of negative feedback. *Cold Spring Harb Perspect Biol* 1 (2):a002014.

Rohatgi, R., L. Milenkovic, and M. P. Scott. 2007. Patched1 regulates hedgehog signaling at the primary cilium. *Science* 317 (5836):372-6.

Sadagurski, M., Z. Cheng, A. Rozzo, I. Palazzolo, G. R. Kelley, X. Dong, D. Krainc, and M. F. White. 2011. IRS2 increases mitochondrial dysfunction and oxidative stress in a mouse model of Huntington disease. *J Clin Invest* 121 (10):4070-81.

Sasaki, H., C. Hui, M. Nakafuku, and H. Kondoh. 1997. A binding site for Gli proteins is essential for HNF-3beta floor plate enhancer activity in transgenics and can respond to Shh in vitro. *Development* 124 (7):1313-22.

Sasaki, H., Y. Nishizaki, C. Hui, M. Nakafuku, and H. Kondoh. 1999. Regulation of Gli2 and Gli3 activities by an amino-terminal repression domain: implication of Gli2 and Gli3 as primary mediators of Shh signaling. *Development* 126 (17):3915-24.

Scales, S. J., and F. J. de Sauvage. 2009. Mechanisms of Hedgehog pathway activation in cancer and implications for therapy. *Trends Pharmacol Sci* 30 (6):303-12.

Scholey, J. M. 2008. Intraflagellar transport motors in cilia: moving along the cell's antenna. *J Cell Biol* 180 (1):23-9.

Shahi, M. H., M. Afzal, S. Sinha, C. G. Eberhart, J. A. Rey, X. Fan, and J. S. Castresana. 2010. Regulation of sonic hedgehog-GLI1 downstream target genes PTCH1, Cyclin D2, Plakoglobin, PAX6 and NKX2.2 and their epigenetic status in medulloblastoma and astrocytoma. *BMC Cancer* 10:614.

Shay, J. W., W. E. Wright, and H. Werbin. 1991. Defining the molecular mechanisms of human cell immortalization. *Biochim Biophys Acta* 1072 (1):1-7.

Sheedfar, F., M. Vermeer, V. Pazienza, J. Villarroya, F. Rappa, F. Cappello, G. Mazzoccoli, F. Villarroya, H. van der Molen, M. H. Hofker, D. P. Koonen, and M. Vinciguerra. 2014. Genetic ablation of macrohistone H2A1 leads to increased leanness, glucose tolerance and energy expenditure in mice fed a high fat diet. *Int J Obes (Lond)*.

Shen, T., X. M. Yan, and C. J. Xiao. 2013. [Current status and implication of research on Bardet-Biedl syndrome]. *Zhonghua Yi Xue Yi Chuan Xue Za Zhi* 30 (5):570-3.

Shih, J., and S. E. Fraser. 1996. Characterizing the zebrafish organizer: microsurgical analysis at the early-shield stage. *Development* 122 (4):1313-22.

Simonin, F., P. Karcher, J. J. Boeuf, A. Matifas, and B. L. Kieffer. 2004. Identification of a novel family of G protein-coupled receptor associated sorting proteins. *J Neurochem* 89 (3):766-75.

Sorenson, R. L., and T. C. Brelje. 1997. Adaptation of islets of Langerhans to pregnancy: beta-cell growth, enhanced insulin secretion and the role of lactogenic hormones. *Horm Metab Res* 29 (6):301-7.

Soriano, P. 1999. Generalized lacZ expression with the ROSA26 Cre reporter strain. *Nat Genet* 21 (1):70-1.

Sorokin, S. 1962. Centrioles and the formation of rudimentary cilia by fibroblasts and smooth muscle cells. *J Cell Biol* 15:363-77.

Spemann, H., and H. Mangold. 2001. Induction of embryonic primordia by implantation of organizers from a different species. 1923. *Int J Dev Biol* 45 (1):13-38.

Spivak-Kroizman, T. R., G. Hostetter, R. Posner, M. Aziz, C. Hu, M. J. Demeure, D. Von Hoff, S. R. Hingorani, T. B. Palculict, J. Izzo, G. M. Kiriakova, M. Abdelmelek, G. Bartholomeusz, B. P. James, and G. Powis. 2013. Hypoxia triggers hedgehog-mediated tumor-stromal interactions in pancreatic cancer. *Cancer Res* 73 (11):3235-47.

Stamateris, R. E., R. B. Sharma, D. A. Hollern, and L. C. Alonso. 2013. Adaptive beta-cell proliferation increases early in high-fat feeding in mice, concurrent with metabolic changes, with induction of islet cyclin D2 expression. *Am J Physiol Endocrinol Metab* 305 (1):E149-59.

Stolovich-Rain, M., A. Hija, J. Grimsby, B. Glaser, and Y. Dor. 2012. Pancreatic beta cells in very old mice retain capacity for compensatory proliferation. *J Biol Chem* 287 (33):27407-14.

Stumvoll, M., U. Chintalapudi, G. Perriello, S. Welle, O. Gutierrez, and J. Gerich. 1995. Uptake and release of glucose by the human kidney. Postabsorptive rates and responses to epinephrine. *J Clin Invest* 96 (5):2528-33.

Su, C. Y., S. N. Bay, L. E. Mariani, M. J. Hillman, and T. Caspary. 2012. Temporal deletion of Arl13b reveals that a mispatterned neural tube corrects cell fate over time. *Development* 139 (21):4062-71.

Suh, J. M., X. Gao, J. McKay, R. McKay, Z. Salo, and J. M. Graff. 2006. Hedgehog signaling plays a conserved role in inhibiting fat formation. *Cell Metab* 3 (1):25-34.

Supp, D. M., D. P. Witte, S. S. Potter, and M. Brueckner. 1997. Mutation of an axonemal dynein affects left-right asymmetry in inversus viscerum mice. *Nature* 389 (6654):963-6.

Svard, J., K. Heby-Henricson, M. Persson-Lek, B. Rozell, M. Lauth, A. Bergstrom, J. Ericson, R. Toftgard, and S. Teglund. 2006. Genetic elimination of Suppressor of fused reveals an essential repressor function in the mammalian Hedgehog signaling pathway. *Dev Cell* 10 (2):187-97.

Szymczak, A. L., C. J. Workman, Y. Wang, K. M. Vignali, S. Dilioglou, E. F. Vanin, and D. A. Vignali. 2004. Correction of multi-gene deficiency in vivo using a single 'self-cleaving' 2A peptide-based retroviral vector. *Nat Biotechnol* 22 (5):589-94.

Takagi, T., H. Furuta, M. Miyawaki, K. Nagashima, T. Shimada, A. Doi, S. Matsuno, D. Tanaka, M. Nishi, H. Sasaki, N. Inagaki, N. Yoshikawa, K. Nanjo, and T. Akamizu. 2013. Clinical and functional characterization of the Pro1198Leu ABCC8 gene mutation associated with permanent neonatal diabetes mellitus. *J Diabetes Investig* 4 (3):269-73.

Takaoka, K., and H. Hamada. 2012. Cell fate decisions and axis determination in the early mouse embryo. *Development* 139 (1):3-14.

Tallila, J., E. Jakkula, L. Peltonen, R. Salonen, and M. Kestila. 2008. Identification of CC2D2A as a Meckel syndrome gene adds an important piece to the ciliopathy puzzle. *Am J Hum Genet* 82 (6):1361-7.

Tam, P. P., and J. Rossant. 2003. Mouse embryonic chimeras: tools for studying mammalian development. *Development* 130 (25):6155-63.

Tam, P. P., K. A. Steiner, S. X. Zhou, and G. A. Quinlan. 1997. Lineage and functional analyses of the mouse organizer. *Cold Spring Harb Symp Quant Biol* 62:135-44.

Tamplin, O. J., D. Kinzel, B. J. Cox, C. E. Bell, J. Rossant, and H. Lickert. 2008. Microarray analysis of Foxa2 mutant mouse embryos reveals novel gene expression and inductive roles for the gastrula organizer and its derivatives. *BMC Genomics* 9:511.

Tanaka, Y., Y. Okada, and N. Hirokawa. 2005. FGF-induced vesicular release of Sonic hedgehog and retinoic acid in leftward nodal flow is critical for left-right determination. *Nature* 435 (7039):172-7.

Taniguchi, C. M., K. Ueki, and R. Kahn. 2005. Complementary roles of IRS-1 and IRS-2 in the hepatic regulation of metabolism. *J Clin Invest* 115 (3):718-27.

te Welscher, P., M. Fernandez-Teran, M. A. Ros, and R. Zeller. 2002. Mutual genetic antagonism involving GLI3 and dHAND prepatterns the vertebrate limb bud mesenchyme prior to SHH signaling. *Genes Dev* 16 (4):421-6.

te Welscher, P., A. Zuniga, S. Kuijper, T. Drenth, H. J. Goedemans, F. Meijlink, and R. Zeller. 2002. Progression of vertebrate limb development through SHH-mediated counteraction of GLI3. *Science* 298 (5594):827-30.

Thomas, M. K., N. Rastalsky, J. H. Lee, and J. F. Habener. 2000. Hedgehog signaling regulation of insulin production by pancreatic beta-cells. *Diabetes* 49 (12):2039-47.

Tobin, J. L., and P. L. Beales. 2008. Restoration of renal function in zebrafish models of ciliopathies. *Pediatr Nephrol* 23 (11):2095-9.

Tran, P. V., C. J. Haycraft, T. Y. Besschetnova, A. Turbe-Doan, R. W. Stottmann, B. J. Herron, A. L. Chesebro, H. Qiu, P. J. Scherz, J. V. Shah, B. K. Yoder, and D. R. Beier. 2008. THM1 negatively modulates mouse sonic hedgehog signal transduction and affects retrograde intraflagellar transport in cilia. *Nat Genet* 40 (4):403-10.

Troy, S., M. Soty, L. Ribeiro, L. Laval, S. Migrenne, X. Fioramonti, B. Pillot, V. Fauveau, R. Aubert, B. Viollet, M. Foretz, J. Leclerc, A. Duchampt, C. Zitoun, B. Thorens, C. Magnan, G. Mithieux, and F. Andreelli. 2008. Intestinal gluconeogenesis is a key factor for early metabolic changes after gastric bypass but not after gastric lap-band in mice. *Cell Metab* 8 (3):201-11.

Tschische, P., E. Moser, D. Thompson, H. F. Vischer, G. P. Parzmair, V. Pommer, W. Platzer, T. Schwarzbraun, H. Schaider, M. J. Smit, L. Martini, J. L. Whistler, and M. Waldhoer. 2010. The G-protein coupled receptor associated sorting protein GASP-1 regulates the signalling and trafficking of the viral chemokine receptor US28. *Traffic* 11 (5):660-74.

Tuson, M., M. He, and K. V. Anderson. 2011. Protein kinase A acts at the basal body of the primary cilium to prevent Gli2 activation and ventralization of the mouse neural tube. *Development* 138 (22):4921-30.

Tuszynski, G. P., V. L. Rothman, X. Zheng, M. Gutu, X. Zhang, and F. Chang. 2011. G-protein coupled receptor-associated sorting protein 1 (GASP-1), a potential biomarker in breast cancer. *Exp Mol Pathol* 91 (2):608-13.

Ulloa, F., and E. Marti. 2010. Wnt won the war: antagonistic role of Wnt over Shh controls dorso-ventral patterning of the vertebrate neural tube. *Dev Dyn* 239 (1):69-76.

Umeda, H., N. Ozaki, N. Mizutani, T. Fukuyama, H. Nagasaki, H. Arima, and Y. Oiso. 2010. Protective effect of hedgehog signaling on cytokine-induced cytotoxicity in pancreatic beta-cells. *Exp Clin Endocrinol Diabetes* 118 (10):692-8.

Wang, G., K. Amanai, B. Wang, and J. Jiang. 2000. Interactions with Costal2 and suppressor of fused regulate nuclear translocation and activity of cubitus interruptus. *Genes Dev* 14 (22):2893-905.

Wang, Y., F. Quagliarini, V. Gusarova, J. Gromada, D. M. Valenzuela, J. C. Cohen, and H. H. Hobbs. 2013. Mice lacking ANGPTL8 (Betatrophin) manifest disrupted triglyceride metabolism without impaired glucose homeostasis. *Proc Natl Acad Sci U S A* 110 (40):16109-14.

Wang, Y., Z. Zhou, C. T. Walsh, and A. P. McMahon. 2009. Selective translocation of intracellular Smoothened to the primary cilium in response to Hedgehog pathway modulation. *Proc Natl Acad Sci U S A* 106 (8):2623-8.

Ware, S. M., M. G. Aygun, and F. Hildebrandt. 2011. Spectrum of clinical diseases caused by disorders of primary cilia. *Proc Am Thorac Soc* 8 (5):444-50.

Wareham, N. J. 2014. The long-term benefits of lifestyle interventions for prevention of diabetes. *Lancet Diabetes Endocrinol*.

Warming, S., N. Costantino, D. L. Court, N. A. Jenkins, and N. G. Copeland. 2005. Simple and highly efficient BAC recombineering using galK selection. *Nucleic Acids Res* 33 (4):e36.

Waters, A. M., and P. L. Beales. 1993. Bardet-Biedl Syndrome. In *GeneReviews*, edited by R. A. Pagon, M. P. Adam, T. D. Bird, C. R. Dolan, C. T. Fong, R. J. H. Smith and K. Stephens. Seattle (WA).

Weatherbee, S. D., L. A. Niswander, and K. V. Anderson. 2009. A mouse model for Meckel syndrome reveals Mks1 is required for ciliogenesis and Hedgehog signaling. *Hum Mol Genet* 18 (23):4565-75.

Weinstein, D. C., A. Ruiz i Altaba, W. S. Chen, P. Hoodless, V. R. Prezioso, T. M. Jessell, and J. E. Darnell, Jr. 1994. The winged-helix transcription factor HNF-3 beta is required for notochord development in the mouse embryo. *Cell* 78 (4):575-88.

Weissmann, L., P. G. Quaresma, A. C. Santos, A. H. de Matos, V. D'Avila Bittencourt Pascoal, T. M. Zanotto, G. Castro, D. Guadgnini, J. Martins da Silva, L. A. Velloso, J. C. Bittencourt, I. Lopes-Cendes, M. J. Saad, and P. O. Prada. 2014. IKK epsilon is key to induction of insulin resistance in the hypothalamus and its inhibition reverses obesity. *Diabetes*.

Whistler, J. L., J. Enquist, A. Marley, J. Fong, F. Gladher, P. Tsuruda, S. R. Murray, and M. Von Zastrow. 2002. Modulation of postendocytic sorting of G protein-coupled receptors. *Science* 297 (5581):615-20.

White, M. F. 2002. IRS proteins and the common path to diabetes. *Am J Physiol Endocrinol Metab* 283 (3):E413-22.

Winklmayr, M., C. Schmid, S. Laner-Plamberger, A. Kaser, F. Aberger, T. Eichberger, and A. M. Frischauf. 2010. Non-consensus GLI binding sites in Hedgehog target gene regulation. *BMC Mol Biol* 11:2.

Withers, D. J., D. J. Burks, H. H. Towery, S. L. Altamuro, C. L. Flint, and M. F. White. 1999. Irs-2 coordinates Igf-1 receptor-mediated beta-cell development and peripheral insulin signalling. *Nat Genet* 23 (1):32-40.

Wolpert, L., and A. Garcia-Bellido. 1998. Debatable issues. Interview by Alain Ghysen. *Int J Dev Biol* 42 (3):511-8.

Wong, S. Y., and J. F. Reiter. 2008. The primary cilium at the crossroads of mammalian hedgehog signaling. *Curr Top Dev Biol* 85:225-60.

Xu, Y., Y. An, X. Wang, W. Zha, and X. Li. 2014. Inhibition of the Hedgehog pathway induces autophagy in pancreatic ductal adenocarcinoma cells. *Oncol Rep* 31 (2):707-12.

Yang, Y., G. Drossopoulou, P. T. Chuang, D. Duprez, E. Marti, D. Bumcrot, N. Vargesson, J. Clarke, L. Niswander, A. McMahon, and C. Tickle. 1997. Relationship between dose, distance and time in Sonic Hedgehog-mediated regulation of anteroposterior polarity in the chick limb. *Development* 124 (21):4393-404.

Yauch, R. L., S. E. Gould, S. J. Scales, T. Tang, H. Tian, C. P. Ahn, D. Marshall, L. Fu, T. Januario, D. Kallop, M. Nannini-Pepe, K. Kotkow, J. C. Marsters, L. L. Rubin, and F. J. de Sauvage. 2008. A paracrine requirement for hedgehog signalling in cancer. *Nature* 455 (7211):406-10.

Yi, P., J. S. Park, and D. A. Melton. 2013. Betatrophin: a hormone that controls pancreatic beta cell proliferation. *Cell* 153 (4):747-58.

Yki-Jarvinen, H. 2010. Liver fat in the pathogenesis of insulin resistance and type 2 diabetes. *Dig Dis* 28 (1):203-9.

Zaghloul, N. A., Y. Liu, J. M. Gerdes, C. Gascue, E. C. Oh, C. C. Leitch, Y. Bromberg, J. Binkley, R. L. Leibel, A. Sidow, J. L. Badano, and N. Katsanis. 2010. Functional analyses of variants reveal a significant role for dominant negative and common alleles in oligogenic Bardet-Biedl syndrome. *Proc Natl Acad Sci U S A* 107 (23):10602-7.

Zaret, K. S. 2008. Genetic programming of liver and pancreas progenitors: lessons for stem-cell differentiation. *Nat Rev Genet* 9 (5):329-40.

Zeng, N., K. T. Yang, J. A. Bayan, L. He, R. Aggarwal, J. W. Stiles, X. Hou, V. Medina, D. Abad, B. M. Palian, I. Al-Abdullah, F. Kandeel, D. L. Johnson, and B. L. Stiles. 2013. PTEN controls beta-cell regeneration in aged mice by regulating cell cycle inhibitor p16ink4a. *Aging Cell* 12 (6):1000-11.

Zhang, X. M., M. Ramalho-Santos, and A. P. McMahon. 2001. Smoothened mutants reveal redundant roles for Shh and Ihh signaling including regulation of L/R asymmetry by the mouse node. *Cell* 105 (6):781-92.

Zhao, Y., D. H. Hong, B. Pawlyk, G. Yue, M. Adamian, M. Grynberg, A. Godzik, and T. Li. 2003. The retinitis pigmentosa GTPase regulator (RPGR)- interacting protein: subserving RPGR function and participating in disk morphogenesis. *Proc Natl Acad Sci U S A* 100 (7):3965-70.

Zhou, J., E. M. Goldberg, N. A. Leu, L. Zhou, D. A. Coulter, and P. J. Wang. 2014. Respiratory failure, cleft palate and epilepsy in the mouse model of human Xq22.1 deletion syndrome. *Hum Mol Genet*.

Zhu, J., E. Nakamura, M. T. Nguyen, X. Bao, H. Akiyama, and S. Mackem. 2008. Uncoupling Sonic hedgehog control of pattern and expansion of the developing limb bud. *Dev Cell* 14 (4):624-32.

Zhuang, L. N., W. X. Hu, M. L. Zhang, S. M. Xin, W. P. Jia, J. Zhao, and G. Pei. 2011. Beta-arrestin-1 protein represses diet-induced obesity. *J Biol Chem* 286 (32):28396-402.

Zung, A., E. Petek, B. Ben-Zeev, T. Schwarzbraun, and S. J. Ben-Yehoshua. 2011. MODY type 2 in Greig cephalopolysyndactyly syndrome (GCPS) as part of a contiguous gene deletion syndrome. *Am J Med Genet A* 155A (10):2469-72.

Additional

Kurth, B.M., C. Lange, P. Kamtsiuris. 2009. Gesundheitsmonitoring am Robert Koch-Institut. Sachstand und Perspektiven. Bundesgesundheitsbl–Gesundheitsforsch–Gesundheitsschutz 52(5): 557-570

Jung, B., D. Padula, I. Burtscher, E. Kremmer, K. Boldt, M. Ueffing, H. Lickert. 2014. Pitchfork and Gprasp2 target Smoothened to the primary cilium for Hedgehog pathway activation. JCB (submitted)

7 Publications

Article

Pitchfork and Gprasp2 target Smoothened to the primary cilium for Hedgehog pathway activation. Jung B, **Padula D**, Burtscher I, Kremmer E, Boldt K, Ueffing M, Lickert H. 2014; JCB (submitted).

Overexpression of dnIKK in mesenchymal stem cells leads to increased migration and decreased invasion upon TNFα stimulation. Haasters F, Prall WC, Westphal I, Böcker W, **Padula D**, Mutschler W, Docheva D, Schieker M. Biochem Biophys Res Commun. 2013 Jun 28.

Probing the interaction forces of prostate cancer cells with collagen I and bone marrow derived stem cells on the single cell level. Sariisik E, Docheva D, **Padula D**, Popov C, Opfer J, Schieker M, Clausen-Schaumann H, Benoit M. PLoS One. 2013 Mar 5.

Effect of collagen I and fibronectin on the adhesion, elasticity and cytoskeletal organization of prostate cancer cells. Docheva D, **Padula D**, Schieker M, Clausen-Schaumann H. Biochem Biophys Res Commun. 2010 Nov 12.

Establishment of immortalized periodontal ligament progenitor cell line and its behavioural analysis on smooth and rough titanium surface. Docheva D, **Padula D**, Popov C, Weishaupt P, Prägert M, Miosge N, Hickel R, Böcker W, Clausen-Schaumann H, Schieker M. Eur Cell Mater. 2010 May.

Researching into the cellular shape, volume and elasticity of mesenchymal stem cells, osteoblasts and osteosarcoma cells by atomic force microscopy. Docheva D, **Padula D**, Popov C, Mutschler W, Clausen-Schaumann H, Schieker M. J Cell Mol Med. 2008 Apr.

Non-Impact Article

Burtscher I, Engert S, Hasenöder S, Padula D, Lickert H. Steuerungsmechanismen der Entodermentwicklung in der Maus. BIOspektrum September 2011, Volume 17, Issue 5, pp 520-523